LUND UNIVERSITY

Beyond Massive MIMO

Trade-offs and Opportunities with Large Multi-Antenna Systems

Vidal Alegría, Juan

2023

Document Version:
Publisher's PDF, also known as Version of record

Link to publication

Citation for published version (APA):
Vidal Alegría, J. (2023). *Beyond Massive MIMO: Trade-offs and Opportunities with Large Multi-Antenna Systems*. Electrical and Information Technology, Lund University.

Total number of authors:
1

General rights
Unless other specific re-use rights are stated the following general rights apply:
Copyright and moral rights for the publications made accessible in the public portal are retained by the authors and/or other copyright owners and it is a condition of accessing publications that users recognise and abide by the legal requirements associated with these rights.
• Users may download and print one copy of any publication from the public portal for the purpose of private study or research.
• You may not further distribute the material or use it for any profit-making activity or commercial gain
• You may freely distribute the URL identifying the publication in the public portal

Read more about Creative commons licenses: https://creativecommons.org/licenses/

Take down policy
If you believe that this document breaches copyright please contact us providing details, and we will remove access to the work immediately and investigate your claim.

LUND UNIVERSITY

PO Box 117
221 00 Lund
+46 46-222 00 00

Beyond Massive MIMO

Trade-offs and Opportunities with Large Multi-Antenna Systems

Juan Vidal Alegría

Lund 2023

© Juan Vidal Alegría, 2023

"Beyond Massive MIMO:
Trade-offs and Opportunities with Large Multi-Antenna Systems"

Published articles have been reprinted with permission from the respective copyright holder. Reprints may include reformatting and minor corrections.

Series of licentiate and doctoral theses
No. 159
ISSN 1654-790X159
ISBN 978-91-8039-615-8 (print)
ISBN 978-91-8039-616-5 (pdf)

This thesis is produced by using the LaTeX Documentation System
Printed in Sweden by *Tryckeriet i E-huset*, Lund.

Department of Electrical and Information Technology
Lund University, Box 118, SE-221 00 Lund, Sweden

A mi abuelo Juan

Popular Science

When I turned 12, my godfather got me as a present my first mobile phone, a cool Sony Ericsson K300. Back then, mobile phones were already more than a portable version of an ordinary telephone, my K300 could be used for taking photos, sending SMSs, and even downloading fancy polytones; why would anyone need more than that? However, 6 years later—I was a bit late among my friends—came my first smartphone, an average Samsung Galaxy Y. Data subscriptions were a bit expensive then, but even without it I could connect my smartphone to free WiFi networks to watch videos, listen to music, and send "WhatsApps".

Nowadays, a majority of the people in the World own a smartphone which can stream high-quality video (and audio), perform live video-calls, or even run elaborate online games. Plus, we have access to all these features almost anywhere and anytime by just paying a relatively cheap mobile broadband subscription fee. Sustaining this increasing traffic demand while reducing costs to keep affordable subscription prices is already a challenging task by itself, which largely justifies the current research efforts in wireless communications. However, we can already read tweets about novel applications including virtual and extended reality for "the metaverse", autonomous mobility (a.k.a., self-driving vehicles), smart homes/cities, and many unimaginable ones may soon emerge—at least I couldn't imagine we would reach this point when I was playing around with my K300. These novel applications will certainly contribute to the traffic burden on mobile broadband networks, but they may even create further requirements for these networks in terms of peak data-rates, delays, reliability, energy efficiency, etc.

The main focus of this thesis is to study technologies intended to support the increasing demand in data-rates. However, there is typically a close connection between data-rate, reliability, and energy efficiency, so we could measure our contributions within an intersection of these metrics. During the last decade, an important trend emerged with the aim of increasing the data-rates that can be supported by mobile broadband networks: increasing the number of antennas at the base stations. You might have heard of "Massive MIMO"

for 5G, which considers base stations with hundreds of antennas, but we are currently witnessing even more massive proposals as large intelligent surfaces (LISs), which consider whole walls having thousands of antennas. The main idea is that, by increasing the number of antennas, we can be more precise in distinguishing users in the space. This means that we can serve several users with the resources typically required for only one of them simply by having them at slightly different positions—within the order of centimeters apart or even less if we have enough antennas.

Although increasing the number of antennas at the base stations—and even its physical size—has clear advantages, it comes at a cost. For example, in order to distinguish users in space, base stations with many antennas may need to effectively treat the signals received at each of their antennas. Typically, this means that they need to transmit all these signals to one computer that tries to analyze them and extract the information from the users. This corresponds to what we call a *centralized architecture*. However, in base stations with a huge number antennas, the amount of signals that have to be sent to this computer would also become huge, so, to be able to send them to a computer, we may need links carrying enormous amounts of data. This becomes even more challenging if the antennas are distributed throughout large areas, since these signals would then have to travel greater distances. A large part of this thesis deals with how to perform transformations on these signals so that the data rates required to send them to a computer are effectively reduced, leading to what we call *decentralized architectures*. On the other hand, we also present some results on the limitations of decentralized architectures, as well as on how to exploit systems with different levels of decentralization that have no performance loss as compared to centralized systems.

Another technology that is trending these days in the research community to support the increasing demand for high data-rates is the use of surfaces that are reflecting the waves in a controlled manner. These surfaces usually have a large number of reconfigurable elements, each of which can interact with the incoming waves so that they can redirect the reflected waves towards the desired directions, e.g., towards the WiFi router. A small part of this thesis presents some ideas on how to use these surfaces, or variations of them, to create favorable channels between users and base stations so that it becomes easier to serve several users with the same resources.

To sum up, we can say that this thesis is about base stations with many antennas, and reconfigurable surfaces of various kinds. Although the scope seems quite broad, the results presented lie mainly in the intersection between signal processing and information theory.

Abstract

After the commercial emergence of 5G, the research community is already putting its focus on proposing innovative solutions to enable the upcoming 6G. One important lesson put forth by 5G research was that scaling up the conventional multiple-input-multiple-output (MIMO) technology by increasing the number of antennas could be extremely beneficial for effectively multiplexing data streams in the spatial domain. This idea was embodied in massive MIMO, which constitutes one of the major technical advancements included in 5G. Consequently, 6G research efforts have been largely directed towards studying ways to further scale up wireless systems, as can be seen in some of the proposed 6G enabling technologies like large intelligent surface (LIS), cell-free massive MIMO, or even reconfigurable intelligent surface (RIS). This thesis studies the possibilities offered by some of these technologies, as well as the trade-offs that may naturally arise when scaling up such wireless systems.

An important part of this thesis deals with decentralized solutions for base station (BS) technologies including a large number of antennas. Already in the initial massive MIMO prototypes, the increased number of BS antennas led to scalability issues due to the high interconnection bandwidths required to send the received signals—as well as the channel state information (CSI)—to a central processing unit (CPU) in charge of the data processing. These issues can only be exacerbated if we consider novel system proposals like LIS, where the number of BS antennas may be increased by an order of magnitude with respect to massive MIMO, or cell-free massive MIMO, where the BS antennas may be located far from each other. We provide a number of decentralized schemes to process the received data while restricting the information that has to be shared with a CPU. We also provide a framework to study architectures with an arbitrary level of decentralization, showing that there exists a direct trade-off between the interconnection bandwidth to a CPU and the complexity of the decentralized processing required for fixed user rates.

Another part of this thesis studies RIS-based solutions to enhance the multiplexing performance of wireless communication systems. RIS constitutes one of the most attractive 6G enabling technologies since it provides a cost- and

energy-efficient solution to improve the wireless propagation links by generating favorable reflections. We extend the concept of RIS by considering reconfigurable surfaces (RSs) with different processing capabilities, and we show how these surfaces may be employed for achieving perfect spatial multiplexing at reduced processing complexity in general multi-antenna communication settings. We also show that these surfaces can exploit the available degrees of freedom—e.g., due to excess of BS antennas—to embed their own data into the enhanced channel.

Preface

This doctoral thesis summarizes the most relevant research contributions from my PhD studies at the department of Electrical and Information Technology (EIT), Lund University, Sweden. However, the journey that brought me here has been much longer than the roughly four and a half years that took me to complete this work. I would say it may have started when my best friend convinced me to join with him a bachelor's degree in telecommunication engineering. At the time, I only knew that I wanted to pursue a technical career—potentially in engineering—but I didn't have a clear direction until my friend's suggestion. Unfortunately, we only studied together during the first year of the bachelor's, but in the meantime, I realized that this choice seemed to align perfectly well with my preferences and skills.

It was three years into my university education when I managed to put my foot into research by becoming a research intern at the microwave and radar group (GMR-UPM), where I participated in some projects including implementation and evaluation of communication systems making use of multi-antenna technology. I still didn't have any desire to pursue a PhD until I crossed paths with Fredrik Rusek. I guess it was the "learning experience" part that caught my attention, or the desire to get to "a higher level of understanding"—which suddenly became one of my major goals. I soon realized, again, that following this path may be one of the most rewarding experiences I could go through. I'm still amazed how far such random choices can take you...

The current thesis is comprised of Part I and Part II. Part I contains an overview of the research field in which I have been working during my PhD, including some useful preliminary knowledge and a brief contextualization of my contributions in this field. Part II is composed of eight papers that constitute my contribution to the research field. The included papers are listed next:

Paper I J. Vidal Alegría, J. Rodríguez Sánchez, F. Rusek, L. Liu and O. Edfors "Decentralized Equalizer Construction for Large Intelligent Surfaces," in *Proc. 2019 IEEE 90th Vehicular Technology Conference (VTC-Fall)*, Honolulu, HI, USA, 2019, pp. 1-6.

Personal contributions: This paper was based upon previous work

of the other authors, which gave the baseline and motivation for it. The framework was discussed among the authors. I came up with the novel decentralized algorithms presented in this work, and performed the analysis and simulations. I also took the lead role in writing the paper except for the Introdution section.

Paper II J. Vidal Alegría, F. Rusek and O. Edfors, "Trade-offs in Decentralized Multi-Antenna Architectures: The WAX Decomposition," in *IEEE Transactions on Signal Processing*, vol. 69, pp.36277-3641, 2021.

Personal contributions: The framework was initially proposed by the second author and discussed among the authors. I performed the theoretical analysis with help from the second author, who contributed to the proof of Theorem 1 and provided the validity conditions for the combining modules. I also did the simulation work and I took the lead role in writing the paper.

Paper III J. Vidal Alegría, J. Huang and F. Rusek, "Cell-Free Massive MIMO: Exploiting The WAX Decomposition," in *Proc. 2022 IEEE International Conference on Acoustics, Speech and Signal Processing (ICASSP)*, Singapore, Singapore, 2022, pp. 5393-5397.

Personal contributions: I proposed framework of the paper upon discussion with the other authors. I performed the whole theoretical and numerical analysis. I also took the lead role in writing the paper.

Paper IV J. Vidal Alegría, F. Rusek and A. Lozano "Impact of Quantization in Decentralized Processing for Large Multi-Antenna Architectures," in *Proc. 2022 56th Asilomar Conference on Signals, Systems, and Computers*, Pacific Grove, CA, USA, 2022, pp. 1351-1356.

Personal contributions: I proposed the framework of the paper, and discussed it with the other authors. I performed the theoretical analysis with advice from the other authors, where the third author proposed the use of the Bussgang decomposition and suggested some relevant bibliography. I also did the simulation work and I took the lead role in writing the paper.

Paper V J. Vidal Alegría and F. Rusek "Channel Orthogonalization with Reconfigurable Surfaces," in *Proc. 2022 IEEE Globecom Workshops (GC-Wkshps)*, Rio de Janeiro, Brazil, 2022, pp. 37-42.

Personal contributions: I came up with the idea of using reflective surfaces with extended capabilities to perfectly orthogonalize the propagation channel. I also came up with the proposed channel estimation methods. I performed the theoretical analysis with advice from the second author, who provided relevant bibliography regarding the use of optimization tools in the unitary matrix space. I also did the simulation work and I took the lead role in writing the paper.

Paper VI J. Vidal Alegría and F. Rusek, "Trade-offs in Decentralized Multi-Antenna Architectures: Sparse Combining Modules for WAX De-

composition," submitted to *IEEE Transactions on Signal Processing* (second review in process).

Personal contributions: The paper was a continuation of previous work which was discussed among the authors. I proposed the general algorithm and the decentralized scheme, while the combining modules were a result of discussions and contributions from both authors. I performed the theoretical analysis, proving the validity of the proposed structures. I also did the numerical analysis and I took the lead role in writing the paper.

Paper VII J. Vidal Alegría, Joao Vieira and F. Rusek "Increased Multiplexing Gain with Reconfigurable Surfaces: Simultaneous Channel Orthogonalization and Information Embedding," submitted to GLOBECOM 2023.

Personal contributions: I proposed the framework and discussed it with the rest of the authors. I performed the theoretical analysis with advice from the last author, who suggested relevant bibliography regarding the derivation of the PDFs. I also did the numerical analysis and I took the lead role in writing the paper.

During my PhD, I have also contributed to a number of papers that are not included in this thesis:

- R. Blázquez-García et al., "Smart Relay Architecture for Over-the-Horizon High Quality Communications With Unmanned Aerial Vehicles," in *IEEE Access*, vol. 7, pp. 76317-76327, 2019.
- J. R. Sánchez, J. Vidal Alegría and F. Rusek, "Decentralized Massive MIMO Systems: Is There Anything to be Discussed?," in *Proc. 2019 IEEE Int. Symposium on Information Theory (ISIT)*, Paris, France, 2019, pp. 787-791.
- J. Vidal Alegría and F. Rusek, "Cramér-Rao Lower Bounds for Positioning with Large Intelligent Surfaces using Quantized Amplitude and Phase," in *Proc. 2019 53rd Asilomar Conference on Signals, Systems, and Computers*, Pacific Grove, CA, USA, 2019, pp. 10-14.
- J. Vidal Alegría and F. Rusek, "Achievable Rate with Correlated Hardware Impairments in Large Intelligent Surfaces," in *Proc. 2019 IEEE 8th Int. Workshop on Computational Advances in Multi-Sensor Adaptive Processing (CAMSAP)*, Le Gosier, Guadeloupe, 2019, pp. 559-563.
- J. Vidal Alegría, F. Rusek, J. R. Sánchez and O. Edfors, "Trade-Offs in Quasi-Decentralized Massive MIMO," in *Proc. 2020 IEEE Int. Conference on Communications Workshops (ICC-Wkshps)*, Dublin, Ireland, 2020, pp. 1-6.
- J. Vidal Alegría, F. Rusek, J. R. Sánchez and O. Edfors, "Modular Binary Tree Architecture for Distributed Large Intelligent Surface," in *Proc. 2021 IEEE Int. Conference on Acoustics, Speech and Signal Processing (ICASSP)*, Toronto, ON, Canada, 2021, pp. 4565-4569.
- J. Vidal Alegría and F. Rusek, "Enabling Decentralized Computation of the WAX Decomposition," in *Proc. IEEE Int. Conference on Communications (ICC)*, Seoul, Republic of Korea, 2022, pp. 1-6.

Acknowledgements

I couldn't start but thanking the greatest information theoretist of Eslöv, Fredrik Rusek. It wasn't until I first entered your office that I started to feel the honesty and kindness that hides behind your bold humor and tough look. That was soon reinforced by Muris with his "Jackpot supervisor" discourse, and with Joao's convincing arguments about how there couldn't be any better option than doing a PhD with you. They were right, you managed to light up my eagerness for knowledge and satisfied it with deep discussions and invaluable lessons. More importantly, you made it fun and easy. I can't be more grateful for your help and support, thanks for becoming a friend to me!

I would also like to thank my colleagues from the Com Division, the ones that are gone—Umar, Jesús, Pepe, Andreia, Qiunyan, Muris, Joao—and the ones that are still here—Xuhong, Guoda, Michiel, Christian, Xuesong, Sara, Ashkan, Dino, Ross, Aleksei, Neharika, Hedie, Makambi, Junshi, Juan S, Hanieh, Yuyan, Ove, Vincent, Michael, Anders, Fredrik T, Kentaro, Leif, John B. Thank you for all the interesting lunch talks, for the generous fikas, and for the good times that made me want to come to office every day. I extend my gratitude to the rest of people at EIT, for creating such an inclusive and comfortable environment. Moreover, I would like to thank my host at universitat Pompeu Fabra (UPF), Angel Lozano, thank you for welcoming me and offering me the opportunity to experience a different way of doing research, which turned out to be really helpful during the end of my Ph.D. I'm also thankful to the rest of the people I met at UPF for making me feel like at home: Rasoul, Mohamed, Giovanni, Andrea, Abhi, Ramona, and all the rest.

I'm also grateful to the people I met along the way. A Iván, por las lecciones de basket y las charlas prolongadas en el balcón de Ulrikedal. A Manu, por las tardes primaverales en busca de alguna pista de tenis bajo el cielo rosa de Lund. A David, por hacerme confiar en el proceso. Al payico Agus, por más festis recogiendo basura. A Luca, por las noches de Sydskånska estirando el reloj. To Raoul, for being the perfect rave and chess buddie. To Umar, for the deep talks to disconnect from the long days at the department. A Arturo, por ser un pilar estos últimos años. To Kostas, for the film nights and random

hangouts that made us through the pandemic. To Konstantin, for the support during the first months of Swedish darkness. To the "EOS Warriors": Emil, Gad, Valentin, Rokas, Jim. To Alexandros and the "bruhs". To Mahdi, for the cofferete Fridays and tough tennis lessons. A Álvaro T por mantener vivo ese "party radar". A Ainoa, por las conversaciones intensas y reveladoras. A Juampi, por ser el mejor comentarista de beer-pong de la historia. A Jaime, por ayudarme a darme cuenta de que era esto lo que realmente quería hacer.

A Fuente, porque no sé si nos uniría "el Destino", o aquél viaje a Berlín en 4º de la ESO, pero desde entonces no has dejado de ser mi mejor amigo. A Álvaro G, porque te quiero mucho tío, aunque me fundas al basket y me levantes por los aires. A Alex, por las risas durante las clases de la carrera, y por los momentos de oro después de ella. A Herradón y Nieto, por las buenas noches madrileñas. A Murillo, por los viajes en metro llenos de historias random. A Fer, el referente durante la carrera, por aguantar sin reproche mis incesables interrogatorios. A los "Q de Quantum B de Blunder", por los mejores momentos en la ETSIT. A los compis del GMR, en especial a Mateo, por marcar mis primeros pasos en el mundo de la investigación. A Diego Scots, por mantenerme conectado a lo que realmente importa, y por ser como un hermano mayor.

A los Vidalines, por seguir estando siempre tan cerca, os quiero un huevo—a Marimar (la TÍA con mayúsculas), a Óscar (el tío guay), a Endika y Jon (los primos Zumosol), a Diego, Miguel, Mario y Lucía (por más noches extendidas en el puerto de Vilaxoán), a los más peques, y a todos los demás Vidales. A mi abuela Matilde. A mi abuela Rosario. A los Alegría, que aunque nos veamos de boda en boda os sigo sintiendo muy cerca y os quiero mucho. A mis padrinos, Zulema y Fernando. Y por supuesto, a mis amigos de la Arenas, porque siempre os sentiré como familia.

A mi hermano, mi referencia en la sombra, la persona que mejor me conoce y por la que antes moriría. Gracias por crecer conmigo, por enseñarme tanto, y por no dejar de estar presente. A mi madre, porque todo es más fácil cuando sé que hay alguien que confía en mí tan incondicionalmente como tú, y porque no has dejado de allanarme el terreno toda mi vida. Gracias por aportarme esa visión práctica y realista de las cosas que tan imprescindible me ha resultado para poder llevar a cabo todos mis proyectos. A mi padre, mi gran referente, el que tanto me ha ayudado a marcar y a valorar este camino extraordinario, mi camino. Gracias por aportarme esa ilusión y sensibilidad por las cosas que tantas alegrías—y no menos valiosas tristezas—me ha permitido experimentar.

Por último, a Laura, porque desde que apareciste en mi vida mi suerte también cambió. Gracias por ayudarme a luchar contra mis dudas y mi negatividad, por escucharme y apoyarme tanto, y por darme energías para afrontar los días con una sonrisa. Te quiero mucho!

Big hug to all of you, and to the hidden contributors I may have forgotten!

Juan

List of Acronyms and Abbreviations

1D	One-Dimensional
2D	Two-Dimensional
3D	Three-Dimensional
3G	The 3rd Generation of Mobile Broadband Communications
4G	The 4th Generation of Mobile Broadband Communications
5G	The 5th Generation of Mobile Broadband Communications
6G	The 6th Generation of Mobile Broadband Communications
ADC	Analog-to-Digital Converter
AoA	Angle-of-Arrival
AoD	Angle-of-Departure
AP	Access Point
ARIS	Amplitude-Reconfigurable Intelligent Surface
AWGN	Additive White Gaussian Noise
BER	Bit Error Rate
BS	Base Station
CDMA	Code-Division Multiple Access
CPU	Central Processing Unit
CSI	Channel State Information
DAC	Digital-to-Analog Converter
DFT	Discrete Fourier Transform
DL	Downlink

ELAA	Extremely Large Aperture Array
FDMA	Frequency-Division Multiple Access
FRIS	Fully-Reconfigurable Intelligent Surface
GCD	Greatest Common Divisor
IID	Independent and Identically Distributed
IRS	Intelligent Reflective Surface
ISI	Inter-Symbol Interference
LHS	Left-Hand Side
LIS	Large Intelligent Surface
LMMSE	LinearMMSE
LoS	Line-of-Sight
LPU	Local Processing Unit
LS	Least Squares
MF	Matched-Filter
MIMO	Multiple-Input-Multiple-Output
MIMO-BC	MIMO Broadcast Channel
MIMO-MAC	MIMO Multiple Access Channel
ML	Maximum-Likelihood
MMSE	Minimum MSE
mmWave	Millimeter-Wave
MRC	Maximum-Ratio Combining
MRT	Maximum-Ratio Transmission
MSE	Mean-Square Error
MU-MIMO	Multi-User MIMO
NLoS	Non-LoS
OFDM	Orthogonal Frequency-Division Multiplexing
OFDMA	Orthogonal FDMA
PDF	Probability Density Function
PMF	Probability Mass Function
RF	Radio-Frequency
RHS	Right-Hand Side
RIS	Reconfigurable Intelligent Surface

RS	Reconfigurable Surface
Rx	Receiver
SDMA	Space-Division Multiple Access
SDR	Software-Defined Radio
SINR	Signal-to-Interference-plus-Noise Ratio
SIR	Signal-to-Interference Ratio
SISO	Single-Input-Single-Output
SNR	Signal-to-Noise Ratio
SVD	Singular Value Decomposition
TDD	Time-Division Duplex
TDMA	Time-Division Multiple Access
THz	TeraHertz
Tx	Transmitter
UE	User Equipment
UL	Uplink
ULA	Uniform Linear Array
W	Watts
XL-MIMO	Extra-Large Scale MIMO
ZF	Zero-Forzing
ZMCSCG	Zero-Mean Circularly-Symmetric Complex Gaussian

Notation

The mathematical notation which will be employed throughout the rest of this thesis is as follows:

- Lowercase, bold lowercase and bold uppercase letters stand for scalars, column vectors, and matrices, respectively.
- The operations $(\cdot)^{\mathrm{T}}$, $(\cdot)^*$ and $(\cdot)^{\mathrm{H}}$ denote transpose, conjugate, and conjugate transpose, respectively.
- The operator $\mathrm{vec}(\cdot)$ transforms a matrix into a vector by concatenating its columns.
- $\mathbb{E}\{\cdot\}$ denotes the expectation operator.
- $\mathbf{I}_i$ corresponds to the identity matrix of size i, $\mathbf{1}_{i\times j}$ denotes the $i \times j$ all-ones matrix, and $\mathbf{0}_{i\times j}$ denotes the $i \times j$ all-zeros matrix. In cases where the dimensions can be obtained by the context, the sub-indices may be omitted.
- $\Re\{\cdot\}$ and $\Im\{\cdot\}$ denote real and imaginary part, respectively.
- The symbol $\jmath$ denotes the imaginary unit, $\jmath = \sqrt{-1}$.
- The operation $\mathrm{diag}(\cdot)$ applied to a set of scalars/blocks outputs a matrix with said scalars/blocks along the main diagonal.
- $[\boldsymbol{A}]_{i:j,\ell:k}$ denotes a matrix formed by rows i to j and columns ℓ to k of some matrix $\boldsymbol{A}$. Absence of one such index indicates that the included rows start/end corresponds to the first/last row/column of $\boldsymbol{A}$, respectively (i.e., as in Python notation).

Contents

Part I

Overview of Research Field

Chapter 1

Introduction

The idea of exploiting the spatial domain to increase the throughput of wireless digital communication links was originally proposed in the 1990s [1], [2]. At that time, cellular systems had access to advanced techniques for multiplexing users in the frequency domain and in the time domain—namely FDMA and TDMA, respectively [3]—so an interesting challenge was to find a new dimension that would allow using the same time-frequency resource for simultaneous streams of symbols. CDMA offered a way to multiplex users in the code domain, which even made it to the 3G standard due to its suitable characteristics for the cellular propagation environment. However, in order to multiplex users in the code domain, CDMA required to spread the spectrum of the signals to be transmitted, thus sacrificing spectral efficiency per user and leading to the same capacity bounds as those for FDMA or TDMA [4]. Instead, MIMO—combined with a suitable FDMA technique such as OFDMA—allowed to exploit the degrees of freedom available in the spatial domain to transmit simultaneous streams of data in the same time-frequency resource. This posed an important advancement towards extending the throughput of wireless links, which was already exploited in 4G, as well as in several WiFi standards.

This chapter intends to give a high-level introduction to the research area where the thesis stands. The aim is to describe the main technologies being considered in this work, and to provide a brief summary of the state-of-the-art.

1.1 From MIMO to Massive MIMO

Let us think of a wireless communications scenario where a Tx is sending information to an Rx through a wireless link. The idea behind MIMO is to equip both the Tx and the Rx with a number of antennas greater than 1. This way, if the antenna spacing is large enough and/or there is a sufficiently rich multipath environment, the information sent by the Tx may leave at different AoD and arrive at the Rx antennas from different AoA—possibly statistically independent too. As a result, MIMO offers a number of advantages which can be divided into three categories: array gain, diversity gain, and multiplexing gain [5], [6]. These three categories may be briefly explained as follows:

- Array gain, also denoted beamforming gain, corresponds to the SNR gain that results from exploiting the increased directivity of arrays with more than one antenna, which translates into a logarithmic gain in capacity.
- Diversity gain corresponds to the exponential decrease in the BER associated to transmitting the same data over statistically independent paths.
- Multiplexing gain corresponds to the linear capacity gain associated to the simultaneous transmission of several streams of data through different spatial modes.

In this thesis we are mostly interested in the capacity metric since we believe it is a more fundamental metric of digital communication performance than BER, which can be made arbitrarily small by means of channel coding when working within the capacity boundary [7]. Thus, we mostly disregard the diversity gain, and we put special emphasis on the multiplexing gain, which we consider the major advancement of MIMO due to its unprecedented capacity improvement [8].

Initial results on MIMO largely focused on the communication between a single multi-antenna Tx and a single multi-antenna Rx [2], also known as point-to-point MIMO [5]. Thus, the Tx would send an arbitrary combination of symbols through each antenna, and the Rx would combine as desired the symbols received at its antennas. However, in mobile broadband communication scenarios, it becomes especially interesting to consider the bidirectional communication between a BS and a set of UEs. These UEs are, in general, not supposed to collaborate with each other to perform joint transmission or decoding. Thus, another fashion of MIMO gained popularity, namely MU-MIMO [1], [9], [10]. In the DL, referred to as MIMO-BC [5], [10], MU-MIMO typically considers a multi-antenna BS transmitting precoded symbols to a set of single- or multi-antenna UEs. As for the UL, referred to as MIMO-MAC [5]—also known as SDMA [1]—all the UEs transmit their symbols simultaneously, and the multi-antenna BS is the one in charge of performing equalization to remove

interference and extract the information sent by each UE. The comparison between point-to-point MIMO and MU-MIMO is illustrated in Fig. 1.1. The system models considered in all the papers included in this thesis fall within the broad framework of MU-MIMO.

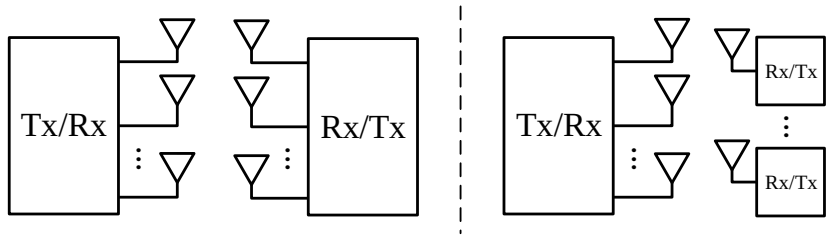

Figure 1.1: Point-to-point MIMO (left) v.s. MU-MIMO (right).

In the 2010s, motivated by the seminal paper [11], a new trend in mobile broadband communication systems emerged: increasing drastically the number of antennas at the BS. In [11], it is shown that, as the number of BS antennas grows large in a MU-MIMO scenario, noise and fading vanish due to averaging effects, whereas pilot contamination is the only factor limiting capacity. These results led to the development of massive MIMO, which corresponds to a special case of MU-MIMO where the number of BS antennas is considerably larger than the number of UEs it intends to serve simultaneously—initial research on MU-MIMO considered it enough to have a number of BS antennas on the order of the number of UEs being served. Massive MIMO allows for unprecedented spatial resolution so that a large number of UEs can be spatially-multiplexed at reduced cost [12]–[14]. More specifically, the excess in BS antennas offers extra degrees of freedom which can compensate for the negative effects caused by e.g., unfavorable propagation, hardware impairments from cheap components, inaccurate CSI estimation, simple linear precoding/equalization, etc. Hence, massive MIMO offers a scalable solution for implementing BSs achieving high spectral efficiency.

1.2 Beyond Massive MIMO

With commercial deployments already in place, and after becoming one of the core technologies in 5G [15], it feels natural to say that massive MIMO has reached maturity. Thus, the research community is already pushing towards more disruptive solutions—many of them based upon massive MIMO—with the aim of facilitating the emergence of 6G. We will now present a number of these solutions which have been directly or indirectly studied within this thesis.

1.2.1 Large Intelligent Surfaces

A natural evolution of massive MIMO is to keep increasing the number antennas at the BS so that more UEs can be effectively multiplexed in space. In the framework of massive MIMO, a typical consideration is to have UEs in the so called far-field, which means that the size of the BS antenna array is relatively small as compared to the distance towards the UEs. Furthermore, in massive MIMO scenarios, it is typically assumed that there exists rich multipath propagation, which favors spatial multiplexing when operating in the far-field, and the presence of strong LoS paths is often disregarded. However, if we keep adding antennas, the size of the BS will also increase, which should then be taken into consideration, and the probability of having strong LoS propagation increases—at least within a subset of the BS antennas. These effects are even more noticeable if we go to higher frequency bands, such as the mmWave or THz bands, due to the drop in transmission ranges, as well as the reduced reflectivity at these bands [16]–[18].

LIS is the most clear evolution of massive MIMO since it mitigates—and even takes advantage of—the previous issues by considering the use of BSs whose antennas are densely deployed throughout large surfaces. This technology was initially proposed in [19], which demonstrates the potential (sum-rate) capacity gains that can be achieved when using large surfaces of electromagnetically active material in a pure LoS scenario. Simultaneous to [19], [20] shows that LIS has also great potential in the task of UE positioning, which we do not address in this thesis. [19] uses a continuous model of LIS where any point of a continuous surface can transmit and receive as desired. However, since there is no evidence that this kind of technology can be implemented in the near future, we see this model as a purely theoretical concept useful for understanding the limits of LIS. Instead, we believe that a real LIS will likely be implemented using dense antenna arrays deployed throughout a large surface, leading to the sampled version of LIS. In fact, [19] shows that, if sampling is dense enough, the continuous and sampled versions of LIS are essentially equivalent due to the spatially-bandlimited nature of the resulting channels. This equivalence has been further strengthened in [21], which shows that even in the NLoS scenario the propagating electromagnetics waves are also spatially-bandlimited. On the other hand, practical implementations of LIS also consider dividing these surfaces into panels (or LIS units) with a lower number of antennas, such that some of these panels can be turned-off to save energy when they have no users nearby [22]–[24].

The terminology in the research community is a bit inconsistent, and sometimes the term LIS is used for referring to surfaces used for reflecting signals instead of for directly transmitting or receiving them—e.g., [25]–[27]. On the other hand, some literature has also referred to LIS with the term holographic MIMO—e.g., [21], [28], [29]. However, the term holographic MIMO typically

excludes the sampled versions of LIS, which can also be identified with the term XL-MIMO [30]. In this work we use the term LIS for those surfaces (sampled or not) that can be directly used as BSs.

1.2.2 Cell-free Massive MIMO

Another interesting evolution of massive MIMO is embodied in cell-free massive MIMO. As initially proposed in [31], cell-free massive MIMO eliminates the need of cells by distributing a large number of coherently coordinated APs throughout large geographical areas. These APs can be seen as distributed BS antennas which coherently serve a large number of UEs within a single time-frequency resource. The main benefit with respect to massive MIMO is that, by not having the BS antennas co-located, the channels between different antennas and UEs have less dependency on each other, leading to improved diversity and multiplexing gains even in the absence of rich multipath propagation.

There is a number of technologies falling within the same umbrella as cell-free massive MIMO. These include coordinated multi-point [32], distributed MIMO [33], network MIMO [34], etc. In [29], the authors employ the term ELAA to refer to this broad umbrella. However, in this thesis we may loosely employ the term cell-free massive MIMO to refer to any of the technologies falling within this framework, as long as the total number of APs is large with respect to the number of UEs.

1.2.3 Reconfigurable Intelligent Surfaces

RIS [35]–[37] is a novel technology with potential to play a big role in the upcoming 6G systems [38], [39]. An RIS consists of a large number of reconfigurable elements deployed throughout a surface. These reconfigurable elements interact with the incoming waves in a controlled manner such that the waves arriving at the whole RIS from a given direction can be reflected towards some beneficial direction, e.g., towards the BS or the UEs. This technology is fundamentally different from massive MIMO in the sense that it cannot be used as a BS technology for serving UEs by itself. Instead, RIS can be used as a support for improving the channel conditions in a communication link between a BS and one or more UEs. However, RIS can also be employed as an energy-efficient transmitter by embedding information in the reflected waves [37], [40], [41]. The main benefit of RIS is that, since it can be constructed through passive metasurfaces, it offers a reduced-cost, low-power, and thus scalable solution to improve the comunication links.

As previously discussed, initial work on RIS also referred to these surfaces with the term LIS—e.g., [25], [27], [38]—which we reserve for surfaces that can be directly used as BSs. Other terms in the literature for these types of surfaces include IRS [39], passive holographic surfaces [42], (software-controlled)

metasurfaces [43], etc. Furthermore, there is still open discussion on how these surfaces should be implemented and what their capabilities should be—e.g., if they should include amplification or not [44]. In this thesis, we employ the broad term RS to refer to any surface used for reflecting waves in a controlled manner, while RIS is used to refer to RSs whose elements are essentially passive and can thus be modeled as phase-shifts.

1.3 Goals and Motivation

The motivation for this thesis can be divided into two categories: (i) the need for decentralized architectures, (ii) the multiplexing capabilities of RS. These two categories give rise to two of the forthcoming chapters, which describe the contributions of this thesis within these two areas. We will next summarize the motivation of this thesis within each of the two mentioned categories.

1.3.1 The Need for Decentralized Processing

Increasing the number of antennas at the BSs has shown to be beneficial due to the improved spatial multiplexing performance even with subotimal hardware and software, as explained when we introduced the concept of massive MIMO. However, practical implementations of massive MIMO still face one major challenge, namely that the interconnection bandwidth and complexity required to process the information coming from so many antennas at one point become excessively large since it scales with the number of BS antennas. Initial prototypes of massive MIMO, such as [45], [46], already noticed these issues, which were tackled by pragmatic solutions sacrificing performance. On the other hand, these issues can become especially concerning in future technologies as LIS or cell-free massive MIMO where, not only the number of antennas is huge—in LIS it can even be orders of magnitude greater than massive MIMO—but the distance between antennas can also be considerably large. Thus, to be able to exploit the full benefits of these technologies, we may need to depart from the classical centralized architectures, where a CPU is in charge of gathering and processing the information received from all antennas. Instead, we can think of decentralized architectures where part of the processing is performed locally at the antennas/panels/APs (or nearby), so that the amount of information that has to reach the CPU—as well as the corresponding processing complexity—can get considerably reduced.

Before the beginning of this PhD, some early work on decentralized architectures was already available [47]–[49] in the context of massive MIMO. Moreover, throughout the course of this PhD, decentralized architectures and algorithms have further gained popularity within the broad research area of large multi-antenna systems, as seen from [50]–[57]. One of the goals of this

thesis is to contribute to the development of this field by proposing decentralized solutions especially tailored for technologies beyond massive MIMO, e.g., making use of the structure of LIS panels for reducing the large delays associated to decentralized solutions like [49], [54].

Decentralized solutions as [49], [50], [53], [54] have been successful at reducing the interconnection bandwidth to a CPU, as well as the required processing complexity at said CPU. The result is that the information that has to reach and be processed at a CPU can be made to scale with the number of UEs instead of with the number of BSs antennas. However, in order to achieve these reductions, the complexity of the decentralized processing applied in the antennas/panels has to scale with the number of UEs, which in some cases may also be excessive. For example, cell-free massive MIMO APs and LIS panels should be desirably cost- and energy efficient to favor scalability, so the processing capabilities at these systems may be limited. Thus, an important goal of this thesis is to study the interplay between the decentralized processing complexity and the level of decentralization, which has not been considered in previous literature.

1.3.2 The Multiplexing Capabilities of RS

Throughout the course of this PhD, RIS has gained popularity and massive amount of research has studied the benefits of using this technology for improving wireless links between a BS and one or more UEs [35], [37], [58]–[60]. Most of the available work on RIS focuses on the exploitation of its impressive beamforming gains, which can be made to scale with the square of the number of RIS elements in general far-field scenarios [37], [59]. However, as pointed out in [61], the available beamforming gains in realistic RIS scenarios are limited by the law of conservation of energy. Moreover, as happens in conventional MIMO, beamforming gains only translate to logaritmic capacity gains. Thus, we believe that the potential of RS technology largely lies in the possibility to improve the multiplexing capabilities of current multi-antenna systems. Only limited work has been done in this regard, e.g., indirectly improving multiplexing gain by improving user rates through time consuming alternating optimization schemes [60], [62], or directly improving multiplexing gain through channel rank improvement as in [63] for a specific single UE scenario. One goal of this thesis is to explore RS technologies with the aim of achieving improved spatial multiplexing in general MU-MIMO scenarios. Furthermore, to be able to exploit the benefits of RIS, the available literature typically relies on full-CSI knowledge, while this task is extremely challenging in the context of RIS [42], [61]. A minor part of this thesis will address the problem of channel estimation for RS.

1.4 Thesis Outline

The rest of the thesis is organized as follows. Chapter 2 provides some preliminary knowledge and assumptions that may be helpful for understanding the results presented in this thesis. Chapter 3 and 4 present an overview of the two main research topics that are studied in this thesis, together with a brief description of our main contributions in these areas. Chapter 5 concludes Part I of the thesis by summarizing the main findings, and by proposing interesting directions for extending this work. Part II of thesis includes a reformatted version of the publications listed in the Preface.

Chapter 2

Useful Knowledge and Considerations

During my PhD studies I have been teaching assistant for the courses "Multiple Antenna Systems" and "Digital Communications, Advanced Course". Teaching these courses—which I also took myself before starting my PhD studies—helped me acquire deep understanding of the digital communication techniques and related problems, especially in the context of multi-antenna communications, which turned out to be very useful in the development of this thesis. I also acquired useful knowledge by taking specialized courses in e.g., probability theory, matrix theory, information theory, etc, as well as by discussing with my supervisor—every time I went to Fredrik's office I came out smarter. In this chapter we summarize some important results in these fields, which may serve as a basic knowledge base for understanding the main findings of this thesis.

2.1 General considerations

The work presented in this thesis considers generic mobile broadband communication scenarios within the broad framework of MU-MIMO. However, most of the included results deal with the challenges and opportunities arising in systems with a large number of BS antennas—i.e., massive MIMO and beyond. Motivated by the available massive MIMO literature [64], [65], the operation of the systems envisioned in this thesis is characterized by

(i) TDD operation: The UL and DL transmissions are done over different time slots, but within the same frequency slots.

(ii) Channel reciprocity: The UL-DL CSI is reciprocal, or, at least, the DL can be obtained from the UL channel through calibration—e.g., [66].

(iii) CSI aquisition through UL pilots: The UEs send orthogonal pilots to the BS, which then performs CSI estimation based on these pilots—note that assumption (ii) is hereby required.

(iv) Perfect-CSI estimates: In this thesis, the CSI estimates are typically assumed to be error-free to simplify the analysis.

(v) Block-fading: The channel remains constant throughout a number of symbol transmissions—i.e., the channel coherence time is greater that the symbol rate.

(vi) Non-interfering narrowband symbols: The underlying modulation allows to consider orthogonal narrowband symbols with no ISI—e.g., OFDM with large enough cyclic-prefix.

(vii) Fully-digital linear equalization and precoding: In the UL the BS spatially filters the symbols sent by the UE through digital linear equalization based on the UL CSI. In the DL the BS sends linearly (and digitally) precoded symbols based on the reciprocal channel from the UL CSI.

(viii) Single-antenna UEs: The UEs are assumed to have a single antenna so that they can receive at maximum one spatial stream.

Most of these assumptions are a result of the common functioning of MU-MIMO systems [5], [6]. On the other hand, the extension of this work to multi-antenna UEs is generally trivial—e.g., the UE antennas can be used for improved array gain without remarkable effect on the results in this work, or several UE antennas could be identified with several single-antenna UEs for considering transmission of several spatial streams to a single UE. Most of the results presented are also applicable to the imperfect CSI scenario, as discussed in part of this work. Finally, as pointed out in [12], linear equalization achieves close to optimal performance when the number of BS antennas is considerably larger than the number of UEs it serves at a given time-frequency resource.

The reader may also notice a general preference for the consideration of UL scenarios, i.e., where the UEs are transmitting simultaneously to the BS. This choice is mainly due to authors' taste, while the extension to DL scenarios is typically straightforward under some considerations—e.g., channel reciprocity and per-line (per-UE) capacity—as discussed in part of the presented work.

2.2 The MU-MIMO framework

As previously mentioned, the results presented in this thesis are based on generalizations of the MU-MIMO framework. Thus, we will now present a theoretical description of this framework, as well as some important results that may be

useful for understanding the rest of the thesis. Much of what is presented next can be found in common MIMO text books—e.g., [5], [6]—while we merely make a selection of the explanations that are important for understanding this thesis. Thus, some results may be presented without citation to avoid excessive repetition, in which cases the reader can refer to [5], [6] for further clarification.

In the UL, let us assume that K UEs are simultaneously transmitting to a BS with M antennas, where $M \geq K$. Due to the general consideration (vi), we can focus on a single narrowband subcarrier and time-slot since, in case we have an OFDM-like modulation with more subcarriers, these can be processed independently. The received narrowband symbol associated to one subcarrier can then be described in complex baseband by

$$\boldsymbol{y} = \boldsymbol{H}\boldsymbol{s} + \boldsymbol{n}, \tag{2.1}$$

where $\boldsymbol{H}$ is the $M \times K$ channel matrix, $\boldsymbol{s}$ is a $K \times 1$ vector containing the complex baseband symbols transmitted by the UEs, and $\boldsymbol{n}$ is an $M \times 1$ vector modelling the noise at the receiver. The standard receiver noise model assumes $\boldsymbol{n}$ to be IID ZMCSCG, i.e., $\boldsymbol{n} \sim \mathcal{CN}(\boldsymbol{0}, N_0\mathbf{I}_M)$, where N_0 corresponds to the noise variance—which is further related to the underlying power spectral density. Note that equation (2.1) describes the received signal per channel use, so for each time slot and each frequency subcarrier we have an equation like (2.1). The scenario under consideration is illustrated in Fig. 2.1. In the DL a similar equation as (2.1) arises, where only the dimensions have to be adapted—$\boldsymbol{H}$ would be substituted by its transpose $\boldsymbol{H}^{\mathrm{T}}$ in case of perfect channel reciprocity.

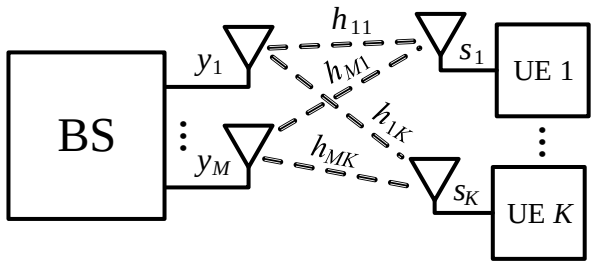

Figure 2.1: The UL MU-MIMO framework.

2.2.1 Capacity

Given a transmitted random vector $\boldsymbol{s}$, and a received random vector $\boldsymbol{y}$, the capacity is defined as [7]

$$C = \max_{p(\boldsymbol{s})} \mathcal{I}(\boldsymbol{y}; \boldsymbol{s}), \tag{2.2}$$

where $p(\boldsymbol{s})$ is the PDF of $\boldsymbol{s}$, and $\mathcal{I}(\boldsymbol{y}; \boldsymbol{s})$ corresponds to the mutual information between $\boldsymbol{y}$ and $\boldsymbol{s}$ given by

$$\mathcal{I}(\boldsymbol{y}; \boldsymbol{s}) = \mathfrak{h}(\boldsymbol{y}) - \mathfrak{h}(\boldsymbol{y}|\boldsymbol{s}), \tag{2.3}$$

where $\mathfrak{h}(\cdot)$ is the (differential)[1] entropy operator, which corresponds to a measure of the uncertainty of a random variable [7]. In his celebrated paper [67], Shannon proved that C, as defined in (2.2), gives the limit on the amount of information embedded in $\boldsymbol{s}$ that can be decoded from $\boldsymbol{y}$ with arbitrarily small error when considering an asymptotically large number of channel uses. On the other hand, for an arbitrary $p(\boldsymbol{s})$, $\mathcal{I}(\boldsymbol{y}; \boldsymbol{s})$, as defined in (2.3), gives the achievable information rate for that input distribution—i.e., the amount of information from the random variable $\boldsymbol{s}$ that can be obtained from $\boldsymbol{y}$ with arbitrarily small error when considering an asymptotically large number of realizations of $\boldsymbol{s}$.

If we now consider the MIMO input-output relation defined in (2.1)—where we assume perfect knowledge of the current channel realization $\boldsymbol{H}$—we can obtain the channel capacity by the famous *log-det* formula [68]

$$C_{\text{MIMO}} = \max_{\boldsymbol{R_{ss}}} \log\det\left(\mathbf{I}_M + \frac{1}{N_0}\boldsymbol{H}\boldsymbol{R_{ss}}\boldsymbol{H}^{\text{H}}\right), \tag{2.4}$$

which is given by substituting the optimal input distribution $\boldsymbol{s} \sim \mathcal{CN}(\mathbf{0}, \boldsymbol{R_{ss}})$ in (2.2). $\boldsymbol{R_{ss}}$ is then optimized by combining diagonalization of $\boldsymbol{H}$ with the *water-filling* method [68]. However, in UL MU-MIMO we usually have the restriction that the UEs are not able to cooperate, so $\boldsymbol{R_{ss}}$ is restricted to be diagonal, where its diagonal elements correspond to the power transmitted by each UE. Assuming further that all UEs transmit with full (equal) power—which is the best thing to do if the UEs have no knowledge about the channel to other UEs—the UL MU-MIMO capacity results in

$$C_{\text{UL}} = \log\det\left(\mathbf{I}_M + \frac{E_s}{N_0}\boldsymbol{H}\boldsymbol{H}^{\text{H}}\right), \tag{2.5}$$

which is achieved for $\boldsymbol{s} \sim \mathcal{CN}(\mathbf{0}, E_s\mathbf{I}_K)$, with E_s corresponding to the power

[1] The initial results from Shannon [67] considered random variables of discrete nature, giving rise to the concept of entropy. Differential entropy corresponds to generalization of said concept for continuous random variables.

transmitted by every UE. Note that, in real systems, embedding information in $\boldsymbol{s}$ is typically done by using predefined symbol constellations $\boldsymbol{s} \in \mathcal{S}^K$,[2] with $\mathcal{S}$ having finite cardinality—e.g., M_{Q}-QAM with $|\mathcal{S}| = M_{\mathrm{Q}}$. In these cases, $\boldsymbol{s}$ would be modeled as a discrete random variable, thus incurring some loss with respect to (2.5). However, the capacity expression (2.5) will be extremely useful for evaluating the performance of the methods proposed in this thesis since it defines the limits of the information rates that can be transmitted in the UL MU-MIMO framework considered.

Another information theory concept which will be useful as a performance metric in this thesis is the achievable rate for a mismatched receiver. The idea is that, in some real scenarios, the received signal may not be perfectly modeled by a simple input-output relation as (2.1). For example, the received vector $\boldsymbol{y}$ may have a complicated non-linear relation with the transmitted vector $\boldsymbol{s}$ due to, e.g., quantization distortion, amplifier non-linearities, etc. In these cases, the receiver may assume a model for the input-output relation which does not correspond to its true distribution—i.e., it may assume that the conditional PDF of $\boldsymbol{y}$ given $\boldsymbol{s}$ corresponds to $q(\boldsymbol{y}|\boldsymbol{s})$ instead of the true $p(\boldsymbol{y}|\boldsymbol{s})$. In this case, we have an expression that, not only lower bounds the capacity for the true $p(\boldsymbol{y}|\boldsymbol{s})$, but also the achievable rate for a decoder considering $q(\boldsymbol{y}|\boldsymbol{s})$ as decoding rule instead of the true $p(\boldsymbol{y}|\boldsymbol{s})$ [69], [70]. This expression is given by [71]

$$\mathrm{I}_{\mathrm{LB}} \triangleq -\mathbb{E}_{\boldsymbol{y}} \log(q(\boldsymbol{y})) + \mathbb{E}_{\boldsymbol{y},\boldsymbol{s}} \log(q(\boldsymbol{y}|\boldsymbol{s})), \tag{2.6}$$

where the expectation operators consider the true distributions of $\boldsymbol{s}$ and $\boldsymbol{y}$, and where $q(\boldsymbol{y})$ is given by

$$q(\boldsymbol{y}) = \int q(\boldsymbol{y}|\boldsymbol{s}) p(\boldsymbol{s}) d\boldsymbol{s}. \tag{2.7}$$

2.2.2 Maximum-Likelihood Decoding

The optimal way to extract the transmitted vector $\boldsymbol{s}$ from a noisy observation $\boldsymbol{y}$ is to apply the so called ML decoder—assuming no channel coding or prior information on the transmitted data.[3] This decoder corresponds to the decoding rule

$$\hat{\boldsymbol{s}}_{\mathrm{ML}} = \arg \max_{\boldsymbol{s} \in \mathcal{S}^K} p(\boldsymbol{y}|\boldsymbol{s}).^4 \tag{2.8}$$

Considering the UL MU-MIMO scenario with perfect knowledge of $\boldsymbol{H}$, the relation described in (2.1) leads to

$$\hat{\boldsymbol{s}}_{\mathrm{ML}} = \arg \min_{\boldsymbol{s} \in \mathcal{S}^K} \|\boldsymbol{y} - \boldsymbol{H}\boldsymbol{s}\|^2. \tag{2.9}$$

[2] For notation simplicity, we assume UEs using identical constellations.

[3] In order to achieve capacity (2.2), ML decoding should be jointly performed over an asymptotically large set of symbol transmissions.

[4] In case of a mismatched decoding rule $q(\boldsymbol{y}|\boldsymbol{s})$, we would substitute it for $p(\boldsymbol{y}|\boldsymbol{s})$.

If we restrict ourselves to finite constellations for the transmitted symbols—i.e., $|\mathcal{S}| = M_{\mathrm{Q}}$ for finite M_{Q}—solving (2.9) would essentially require an exhaustive search over $(M_{\mathrm{Q}})^K$ possible transmitted symbol vectors, where in each evaluation the required computations scale with the number of BS antennas M. This becomes extremely restrictive if we want to spatially-multiplex several UEs with high data-rates by using a BS with a large number of antennas. Thus, more efficient schemes should be explored to deal with these complexity issues, as we discuss next. One common sub-optimal approach is to generate a continuous estimate $\hat{\boldsymbol{s}}$ of $\boldsymbol{s}$, and then perform individual detection upon each entry of the estimated $\hat{\boldsymbol{s}}$, which leads to an exponential reduction—from $(M_{\mathrm{Q}})^K$ to KM_{Q}, or even better if further assumptions are taken. We will next look at some methods for obtaining such estimates, as well as for reducing the amount of computations.

2.2.3 Linear Equalization

In the UL MU-MIMO framework, linear equalization generates a post-processed vector which corresponds to a linear combination of the received vector. Considering (2.1), the post-processed vector resulting from an arbitrary linear equalization process can be expressed as

$$\boldsymbol{z} = \boldsymbol{F}\boldsymbol{y}, \tag{2.10}$$

where $\boldsymbol{F}$ is the $T \times M$ matrix associated to the linear equalizer. Assuming $\boldsymbol{F}$ is already defined—which is usually the most tricky part of the process—this type of processing is relatively simple since it corresponds to a matrix multiplication, which can be implemented by a fixed number of multiplications and additions determined by the size of the vectors.[5]

We differentiate two main reasons for employing linear equalization in UL MU-MIMO:

1. To directly generate an estimate of the aggregate vector transmitted by the UEs—e.g., a ZF estimate.[6] This can also be used in the DL, where $\boldsymbol{F}$ would correspond instead to the linear precoder matrix applied at the BS, which may require further normalization.

2. To merely reduce the dimension of the received data—hence simplifying upcoming detection—e.g., by generating sufficient statistics with lower dimensions than the original received vector.

[5] For received vectors of large dimension—e.g., in massive MIMO and beyond—the complexity of linear equalization will grow linearly with the size of the matrices being multiplied.

[6] Considering discrete constellations, symbol estimation does not preclude a detection step where the estimated symbols are matched to symbols from the constellation.

For the cases where the linear equalizer is used to generate an estimate of the transmitted vector we have the extra restriction $T = K$, so that the dimensions allow to have the estimate $\hat{\boldsymbol{s}} = \boldsymbol{z}$. Otherwise, we can consider the general restriction $T < M$ so as to achieve at least some dimension reduction. If symbol detection is performed upon the full post-processed vector $\boldsymbol{z}$ from (2.10), and assuming full-rank $\boldsymbol{F}$, the capacity in (2.5) degenerates to

$$C_{\mathrm{UL,eq}} = \log\det\left(\mathbf{I}_M + \frac{E_s}{N_0}(\boldsymbol{F}\boldsymbol{F}^{\mathrm{H}})^{-1}\boldsymbol{F}\boldsymbol{H}\boldsymbol{H}^{\mathrm{H}}\boldsymbol{F}^{\mathrm{H}}\right). \tag{2.11}$$

However, when linear equalization is used for symbol estimation—given by $\hat{\boldsymbol{s}} = \boldsymbol{z}$—each entry of $\boldsymbol{z}$ is often treated independently thereafter for simplifying subsequent detection, leading to some loss in capacity per line[7]—in DL this restriction is enforced by assuming non-cooperating UEs.

In this thesis, we have a special interest in linear equalizers $\boldsymbol{F}$ such that (2.11) leads to same capacity value as (2.5), which correspond to what we call *information-lossless linear transformations*. In other words, an information-lossless linear transformation is a linear equalizer that gives a post-processed vector constituting a sufficient statistic for $\boldsymbol{s}$ [7]. Such transformations would thus achieve the capacity value from (2.5) when ML decoding is jointly applied to its outputs throughout an asymptotically large number of symbol transmissions with optimum input distribution. Any information-lossless linear transformation can be expressed as

$$\boldsymbol{F} = \left[\widetilde{\boldsymbol{F}}_{\mathrm{L}} \;\; \widetilde{\boldsymbol{F}}_{\mathrm{R}}\right]\boldsymbol{U}^{\mathrm{H}}, \tag{2.12}$$

where $\boldsymbol{U}$ corresponds to the left unitary matrix from the SVD of $\boldsymbol{H}$, $\widetilde{\boldsymbol{F}}_{\mathrm{L}}$ is a $T \times K$ full-rank matrix, and $\widetilde{\boldsymbol{F}}_{\mathrm{R}}$ is an unrestricted $T \times (M - K)$ matrix. The reason is that the signal space of $\boldsymbol{s}$ in $\boldsymbol{y}$ is contained within the first K left singular vectors of $\boldsymbol{H}$—i.e., associated to (potentially-) non-zero singular values.

Next, we present the most common linear equalizers for MU-MIMO, which are also information-lossless linear transformations, but whose main practicality lies in using them as direct estimators for the transmitted symbol vector $\boldsymbol{s}$.

Maximum Ratio Combining/Matched Filter

MRC, also called (spatially-) MF since it is the spatial equivalent of the common MF [72], is given by

$$\boldsymbol{F}_{\mathrm{MF}} = \boldsymbol{H}^{\mathrm{H}}. \tag{2.13}$$

[7]For per-line detection upon symbol estimates $\hat{\boldsymbol{s}} = \boldsymbol{z}$, the capacity of the ith UE is given by the common $\log(1 + \mathrm{SINR}_i)$, with the post-processed SINR from the ith entry of $\boldsymbol{z}$.

Considering symbol estimation, this linear equalization gives a post-processed vector $\boldsymbol{z}$ with maximum output SNR per line—i.e., per entry of $\boldsymbol{z}$. However, the entries of $\boldsymbol{z}$—identified with symbol estimates by $\hat{\boldsymbol{s}} = \boldsymbol{z}$ if we ignore entry scaling—may have interference from other UEs. Thus, this linear equalization is useful for symbol estimation mainly when $\boldsymbol{H}$ and N_0 lead to a noise-limited scenario—i.e., in low SNR and/or highly orthogonal channels.

Zero-Forzing

ZF estimation is typically performed by selecting the equalizer

$$\boldsymbol{F}_{\mathrm{ZF}} = (\boldsymbol{H}^{\mathrm{H}}\boldsymbol{H})^{-1}\boldsymbol{H}^{\mathrm{H}}, \tag{2.14}$$

which corresponds to the left pseudo-inverse of $\boldsymbol{H}$ with minimum power.[8] Furthermore, (2.14) can also be identified with the LS estimator, which gives the estimate $\hat{\boldsymbol{s}} = \boldsymbol{z}$ minimizing the norm $\|\boldsymbol{y} - \boldsymbol{H}\hat{\boldsymbol{s}}\|$—note that $\boldsymbol{s}$ is here unconstrained, unlike in the ML-decoding approach from (2.9). The resulting estimate achieves perfect inter-UE interference at all its lines. However, it does so by enhancing noise—i.e., leading to lower post-processed SNR per line than MF—and by generating (potentially) correlated noise entries for different UEs. Thus, ZF estimation is suitable for settings which are interference-limited—i.e., high-SNR regime and/or highly non-orthogonal channels.

Minimum Mean Square Error

The MSE, given by $\mathbb{E}\{\|\boldsymbol{s} - \hat{\boldsymbol{s}}\|^2\}$, corresponds to the most standard way to measure estimation error—-since ancient Greece. Thus, MMSE estimation is usually considered the optimum estimation method since it leads to the smallest MSE possible. In general settings, the MMSE estimator may result in a non-linear transformation—if it can even be found in closed-form. However, for the linear model described by (2.1), and assuming Gaussian input distribution, the MMSE estimator is also linear—thus coinciding with the LMMSE estimator—and can be obtained by selecting the equalizer as

$$\boldsymbol{F}_{\mathrm{MMSE}} = \left(\boldsymbol{H}^{\mathrm{H}}\boldsymbol{H} + \frac{N_0}{E_s}\mathbf{I}_K\right)^{-1}\boldsymbol{H}^{\mathrm{H}}. \tag{2.15}$$

From the previous expression, we can note that the MMSE equalizer approximates the ZF equalizer in the high-SNR regime ($E_s \gg N_0$), and the MF in the low-SNR regime ($E_s \ll N_0$). The MMSE estimator is optimum for symbol estimation, since it achieves the best trade-off between interference and noise

[8] Other pseudo-inverses than (2.14) may be considered for interference cancellation, but they lose practicality due to greater noise enhancement.

cancellation—i.e., optimum post-processed SINR per line. However, we may still have some loss with respect to (2.5) when performing individual symbol detection upon the estimated symbols at each UE, since, in general settings, there would still be leftover interference and/or noise correlation between estimated symbols for different UEs.

2.2.4 Channel Models

Channel modelling in MU-MIMO systems is a research field by itself. One reason is that accurate (statistical/deterministic) description of MU-MIMO channels largely depends on the operating frequencies, the geographical area, the number of BS antennas, etc. In this thesis we do not enter the discussion on how to model the propagation channel, but we employ some simple channel models which allow us to evaluate the performance of our results—as well as their restrictions. Note that what we denote as channel in the context of MU-MIMO directly corresponds to the channel matrix $\boldsymbol{H}$, as given in (2.1). Next, we present the channel models which are considered in this thesis.

IID Rayleigh Fading Channel

The IID Rayleigh fading channel corresponds to a channel model assuming $\boldsymbol{H}$ to have IID random entries with standard ZMCSCG distribution. Thus, we can write

$$\mathrm{vec}(\boldsymbol{H}) \sim \mathcal{CN}(\mathbf{0}_{MK\times 1}, \mathbf{I}_{MK}). \tag{2.16}$$

Note that the term *Rayleigh fading* comes from the fact that the amplitude of the entries of $\boldsymbol{H}$ have Rayleigh distribution—the square root of the sum of two squared Gaussian random variables gives a Rayleigh random variable.

The IID Rayleigh fading channel model characterizes the small scale fading for NLoS propagation in the presence of isotropic scattering, i.e., where the AoA of the signals reaching the receiving antenna array can be assumed to be uniformly distributed over $[0, 2\pi)$. This type of propagation may arise in scenarios where there is a large number of multipath reflections coming from random directions [73]. We should point out that the IID condition for the different channel coefficients is only accurate if we consider isotropic 3D propagation with receivers consisting of a ULA of antennas with $\lambda/2$ spacing; otherwise, the structure of the antenna array would naturally lead to spatial correlation [28], [73], [74]. Nevertheless, the IID Rayleigh fading model is widely used in the analysis of general massive MIMO systems and beyond due to its analytical tractability, which can still lead to insightful results [64].

Randomly chosen channel

The previously described IID Rayleigh fading model has been the main channel model used for generating simulation results throughout this thesis due to its simplicity and practicality. However, most of the analytical results from the thesis have a much looser requirement on the properties of the underlying channel. We thus feel the need to present a considerably broader family of statistical channel models (or random matrix distributions) where the IID Rayleigh fading channel is included, and which captures the main restrictions that are assumed on the channel models for our main analytical results to apply.

We employ the term *randomly chosen matrix* to refer to any random matrix realization whose elements are drawn from arbitrary continuous distributions, but such that any submatrix of it is full-rank with probability 1—i.e., the set of randomly chosen matrices having some rank-deficient submatrix is of measure 0. A *randomly chosen channel* is then obtained from any channel model where the channel matrix $\boldsymbol{H}$ corresponds to a randomly chosen matrix. This definition may seem a bit arbitrary, but many of the broadly employed statistical channel models give rise to randomly chosen channels, since they inherently fulfill these restrictions. The IID Rayleigh fading model may be the most obvious one, but if we consider a general correlated Rayleigh fading model, where we have

$$\mathrm{vec}(\boldsymbol{H}) \sim \mathcal{CN}(\mathbf{0}_{MK\times 1}, \boldsymbol{R}), \tag{2.17}$$

for some $MK \times MK$ correlation matrix $\boldsymbol{R}$, we also get a randomly chosen as long as $\boldsymbol{R}$ is full-rank. The same is true for a Rician channel model whenever there is non-zero random fading component with full-rank correlation.

Cell-Free Massive MIMO Channel

An interesting scenario where considering a randomly chosen channel may not be accurate enough is in cell-free massive MIMO. The reason is that, in general cell-free massive MIMO scenarios, the BS station antennas may be distributed through a number of APs that may be geographically far from each other. Hence, there may be UEs that are only visible to some of the APs, which would lead to having some submatrices of $\boldsymbol{H}$ being zero. To be able to capture such scenarios we define a more general channel model which we hereby denote the *cell-free massive MIMO channel*. Assuming a total number of P APs, this model corresponds to having $\boldsymbol{H}$ defined as follows

$$\boldsymbol{H} = \begin{bmatrix} b_{11}\boldsymbol{H}_{11} & b_{12}\boldsymbol{H}_{12} & \cdots & b_{1C}\boldsymbol{H}_{1C} \\ b_{21}\boldsymbol{H}_{21} & b_{22}\boldsymbol{H}_{22} & \cdots & b_{2C}\boldsymbol{H}_{1C} \\ \vdots & \vdots & \ddots & \vdots \\ b_{P1}\boldsymbol{H}_{P1} & b_{P2}\boldsymbol{H}_{P2} & \cdots & b_{PC}\boldsymbol{H}_{PC} \end{bmatrix}, \tag{2.18}$$

where $C = 2^P - 1$, $\boldsymbol{b}_j = (b_{1j}b_{2j}\cdots b_{Pj})_2$ corresponds to the binary expansion of j—i.e., each $\boldsymbol{b}_j$ is fixed since it can be obtained from P and j—and $\boldsymbol{H}_{ij}$ are randomly chosen channels of dimension $N_i \times K_j$. Note that N_i would correspond to the number of antennas at the ith AP, and K_j would correspond to the number of UEs which are simultaneously visible to the APs indexed by the non-zero elements of $\boldsymbol{b}_j$. We believe that this channel model is the most general representation of a channel which has an arbitrary set of UEs hidden to an arbitrary set of APs, since the fixed binary expansions allow us to consider all possible combinations of hidden/visible UEs. To get a feeling of what this channel would look like in some specific setting, we show an example where (2.18) is particularized to the case where there are only 2 APs, which would lead to the channel matrix

$$\boldsymbol{H} = \begin{pmatrix} \boldsymbol{H}_{11} & \boldsymbol{0}_{N_1\times K_2} & \boldsymbol{H}_{13} \\ \boldsymbol{0}_{N_2\times K_1} & \boldsymbol{H}_{22} & \boldsymbol{H}_{23} \end{pmatrix}, \tag{2.19}$$

where $\boldsymbol{H}_{11}$ is the channel from AP 1 to the K_1 UEs hidden from AP 2, $\boldsymbol{H}_{22}$ is the channel from AP 2 to the K_2 UEs hidden from AP 1, while $\boldsymbol{H}_{13}$ and $\boldsymbol{H}_{23}$ are the channels from AP 1 and AP 2, respectively, to the K_3 UEs which are seen by both APs.

Orthogonal Channel

The most desirable channel for multiplexing UEs in the spatial domain is the so-called *orthogonal channel*. In this thesis, we define the orthogonal channel by

$$\boldsymbol{H} = \sqrt{\beta}\widetilde{\boldsymbol{U}} \tag{2.20}$$

where $\widetilde{\boldsymbol{U}}$ is an $M \times K$ matrix such that $\widetilde{\boldsymbol{U}}^{\mathrm{H}}\widetilde{\boldsymbol{U}} = \mathbf{I}_K$—recall the assumption $M \geq K$ which is hereby considered. This means that we can write without loss of generality

$$\widetilde{\boldsymbol{U}} = \boldsymbol{U}\begin{bmatrix} \mathbf{I}_K \\ \boldsymbol{0}_{(M-K)\times K} \end{bmatrix}, \tag{2.21}$$

where $\boldsymbol{U} \in \mathcal{U}(M)$—i.e., it is an $M \times M$ unitary matrix. Note that a random orthogonal channel formed by a unitary matrix $\boldsymbol{U}$ uniformly distributed in $\mathcal{U}(M)$ also constitutes a randomly chosen channel. Furthermore, the IID Rayleigh channel from (2.16)—i.e., with normalized entries having unit-power on average—approximates an orthogonal channel as the number of antennas at the base station grow large, i.e., $M \to \infty$. This is often referred to as the *channel hardening* effect, which constitutes one of the main advantages of massive MIMO systems [75].

Having an orthogonal channel like (2.20) is incredibly advantageous, since it leads to maximum multiplexing gain at low complexity. It is enough to con-

sider the previously mentioned MF equalizer to achieve optimum processing—in fact, any of the common linear equalizers described before lead to the same processing matrix up to scaling. The reason is that these channels allow for perfect interference cancellation while simultaneously maximizing post-processed SNR—i.e., leading also to optimum SINR per line. Furthermore, performing per-line ML-detection upon the MF estimates—given by $\hat{\boldsymbol{s}} = \boldsymbol{z}$ with (2.13)—still allows for maximum UL capacity (2.5). This is because unitary matrices induce no correlation on the noise, so all the entries of $\boldsymbol{z}$ are perfectly independent from each other. On top of that, the general expression for the MIMO capacity (2.4) is also achievable in this case since all the singular values of the channel are equal, so there is no gain from using water-filling at the UEs, which are further served at equal rates. However, a more general description of the orthogonal channel could be considered by multiplying an arbitrary diagonal matrix from the right—e.g., accounting for different fading factors at each UE—leading to (potentially) non-zero capacity gain from water-filling.

Chapter 3

Decentralized Multi-Antenna Architectures

When I landed at EIT, Jesús and Fredrik were working together in decentralized solutions for massive MIMO systems. Jesús had derived some interesting results and I got immersed in the discussions that led to a conference publication which I had the pleasure to present at ISIT'19, opening my eyes to the academic research community. Jesús had also been working earlier in decentralized solutions for interference cancellation in massive MIMO systems based on Daisy-chain architectures, and we started looking at how we could extend these ideas to architectures based on LIS—which was my initial research topic. After long discussions and a bunch of simulation work, I was lucky to develop some algorithms making use of the structure of LIS panels to achieve reasonable performance improvements, leading to the first conference publication included in this thesis. After this first publication, I started working in more fundamental LIS problems, and I managed to drop some more conference publications which are not included in the thesis.

I was presenting again the ideas from the first paper in a small conference in Lund when, from the back of the room, Fredrik overheard a conversation between two guys from Ericsson that were doubtful about the difficulty to perform such processing in real systems. Of course, this was just enough for Fredrik to take it personal, so the next day he was waiting in his office with some ideas on finding a fundamental trade-off between complexity and level of decentralization in multi-antenna architectures. This problem turned out to be quite challenging—as well as motivating—so it kept us busy for a long time with countless discussions, MATLAB scripts, and sheets full of failed at-

tempts to solve the problem. We ended up with the definition of the WAX decomposition—named after the letters we were using for the three matrices it consists of—which allowed us to get some interesting results and opened a whole research quest for us. The work on the WAX decomposition, and the decentralized trade-offs associated, constitutes the main contribution of this thesis, which comprises the two journal publications, as well one conference publication that I worked on during my short virtual internship at Huawei. In this line of work, also lies one more included conference publication that was a result of my research visit to Barcelona with Angel Lozano. I had the opportunity to present the WAX decomposition results there and one of Angel's students questioned that an information-losless dimension reduction—as that given by WAX—may not reduce the interconnection bandwidth for given information-loss if quantization is considered. I followed Fredrik's example and I took it personal.

3.1 From Centralized to Decentralized

From now on, let us focus, without much loss of generality, on the UL MU-MIMO scenario described in the previous chapter, where K UEs are simultaneously communicating with an M-antenna BS. In order to go from the electromagnetic signals received at the antennas to the received symbol vector $\boldsymbol{y}$ from (2.1)—assuming synchronization is established—there is a number of initial steps that should be taken:

1) First, we should use RF circuitry to amplify, filter, and down-convert the signals to low frequencies.

2) Then, we can use ADCs to be able to transform the signals to bits so they can be digitally processed—e.g., by a computer.

3) Finally, we can demodulate the narrowband subcarrier of interest from each antenna to obtain $\boldsymbol{y}$. In OFDM-like modulations this involves applying a DFT to the received digital signals to isolate the narrowband subcarriers.

These steps are typically integrated in specific modules which may also possess further processing capabilities—including CSI estimation capabilities. In systems with a small number of antennas, it may be enough to have a single module implementing all these computations, as well as the detection and decoding. This module could then be identified with the CPU (or central node) of the common centralized approach. However, systems with a large number of antennas potentially require several of these modules—which may be implemented through SDRs—since each of them may have physical restrictions on the number of antennas it can accommodate. For example, in initial massive MIMO prototypes like [45], one SDR is employed for each group of 4 antennas

out of 64, while in [46] one SDR is employed for every pair of antennas out of 100. In this context, the centralized approach would consist of transmitting all the data from the SDRs—including the estimated CSI—to a powerful-enough CPU, which would then have full freedom to jointly process the received complex baseband vector $\boldsymbol{y}$ for each narrowband subcarrier using the channel estimates. However, as already noticed in [45] and [46], the amount of data that would have to be transmitted to the CPU in this approach scales with the number of antennas, so it would require impractically large interconnection bandwidths. This led the authors in [45] and [46] to consider some initial pragmatic decentralized approaches, i.e., by applying simple preprocessing of the data at the SDRs to reduce the amount of data that had to be transmitted to the CPU at the cost of some performance loss.

3.1.1 Centralized Multi-Antenna Architecture

Following our previous exposition, a *centralized multi-antenna architecture* can then be defined as a multi-antenna architecture where the full complex baseband symbols $\boldsymbol{y}$ from (2.1), as well as the estimates of $\boldsymbol{H}$, are accumulated at a CPU in charge of performing equalization, detection, decoding, etc.[1] An equivalent complex baseband description of a centralized architecture is then illustrated in Fig. 3.1, where the respective SDRs (or equivalent modules) can be located close to the antennas or close to the CPU, indifferently.

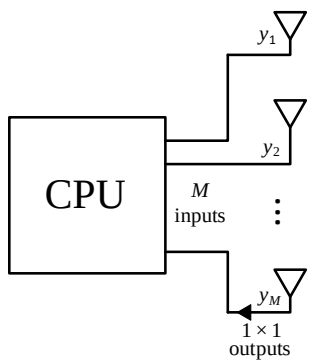

Figure 3.1: Centralized multi-antenna architecture.

[1] For the DL, a centralized architecture would only select at a CPU the precoded symbols to be transmitted from its antennas, since detection would be performed by the UEs.

3.1.2 Decentralized Multi-Antenna Architectures

As opposed to the centralized case, the definition of a decentralized multi-antenna architecture can lead to some discussion. Some decentralized approaches may consider data detection capabilities at the decentralized modules—e.g., [50], [56], [76]—while for others it may be enough to perform linear estimation of the symbols—e.g., [49], [54]—or even just some dimension reduction—e.g., [51]. In any case, as we argue in [53], the data arriving at a BS from a set of UEs has to end up eventually in a central node so that it can travel further through the core network—e.g., to some server, to the other party of a video-call, etc. This means that we can always assume that a CPU will be present in the process, which would likely have enough capabilities for performing symbol detection, channel decoding, etc. In this thesis, we thus limit the decentralized processing capabilities to linear equalization schemes, which could potentially be implemented using cost-efficient SDRs (or equivalent decentralized modules) and where complexity is essentially given by the number of multiplications that have to be performed. The *level of decentralization* is then measured in terms of the interconnection bandwidth—i.e., the amount of information that is being shared—between the decentralized nodes and the CPU for effectively decoding the data from the UEs. We can now give a broad definition of a *decentralized multi-antenna architecture* as a multi-antenna architecture where the interconnection bandwidth to a CPU is effectively reduced in comparison to a centralized architecture by performing data preprocessing at some decentralized modules close to the antennas—e.g., SDRs. On the other hand, a *fully-decentralized multi-antenna architecture* would correspond to a decentralized multi-antenna architecture where the interconnection bandwidth to a CPU only scales with the number K of UEs being served—and not with the number M of BS antennas—as we discuss in [53].

In Fig. 3.2 we illustrate an equivalent complex baseband description of a fully-decentralized architectures which falls within our definition, and which will be further considered in upcoming sections since it generalizes a large part of the fully-decentralized approaches being considered. In this architecture, each decentralized module m multiplies its input complex baseband entry, y_m from (2.1), by $K \times 1$ vectors $\boldsymbol{w}_m$. The outputs are then combined through a big sum module—which could potentially be implemented in a sequential way, or through alternative decentralized approaches—and the output sum is then sent to the CPU for subsequent detection, decoding, etc. The post-processed vector arriving the CPU can then be described as in (2.10)—since it results also in a linear equalization process—but where the equalizer $\boldsymbol{F}$ is now a $K \times M$ matrix given by

$$\boldsymbol{F}_{\text{FD}} = \begin{bmatrix} \boldsymbol{w}_1 & \cdots & \boldsymbol{w}_m \end{bmatrix}. \tag{3.1}$$

We can note that, if we group the antennas such that each decentralized module

is associated to an arbitrary number N of antennas, we would be able to achieve the same equalization without loss, where the vector multiplication in each module would be changed for a multiplication by a $K \times N$ matrix.

Let $\boldsymbol{H} = [\boldsymbol{h}_1 \ \cdots \ \boldsymbol{h}_M]^{\mathrm{T}}$. If we select $\boldsymbol{w}_m = \boldsymbol{h}_m^*$—i.e., the conjugate transpose of the mth row of channel matrix $\boldsymbol{H}$—this architecture achieves perfect MF equalization $\boldsymbol{F}_{\mathrm{FD}} = \boldsymbol{H}^{\mathrm{H}}$, which corresponds to the approach followed in the initial massive MIMO prototypes from [45], [46] to deal with the problem of high interconnection bandwidth. The main advantage of these approaches is that the information that has to be transmitted to the CPU now scales with the number of users K instead of with the number of BS antennas M, thus leading to practical interconnection bandwidths even in large multi-antenna systems like massive MIMO and beyond technologies. However, in interference limited scenarios the performance may be severely restricted since MF equalizer does not have good interference cancellation properties for general channels, as discussed in the previous chapter.

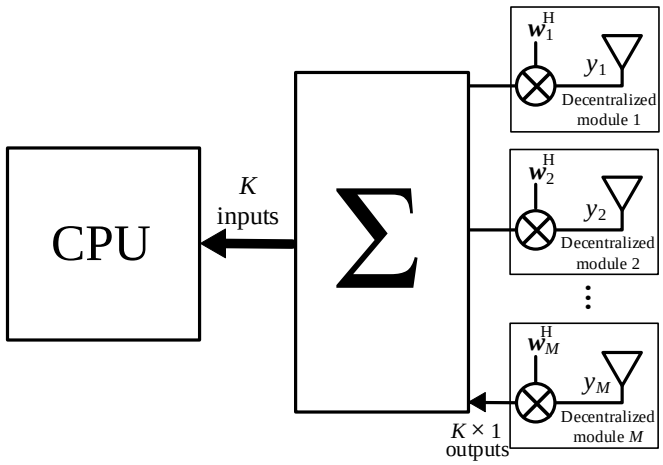

Figure 3.2: Fully-decentralized multi-antenna architecture.

In principle, an architecture like the one from Fig. 3.2 can implement any of the linear equalizers presented in the previous chapter—note that a matrix multiplication is just a sum of vector multiplications. However, for implementing some of the studied equalizers the full channel matrix has to be known at all the decentralized modules. An important restriction of decentralized architectures is that the channel estimation is performed in the decentralized modules, so each decentralized module would only have access to the channel vector (or matrix) between the UEs and the antenna (or antennas) associated to it. In the

architecture from Fig. 3.2, we can thus assume that only $\boldsymbol{h}_m$ is known at decentralized module m, so perfect MF equalizer is straightforward—as seen from our previous description. However, in order to apply other linear equalizers, we should study decentralized schemes that allow to have, at each decentralized module, some knowledge of the channel and/or the processing applied at other decentralized modules. We thus define the term *decentralized scheme* as an information sharing strategy between the decentralized modules—and possibly with the CPU—in a decentralized architecture to be able to implement certain equalization processes. Note that decentralized schemes are mainly employed during the training phase to find the decentralized processing to be applied. Furthermore, a decentralized scheme may be associated to an architecture—or rather a topology, as in [77]—showing how the decentralized modules are connected to share data, but we will restrict the term decentralized architecture for describing the equivalent architecture employed during the data phase, as in Fig. 3.2. Part of this thesis defines decentralized schemes for achieving specific equalization processes, some of these schemes will be discussed next.

3.2 Fully-Decentralized Interference Cancellation Schemes

Let us consider the fully-decentralized architecture from Fig. 3.2. Since in this architecture each decentralized module has only access to the channel estimates associated to its antenna—i.e., module m only knows the estimate of the mth row of $\boldsymbol{H}$, $\boldsymbol{h}_m^{\mathrm{T}}$—applying any equalization other than MF requires a suitable decentralized scheme to convey the relevant information to the decentralized modules. In particular, in systems whose performance is limited by the interference between UEs—e.g., where $\boldsymbol{H}$ is far from being orthogonal—we would like to find decentralized schemes to achieve a processing matrix which is close to a ZF equalizer.

We will now take a look at how we can quantify the interference cancellation properties—inspired by the ZF solution—when using the fully-decentralized architecture, which will be useful for defining suitable decentralized schemes. The ZF equalizer achieves perfect interference cancellation by performing a left pseudo-inverse of the channel matrix, i.e., leading to an equivalent channel

$$\boldsymbol{F}_{\mathrm{ZF}}\boldsymbol{H} = \mathbf{I}_K. \tag{3.2}$$

Given the equivalent processing matrix $\boldsymbol{F}_{\mathrm{FD}}$ from (3.1), in order to have good interference cancellation properties it would thus be desirable to construct $\boldsymbol{F}_{\mathrm{FD}}$

such that it is close to a left pseudo-inverse of $\boldsymbol{H}$.[2] One straightforward way to measure how close is $\boldsymbol{F}_{\mathrm{FD}}$ to a left pseudo-inverse of $\boldsymbol{H}$ is given by

$$\begin{aligned} \mathrm{I}_{\mathrm{UE}} &= \|\boldsymbol{F}_{\mathrm{FD}}\boldsymbol{H} - \mathbf{I}_K\|_{\mathrm{F}}^2 \\ &= \left\| \sum_{m=1}^{M} \boldsymbol{w}_m \boldsymbol{h}_m^{\mathrm{T}} - \mathbf{I}_K \right\|_{\mathrm{F}}^2, \end{aligned} \tag{3.3}$$

which for $\boldsymbol{F}_{\mathrm{FD}} = \boldsymbol{F}_{\mathrm{ZF}}$ would give 0. In fact, assuming the diagonal elements of the product $\boldsymbol{F}_{\mathrm{FD}}\boldsymbol{H}$ are normalized to 1, I_{UE} is directly related to the power of the interference between different UEs when applying $\boldsymbol{F}_{\mathrm{FD}}$. The nice thing about (3.3) is that it provides a simple objective function that can be minimized in different ways to achieve good interference cancellation under different settings, as we will see next.

3.2.1 Sequential Decentralized Schemes Based on Daisy Chain

In [49], [54] decentralized schemes based on the Daisy chain topology are proposed to achieve interference cancellation in a fully-decentralized architecture like the one from Fig. 3.2. The idea is to iteratively minimize the expression for I_{UE}—given in (3.3)—so that the resulting equivalent equalizer $\boldsymbol{F}_{\mathrm{FD}}$ has good interference-cancellation properties. In Fig. 3.3 we can see a schematic of a Daisy chain topology, where the discontinuous line between decentralized modules 1 and M is because this connection may be included or not—as discussed in [54].

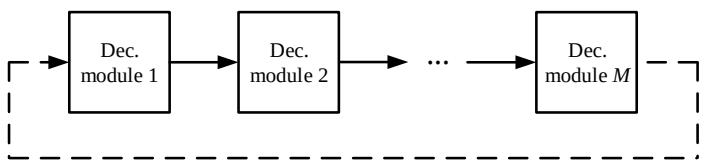

Figure 3.3: Schematic of Daisy chain topology.

The Daisy chain topology allows for the implementation of coordinate descent minimization of I_{UE} from (3.3). In the initial round, decentralized module

[2] To be strictly general, achieving perfect interference cancellation would only require that the equivalent channel is a diagonal matrix. However, we focus on the pseudo-inverse formulation for simplicity and tractability.

m would compute its filter $\boldsymbol{w}_m$ by solving the minimization problem

$$\begin{aligned} \arg\min_{\boldsymbol{w}_m} \quad & \left\| \boldsymbol{S}_m + \boldsymbol{w}_m \boldsymbol{h}_m^{\mathrm{T}} - \mathbf{I}_K \right\|_{\mathrm{F}}^2 \\ \text{s.t.} \quad & \|\boldsymbol{w}_m\|^2 = \mu, \end{aligned} \tag{3.4}$$

where $\boldsymbol{S}_m$ corresponds to a $K \times K$ matrix which should be shared from decentralized module $m-1$ in the previous step, and which is given by

$$\boldsymbol{S}_m = \sum_{i=1}^{m-1} \boldsymbol{w}_i \boldsymbol{h}_i^{\mathrm{T}}, \tag{3.5}$$

i.e., it contains the contribution of the previous $m-1$ decentralized modules to the equivalent channel. Note that the power constraint $\|\boldsymbol{w}_m\|^2 = \mu$ comes from assuming that all decentralized modules apply equal amplification, but it could potentially be disregarded—especially considering the UL scenario. After finding $\boldsymbol{w}_m$ from (3.4), which has closed form solution

$$\boldsymbol{w}_m = \mu \frac{(\mathbf{I}_K - \boldsymbol{S}_m)\boldsymbol{h}_m^*}{\|(\mathbf{I}_K - \boldsymbol{S}_m)\boldsymbol{h}_m^*\|}, \tag{3.6}$$

decentralized module m can then compute $\boldsymbol{S}_{m+1} = \boldsymbol{S}_m + \boldsymbol{w}_m \boldsymbol{h}_m^{\mathrm{T}}$ and send it to the next decentralized module so that it can similarly compute its own decentralized filter $\boldsymbol{w}_{m+1}$. Note that, in the first decentralized module, we would have $\boldsymbol{S}_1 = \mathbf{0}$ as starting assumption. After going through the whole chain once, and if the connection between the last and the first decentralized modules is in place, we could have another round of the process to further improve the interference cancellation performance. In this case, each panel would directly have access to the whole expression (3.3)—although it can only optimize its own decentralized filter—so it would use $\boldsymbol{S}_m = \sum_{i \neq m} \boldsymbol{w}_i \boldsymbol{h}^{\mathrm{T}}$—i.e., by subtracting its previous contribution to the accumulated sum received from the preceding decentralized module.

One of the main drawbacks of the decentralized schemes based on Daisy chain is that, since each decentralized module has to perform some operations and send information to the following decentralized module, the accumulated delay required to go through the whole process scales with the number of decentralized modules, and thus with the number of antennas M. This becomes an issue in massive MIMO systems, and even more in LIS, since these systems consider BSs with a huge number of antennas, so the associated delays to implement such decentralized schemes would make them impractical.

3.2.2 Parallel Decentralized Schemes

Instead of considering sequential solutions, as in the Daisy chain schemes from [49], [54], we could potentially get rid of the scaling of the delay with the number of antennas by considering schemes where all decentralized modules are simultaneously trying to compute their equalizer by minimizing some metric similar to I_{UE}. As in the sequential case, in parallel schemes, the decentralized modules would also compute their equalizer iteratively and—after each iteration—share some information related to the resulting equalization, as well as to the local CSI. However, parallel schemes allow for more freedom in the way information in being shared, since there is no need to connect one module after another. Thus, we could consider decentralized schemes making use of information sharing topologies like the one described by Fig. 3.4, which includes two-way connections between decentralized modules as opposed to Fig. 3.3. Furthermore, we could even make use of the antenna arrangement to make the information sharing faster, while favoring integration in 2D panels of antennas—e.g., LIS panels. For example, Fig. 3.5 (left) shows such a 2D topology, where each decentralized module can be described by Fig. 3.5 (right).

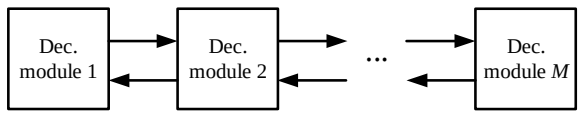

Figure 3.4: 1D topology for parallel decentralized schemes.

In **Paper I**, we will propose decentralized schemes employing the topologies from Fig. 3.4 and Fig. 3.5 for achieving improved interference cancellation with reduced delays by extending the concepts described before for Daisy chain topologies from [49], [54]. The idea is that the information being shared should also scale with the number of UEs instead of with the number of BS antennas—i.e., we still allow sharing $K \times K$ matrices.

3.2.3 Alternative Schemes with CPU processing

Another straightforward way to use the fully-decentralized architecture from Fig. 3.2 to perform interference cancellation would be to consider decentralized schemes where the decentralized modules may send some channel information to the CPU, as discussed in [53]. In fact, by simply sharing with the CPU the Gramian of the channel—i.e., $\boldsymbol{H}^{\mathrm{H}}\boldsymbol{H}$—which still scales with the number of UEs since it is a $K \times K$ matrix, the CPU can perform perfect ZF equalization, and even MMSE equalization. In this case, the decentralized modules would only

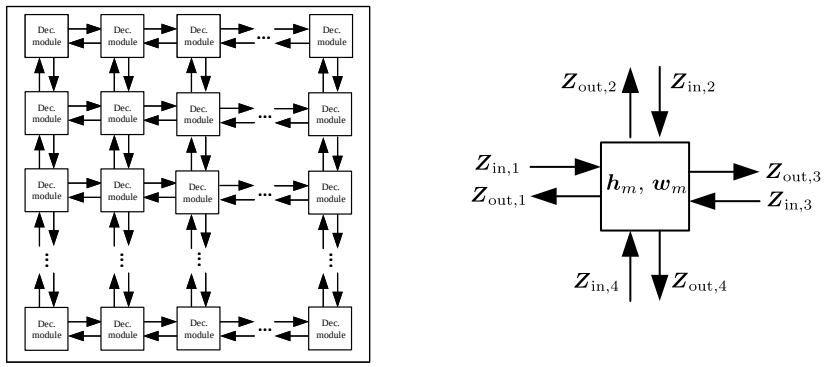

Figure 3.5: 2D topology (left), and schematic of a decentralized module (right) for parallel decentralized schemes. Notation will be further explained in **Paper I**.

have to apply the equivalent MF by simply selecting $\boldsymbol{w}_m = \boldsymbol{h}_m^*$, as previously discussed. The CPU would then use the shared Gramian to perform ZF—i.e., by inverting it and applying it to the MF-equalized vector—or MMSE—i.e., by summing it to an identity scaled by the inverse SNR[3] before inverting, and applying the result to the MF-equalized vector.

One goal of the thesis is to extend these types of decentralized schemes to architectures with arbitrary level of decentralization. This will be addressed to a certain extent in **Papers II**, **III** and **VI**. Next, we will present a formal description for architectures with arbitrary level of decentralization.

3.3 Architectures with Arbitrary Level of Decentralization

If we consider our previous definition of fully-decentralized multi-antenna architectures—i.e., where the interconnection bandwidth scales with K—we can define the *level of decentralization* as the scaling of the interconnection bandwidth of a decentralized multi-antenna architecture. This scaling would then be between K—as in the fully-decentralized architectures—and M—as in the centralized architectures.[4] If we look at the fully-decentralized architecture from Fig. 3.2—where the equivalent equalization is given by the $K \times M$ matrix $\boldsymbol{F}_{\text{FD}}$ from (3.1)—we could straightforwardly increase the scaling of the

[3]The CPU should have an estimate of the SNR, which is a common assumption.

[4]In principle, we could also consider decentralized architectures where the scaling of the interconnection bandwidth goes below K, but these require to sacrifice performance since the end data from K UEs that has to be received at the BS obviously scales with K.

data sent to the CPU by increasing the size of the $\boldsymbol{w}_m$ vectors to an arbitrary T. However, by doing that, we are also increasing the complexity of the processing—i.e., the number of multiplications—that have to be applied at the decentralized modules, so we see no benefit whatsoever in doing that.

An important motivation for considering architectures with arbitrary level of decentralization is to simplify the processing that has to be applied at the decentralized modules. In the fully-decentralized architecture from Fig. 3.2, we can note that, throughout every UL reception, each decentralized module has to be able to apply K multiplications—i.e., to multiply by the $\boldsymbol{w}_m$ vector. Although the number of UEs may be considerably smaller than the number of BS antennas, the decentralized modules may also have much more limited processing capabilities than the main CPU, since they should be implemented close to the antennas in a cost-efficient, and possibly space-constrained manner. For example, these modules may be designed such that the number of multiplications that the hardware can handle may not exceed some threshold, while the number of UEs in the network can be flexible, so there may be situations where the number of UEs exceeds said threshold. Thus, let us define the *decentralized processing complexity* as the scaling of the operations that a decentralized module has to apply. This scaling would then be between K—as in fully-decentralized architectures like the one from Fig. 3.2—and 0—as in common centralized architectures.

Taking into account our previous definitions, we can now extend the fully-decentralized architecture from Fig. 3.2 to consider an arbitrary level of decentralization for some fixed decentralized processing complexity. This can be done by selecting an arbitrary number of CPU inputs T, while fixing the number of multiplications per decentralized module to some number L. Fig. 3.6 describes a generalized multi-antenna architecture during an UL data transmission which fulfills the previous considerations. This architecture corresponds to a generalization of the fully-decentralized architecture from Fig. 3.2 where the $\boldsymbol{w}_m$ vectors are now resized to L—corresponding to the multiplications per antenna—and the sum module is now substituted by a combining module which generates T outputs—corresponding to the number of CPU inputs. The combining module is now described through a matrix $\boldsymbol{A}^{\mathrm{H}}$ instead of a big sum module since the dimensions have to be adapted, but the idea is to have these modules constructed through smaller sum modules that can be implemented by simple hardware and remain fixed once such systems are deployed. Moreover, the CPU can apply further processing to readapt the dimensions so that common symbol estimation procedures may be applied. We can thus model the CPU processing (or part of it) as a multiplication by a $K \times T$ matrix $\boldsymbol{X}^{\mathrm{H}}$ which adapts the dimensions to the number of UE streams. The resulting

post-processed vector can then be described by the $K \times 1$ vector

$$\boldsymbol{z} = \boldsymbol{X}^{\mathrm{H}} \boldsymbol{A}^{\mathrm{H}} \boldsymbol{W}^{\mathrm{H}} \boldsymbol{y}, \tag{3.7}$$

[5]

where $\boldsymbol{W}^{\mathrm{H}}$ is a $ML \times M$ block diagonal matrix

$$\boldsymbol{W}^{\mathrm{H}} = \mathrm{diag}\big(\boldsymbol{w}_1, \cdots, \boldsymbol{w}_M\big). \tag{3.8}$$

Note that if we solely consider the decentralized processing being applied, we would have a $T \times 1$ post-processed-vector

$$\boldsymbol{z}_{\mathrm{D}} = \boldsymbol{F}_{\mathrm{AD}} \boldsymbol{y}, \tag{3.9}$$

with $\boldsymbol{F}_{\mathrm{AD}} = \boldsymbol{A}^{\mathrm{H}} \boldsymbol{W}^{\mathrm{H}}$. However, including the CPU processing will help giving a better understanding of the possibilities of such framework. In fact, in the fully-decentralized approach from [53]—described in Section 3.2.3—a similar consideration is made since the decentralized processing there is restricted to MF, and the CPU uses the shared Gramian to be able to apply ZF or MMSE.

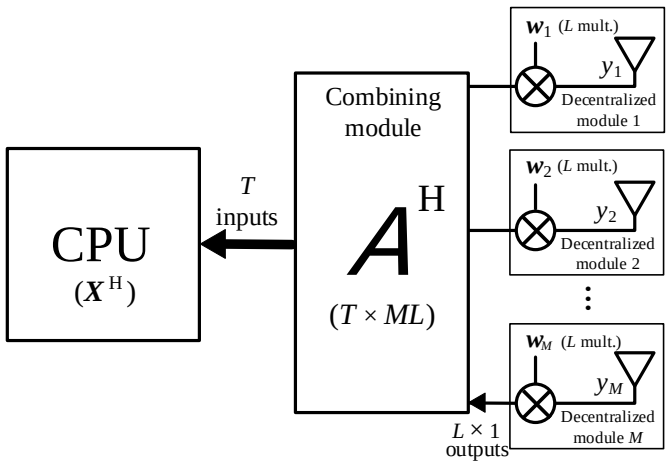

Figure 3.6: Architecture with arbitrary level of decentralization.

If we assume some desirable structure for $\boldsymbol{A}$ such that the output of every group of L adjacent antennas are directly summed, we can consider an alternative description of multi-antenna architectures with arbitrary level of

[5] The usage of conjugate transpose matrices is mainly for presentation purposes since this will lead to a more neat description of the WAX decomposition, which will be later presented.

decentralization in which each decentralized module is performing decentralized processing upon a group of L antennas. The $L \times 1$ $\boldsymbol{w}_m$ vectors would then turn into $L \times L$ matrices, which still allows to achieve the same processing as before, but without increasing the dimension of the data sent to the remaining combining module. This consideration has been used in much of the included work related to muti-antenna architectures with arbitrary level of decentralization since, apart from gaining some practicality, it leads to better analytical tractability. Nevertheless, this consideration does not affect the validity of the results, which can still be trivially adapted to the description from Fig. 3.6, as further discussed in **Paper II**.

3.3.1 Trade-off Between Level of Decentralization and Decentralized Processing Complexity

Let us consider the general architecture from Fig. 3.6. In this general framework, we can find a combination of parameters L, T, and $\boldsymbol{A}$ that allows representing the centralized architecture from Fig. 3.1, as well as the fully-decentralized architecture from Fig. 3.2. For the centralized case, this is achieved by selecting $L = 0$,[6] $T = M$, and $\boldsymbol{A} = \mathbf{I}_M$, while for the fully-decentralized case we would select $L = K$, $T = K$, and $\boldsymbol{A} = [\mathbf{I}_K \ \cdots \ \mathbf{I}_K]^{\mathrm{T}}$. If we ignore the complexity of the combining module, which may be implemented by fixed hardware, we can identify a trade-off between these two architectures in terms of level of decentralization and decentralized processing complexity which is depicted in Fig. 3.7.

An important observation is that, although implementing specific equalizers may require non-trivial approaches, the fully-decentralized architecture from Fig. 3.6 trivially allows the application of information lossless linear transformations to the received vector $\boldsymbol{y}$. The most obvious example is when we simply select $\boldsymbol{w}_m = \boldsymbol{h}_m^*$, leading to the MF equalizer, which corresponds to an information lossless linear transformation since it only removes dimensions in the noise space. Thus, assuming optimal decoding at the CPU, the fully-decentralized architecture would be able to achieve the same user rates as the centralized architecture. This suggests the existence of a fundamental information-lossless trade-off between level of decentralization and decentralized processing complexity. A major goal of this thesis is to fully characterize said trade-off—i.e., to find the region from Fig. 3.7 where information-lossless linear transformations are available using a framework like that of Fig. 3.6. We will also study how to achieve practical exploitation of said trade-off—e.g., by proposing decentral-

[6] Considering the framework from Fig. 3.6, choosing $L = 0$ would paradoxically lead to 0 inputs to the combining module. It would thus be more accurate to represent this case by considering $L = 1$ and $w_m = 1$. However, we prefer to link L with the number of multiplications—i.e., regarding this as a special case—since even one multiplication, when properly exploited, may lead to a reduction in the required inputs to CPU.

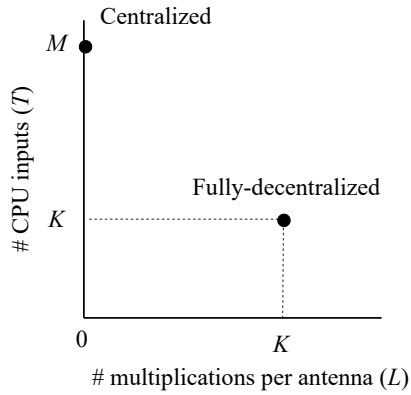

Figure 3.7: Trade-off between fully-decentralized and centralized architectures.

ized schemes, designing practical combining modules, or considering specific channel models.

3.3.2 The WAX Decomposition

From our previous discussion, we can note that one of the simplest way to achieve an information-lossless linear transformation in the fully-decentralized architecture from Fig. 3.2 is to perform decentralized MF, since we can select $\boldsymbol{w}_m = \boldsymbol{h}_m^*$ without the need to share any information between the different decentralized modules. Thus, a straightforward way to study the information-lossless trade-off in architectures with arbitrary level of decentralization based on Fig. 3.6, would be to characterize the conditions under which such architectures can achieve perfect MF equalization. The ability to perform MF equalization turns out to be also a necessary condition for achieving information-lossless linear transformations, as we discuss in **Paper II**. Considering the equivalent processing from (3.7), performing MF equalization in such a framework translates to finding $\boldsymbol{W}$ and $\boldsymbol{X}$ such that

$$\boldsymbol{H} = \boldsymbol{W}\boldsymbol{A}\boldsymbol{X}, \tag{3.10}$$

where $\boldsymbol{W}$ should have the block diagonal structure from (3.8). The expression from (3.10) is what we define as *the WAX decomposition* of $\boldsymbol{H}$. The main peculiarities of such a decomposition are the block-diagonal structure of $\boldsymbol{W}$, and the fact that $\boldsymbol{A}$ is a fixed matrix—i.e., a suitable WAX decomposition should involve an $\boldsymbol{A}$ matrix that allows decomposing all (or at least most) possible $\boldsymbol{H}$ matrices.

The WAX decomposition gives the requirement that a multi-antenna ar-

chitecture with arbitrary level of decentralization—based on Fig. 3.6—has to fulfill in order to be able to apply information-lossless processing. Note that, even disregarding the application of $\boldsymbol{X}^{\mathrm{H}}$ at the CPU, if we can perform WAX decomposition of $\boldsymbol{H}$ (3.10), the decentralized processing applied before arriving the CPU—i.e., $\boldsymbol{F}_{\mathrm{AD}} = \boldsymbol{A}^{\mathrm{H}}\boldsymbol{W}^{\mathrm{H}}$ as in (3.9)—would also correspond to an information-lossless linear transformation due to the data-processing inequality [7]. Characterizing the conditions of existence of the WAX decomposition for all (or most) possible channel matrices $\boldsymbol{H}$ would then be equivalent to characterizing the information-lossless trade-off in Fig. 3.7. We will see that the channel model employed, as well as the design of $\boldsymbol{A}$, can have an important impact on this trade-off. Furthermore, since $\boldsymbol{A}$ should be associated to a hardware combining module—i.e., similar to the sum module from Fig. 3.2—we should consider the use of $\boldsymbol{A}$ matrices comprised of sparse structures with 1s and 0s so that they have straightforward implementation using simple sum modules. These and other considerations will be thoroughly studied in **Papers II, IV, VI**.

3.4 Quantization Effects in Decentralized Processing

In the previous sections of this chapter we have been measuring the interconnection bandwidth to a CPU using the dimension of the vectors that are being transmitted between different nodes. However, in real systems the complex baseband vectors are actually stored and transmitted using bits since, as we discussed earlier, in order to get the received vector $\boldsymbol{y}$ from the electromagnetic signals received at the BS antennas one of the steps is to use an ADC to transform the analog signals into bits. These bits can then be digitally processed, sent, and stored. In principle, if the number of output bits from each ADC—given by the quantization bits—is large enough, we would be able to represent the complex baseband numbers with very small error. However, another way to reduce the volume of information that has to be sent to a CPU, is to reduce the amount of quantization bits so that each complex baseband number requires less bandwidth to be transmitted. Of course, having less quantization bits translates to having a less accurate description of these complex baseband numbers, so the resulting transmission rates from the UEs to the BS may have to be reduced to compensate for the quantization error.

Following our previous discourse we may naturally ask ourselves, is it better to reduce quantization bits or to perform information-lossless dimension reductions? To the best of our knowledge, the available literature has not been able to clearly address such question, so **Paper IV** includes some initial work in this direction. Specifically, we study transmission rates in simplified model

where quantization is considered for reducing the bits that have to be transmitted to a CPU after an information-lossless dimension reduction, as depicted in Fig. 3.8.

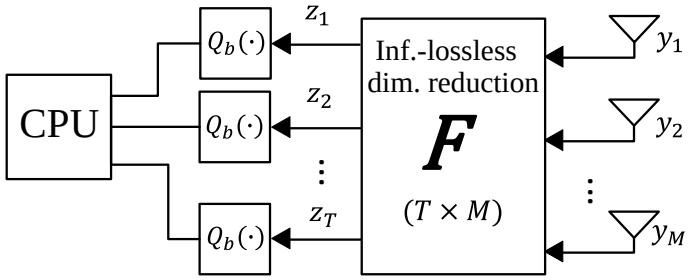

Figure 3.8: Quantization in centralized architecture (left) v.s. quantization after dimension reduction (right).

3.5 Thesis Contributions

The contributions of this thesis in the topics described throughout this chapter are summarized next.

3.5.1 Paper I

In this paper, we define parallel decentralized schemes for achieving interference cancellation using a fully-decentralized architecture as the one described by Fig. 3.2. We consider the topologies from Figs. 3.4 and 3.5, which allow us to take into account the physical structure of LIS panels. For each of the considered topologies, we propose algorithms which achieve good interference cancellation performance while incurring lower delay than the Daisy chain approaches from [49], [54]. These algorithms employ novel message passing schemes for effectively sharing the necessary information between the decentralized modules without increasing the interconnection bandwidths as compared to the Daisy chain approaches.

3.5.2 Paper II

This paper presents the first results on architectures with arbitrary level of decentralization. A general framework like the one from Fig. 3.6 is studied, leading to the definition of the WAX decomposition, which delimits the equalization that can be applied in such framework. We show how to perform

the WAX decomposition, and find the conditions to be able to perform such decomposition to any randomly chosen channel $\boldsymbol{H}$ using a randomly chosen (although still fixed) matrix $\boldsymbol{A}$ as combining module. This leads to the characterization of the information-lossless trade-off between level of decentralization and decentralized processing complexity for randomly chosen $\boldsymbol{A}$. The paper also includes some validity conditions on the combining module $\boldsymbol{A}$, as well as simulations showing that this module can be potentially implemented using sparse structures of 1s and 0s.

3.5.3 Paper III

This paper continues the work on architectures with arbitrary level of decentralization by considering a cell-free massive MIMO scenario where the channel matrix cannot be modeled as a randomly chosen matrix. The general framework from Fig. 3.6 is readapted to consider physically distant APs with an arbitrary number of antennas, leading to cell-free massive MIMO channels like (2.18). The conclusion is that having zero blocks at the channel matrix can have a negative impact on the achievable information-lossless trade-off between level of decentralization and decentralized processing complexity.

3.5.4 Paper IV

This paper studies the trade-off between achievable user rate and interconnection bandwidth to a CPU when quantization is considered. We employ the framework from Fig. 3.8 and characterize the achievable user rates for fixed quantization bits when applying different information-lossless dimension reductions. The conclusion is that, even in the presence of coarse quantization, information-lossless transformations can effectively reduce the interconnection bandwidth to a CPU for given user rates. However, there seems to be a slight performance loss when using specific dimension reductions under coarse quantization, which should be further characterized.

3.5.5 Paper VI

This paper extends the work on architectures with arbitrary level of decentralization by putting the focus on the design of practical combining modules. We present a number of constructions for $\boldsymbol{A}$ consisting of sparse structures of 1s and 0s, and prove their validity for WAX decomposition. Some of these structures have marginal loss in the information-lossless trade-off from **Paper II**, which we also prove to be fundamental since no $\boldsymbol{A}$ can perform beyond it. Furthermore, we present decentralized schemes making use of the structure of $\boldsymbol{A}$ to obtain the processing matrix $\boldsymbol{W}$ to be applied at the decentralized modules for information-lossless processing.

Chapter 4

Reconfigurable Surfaces

I didn't start my work on RS until the last year of my PhD. I was presenting some WAX results at ICC'22, when I listened to a talk from Merouane Debbah where he commented on the open problem of orthogonalizing the channel with RIS. Given the matrix theory skills I acquired during my work on WAX, I felt pretty confident I could get some interesting solutions for this problem, so I became obsessed with it and started writing some initial attempts in my tablet during the conference coffee breaks. I was also attending ICASSP'22 immediately afterwards, where I got some ideas from Robert W. Heath on information theoretical formulations for RIS frameworks. So when I got back home, I had two interesting lines of work which ended up in the two included conference publications on RS.

4.1 Reconfigurable Surfaces for Adjusting the MU-MIMMO Channel

RSs comprise a family of technologies that allow for adjustment of the propagation environment by offering a tunable reflection. They are thus complementary to the communication link between two ends and their main goal is to improve the properties of the resulting link. In this thesis we focus on the utilization of RS as a complementary technology for the UL MU-MIMO framework presented in Chapter 2. In this context, we can still assume the input-output relation defined by (1), which considers a single narrowband subcarrier. The main effect of including an RS is then manifested in the resulting channel matrix $\boldsymbol{H}$, which can now be described by

$$\boldsymbol{H} = \boldsymbol{H}_0 + \boldsymbol{H}_1 \boldsymbol{\Theta} \boldsymbol{H}_2, \tag{4.1}$$

where, assuming the RS has a total of N reconfigurable elements, we have that:

- $\boldsymbol{H}_0$ is the $M \times K$ direct channel matrix between the UEs and the BS antennas.
- $\boldsymbol{H}_1$ is the $M \times N$ channel matrix between the RS elements and the BS antennas.
- $\boldsymbol{H}_2$ is the $N \times K$ channel matrix between the UEs and the RS elements.
- $\boldsymbol{\Theta}$ is the $N \times N$ reflection matrix associated to the controllable interaction of the RS elements with the incoming waves.

Fig. 4.1 illustrates the scenario under consideration. The main challenge in this framework is to find useful ways to exploit the controllability of the channel when using the RS. This translates into finding the RS configuration such that the resulting reflection matrix $\boldsymbol{\Theta}$ leads to a channel matrix $\boldsymbol{H}$ attaining gains in some metric—e.g., received power, sum rate, energy efficiency.

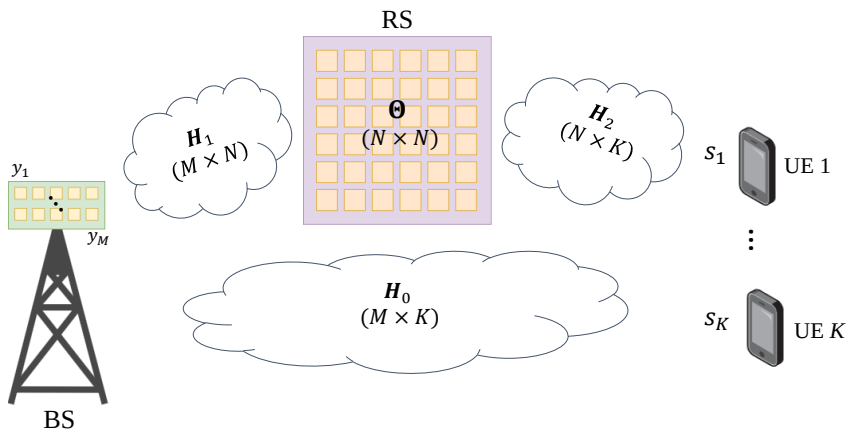

Figure 4.1: UL MU-MIMO scenario employing a square $\sqrt{N} \times \sqrt{N}$ RS.

The way in which the RS is implemented has major impact on the restrictions for the reflection matrix $\boldsymbol{\Theta}$ that should be considered. One of the key requirements for RS is to offer a cost- and energy-efficient solution. Thus, a compromise should be found between the capabilities of these surfaces, and their energy consumption together with their implementation costs. The main RS technology that has been considered in the literature is RIS, which corresponds to an RS whose elements have only phase-shifting capabilities and

which have no interaction with one another. This leads to the common RIS model for the reflection matrix given by

$$\boldsymbol{\Theta}_{\text{RIS}} = \text{diag}\big(\exp(\jmath\theta_1), \ldots, \exp(\jmath\theta_N)\big), \tag{4.2}$$

where $\theta_n \in [0, 2\pi)$ corresponds to the phase-shift applied at the nth RIS element. This simple model is considered in many of the results presented in the following section for demonstrating the potential of RIS technology.

A Note on Practical Implementations

Although in the general RIS model, the phase shifts that can be applied have no restrictions whatsoever, in real systems, the RIS elements would be controlled through digital signals. Thus, the resolution of the DACs will limit the set of phase-shifts that can be applied in practice. Furthermore, the lower the resolution of these DACs the lower their cost and energy consumption, so initial RIS prototypes typically employ low resolution DACs, meaning that each θ_n may only be selected from a small finite set of phase-shift values. For example, in [78], the authors implement a RIS with 1 bit configuration—i.e., each reflecting element can only select 2 phase-shift values—while in [79] they use 2 bit configuration—i.e., each reflecting element can select among 4 phase-shift values. However, for a large number N of RIS elements this may still allow a huge number of possible reflection matrices—e.g., 2^N with $N = 1100$ in [78], or 4^N with $N = 256$ in [79]. Thus, a great part of the benefits from RIS technology may still be exploited through these practical implementations, while the cost and energy-consumption may be kept low. For example, [78] can achieve beamforming gains of 27 dB with an impressively low power consumption of 1 W, while [79] achieves 21.7 dB gain with a considerably higher power consumption of 153 W.

Another thing to keep in mind is that, since practical implementations rely on devices like varactor diodes—which offer capacitance configurability—the reflection coefficients may also have spurious amplitude variability. Furthermore, these technologies typically have wide-band operation—i.e., with further spurious frequency variability—so a single-subcarrier analysis for these systems may not be fully accurate. For example, considering frequency selective channels, optimal configuration of the RIS at one frequency sub-band may lead to far-from-optimal performance at other sub-bands. Nevertheless, RS technology is still in an initial research stage, and we believe that a thorough analysis of the implementation trade-offs for these surfaces should still be addressed. Thus, we will focus our analysis in simplified narowband models like the one described in Fig. 4.1, and where a RIS reflection matrix may be described through (4.2).

4.2 Reconfigurable Intelligent Surface

The recent years have seen a colossal increase in the number of research publications dealing with RIS technology. This trend is still ongoing, with most conferences in the field of communications reserving even special tracks for this technology. Thus, it becomes especially challenging to summarize these results in a thesis section, which is getting outdated during the time it is being written. In this section, we will try to summarize a small part of the RIS results from literature which may be helpful for understanding the motivation of some of the research contributions included in this thesis.

4.2.1 Power Scaling Laws

One of the most clear advantages of RIS is that it allows concentrating the reflected power towards the desired directions. For example, in the UL MU-MIMO scenario, a RIS could be used to reflect the power of one UE towards the BS. This translates into a beamforming gain that allows for an increase in the received power (and the SNR) at the BS—or rather a reduction in the power which is lost in other directions.

In order to analyze the achievable beamforming gains when using RIS, let us focus on a SISO scenario where we have a single UE transmitting to a single-antenna BS—i.e., we can take the UL MU-MIMO scenario with $M = 1$, $K = 1$. We further assume that the direct channel is non-existent—e.g., it is blocked by an obstacle, leading to $h_0 = 0$. We can then express the received baseband narrowband signal as

$$\begin{aligned} y &= \boldsymbol{h}_1^{\mathrm{T}} \boldsymbol{\Theta}_{\mathbf{RIS}} \boldsymbol{h}_2 s + n \\ &= \sum_{n=1}^{N} h_{1n} h_{2n} \exp(\jmath\theta_n) s + n, \end{aligned} \tag{4.3}$$

where $\boldsymbol{h}_1 = [h_{11} \ \cdots \ h_{1N}]^{\mathrm{T}}$ $\boldsymbol{h}_2 = [h_{21} \ \cdots \ h_{2N}]^{\mathrm{T}}$ are the RIS-BS and UE-RIS channel vectors, respectively, s is the symbol transmitted by the UE with $\mathcal{E}\{|s|^2\} = E_s$, and $n \sim \mathcal{CN}(0, N_0)$ is AWGN. If we want to maximize the received power, and thus the SNR,[1] we should select the RIS phase-shift values such that the sum in (4.3) generates a constructive interference—i.e., all the elements are summed in-phase leading to a coherent combination. Since h_{1n} and h_{2n} may be arbitrary scalar complex numbers, we may express their product as

$$h_{1n} h_{2n} = |h_{1n}||h_{2n}| \exp(\jmath\phi_n), \tag{4.4}$$

[1] Note that, since the RIS is assumed to have no active amplification, the noise that may be originated at the RIS would arrive at the BS with negligible power.

where ϕ_n would correspond to the sum of the phases of h_{1n} and h_{2n}. Assuming that the RIS has access to the phase values ϕ_n of the cascaded channel, constructive interference can then be generated by selecting $\theta_n = \varphi - \phi_n$, where φ would be the output phase. Let us disregard, without loss of generality, the output phase by assuming $\varphi = 0$. The resulting received SNR is then given by

$$\rho = \frac{(\sum_{n=1}^{N} |h_{1n}||h_{2n}|)^2 E_s}{N_0}. \tag{4.5}$$

From (4.5), we can identify the beamforming gain achieved by the RIS with the term $(\sum_{n=1}^{N} |h_{1n}||h_{2n}|)^2$. This term corresponds to the square of a sum of N positive contributions—associated to the $|h_{1n}||h_{2n}|$ product terms—which, assuming these contributions are approximately independent of N, leads to the famous N^2 power scaling achieved with RIS. This scaling can be easily derived in closed form if we consider simple statistical models for the channel—e.g., IID Rayleigh fading as in [37]—and even if we consider LoS channels in the far-field—as shown by [59]. However, as we increase the size of the RIS, the product terms $|h_{1n}||h_{2n}|$ will eventually decrease since either the far-field assumption, and/or the isotropic scattering assumption, would start to lose validity.[2] This can be easily understood by the law of conservation of energy, since the N^2 power scaling in principle allows the power to go to infinity, but in reality we cannot receive more power than what was transmitted. For example, if we would cover all the walls, ceiling, and floor of a room with RIS elements spaced according to Nyquist sampling theory for electromagnetic fields—which leads to $\lambda/2$ spacing, as suggested by [19] for the LoS scenario, or [21] for the rich scattering scenario—we would be able to focus all the power transmitted from a UE to the 3D point where the BS antenna lies—i.e., reaching the limit of these beamforming gains. Thus, in this hypothetical scenario, adding more RIS elements would not increase the received power any further. A thorough analysis of these scaling laws in LoS scenarios can be found in [59], which offers a practical comparison between different methods to achieve these beamforming gains.

4.2.2 Improved Multiplexing Performance

As we have mentioned earlier, beamforming gains can only achieve a logarithmic increase in capacity, since they only give a polynomial SNR increase. On the other hand, MU-MIMO has already been successful at exploiting the spatial dimensions to multiplex UEs under rich multipath propagation, leading to linear gains in capacity associated to the multiplexing gain. However, in

[2] We may further note that the terms $|h_{1n}||h_{2n}|$ are subject to a squared path-loss, which, in general, leads to an overall path-loss much greater than having a single path with the same total length.

MU-MIMO scenarios with scarce multipath propagation—which may become more common as we go towards higher frequency bands [16]–[18]—the number of spatial modes may be insufficient for multiplexing UEs located close to each other [80]—i.e., the channel matrix $\boldsymbol{H}$ may be rank deficient. These issues become even more concerning in point-to-point MIMO scenarios, where the Tx and Rx antennas are usually co-located. In these cases, RIS may be a helpful tool, since it may offer some controllable multipath components which could allow for an increase in the number of spatial modes of the resulting $\boldsymbol{H}$.

Although a major part of the research on RIS focuses on exploiting its beamforming gains, we can also find in the literature a reasonable number of papers focusing on the use of RIS for improved multiplexing performance. For example, in [63] a RIS-based solution is proposed to turn a far-field LoS single-user MIMO channel—i.e., where the channel matrix is of rank 1—into a MIMO channel with two effective spatial modes—i.e., where the channel matrix is of rank 2 with a reasonable condition number. In this line of work, we can also find papers like [81] or [82], which also consider far-field LoS MIMO scenarios, but with the presence of several RISs whose configuration is optimized according to some rate-maximization problem which leads to increased multiplexing performance. Some important weaknesses of these methods are that they are hugely dependent on the considered scenario—e.g., pure LoS, fixed positions of RIS, Tx, and Rx—and that they rely on full-CSI knowledge—i.e., including the channels to and from the RIS elements—which is still a major challenge in RIS scenarios [37].

As a general comment, if we optimize the RIS configuration according to some capacity based metric—e.g., user sum-rate—the solution may attain a desirable compromise between beamforming and multiplexing performance, so works like [60], [62] may also lead to multiplexing improvements if they were applied over ill-conditioned channels at high-SNR regimes. However, much of these results also face the weaknesses of impractical CSI knowledge and scenario-specific assumptions.

4.2.3 RIS as Passive Transmitter

Apart from considering RIS as a passive reflector to improve the propagation channel between a Tx and an Rx, we can also consider the use of RIS as a cost- and energy-efficient passive transmitter. The idea is that incoming waves can be modulated through the controllable reflection at the RIS, which may embed its own data in the reflected waves. This corresponds to a fundamentally different use case than what was considered in the previous sections, since now

the RIS would act as a pseudo-BS technology.[3] Furthermore, such use case for RIS can be included within the general topic of symbiotic radio [83], which considers the use of general backscatter devices—such as RIS—to passively modulate information on the scattered waves.

There is a fair amount of publications dealing with how to configure RIS to embed information into the reflected waves. In [84], index modulation is defined as a method to embed information into both unmodulated and modulated carrier signals reflected at the RIS. We can also find practical implementations of RIS modulation such as [85], which employs a 256-element RIS—implemented through varactor diodes connected to DACs—to perform 8-PSK modulation on a pure RF tone transmitted towards the RIS. The survey from [37] includes further examples of these techniques.

There is also a substantial amount of work dealing with how to simultaneously employ RIS for improving the propagation channel between a Tx and an Rx, while embedding its own information. For example, [86] presents a solution for configuring RIS to achieve beamforming gains in a communication link between a multi-antenna BS and a UE, while sending information from the RIS to the BS by turning on/off some of its reconfigurable elements—which can be done by, e.g., pointing their reflection away from the BS. However, turning off elements would correspond to lowering the number of RIS elements, thus such solution may incur a residual loss in beamforming performance. In [87], the authors study bounds on the capacity when employing RIS for simultaneous beamforming and information transmission. In this case, the RIS information is embedded by selecting from a predefined constellation of reflection matrices which should be optimized for beamforming performance. We can also find a number of papers dealing with similar problems—e.g., [88]–[90]—for a survey on these solutions the reader may refer to [91]. Many of these solutions still face important challenges since they are generally tailored to single-UE scenarios, the RIS-information embedding usually comes at the cost of beamforming performance, and they usually rely on impractical CSI knowledge. Part of the scope of this thesis is to study RS solutions for simultaneously embedding information while improving the multiplexing performance in general MU-MIMO frameworks, which, to the best of our knowledge, has not yet been considered in the available literature.

[3]The reader may argue that such use case of RIS could be included within our definition of LIS since it would be employed as a BS. However, this application of RIS would still require of external wave generators, while we envision LIS as a self-contained BS technology. An RIS together with a wave generator could however be seen as an implementation of LIS.

4.3 Channel Orthogonalization with RS

As we already discussed in Chapter 2, orthogonal channels are extremely desirable channels in MU-MIMO frameworks since they allow for perfect multiplexing of UEs at reduced complexity. Thus, we believe that the problem of employing RS technology for orthogonalizing MU-MIMO channels is of fundamental importance. If we restrict ourselves to the RIS model from (4.2) we can immediately note that achieving a perfectly orthogonal channel—as described by (2.20)—seems out of reach, except in very specific scenarios—e.g., under certain favorable combinations of $\boldsymbol{H}_0$, $\boldsymbol{H}_1$ and $\boldsymbol{H}_2$, or in asymptotic regimes with certain statistical channel models. However, we can formulate optimization problems to find the RIS configuration maximizing some metric for orthogonality. For example, we could use the condition number $\kappa(\cdot)$ of the resulting channel matrix as a metric for orthogonality, which corresponds to the ratio between its maximum and minimum singular values $\kappa(\cdot) = \sigma_{\max}(\cdot)/\sigma_{\min}(\cdot)$—i.e., $\kappa(\cdot) \geq 1$ with equality only for orthogonal matrices as the one from (2.20). We would then have to solve

$$\min_{\theta_1,\ldots,\theta_N} \kappa(\boldsymbol{H}_0 + \boldsymbol{H}_1 \boldsymbol{\Theta}_{\text{RIS}} \boldsymbol{H}_2). \tag{4.6}$$

Finding a closed-form solution for such problem seems highly non-trivial, so numerical optimization tools may be required. Moreover, performing a maximization like (4.6) may lead to impractical solutions—e.g., where the resulting SNR is extremely low—so it may further be necessary to include extra constraints to achieve practical solutions. On the other hand, as in many of the RIS optimization problems from the literature, we may require full knowledge of all the involved channels, which is an extremely impractical constraint [37].

Given the limited potential of the common RIS framework for achieving perfectly orthogonal channels, we will also consider extended RS models for this task. Specifically, we will consider an extended RS technology which can perform controlled amplitude-shifting apart from the pure phase-shifting. We will employ the term ARIS for such technology, whose reflection matrix can be modeled as

$$\boldsymbol{\Theta}_{\text{ARIS}} = \text{diag}\left(\alpha_1, \ldots, \alpha_N\right), \quad \alpha_i \in \mathbb{C} \ \ \forall i. \tag{4.7}$$

The reader may argue that considering such an RS system would require to add amplification to a RIS, which has already been proposed in the literature—e.g., [92], [93]. However, we will consider power restrictions so that amplification is not strictly required, since this would lead to the appearance of extra correlated noise from the amplified reflection.

We will also consider another extended RS technology which may include interaction between different reconfigurable elements. We will use the term FRIS for such RS, whose reflection matrix may now be arbitrarily selected,

leading to

$$\boldsymbol{\Theta}_{\text{FRIS}} \in \mathbb{C}^{N \times N}. \tag{4.8}$$

Again, we will consider specific power restrictions on the FRIS reflection matrices such that amplification is not strictly needed.

An important reason for considering these two extended RS technologies—and not only one of them—is to take some initial steps towards a characterization of the trade-offs between RS capabilities and, e.g., performance, efficiency, required size, etc. However, the reader may also take our results as upper limits for the potential of RIS-aided systems. In this thesis, we will not have a deep discussion about the implementation issues of these RS technologies. In principle, ARIS could be implemented through adjustable impedance networks in a similar fashion as RIS, since these networks also have a predictable effect on the amplitude, which may be exploited. The main issue would then be the wideband reconfigurability of such systems, which may lead to a loss in channel orthogonality when considering subcarriers that are beyond the coherence banbdwidth from the subcarrier at which the ARIS was configured. Thus, for perfect exploitation of its benefits, we may require to perform per-subcarrier (or at least per-coherence-band) processing, which means that fully-digital architectures may be of interest, thus increasing cost and energy consumption—note that this problem also arises in the common RIS framework assuming (4.2). As of FRIS, we can also think of analog combiners using vector modulators as in [94], but we would face a similar problem when per-subcarrier (or per-coherence-band) processing is required. Instead, fully-digital implementations may be considered by, e.g., identifying FRIS with inactive APs having a low-power operation mode. These are just preliminary ideas, but our main focus will be on showing the possibilities of such models, which, as we will see, allow for perfect channel orthogonalization while relying on reasonably-efficient channel estimation methods.

4.4 Thesis Contributions

4.4.1 Paper V

In this paper, we study the use of RS technology to perform channel orthogonalization in MU-MIMO, thus taking an important step in characterizing the multiplexing performance of such surfaces. We introduce the concepts of ARIS and FRIS and derive the configuration that should be applied at these RSs for achieving perfectly orthogonal channels. We also present pragmatic methods for channel estimation that enable effective application of this configuration to ARIS and FRIS. Furthermore, we characterize the minimum power that these surfaces should apply for achieving channel orthogonalization. The results show that, in most practical scenarios, these surfaces can potentially achieve channel

orthogonalization without the need of amplification, thus offering an energy-efficient solution to effectively improve multiplexing performance in general MU-MIMO scenarios.

4.4.2 Paper VII

This paper builds upon the results from **Paper V** by considering ARIS and FRIS for orthogonalizing MU-MIMO channels. However, in this work we include the extra consideration that the RS can embed its own information in the orthogonal channels that are generated. We characterize the achievable bounds of such a communication framework, and study the high-SNR regime to obtain the resulting multiplexing performance. The results show that, by including this simultaneous RS-BS communication link, we can potentially exploit without extra resources the remaining spatial degrees of freedom associated to the excess of BS antennas (with respect to UEs) in general MU-MIMO frameworks.

Chapter 5

Conclusions and Future Work

5.1 Conclusions

In this thesis, we have studied the trade-offs and opportunities that arise when scaling up multi-antenna systems. The main conclusions of this thesis can be summarized as follows:

- We have presented novel algorithms for decentralized processing exploiting the structure of LIS panels.
- We have defined a fundamental trade-off between the level of decentralization of a system and the complexity of the decentralized processing in large multi-antenna systems.
- We have defined and studied a matrix decomposition which is especially useful in the analysis of multi-antenna systems with an arbitrary level of decentralization.
- We have generalized the previously mentioned trade-off for practical scenarios, e.g., considering cell-free massive MIMO scenarios, or considering the restriction of having practical combining modules.
- We have showed that, even when considering coarse quantization, reducing the dimension of the vectors to be transmitted to a CPU translates to a reduction of the data that has to be sent to said CPU without sacrificing data rates.

- We have presented two novel proposals for RS technologies, and proved that these can achieve perfectly orthogonal propagation channels for effective multiplexing of UEs in the spatial domain without the need of amplification.
- We have presented practical channel estimation for the defined RS technologies so that the BS can arbitrarily select the desired propagation channel and configure the RS accordingly.
- We have showed how the proposed RS technologies can be used to exploit additional multiplexing gains, as compared to common large multi-antenna systems, by embedding their own information in the adjusted propagation channel.

Altogether, the findings of this thesis show that, if hardware development goes along, we may be able to implement a BS with an arbitrary level of decentralization such that the decentralized processing may be applied through reduced interaction with a CPU. Moreover, with the help of RS technology, this BS may effectively multiplex a set of UEs through an orthogonal channel—i.e., leading to fair UE rate allocation at reduced complexity—and the RS may further communicate with the BS without the need of extra resources.

5.2 Future Work

The results presented in this thesis have opened a number research directions where we can still find a large number of interesting problems and unanswered questions. We may classify the main research directions associated to this thesis into: WAX decomposition results and applications, decentralized schemes, quantization effects in decentralized processing, RS technology—as well as combinations of the previous. We will next present a list with some ideas that may be considered for extending our work in these directions.

- An extension of **Paper III** may be considered by studying the degradation of the WAX decomposition trade-off arising from general rank deficiencies in the channel matrix, instead of just blocks of zeros.
- The WAX decomposition trade-offs have been studied independently in the cases of sparse combining module and sparse channel matrix. A characterization of the WAX decomposition trade-offs where sparse combining modules are simultaneously considered with sparse channel matrices still remains an open question.
- A complete characterization of the information-loss in the regime where the WAX decomposition trade-off is not fulfilled also constitutes another interesting research problem.

- The current results on architectures with arbitrary level of decentralization only include decentralized schemes for computing the decentralized filters achieving information-lossless processing. However, it may be interesting to explore specific interference cancellation schemes in the WAX decomposition framework, e.g., by defining what processing should be further applied at the CPU and how to achieve such processing with reduced interconnection bandwidth.

- It may also be interesting to extend the results from **Paper I** to other topologies. For example, if we assume we have distributed APs instead of antennas in a LIS panel, it may be interesting to consider hexagonal arrangements.

- The work on quantization effects in decentralized processing from **Paper IV** considers a naive model for information-lossless transformations that lead to closed-form analitical results. We may extend this model by considering an extra unitary transformation on the uncorrelated post-processed vector, which may be optimized for maximum achievable rates using similar tools as those employed in **Paper V**.

- We may also extend the work on quantization effects in decentralized processing by combining it with the WAX decomposition results to characterize the trade-off between level of decentralization and decentralized processing complexity when quantization comes into play.

- Regarding our work on RS, future work may aim at providing implementation proposals for ARIS and FRIS. This may also include extending our results to characterize the losses in realistic scenarios—e.g., in the presence of hardware impairments or imperfect CSI.

- It may also be interesting to try to make a proper characterization of the trade-off between RS capabilities/overall performance and energy consumption/implementation cost.

- Another interesting direction would be to combine the work on RS with the work on WAX decomposition. For example, having an orthogonal channel may simplify the computation of the processing performed at the decentralized modules, or at the CPU.

- In **Paper VII** we perform an information-theoretic characterization of the achievable rates when the studied RS technologies are also embedding information on the channel. However, it may be interesting to study specific transmission schemes in this framework that can potentially be implemented in real systems.

References

[1] R. H. Roy III and B. Ottersten, *Spatial division multiple access wireless communication systems*, US Patent 5,515,378, 1996.

[2] A. J. Paulraj and T. Kailath, *Increasing capacity in wireless broadcast systems using distributed transmission/directional reception (dtdr)*, US Patent 5,345,599, 1994.

[3] A. Kucar, "Mobile radio: An overview," *IEEE Communications Magazine*, vol. 29, no. 11, pp. 72–85, 1991.

[4] W. Lee, "Overview of cellular CDMA," *IEEE Transactions on Vehicular Technology*, vol. 40, no. 2, pp. 291–302, 1991.

[5] A. Paulraj, R. Nabar, and D. Gore, *Introduction to Space-Time Wireless Communications*, 1st. USA: Cambridge University Press, 2008.

[6] R. W. Heath Jr. and A. Lozano, *Foundations of MIMO Communication*. Cambridge University Press, 2018.

[7] T. M. Cover and J. A. Thomas, *Elements of Information Theory (Wiley Series in Telecommunications and Signal Processing)*. USA: Wiley-Interscience, 2006.

[8] A. Lozano and N. Jindal, "Transmit diversity vs. spatial multiplexing in modern MIMO systems," *IEEE Transactions on Wireless Communications*, vol. 9, no. 1, pp. 186–197, 2010.

[9] P. Viswanath and D. Tse, "Sum capacity of the vector gaussian broadcast channel and uplink–downlink duality," *IEEE Transactions on Information Theory*, vol. 49, no. 8, pp. 1912–1921, 2003.

[10] G. Caire and S. Shamai, "On the achievable throughput of a multiantenna gaussian broadcast channel," *IEEE Transactions on Information Theory*, vol. 49, no. 7, pp. 1691–1706, 2003.

[11] T. L. Marzetta, "Noncooperative cellular wireless with unlimited numbers of base station antennas," *IEEE Transactions on Wireless Communications*, vol. 9, no. 11, pp. 3590–3600, 2010.

[12] F. Rusek, D. Persson, B. K. Lau, *et al.*, "Scaling up MIMO: Opportunities and challenges with very large arrays," *IEEE Signal Processing Magazine*, vol. 30, no. 1, pp. 40–60, 2013.

[13] E. G. Larsson, O. Edfors, F. Tufvesson, and T. L. Marzetta, "Massive MIMO for next generation wireless systems," *IEEE Communications Magazine*, vol. 52, no. 2, pp. 186–195, 2014.

[14] H. Q. Ngo, E. G. Larsson, and T. L. Marzetta, "Energy and spectral efficiency of very large multiuser MIMO systems," *IEEE Transactions on Communications*, vol. 61, no. 4, pp. 1436–1449, 2013.

[15] E. Björnson, L. Sanguinetti, H. Wymeersch, J. Hoydis, and T. L. Marzetta, "Massive MIMO is a reality - What is next? Five promising research directions for antenna arrays," 2019. arXiv: 1902.07678.

[16] M. Shafi, J. Zhang, H. Tataria, *et al.*, "Microwave vs. millimeter-wave propagation channels: Key differences and impact on 5G cellular systems," *IEEE Communications Magazine*, vol. 56, no. 12, pp. 14–20, 2018.

[17] S. Priebe and T. Kurner, "Stochastic modeling of THz indoor radio channels," *IEEE Transactions on Wireless Communications*, vol. 12, no. 9, pp. 4445–4455, 2013.

[18] C. Gentile, P. B. Papazian, N. Golmie, *et al.*, "Millimeter-wave channel measurement and modeling: A NIST perspective," *IEEE Communications Magazine*, vol. 56, no. 12, pp. 30–37, 2018.

[19] S. Hu, F. Rusek, and O. Edfors, "Beyond massive MIMO: The potential of data transmission with large intelligent surfaces," *IEEE Transactions on Signal Processing*, vol. 66, no. 10, pp. 2746–2758, 2018.

[20] S. Hu, F. Rusek, and O. Edfors, "Beyond massive MIMO: The potential of positioning with large intelligent surfaces," *IEEE Transactions on Signal Processing*, vol. 66, no. 7, pp. 1761–1774, 2018.

[21] A. Pizzo, A. d. J. Torres, L. Sanguinetti, and T. L. Marzetta, "Nyquist sampling and degrees of freedom of electromagnetic fields," *IEEE Transactions on Signal Processing*, vol. 70, pp. 3935–3947, 2022.

[22] S. Hu, F. Rusek, and O. Edfors, "Capacity degradation with modeling hardware impairment in large intelligent surface," in *2018 IEEE Global Communications Conference (GLOBECOM)*, 2018, pp. 1–6.

[23] A. Pereira, F. Rusek, M. Gomes, and R. Dinis, "Deployment strategies for large intelligent surfaces," *IEEE Access*, vol. 10, pp. 61 753–61 768, 2022.

[24] M. Jung, W. Saad, Y. Jang, G. Kong, and S. Choi, "Performance analysis of large intelligent surfaces (LISs): Asymptotic data rate and channel hardening effects," *IEEE Transactions on Wireless Communications*, vol. 19, no. 3, pp. 2052–2065, 2020.

[25] C. Huang, A. Zappone, G. C. Alexandropoulos, M. Debbah, and C. Yuen, "Large intelligent surfaces for energy efficiency in wireless communication," 2018. arXiv: 1810.06934.

[26] Y. Han, W. Tang, S. Jin, C.-K. Wen, and X. Ma, "Large intelligent surface-assisted wireless communication exploiting statistical CSI," *IEEE Transactions on Vehicular Technology*, vol. 68, no. 8, pp. 8238–8242, 2019.

[27] E. Basar, "Transmission through large intelligent surfaces: A new frontier in wireless communications," in *2019 European Conference on Networks and Communications (EuCNC)*, 2019, pp. 112–117.

[28] A. Pizzo, T. L. Marzetta, and L. Sanguinetti, "Spatially-stationary model for holographic MIMO small-scale fading," *IEEE Journal on Selected Areas in Communications*, vol. 38, no. 9, pp. 1964–1979, 2020.

[29] E. Björnson, L. Sanguinetti, H. Wymeersch, J. Hoydis, and T. L. Marzetta, "Massive MIMO is a reality—what is next?: Five promising research directions for antenna arrays," *Digital Signal Processing*, vol. 94, pp. 3–20, 2019, Special Issue on Source Localization in Massive MIMO.

[30] E. D. Carvalho, A. Ali, A. Amiri, M. Angjelichinoski, and R. W. Heath, "Non-stationarities in extra-large-scale massive MIMO," *IEEE Wireless Communications*, vol. 27, no. 4, pp. 74–80, 2020.

[31] H. Q. Ngo, A. Ashikhmin, H. Yang, E. G. Larsson, and T. L. Marzetta, "Cell-free massive MIMO versus small cells," *IEEE Transactions on Wireless Communications*, vol. 16, no. 3, pp. 1834–1850, 2017.

[32] *Coordinated Multi-Point in Mobile Communications: From Theory to Practice*. Cambridge University Press, 2011.

[33] U. Madhow, D. R. Brown, S. Dasgupta, and R. Mudumbai, "Distributed massive MIMO: Algorithms, architectures and concept systems," in *2014 Information Theory and Applications Workshop (ITA)*, 2014, pp. 1–7.

[34] S. Venkatesan, A. Lozano, and R. Valenzuela, "Network MIMO: Overcoming intercell interference in indoor wireless systems," in *2007 Conference Record of the Forty-First Asilomar Conference on Signals, Systems and Computers*, 2007, pp. 83–87.

[35] C. Huang, A. Zappone, G. C. Alexandropoulos, M. Debbah, and C. Yuen, "Reconfigurable intelligent surfaces for energy efficiency in wireless communication," *IEEE Transactions on Wireless Communications*, vol. 18, no. 8, pp. 4157–4170, 2019.

[36] Y. Liu, X. Liu, X. Mu, *et al.*, "Reconfigurable intelligent surfaces: Principles and opportunities," *IEEE Communications Surveys & Tutorials*, vol. 23, no. 3, pp. 1546–1577, 2021.

[37] E. Basar, M. Di Renzo, J. De Rosny, M. Debbah, M.-S. Alouini, and R. Zhang, "Wireless communications through reconfigurable intelligent surfaces," *IEEE Access*, vol. 7, pp. 116 753–116 773, 2019.

[38] W. Saad, M. Bennis, and M. Chen, "A vision of 6G wireless systems: Applications, trends, technologies, and open research problems," *IEEE Network*, vol. 34, no. 3, pp. 134–142, 2020.

[39] M. Z. Chowdhury, M. Shahjalal, S. Ahmed, and Y. M. Jang, "6G wireless communication systems: Applications, requirements, technologies, challenges, and research directions," *IEEE Open Journal of the Communications Society*, vol. 1, pp. 957–975, 2020.

[40] W. Tang, J. Y. Dai, M. Chen, *et al.*, "Programmable metasurface-based RF chain-free 8PSK wireless transmitter," *Electronics Letters*, vol. 55, no. 7, pp. 417–420, 2019. eprint: `https://ietresearch.onlinelibrary.wiley.com/doi/pdf/10.1049/el.2019.0400`.

[41] W. Yan, X. Yuan, and X. Kuai, "Passive beamforming and information transfer via large intelligent surface," *IEEE Wireless Communications Letters*, vol. 9, no. 4, pp. 533–537, 2020.

[42] C. Huang, S. Hu, G. C. Alexandropoulos, *et al.*, "Holographic MIMO surfaces for 6G wireless networks: Opportunities, challenges, and trends," *IEEE Wireless Communications*, vol. 27, no. 5, pp. 118–125, 2020.

[43] C. Liaskos, S. Nie, A. Tsioliaridou, A. Pitsillides, S. Ioannidis, and I. Akyildiz, "A new wireless communication paradigm through software-controlled metasurfaces," *IEEE Communications Magazine*, vol. 56, no. 9, pp. 162–169, 2018.

[44] Z. Zhang, L. Dai, X. Chen, *et al.*, "Active RIS vs. passive RIS: Which will prevail in 6G?" *IEEE Transactions on Communications*, pp. 1–1, 2022.

[45] C. Shepard *et al.*, "Argos: Practical many-antenna base stations," in *Proceedings of the 18th Annual International Conference on Mobile Computing and Networking (Mobicom)*, Istanbul, Turkey, 2012, pp. 53–64.

[46] S. Malkowsky *et al.*, "The world's first real-time testbed for massive MIMO: Design, implementation, and validation," *IEEE Access*, vol. 5, pp. 9073–9088, 2017.

[47] K. Li, R. R. Sharan, Y. Chen, T. Goldstein, J. R. Cavallaro, and C. Studer, "Decentralized baseband processing for massive MU-MIMO systems," *IEEE Journal on Emerging and Selected Topics in Circuits and Systems*, vol. 7, no. 4, pp. 491–507, 2017.

[48] E. Bertilsson, O. Gustafsson, and E. G. Larsson, "A scalable architecture for massive MIMO base stations using distributed processing," in *2016 50th Asilomar Conference on Signals, Systems and Computers*, 2016, pp. 864–868.

[49] M. Sarajlic, F. Rusek, J. R. Sanchez, L. Liu, and O. Edfors, "Fully decentralized approximate zero-forcing precoding for massive MIMO systems," *IEEE Wireless Communications Letters*, pp. 1–1, 2019.

[50] C. Jeon, K. Li, J. R. Cavallaro, and C. Studer, "Decentralized equalization with feedforward architectures for massive MU-MIMO," *IEEE Transactions on Signal Processing*, vol. 67, no. 17, pp. 4418–4432, 2019.

[51] F. Wiffen, W. H. Chin, and A. Doufexi, "Distributed dimension reduction for distributed massive MIMO C-RAN with finite fronthaul capacity," in *2021 55th Asilomar Conference on Signals, Systems, and Computers*, 2021, pp. 1228–1236.

[52] K. Li, J. McNaney, C. Tarver, *et al.*, "Design trade-offs for decentralized baseband processing in massive MU-MIMO systems," in *2019 53rd Asilomar Conference on Signals, Systems, and Computers*, 2019, pp. 906–912.

[53] J. R. Sánchez, J. Vidal Alegría, and F. Rusek, "Decentralized massive MIMO systems: Is there anything to be discussed?" In *2019 IEEE International Symposium on Information Theory (ISIT)*, 2019, pp. 787–791.

[54] J. Rodríguez Sánchez, F. Rusek, O. Edfors, M. Sarajlić, and L. Liu, "Decentralized massive MIMO processing exploring Daisy-chain architecture and recursive algorithms," *IEEE Transactions on Signal Processing*, vol. 68, pp. 687–700, 2020.

[55] Z. Zhang, H. Li, Y. Dong, X. Wang, and X. Dai, "Decentralized signal detection via expectation propagation algorithm for uplink massive MIMO systems," *IEEE Transactions on Vehicular Technology*, pp. 1–1, 2020.

[56] A. Amiri, S. Rezaie, C. N. Manchón, and E. de Carvalho, "Distributed receiver processing for extra-large MIMO arrays: A message passing approach," *IEEE Transactions on Wireless Communications*, vol. 21, no. 4, pp. 2654–2667, 2022.

[57] E. Björnson and L. Sanguinetti, "Scalable cell-free massive MIMO systems," *IEEE Transactions on Communications*, vol. 68, no. 7, pp. 4247–4261, 2020.

[58] Q. Wu and R. Zhang, "Intelligent reflecting surface enhanced wireless network via joint active and passive beamforming," *IEEE Transactions on Wireless Communications*, vol. 18, no. 11, pp. 5394–5409, 2019.

[59] Q. Wu and R. Zhang, "Towards smart and reconfigurable environment: Intelligent reflecting surface aided wireless network," *IEEE Communications Magazine*, vol. 58, no. 1, pp. 106–112, 2020.

[60] H. Guo, Y.-C. Liang, J. Chen, and E. G. Larsson, "Weighted sum-rate maximization for reconfigurable intelligent surface aided wireless networks," *IEEE Transactions on Wireless Communications*, vol. 19, no. 5, pp. 3064–3076, 2020.

[61] E. Björnson, O. Özdogan, and E. G. Larsson, "Reconfigurable intelligent surfaces: Three myths and two critical questions," *IEEE Communications Magazine*, vol. 58, no. 12, pp. 90–96, 2020.

[62] Y. Zhang, C. Zhong, Z. Zhang, and W. Lu, "Sum rate optimization for two way communications with intelligent reflecting surface," *IEEE Communications Letters*, vol. 24, no. 5, pp. 1090–1094, 2020.

[63] O. Ozdogan, E. Björnson, and E. G. Larsson, "Using intelligent reflecting surfaces for rank improvement in MIMO communications," in *ICASSP 2020 - 2020 IEEE International Conference on Acoustics, Speech and Signal Processing (ICASSP)*, 2020, pp. 9160–9164.

[64] T. L. Marzetta, E. G. Larsson, H. Yang, and H. Q. Ngo, *Fundamentals of Massive MIMO*. Cambridge University Press, 2016.

[65] E. Björnson, J. Hoydis, and L. Sanguinetti, "Massive MIMO networks: Spectral, energy, and hardware efficiency," *Foundations and Trends® in Signal Processing*, vol. 11, no. 3-4, pp. 154–655, 2017.

[66] J. Vieira, F. Rusek, O. Edfors, S. Malkowsky, L. Liu, and F. Tufvesson, "Reciprocity calibration for massive MIMO: Proposal, modeling, and validation," *IEEE Transactions on Wireless Communications*, vol. 16, no. 5, pp. 3042–3056, 2017.

[67] C. E. Shannon, "A mathematical theory of communication," *The Bell System Technical Journal*, vol. 27, no. 3, pp. 379–423, 1948.

[68] E. Telatar, "Capacity of multi-antenna gaussian channels," *European Transactions on Telecommunications*, vol. 10, no. 6, pp. 585–595, 1999. eprint: `https://onlinelibrary.wiley.com/doi/pdf/10.1002/ett.4460100604`.

[69] F. Rusek and D. Fertonani, "Bounds on the information rate of intersymbol interference channels based on mismatched receivers," *IEEE Transactions on Information Theory*, vol. 58, no. 3, pp. 1470–1482, 2012.

[70] A. Ganti, A. Lapidoth, and I. Telatar, "Mismatched decoding revisited: General alphabets, channels with memory, and the wide-band limit," *IEEE Transactions on Information Theory*, vol. 46, no. 7, pp. 2315–2328, 2000.

[71] D. Arnold, H.-A. Loeliger, P. Vontobel, A. Kavcic, and W. Zeng, "Simulation-based computation of information rates for channels with memory," *IEEE Transactions on Information Theory*, vol. 52, no. 8, pp. 3498–3508, 2006.

[72] G. Turin, "An introduction to matched filters," *IRE Transactions on Information Theory*, vol. 6, no. 3, pp. 311–329, 1960.

[73] R. H. Clarke, "A statistical theory of mobile-radio reception," *Bell System Technical Journal*, vol. 47, pp. 957–1000, 1968.

[74] L. Sanguinetti, E. Björnson, and J. Hoydis, "Toward massive MIMO 2.0: Understanding spatial correlation, interference suppression, and pilot contamination," *IEEE Transactions on Communications*, vol. 68, no. 1, pp. 232–257, 2020.

[75] S. Willhammar, J. Flordelis, L. Van Der Perre, and F. Tufvesson, "Channel hardening in massive MIMO: Model parameters and experimental assessment," *IEEE Open Journal of the Communications Society*, vol. 1, pp. 501–512, 2020.

[76] A. Amiri, C. N. Manchón, and E. de Carvalho, "Uncoordinated and decentralized processing in extra-large MIMO arrays," *IEEE Wireless Communications Letters*, vol. 11, no. 1, pp. 81–85, 2022.

[77] J. Rodríguez Sánchez, "Systems with massive number of antennas: Distributed approaches," English, Defence details Date: 2022-09-02 Time: 09:00 Place: Lecture Hall E:1406, building E, Ole Römers väg 3, Faculty of Engineering LTH, Lund University, Lund. External reviewer(s) Name: Ouitin, Francois Title: Prof. Affiliation: Université libre de Bruxelles, Belgium. —, Ph.D. dissertation, 2022.

[78] X. Pei, H. Yin, L. Tan, *et al.*, "RIS-aided wireless communications: Prototyping, adaptive beamforming, and indoor/outdoor field trials," *IEEE Transactions on Communications*, vol. 69, no. 12, pp. 8627–8640, 2021.

[79] L. Dai, B. Wang, M. Wang, *et al.*, "Reconfigurable intelligent surface-based wireless communications: Antenna design, prototyping, and experimental results," *IEEE Access*, vol. 8, pp. 45 913–45 923, 2020.

[80] J. Flordelis, F. Rusek, X. Gao, G. Dahman, O. Edfors, and F. Tufvesson, "Spatial separation of closely-located users in measured massive MIMO channels," *IEEE Access*, vol. 6, pp. 40 253–40 266, 2018.

[81] J. Choi, G. Kwon, and H. Park, "Multiple intelligent reflecting surfaces for capacity maximization in LOS MIMO systems," *IEEE Wireless Communications Letters*, vol. 10, no. 8, pp. 1727–1731, 2021.

[82] E. Ibrahim, R. Nilsson, and J. van de Beek, "Intelligent reflecting surfaces for MIMO communications in los environments," in *2021 IEEE Wireless Communications and Networking Conference (WCNC)*, 2021, pp. 1–6.

[83] R. Long, Y.-C. Liang, H. Guo, G. Yang, and R. Zhang, "Symbiotic radio: A new communication paradigm for passive internet of things," *IEEE Internet of Things Journal*, vol. 7, no. 2, pp. 1350–1363, 2020.

[84] E. Basar, "Reconfigurable intelligent surface-based index modulation: A new beyond MIMO paradigm for 6G," *IEEE Transactions on Communications*, vol. 68, no. 5, pp. 3187–3196, 2020.

[85] W. Tang, J. Y. Dai, M. Chen, *et al.*, "Programmable metasurface-based rf chain-free 8PSK wireless transmitter," *Electronics Letters*, vol. 55, no. 7, pp. 417–420, 2019. eprint: `https://ietresearch.onlinelibrary.wiley.com/doi/pdf/10.1049/el.2019.0400`.

[86] W. Yan, X. Yuan, and X. Kuai, "Passive beamforming and information transfer via large intelligent surface," *IEEE Wireless Communications Letters*, vol. 9, no. 4, pp. 533–537, 2020.

[87] J. Ye, S. Guo, S. Dang, B. Shihada, and M.-S. Alouini, "On the capacity of reconfigurable intelligent surface assisted MIMO symbiotic communications," *IEEE Transactions on Wireless Communications*, vol. 21, no. 3, pp. 1943–1959, 2022.

[88] J. Hu, Y.-C. Liang, and Y. Pei, "Reconfigurable intelligent surface enhanced multi-user miso symbiotic radio system," *IEEE Transactions on Communications*, vol. 69, no. 4, pp. 2359–2371, 2021.

[89] Y. Ma, R. Liu, M. Li, and Q. Liu, "Passive information transmission in intelligent reflecting surface aided miso systems," *IEEE Communications Letters*, vol. 24, no. 12, pp. 2951–2955, 2020.

[90] M. Wu, X. Lei, X. Zhou, Y. Xiao, X. Tang, and R. Q. Hu, "Reconfigurable intelligent surface assisted spatial modulation for symbiotic radio," *IEEE Transactions on Vehicular Technology*, vol. 70, no. 12, pp. 12 918–12 931, 2021.

[91] X. Lei, M. Wu, F. Zhou, X. Tang, R. Q. Hu, and P. Fan, "Reconfigurable intelligent surface-based symbiotic radio for 6G: Design, challenges, and opportunities," *IEEE Wireless Communications*, vol. 28, no. 5, pp. 210–216, 2021.

[92] R. A. Tasci, F. Kilinc, E. Basar, and G. C. Alexandropoulos, "A new RIS architecture with a single power amplifier: Energy efficiency and error performance analysis," *IEEE Access*, vol. 10, pp. 44 804–44 815, 2022.

[93] R. Long, Y.-C. Liang, Y. Pei, and E. G. Larsson, "Active reconfigurable intelligent surface-aided wireless communications," *IEEE Transactions on Wireless Communications*, vol. 20, no. 8, pp. 4962–4975, 2021.

[94] T. Zirtiloglu, N. Shlezinger, Y. C. Eldar, and R. Tugce Yazicigil, "Power-efficient hybrid MIMO receiver with task-specific beamforming using low-resolution ADCs," in *ICASSP 2022 - 2022 IEEE International Conference on Acoustics, Speech and Signal Processing (ICASSP)*, 2022, pp. 5338–5342.

Part II

Included Papers

Paper I

Decentralized Equalizer Construction for Large Intelligent Surfaces

In this paper we present fully decentralized methods for calculating an approximate ZF equalizer in a LIS. A LIS is intended for wireless communication and facilitates unprecedented MU-MIMO performance, far superior to that of Massive MIMO. Antenna modules in the grid connect to their neighbors to exchange messages of information needed for interference cancellation in a fully-decentralized fashion, making the system scalable. By a careful design of how the messages are routed, we show that the proposed method is able to cancel inter-user interference sufficiently well without any centralized coordination, opening the door for the realization of this type of structures.

©2019 IEEE. Reprinted, with permission, from
J. Vidal Alegría, J. Rodríguez Sánchez, F. Rusek, L. Liu, O. Edfors
"Decentralized Equalizer Construction for Large Intelligent Surfaces,"
in *IEEE Proc. VTC-fall 2019*, Honolulu, HI, USA, 2019, pp. 1-6.

1 Introduction

We envision a future where man-made surfaces are electromagnetically active enabling wireless communication, wireless charging and remote sensing [1]–[4]. These surfaces will be part of our daily lives, interacting with humans and making Internet of Things a reality by allowing the simultaneous connection of an unprecedented number of devices [5].

The concept of LIS has emerged recently as a natural evolution of Massive MIMO [6], where the BS consists of an inmense continuous radiating surface, instead of the discrete antenna array concept which has been dominant in MIMO communication since its conception.

As with antenna arrays, it is expected that each part of the surface is able to receive and transmit electromagnetic waves with a certain control, so the radiation can be focused tightly in 3D space with ultra-high resolution, opening a new world of possibilities for power-efficient communication, sensing, and positioning.

Even though LIS research is gaining momentum, it is believed that a continuous intelligent radiating surface is a theoretical model far from being implemented in the near future due to limitations of current technology. In reality, this would be implemented through a huge number of radiating elements, or antennas, distributed throughout a large surface. Nevertheless, as pointed out in [1], there is no practical difference between a continuous LIS and a grid of antennas, or discrete LIS, as the surface area grows, and provided that the antenna spacing is sufficiently dense.

Assuming that such large number of antennas are connected to a CPU, the equalizer formulation gets unhandleable due to the large computational and inter-connection requirements. To make this problem tractable, the surface is split into LIS-units, where each contains a lower, but still significant, number of antennas. We assume that any surface can be implemented by the connection of such units, making the system fully scalable. The optimal number of antennas in a LIS-unit depends on the number of users to be served, but this is outside the scope of this paper. We focus our research on one M-antenna LIS-unit serving K users.

Even though we simplify the original problem into a tractable one, each of these LIS-units may contain a very high number of antennas, which still presents multiple challenges from the control and inter-connection points of view. It is not only a challenge to connect all antennas to a CPU but also the high amount of data which is required to be collected by this node for baseband processing. At this point, there is a need for fully-decentralized architectures and algorithms which allow for high performance communications with low, or zero, central control.

One approach to alleviate this bottleneck is to obtain CSI locally and apply a MF at each antenna, which fits directly into the decentralized architecture

vision because exchange of CSI is not needed. However, one main application of these structures is spatial multiplexing of a high number of active users by using the same frequency-time resources (MU-MIMO), so some degree of interference-cancellation capabilities is a desirable requirement of any proposed method in order to exploit the promising capacity of the LIS concept. Unfortunately, MF does not always fulfill this requirement, thus, we look for decentralized approximate ZF schemes.

Initial work in this direction can be found in [7], followed by [8]–[10], among others. There are recent activities in this area in [11], [12], where antennas are connected by direct links forming a daisy chain. It has been shown that such a structure is able to achieve approximate ZF performance under IID channel conditions (i.e., zero mean circularly symmetric complex gaussian channel matrix entries) and perfect CSI with very low inter-connection requirements and fully decentralized detection/precoding processing. This approach, which is perfectly valid for Massive MIMO arrays, may not be enough for LIS-units, where the number of antennas can be several orders of magnitude more, with a subsequent increment in the processing latency. Reduction of such latency is one of the scopes of this research.

We propose two topologies, a 1D topology and a 2D topology, for implementing decentralized schemes suitable for a discrete LIS considering a fully-decentralized architecture. The main goal of this paper is to propose methods to construct an approximate-ZF equalizer for these topologies by message-passing between adjacent antenna nodes.

The outline of this paper is as follows. A system model is presented in Section 2. In Section 3 the 1D case is first introduced, where all antennas are connected forming a bidirectional chain as a baseline for our study, to then extend to the 2D case where simultaneous connection in vertical and horizontal directions are allowed. Results are presented in Section 4 and our conclusions are summarized in Section 5.

2 System Model

We consider the transmission from K single antenna users to a discrete LIS containing M antennas. The $M \times 1$ received vector at the LIS is

$$\boldsymbol{y} = \boldsymbol{H}\boldsymbol{x} + \boldsymbol{n}, \tag{1}$$

where $\boldsymbol{x}$ is the $K \times 1$ user data vector, $\boldsymbol{H} = [\boldsymbol{h}_1\, \boldsymbol{h}_2\, \ldots\, \boldsymbol{h}_M]^{\mathrm{T}}$ is the $M \times K$ channel matrix, and $\boldsymbol{n}$ is the noise vector with sample variance N_0. We assume perfect CSI knowledge at the receiver.

2.1 Linear Processing and Zero-Forcing

We limit our study to linear equalization so that the estimated user data vector is computed as

$$\widehat{\boldsymbol{x}} = \boldsymbol{W}\boldsymbol{y}, \tag{2}$$

where $\boldsymbol{W} = [\boldsymbol{w}_1\ \boldsymbol{w}_2\ \ldots\ \boldsymbol{w}_M]$ is a $K \times M$ matrix. If we focus on cancelling interference, which is close to optimum for large M, favorable propagation, and high SNR, $\boldsymbol{W}$ has to be chosen so that the equivalent channel is

$$\boldsymbol{W}\boldsymbol{H} = \boldsymbol{D}, \tag{3}$$

where $\boldsymbol{D}$ is a diagonal matrix. A typical approach is to take $\boldsymbol{D}$ as the $K \times K$ identity matrix $\boldsymbol{I}_K$, achieved by choosing $\boldsymbol{W}$ to be the ZF equalization matrix

$$\boldsymbol{W}_{\mathrm{ZF}} = (\boldsymbol{H}^{\mathrm{H}}\boldsymbol{H})^{-1}\boldsymbol{H}^{\mathrm{H}}. \tag{4}$$

However, the straightforward implementation of (4) essentially implies knowing the complete channel matrix at one node, which is not convenient for a LIS since it may extend over a huge area, and the interconnection bandwidth required for the transmission of the CSI would be extremely high due to the immense amount of antennas. Instead, it would be desirable to consider decentralized approaches in which the antennas of the LIS communicate with each other and independently compute their associated entries of the matrix $\boldsymbol{W}$, which should be then combined by having a large sum module inputting the contributions from all antennas. In this paper we research how to establish an approximation of the matrix $\boldsymbol{W}_{\mathrm{ZF}}$ in a decentralized way.

2.2 Fully-Decentralized Processing

Since we want to establish a decentralized approach to find an approximate $\boldsymbol{W}_{\mathrm{ZF}}$ for a LIS system, we consider the use of iterative algorithms as in [12]. We assume that each antenna is associated to a baseband processing unit that can perform simple matrix calculations. The antennas of the LIS work independently and in parallel, but they are connected to each other so that they share some limited amount of information. We consider two possible topologies for the interconnection between antennas.

1D Topology

In this case, all antennas are connected along a line. Therefore, each of the antennas of the LIS has a direct connection with two of its neighbors (except the first and last antennas, which only have one neighbor).

2D Topology

In this case, all antennas are connected in a grid which is related to their physical location in the LIS. Thus, each of the antennas has a direct connection with their four nearest neighbors, associated to the vertical and horizontal axes (except the ones in the sides and in the corners of the LIS, which are connected to two and three neighbors, respectively).

In Fig. 1 we provide an illustration of the layout of the two proposed topologies. Note that the 1D topology can be seen as a 2D topology in which some connections are removed. The 1D topology could be suitable for long linear arrays or for 2D arrays where one of the dimensions is much longer than the other one.

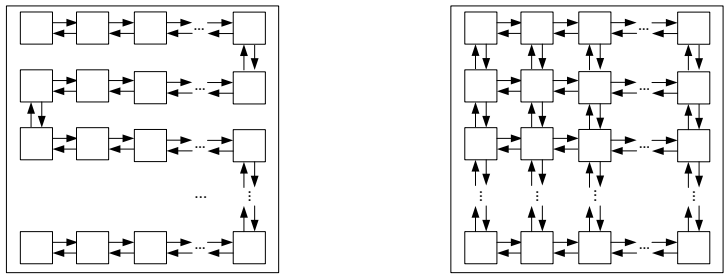

Figure 1: 1D (left) and 2D (right) topologies

3 Algorithms for Decentralized Interference Cancellation

Considering that all antennas of the LIS are identical, and that they work independently and in parallel, we can determine the operation of the LIS by focusing on one of its antennas. Fig. 2 shows a simplified schematic of a single LIS antenna. The antennas in the 1D topology, or the ones located at sides or corners, can discard the corresponding connections.

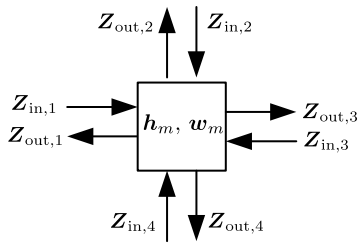

Figure 2: LIS antenna schematic.

Antenna m is in charge of computing its equalization vector $\boldsymbol{w}_m$, corresponding to column m of $\boldsymbol{W}$. Let us define a discrete time variable associated to the iteration number $n = 0, 1, 2, \ldots, N_{\text{it}}$. In every iteration, antenna m computes a new version of $\boldsymbol{w}_m$, $\boldsymbol{w}_m[n]$, using its channel vector $\boldsymbol{h}_m$, and the inputs arriving at the current iteration $\boldsymbol{Z}_{\text{in},\ell}[n]$, $\ell = 1, \ldots, L$, where L is the number of inputs/outputs for antenna m (in the 1D and 2D topologies it is in general 2 and 4, respectively). Also, the outputs $\boldsymbol{Z}_{\text{out},\ell}[n]$ are generated, which are sent to the neighbouring antennas so that they can use them as inputs in the next iteration. To fully define the operations, we must specify the precise generation of $\boldsymbol{w}_m$ and $\boldsymbol{Z}_{\text{out},\ell}$, and we do this next.

We would like to minimize the interference between users so, if we define the sum of the contributions from the other antennas to the equivalent channel at iteration n as

$$\boldsymbol{S}_m[n] = \sum_{i \neq m} \boldsymbol{w}_i[n] \boldsymbol{h}_i^{\mathrm{T}}, \tag{5}$$

we can define an optimization problem as in [12]:

$$\begin{array}{ll} \underset{\boldsymbol{w}_m[n+1]}{\text{minimize}} & \left\| \boldsymbol{I}_K - \boldsymbol{S}_m[n] - \boldsymbol{w}_m[n+1] \boldsymbol{h}_m^{\mathrm{T}} \right\| \\ \text{subject to} & \|\boldsymbol{w}_m[n+1]\| = \mu, \end{array} \tag{6}$$

where $\boldsymbol{I}_K$ is the desired equivalent channel without interference. The operator $\|\,.\,\|$ denotes Frobenius norm. This problem is solved in closed form by

$$\boldsymbol{w}_m^{\text{opt}}[n+1] = \mu \frac{(\boldsymbol{I}_K - \boldsymbol{S}_m[n]) \boldsymbol{h}_m^*}{\|(\boldsymbol{I}_K - \boldsymbol{S}_m[n]) \boldsymbol{h}_m^*\|}. \tag{7}$$

Note that in this paper the optimization problem (6) is tackled using parallel iterative computations of the equalization vectors at the different antennas instead of using a sequential daisy chain structure as in [12].

From this point on, we assume that (7) is used for computing $\boldsymbol{w}_m[n+1]$ in every iteration unless otherwise specified. However, with the limitations of the earlier defined topologies, it is not possible to obtain the whole sum $\boldsymbol{S}_m$ at antenna m. The main reason is that new equalization vectors are being calculated at every antenna of the LIS in each iteration, and these contributions reach antenna m with a delay associated to the number of steps from the antennas where they originated. Therefore, we approximate $\boldsymbol{S}_m$ in every iteration by an incomplete sum including only terms that were at hand during the current iteration and with the delays associated to them. We have the expression

$$\widehat{\boldsymbol{S}}_m[n] = \sum_{i \neq m,\, d_{i,m} \leq n} \boldsymbol{w}_i[n - d_{i,m}] \boldsymbol{h}_i^{\mathrm{T}}, \tag{8}$$

where $d_{i,m}$ is the delay, in iterations, between antenna i and m. As we can see, in every iteration new terms are added to the sum corresponding to the antennas that were unreachable in the previous iteration. However, $\boldsymbol{w}_i$ associated to these terms is outdated by the delay that they needed to reach the current antenna (recall that, in every iteration, a new $\boldsymbol{w}_i$ is computed at every antenna of the LIS). It might be the case that the LIS is so huge that the antennas cannot reach each other in a reasonable number of iterations. Nevertheless, as we converge to a stable solution, the changes in the vectors $\boldsymbol{w}_i$ get smaller over the iterations. In practice, it is reasonable to believe that it suffices to consider $\boldsymbol{w}_i\boldsymbol{h}_i$ of a number of antennas which are not too far from the current antenna for the optimization process to stabilize. This is so since antennas far apart may be subject to different large scale channel statistics, so they have limited influence on each other's equalization construction.

Note that in (8), we have not yet addressed the messages $\boldsymbol{Z}_{\text{in},\ell}$ and $\boldsymbol{Z}_{\text{out},\ell}$; we merely worked with an auxiliary variable $\widehat{\boldsymbol{S}}_m[n]$. Thus, we need to elaborate on the type of messages $\boldsymbol{Z}_{\text{in},\ell}$ and $\boldsymbol{Z}_{\text{out},\ell}$ that would allow us to obtain $\widehat{\boldsymbol{S}}_m[n]$ in all the antennas. In general, we would like to have a message sharing scheme which allows us to get as close as possible to $\boldsymbol{S}_m[n]$ (i.e., minimize $d_{i,m}$, maximizing the number of reachable antennas) so that we obtain a result as close to optimum as possible.

3.1 1D Algorithm

We define the messages, $\boldsymbol{Z}_{\text{in},\ell}$ and $\boldsymbol{Z}_{\text{out},\ell}$, to be $K \times K$ matrices with an accumulated sum of the terms $\boldsymbol{w}_i\boldsymbol{h}_i^{\text{T}}$ that antenna m has been able to reach. We can define at antenna m

$$\widehat{\boldsymbol{S}}_m[n] = \sum_{\ell=1}^{L} \boldsymbol{Z}_{\text{in},\ell}[n]. \tag{9}$$

At iteration 0, the input messages at a given antenna, m, would be initialized to $\mathbf{0}$, i.e.,

$$\boldsymbol{Z}_{\text{in},\ell}[0] = \mathbf{0}. \tag{10}$$

Therefore, the output messages at antenna m after calculating the first equalization vector, which correspond to the input messages for other antennas in iteration 1, would be

$$\boldsymbol{Z}_{\text{out},\ell}[1] = \boldsymbol{w}_m[1]\boldsymbol{h}_m^{\text{T}}. \tag{11}$$

If we consider the 1D topology, each antenna would have two inputs and two outputs (except for the first and last ones). In order to get an expression of the form (8), where we can see that each node is not considering its own contribution or repeated contributions of any other node, we cannot send the

messages freely to all the nodes. We need a way to avoid a contribution from being sent back to the node where it originated, or a contribution reaching a certain node more than once. This can be done by restricting the direction of a message when it leaves a node so that it always travels towards the end nodes. Therefore, if we are at antenna m at iteration n, and we have an input from the left, $\boldsymbol{Z}_{\text{in},1}$, and another from the right, $\boldsymbol{Z}_{\text{in},2}$, then we should output to the left the input that we got from the right, and to the right the input that we got from the left after adding our current contribution, $\boldsymbol{w}_m[n]\boldsymbol{h}_m^{\text{T}}$, i.e.,

$$\begin{aligned} \boldsymbol{Z}_{\text{out},1}[n+1] &= \boldsymbol{Z}_{\text{in},2}[n] + \boldsymbol{w}_m[n+1]\boldsymbol{h}_m^{\text{T}} \\ \boldsymbol{Z}_{\text{out},2}[n+1] &= \boldsymbol{Z}_{\text{in},1}[n] + \boldsymbol{w}_m[n+1]\boldsymbol{h}_m^{\text{T}}. \end{aligned} \tag{12}$$

It should be noticed, that $\boldsymbol{Z}_{\text{in},1}$ and $\boldsymbol{Z}_{\text{in},2}$ are summed inside antenna m, as suggested in (9), to obtain an approximation of (5) which allows us to obtain $\boldsymbol{w}_m[n]$ through (7).

With this method, the expression (9), which is now of the form (8), for $1 \leq n \leq N_{\text{it}}$ becomes

$$\widehat{\boldsymbol{S}}_m[n] = \sum_{\substack{|m-i| \leq n \\ i \neq m}} \boldsymbol{w}_i \left[n - |m-i|\right] \boldsymbol{h}_i^{\text{T}}, \tag{13}$$

where we can see that after every iteration, two terms associated to new previously unreached antennas are added to the sum (and the terms already considered are updated one iteration). This means that the number of reachable antennas from antenna m scales as $\mathcal{O}(n)$.

Algorithm 1 provides a complete algorithmic description of how each antenna would compute its equalization vector at a given iteration considering our message sharing scheme. This algorithm needs to be run simultaneously for every antenna in the LIS, and repeated a number of iterations, N_{it}, for the equalization vectors to cancel the interference reasonably well.

Algorithm 1 Calculation of the equalization vector at antenna m of a LIS at a given iteration using 1D topology.

Require: $\boldsymbol{Z}_{\text{in},1}$, $\boldsymbol{Z}_{\text{in},2}$, $\boldsymbol{h}_m$

Ensure: $\boldsymbol{Z}_{\text{out},1}$, $\boldsymbol{Z}_{\text{out},2}$, $\boldsymbol{w}_m$

1: $\widehat{\boldsymbol{S}}_m = \boldsymbol{Z}_{\text{in},1} + \boldsymbol{Z}_{\text{in},2}$

2: $\boldsymbol{w}_m = \frac{\mu(\boldsymbol{I}_K - \widehat{\boldsymbol{S}}_m)\boldsymbol{h}_m^{\text{T}}}{\left\|(\boldsymbol{I}_K - \widehat{\boldsymbol{S}}_m)\boldsymbol{h}_m^{\text{T}}\right\|}$

3: $\boldsymbol{Z}_{\text{out},1} = \boldsymbol{Z}_{\text{in},2} + \boldsymbol{w}_m\boldsymbol{h}_m^*$

4: $\boldsymbol{Z}_{\text{out},2} = \boldsymbol{Z}_{\text{in},1} + \boldsymbol{w}_m\boldsymbol{h}_m^*$

3.2 2D Algorithm

Now we need to adapt the previous algorithm to make it suitable for the 2D topology. We expect to reduce the stabilization time, in terms of number of iterations, since the number of connections is greater in this case, so the information travels faster across the LIS. The 2D topology is more interesting in a LIS scenario because it takes advantage of the physical structure of a LIS.

For ease of representation, we define $M = M_{\mathrm{x}}M_{\mathrm{y}}$, so that the LIS can be seen as an $M_{\mathrm{x}} \times M_{\mathrm{y}}$ array where M_{x} and M_{y} represent the number of antennas in the horizontal and vertical axes, respectively. Thus, we re-define notation for the equalization vectors and the channel vectors as $\boldsymbol{w}_{m_{\mathrm{x}},m_{\mathrm{y}}}$ and $\boldsymbol{h}_{m_{\mathrm{x}},m_{\mathrm{y}}}$, respectively, with $1 \leq m_{\mathrm{x}} \leq M_{\mathrm{x}}$ and $1 \leq m_{\mathrm{y}} \leq M_{\mathrm{y}}$.

We assume that the messages are initialized as in the 1D topology, thus, (9), (10), and (11) still apply. The simplest way to proceed would be to apply the 1D algorithm in the horizontal and vertical directions at the same time, i.e., to send the $\boldsymbol{Z}_{\mathrm{in},\ell}$ matrices arriving at the current LIS antenna from each of the inputs to the opposite output after adding the contribution of the current antenna in such a way that information moving in horizontal direction do not flow to vertical direction and vice versa. However, this implies that each antenna would only receive information from the antennas situated in its horizontal and vertical axis.

In view of the above-mentioned discussion, we slightly manipulate the algorithm. The two requirements we seek to fulfill are that the number of reachable antennas after n iterations should scale as $\mathcal{O}(n^2)$, and the sum of all incoming messages (9) should be of the form (8) at antenna $(m_{\mathrm{x}}, m_{\mathrm{y}})$. This translates to the contributions, $\boldsymbol{w}_{i,j}[n]\boldsymbol{h}_{i,j}^{\mathrm{T}}$, flowing from each antenna to the rest of the antennas, but using these contributions once, and only once, at other antennas. Algorithm 2 provides an algorithmic description of the proposed approach. As in the 1D topology, this algorithm applies to a single antenna, and thus it is performed simultaneously at every antenna of the LIS, and repeated N_{it} iterations.

Algorithm 2 Calculation of the equalization vector at antenna $(m_{\mathrm{x}}, m_{\mathrm{y}})$ of a LIS at a given iteration using 2D topology.

Require: $\boldsymbol{Z}_{\mathrm{in},1}$, $\boldsymbol{Z}_{\mathrm{in},2}$, $\boldsymbol{Z}_{\mathrm{in},3}$, $\boldsymbol{Z}_{\mathrm{in},4}$, $\boldsymbol{h}_{m_{\mathrm{x}},m_{\mathrm{y}}}$

Ensure: $\boldsymbol{Z}_{\mathrm{out},1}$, $\boldsymbol{Z}_{\mathrm{out},2}$, $\boldsymbol{Z}_{\mathrm{out},3}$, $\boldsymbol{Z}_{\mathrm{out},4}$, $\boldsymbol{w}_{m_{\mathrm{x}},m_{\mathrm{y}}}$

1: $\widehat{\boldsymbol{S}}_{m_{\mathrm{x}},m_{\mathrm{y}}} = \boldsymbol{Z}_{\mathrm{in},1} + \boldsymbol{Z}_{\mathrm{in},2} + \boldsymbol{Z}_{\mathrm{in},3} + \boldsymbol{Z}_{\mathrm{in},4}$

2: $\boldsymbol{w}_{m_{\mathrm{x}},m_{\mathrm{y}}} = \frac{\mu(\boldsymbol{I}_K - \widehat{\boldsymbol{S}}_{m_{\mathrm{x}},m_{\mathrm{y}}})\boldsymbol{h}^*_{m_{\mathrm{x}},m_{\mathrm{y}}}}{\left\|(\boldsymbol{I}_K - \widehat{\boldsymbol{S}}_{m_{\mathrm{x}},m_{\mathrm{y}}})\boldsymbol{h}^*_{m_{\mathrm{x}},m_{\mathrm{y}}}\right\|}$

3: $\boldsymbol{Z}_{\mathrm{out},1} = \boldsymbol{Z}_{\mathrm{in},2} + \boldsymbol{Z}_{\mathrm{in},3} + \boldsymbol{Z}_{\mathrm{in},4} + \boldsymbol{w}_{m_{\mathrm{x}},m_{\mathrm{y}}}\boldsymbol{h}^{\mathrm{T}}_{m_{\mathrm{x}},m_{\mathrm{y}}}$

4: $\boldsymbol{Z}_{\mathrm{out},2} = \boldsymbol{Z}_{\mathrm{in},4} + \boldsymbol{w}_{m_{\mathrm{x}},m_{\mathrm{y}}}\boldsymbol{h}^{\mathrm{T}}_{m_{\mathrm{x}},m_{\mathrm{y}}}$

5: $\boldsymbol{Z}_{\mathrm{out},3} = \boldsymbol{Z}_{\mathrm{in},1} + \boldsymbol{Z}_{\mathrm{in},2} + \boldsymbol{Z}_{\mathrm{in},4} + \boldsymbol{w}_{m_{\mathrm{x}},m_{\mathrm{y}}}\boldsymbol{h}^{\mathrm{T}}_{m_{\mathrm{x}},m_{\mathrm{y}}}$

6: $\boldsymbol{Z}_{\mathrm{out},4} = \boldsymbol{Z}_{\mathrm{in},2} + \boldsymbol{w}_{m_{\mathrm{x}},m_{\mathrm{y}}}\boldsymbol{h}^{\mathrm{T}}_{m_{\mathrm{x}},m_{\mathrm{y}}}$

It can be verified that our algorithm meets both of the previously mentioned requirements. We explain this with an example illustrating how the $\boldsymbol{w}_{i,j}\boldsymbol{h}^{\mathrm{T}}_{i,j}$ terms are shared among the antennas of the LIS when applying the algorithm. If we consider a 5×5 LIS, during iteration n, $\boldsymbol{w}_{3,3}[n]\boldsymbol{h}^{\mathrm{T}}_{3,3}$ is generated at antenna $(3,3)$. Then this contribution is spread across the LIS until it is completely forgotten as described in Fig. 3. The green nodes are the antennas that have used the contribution in the current iteration and send it to the red nodes. Note that, even though the contribution $\boldsymbol{w}_{3,3}\boldsymbol{h}^{\mathrm{T}}_{3,3}$ is summed to other contributions from other antennas on the way, the algorithm assures that it can be treated independently and be seen as one single message.

Considering this message sharing scheme for $1 \leq n \leq N_{\mathrm{it}}$, the expression (8) becomes

$$\widehat{\boldsymbol{S}}_{m_{\mathrm{x}},m_{\mathrm{y}}}[n] = \sum_{\substack{|m_{\mathrm{x}}-i|+|m_{\mathrm{y}}-j|\leq n \\ (i,j)\neq(m_{\mathrm{x}},m_{\mathrm{y}})}} \boldsymbol{w}_{i,j}\,[n-(|m_{\mathrm{x}}-i|+|m_{\mathrm{y}}-j|)]\boldsymbol{h}^{\mathrm{T}}_{i,j}. \tag{14}$$

In this case, after every iteration a total of $4n$ terms associated to previously unreached antennas are added to the sum, which means that the number of reached antennas scales as $\mathcal{O}(n^2)$.

3.3 2D Algorithm Improvement

From performance tests of the previous 2D algorithm, in terms of interference cancellation, one can see that the results are not as good as desired. This might be due to the simultaneous recomputing of $\boldsymbol{w}_m$ in all the antennas of the LIS which makes the delay of the new terms added to $\widehat{\boldsymbol{S}}_m[n]$ a bottleneck. So, after

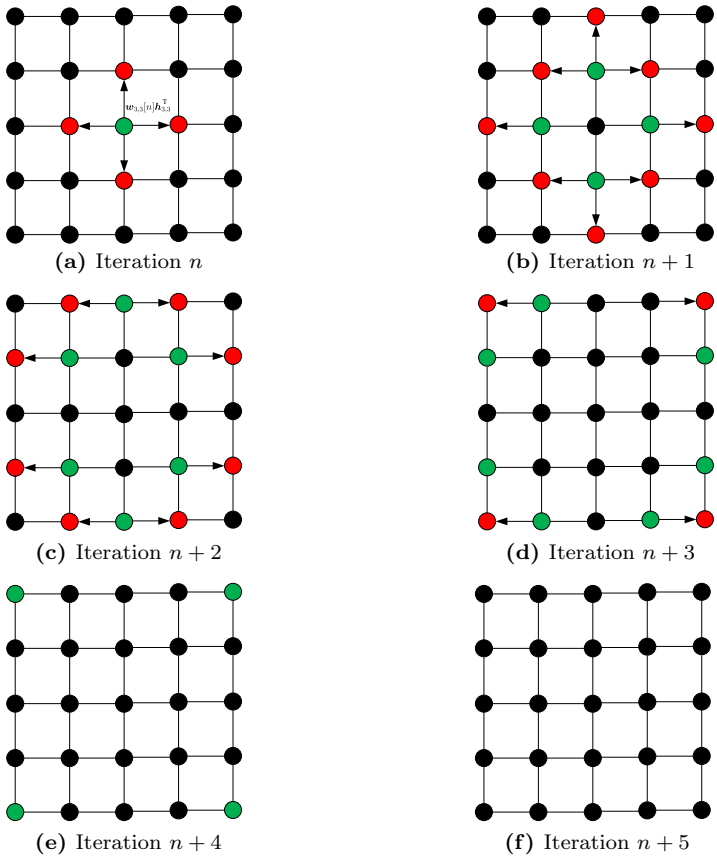

(a) Iteration n **(b)** Iteration $n+1$

(c) Iteration $n+2$ **(d)** Iteration $n+3$

(e) Iteration $n+4$ **(f)** Iteration $n+5$

Figure 3: Example of the transmission of $\boldsymbol{w}_{3,3}[n]\boldsymbol{h}_{3,3}^{\mathrm{T}}$ from node $(3,3)$ to the rest of a 5×5 LIS. Note that the term $\boldsymbol{w}_{3,3}[n]\boldsymbol{h}_{3,3}^{\mathrm{T}}$ is transmitted in the messages $\boldsymbol{Z}_{\mathrm{in},\ell}$ and $\boldsymbol{Z}_{\mathrm{out},\ell}$.

some testing, we developed a new algorithm based on the previous one which takes into account the previously computed $\boldsymbol{w}_m$ when computing the new ones. This way, the changes in $\boldsymbol{w}_m$ from iteration to iteration are smoothened and the delays in $\widehat{\boldsymbol{S}}_m[n]$ are less critical.

The new algorithm is exactly the same as the original 2D algorithm except for the way in which $\boldsymbol{w}_m$ is calculated in every iteration. In this case, we compute the equalization vector $\boldsymbol{w}_{m_\mathrm{x},m_\mathrm{y}}[n+1]$ as

$$\boldsymbol{w}_{m_\mathrm{x},m_\mathrm{y}}[n+1] = \mu \frac{\boldsymbol{w}^{\mathrm{opt}}_{m_\mathrm{x},m_\mathrm{y}}[n+1] + \sum_{k=n+1-N_\mathrm{avg}}^{n} \boldsymbol{w}_{m_\mathrm{x},m_\mathrm{y}}[k]}{\left\| \boldsymbol{w}^{\mathrm{opt}}_{m_\mathrm{x},m_\mathrm{y}}[n+1] + \sum_{k=n+1-N_\mathrm{avg}}^{n} \boldsymbol{w}_{m_\mathrm{x},m_\mathrm{y}}[k] \right\|}, \tag{15}$$

where $\boldsymbol{w}^{\mathrm{opt}}_{m_\mathrm{x},m_\mathrm{y}}[n+1]$ is computed by (7). This can be seen as an average over the current $\boldsymbol{w}^{\mathrm{opt}}_{m_\mathrm{x},m_\mathrm{y}}$ and the N_avg previously computed $\boldsymbol{w}_{m_\mathrm{x},m_\mathrm{y}}$. Note that in (15) N_avg previous versions of $\boldsymbol{w}_{m_\mathrm{x},m_\mathrm{y}}$ are required. These are initially computed through (7) during the first N_avg iterations, and in the successive iterations (15) is used.

The value of N_avg is related to the oldest version of $\boldsymbol{w}_{m_\mathrm{x},m_\mathrm{y}}$ that is considered. In (14), we can approximate the number of $\boldsymbol{w}_{i,j}\boldsymbol{h}^{\mathrm{T}}_{i,j}$ terms associated to reachable antennas at iteration n by n^2. This means that, assuming a square LIS, in iteration $\left\lceil \sqrt{M} \right\rceil$ all the antennas have been reached, so the maximum delay between antennas is approximately

$$\max_{i,j}(d_{i,j}) \approx \left\lceil \sqrt{M} \right\rceil . \tag{16}$$

With this in mind, we can choose N_avg to be precisely $\left\lceil \sqrt{M} \right\rceil$ so that, for $n > N_\mathrm{avg}$, the contribution arriving from antenna $(m_\mathrm{x}, m_\mathrm{y})$ to the antenna with the highest delay to $(m_\mathrm{x}, m_\mathrm{y})$, will still be sufficiently well related to the actual $\boldsymbol{w}_{m_\mathrm{x},m_\mathrm{y}}$ computed in $(m_\mathrm{x}, m_\mathrm{y})$ through (15) (the changes in $\boldsymbol{w}_{m_\mathrm{x},m_\mathrm{y}}$ between iterations become smaller).

4 Numerical Results

In this section we present simulation results of the different algorithms defined for decentralized interference cancellation. We compare our algorithms with an implementation of the daisy chain proposed in [12], which consists of computing the equalization vectors sequentially at each antenna through (7), where in this case

$$\widehat{\boldsymbol{S}}_m = \sum_{i=1}^{m-1} \boldsymbol{w}_i \boldsymbol{h}_i^{\mathrm{T}}. \tag{17}$$

Note that the iteration count in this case corresponds to the antenna number. In order to be able to consider a number of iterations greater than M, we extend the chain by feeding the result from the last antenna back to the first one. Fig. 4 shows an illustration of this topology.

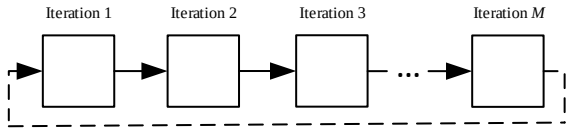

Figure 4: Topology of a daisy chain with feedback loop. The boxes correspond to antennas.

Since we are only interested in the interference level, and the stabilization speed, we will plot the results in terms of SIR vs. number of iterations. The SIR is directly calculated from the resulting equivalent channel (3), where $\boldsymbol{W}$ corresponds to the resulting equalization matrix after applying the algorithms.

As discussed in [12], the value of μ in (7) has a strong effect on the stability of the results. In our simulations, we use $\mu = \sqrt{K}/M$, which is the value proposed in [12], except in the original 2D algorithm, where we use $\mu = 0.85\sqrt{K}/M$ to obtain a stable solution. Lower values of μ work reasonably well, although the SIR results can stabilize at lower levels.

Fig. 5 and 6 show the results of the algorithms presented in this paper for an 8×8 and a 12×12 LIS serving 8 users. The results are averaged over 1000 realizations of an IID channel. In the different channel realizations the SIR levels may vary, but the shape of the curves is approximately maintained. The figures show SIR value at iteration number n, with $1 \leq n \leq N_{\text{it}}$, and $N_{\text{it}} = 2M$. To have a fair comparison, the performance of the daisy chain is measured at an integer number of iterations of loop, N_{fb}; however, the total number of iterations required to obtain the reported SIR level is $N_{\text{fb}}M$.

As can be seen from Fig. 5 and 6, the algorithms proposed always surpass the performance of a single daisy chain realization even before n reaches M. However, the original 2D algorithm saturates before reaching the performance of 2 daisy chain realizations. Both 2D algorithms have a steeper increase of the SIR during the first iterations than the 1D algorithm due to the $\mathcal{O}(n^2)$ spread of the information. The improved 2D algorithm obtains a better performance than the original one as iterations grow, but as the number antennas grows, this algorithm ends up saturating at a lower SIR than the 1D algorithm.

5 Conclusions

In this paper, we have presented three algorithms for estimating an equalization matrix which reduces inter-user interference in a LIS in a decentralized way. We have defined two topologies, the 1D topology and the 2D topology. The

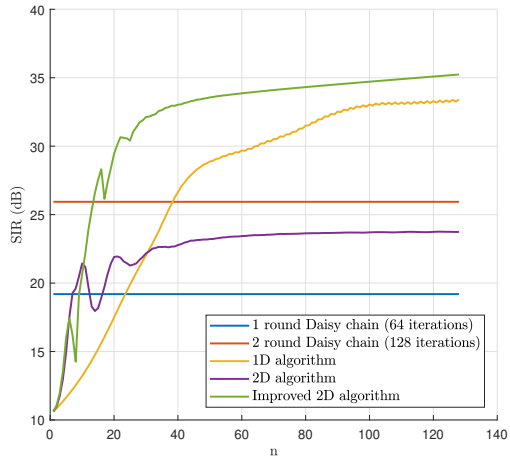

Figure 5: SIR vs. number of iterations, averaged over 1000 IID channel realizations, using the different algorithms for a 8×8 LIS serving 8 users.

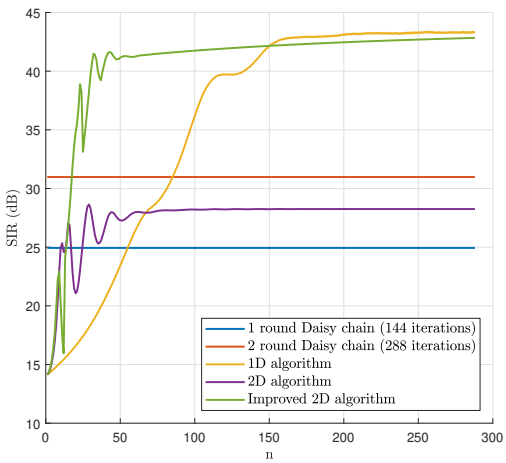

Figure 6: SIR vs. number of iterations, averaged over 1000 IID channel realizations, using the different algorithms for a 12×12 LIS serving 8 users.

2D algorithms have a faster SIR increase during early iterations than the 1D algorithm. However, in later iterations, they tend to saturate at a lower SIR. The improved 2D algorithm reduces this effect.

References

[1] S. Hu, F. Rusek, and O. Edfors, "Beyond massive MIMO: The potential of data transmission with large intelligent surfaces," *IEEE Transactions on Signal Processing*, vol. 66, no. 10, pp. 2746–2758, 2018.

[2] S. Hu, F. Rusek, and O. Edfors, "The potential of using large antenna arrays on intelligent surfaces," in *2017 IEEE 85th Vehicular Technology Conference (VTC Spring)*, 2017, pp. 1–6.

[3] S. Hu, K. Chitti, F. Rusek, and O. Edfors, "User assignment with distributed large intelligent surface (LIS) systems," in *2018 IEEE 29th Annual International Symposium on Personal, Indoor and Mobile Radio Communications (PIMRC)*, 2018, pp. 1–6.

[4] M. Jung, W. Saad, Y. Jang, G. Kong, and S. Choi, "Performance analysis of large intelligent surfaces (LISs): Asymptotic data rate and channel hardening effects," *IEEE Transactions on Wireless Communications*, vol. 19, no. 3, pp. 2052–2065, 2020.

[5] "More than 50 billion connected devices," Ericsson, Ericsson White Paper, 2011, ech. Rep. 284 23–3149 Uen.

[6] F. Rusek, D. Persson, B. K. Lau, *et al.*, "Scaling up MIMO: Opportunities and challenges with very large arrays," *IEEE Signal Processing Magazine*, vol. 30, no. 1, pp. 40–60, 2013.

[7] C. Shepard *et al.*, "Argos: Practical many-antenna base stations," in *Proceedings of the 18th Annual International Conference on Mobile Computing and Networking (Mobicom)*, Istanbul, Turkey, 2012, pp. 53–64.

[8] A. Puglielli, A. Townley, G. LaCaille, *et al.*, "Design of energy- and cost-efficient massive MIMO arrays," *Proceedings of the IEEE*, vol. 104, no. 3, pp. 586–606, 2016.

[9] K. Li, R. R. Sharan, Y. Chen, T. Goldstein, J. R. Cavallaro, and C. Studer, "Decentralized baseband processing for massive MU-MIMO systems," *IEEE Journal on Emerging and Selected Topics in Circuits and Systems*, vol. 7, no. 4, pp. 491–507, 2017.

[10] E. Bertilsson, O. Gustafsson, and E. G. Larsson, "A distributed processing architecture for modular and scalable massive MIMO base stations," Jan. 2018. eprint: `1801.07967`.

[11] J. Rodríguez Sánchez, F. Rusek, O. Edfors, M. Sarajlić, and L. Liu, "Decentralized massive MIMO processing exploring Daisy-chain architecture and recursive algorithms," *IEEE Transactions on Signal Processing*, vol. 68, pp. 687–700, 2020.

[12] M. Sarajlic, F. Rusek, J. R. Sanchez, L. Liu, and O. Edfors, "Fully decentralized approximate zero-forcing precoding for massive MIMO systems," *IEEE Wireless Communications Letters*, pp. 1–1, 2019.

[13] E. Bertilsson, O. Gustafsson, and E. G. Larsson, "A scalable architecture for massive MIMO base stations using distributed processing," in *2016 50th Asilomar Conference on Signals, Systems and Computers*, 2016, pp. 864–868.

[14] A. Puglielli *et al.*, "Design of energy- and cost-efficient massive MIMO arrays," *Proceedings of the IEEE*, vol. 104, no. 3, pp. 586–606, 2016.

Paper II

Trade-offs in Decentralized Multi-Antenna Architectures: The WAX Decomposition

Current research on multi-antenna architectures is trending towards increasing the amount of antennas in the BS so as to increase the spectral efficiency. As a result, the interconnection bandwidth and computational complexity required to process the data using centralized architectures is becoming prohibitively high. Decentralized architectures can reduce these requirements by pre-processing the data before it arrives at a CPU. However, performing decentralized processing introduces also cost in complexity/interconnection bandwidth at the antenna end which is in general being ignored. This paper aims at studying the interplay between level of decentralization and the associated complexity/interconnection bandwidth requirement at the antenna end. To do so, we propose a general framework for centralized/decentralized architectures that can explore said interplay by adjusting some system parameters, namely the number of connections to the CPU (level of decentralization), and the number of multiplications/outputs per antenna (complexity/interconnection bandwidth). We define a novel matrix decomposition, the WAX decomposition, that allows information-lossless processing within our proposed framework, and we use it to obtain the operational limits of the interplay under study. We also look into some of the limitations of the WAX decomposition.

©2020 IEEE. Reprinted, with permission, from
J. Vidal Alegría, F. Rusek, O. Edfors,
"Trade-offs in Decentralized Multi-Antenna Architectures: The WAX Decomposition,"
in *IEEE Trans. Signal Process.*, vol. 69, pp. 3627-3641, 2021.

1 Introduction

Multi-antenna architectures have been widely employed since they were first introduced in the 1990s and they still remain a popular research topic. The main reason is the enormous improvements in data rate and reliability coming from exploiting space-division multiplexing and diversity. Current research and development on multi-antenna architectures is trending towards scaling up the number of antennas so as to increase the spatial resolution, thus increasing the spectral efficiency by serving several users in the same time-frequency resource. Furthermore, the exploitation of millimeter-wave spectrum in modern communications [1] also justifies the increase in the number of antennas. The reason is that the huge path-loss associated to these frequencies when the electrical size of the antennas is kept constant needs to be overcome by focusing the transmitted energy more effectively [2]. Massive MIMO [3], [4] and LIS [5] are some examples of the trend towards increasing the number of antennas, where massive MIMO considers BSs with hundreds of antennas while LIS extends this concept even further by considering whole walls of electromagnetically active material.

Massive MIMO is already a reality and several prototypes have been developed and tested, such as [6]–[8]. In the prototypes presented in [6], [8], the use of centralized processing leads to huge data-rates between the antennas and the CPU, which limits the scalability of the system as the number of antennas grows. This fact is also noticed in [7], which sacrifices performance by relying on simple decentralized beam-forming to favor scalability. The scalability issue is likely to be exacerbated if we consider LIS, where we can think of practical deployments consisting of walls equipped with an even larger number of antennas than massive MIMO (the continuous surfaces are approximately equivalent to the discrete surfaces when the sampling is dense enough, as observed in [5], [9]). Other technologies that are gaining popularity and are likely to face scalability issues include cell-free massive MIMO [10]–[12], or IRS [12]–[14]. We will base our study in a general multi-antenna architecture so that it can be easily extended to more specific applications, such as the ones previously mentioned.

There is a current trend towards more decentralized architectures [15]–[23] so as to reduce the information transmitted to the CPU. The idea is to carry out pre-processing of the data at the antenna end (or close to it), so that the CPU does not need to have access to all the information required to decode raw data. Available literature on decentralized massive MIMO proposes a wide range of solutions from fully-decentralized architectures [15], [19]–[21], where CSI does not have to be available at the CPU, to partially decentralized architectures, where some of the processing tasks are distributed, but either full [16], [23] or partial CSI [18] is available at the CPU.

In this paper we do not address the problem of decentralized CSI estimation; we assume that perfect CSI is available at the CPU. We rely on the fact that

CSI estimation does not limit the overall level of decentralization within our framework since it needs to be carried out only once per coherence block. Thus, CSI estimation takes a minor fraction of the coherence time, and the estimated CSI can be then used for the data phase throughout the rest of the coherence block without affecting the level of decentralization. However, the problem of estimating and sharing CSI in an efficient and scalable way within our framework remains as future work.

In [18] it is argued that an architecture is decentralized enough if it does not need extra hardware apart from the minimum required during the payload data phase. It also states that the volume of data transferred during the data phase has to be independent of the number of antennas at the base station. However, as happens in [18]–[21], in order to reduce this volume of data (related to the number of connections to the CPU) and make it independent of the number of antennas, each antenna has to provide a number of outputs that scales with the number of users. Note that in a centralized architecture we would have only one output per antenna corresponding to one input to the CPU per antenna. We notice the existence of an interesting trade-off between the number of connections to the CPU and the number of outputs from each antenna.

The main goal of this paper is to study the interplay between level of decentralization and the corresponding increase in decentralized processing complexity for multi-antenna architectures. We measure the level of decentralization as the number of connections to a CPU required during the data phase, and we measure the decentralized processing complexity as the number of multiplications/outputs per antenna (or antenna panel)[1] required to achieve a given level of decentralization. So as to study this trade-off, we present a general framework for a multi-antenna architecture which allows us to change the level of decentralization and complexity by adjusting some system parameters. In this framework, the antennas are grouped into panels of a given number of antennas (this number can be 1 as in [24]). Distributed processing is applied by applying a linear transformation to the inputs of each antenna panel, which generates a given number of outputs (complexity). The outputs are then combined using a combining module that is connected to the CPU using a fixed number of CPU inputs (level of decentralization).

To the best of our knowledge, the presented trade-off has not been explored in the available literature and the results we present are completely new. In [17] trade-offs between different decentralized architectures, algorithms, and data precision levels are studied. However, these trade-offs are mainly systematic while we are interested in fundamental trade-offs where information rates are maintained with respect to typical centralized systems. Thus, our framework focuses on complex baseband processing, and we assume that the detection is

[1] Antenna panel refers to a group of co-located antennas.

always performed in a CPU.

This paper extends the work presented in [24]. The list of contributions are summarized next:

- We present a novel general framework for multi-antenna systems that allows us to consider different levels of decentralization and complexity by adjusting the system parameters. This general framework accounts for typical centralized architectures, decentralized architectures such as the one presented in [18], and hybrid architectures in between those two. In [24], a similar framework to the one studied in this paper is considered. However, the architecture presented in the current work is more general since it adds the possibility of arranging the antennas into panels.

- We define the WAX decomposition, a novel matrix decomposition that allows us to define and exploit the trade-offs within our general framework while achieving information-lossless processing. In [24] the WAX decomposition is already introduced, but in the current work we adapt it to use it in a more general framework. Furthermore, we present novel results on the validity and application of said decomposition, e.g., Theorem 2.

- We present the trade-off in terms of number of multiplications/outputs per antenna panel and number of connections to the CPU for achieving information-lossless processing within our general framework. This trade-off is first studied in [24], but considering only the less general version of the current framework.

- We study through simulations the cost of obtaining simple combining modules that accept WAX decomposition within our general framework.

- We study complexity limitations for the combining modules within our general framework that accept WAX decomposition.

- We study the information-loss associated to operating within our framework when WAX decomposition is not available.

- We present a simple non-optimal solution for determining the distributed processing to be applied whenever WAX decomposition is not available. A deeper research on more effective solutions remains as future work.

The rest of the paper is organized as follows. Section 2 presents the general framework under study, as well as the system model and problem formulation. In Section 3 we present the WAX decomposition, which allows the application of information-lossless processing within our general framework. In Section 4 we study the problem of defining a simple, but valid, combining network for our general framework. Section 5 presents some discussion on the resulting trade-offs, and some examples of the usage of WAX decomposition.

Section 6 explores broadly the case where WAX decomposition is not available and other information-lossy processing has to be applied to maximize the data-rates within our framework. We conclude the paper in Section 7 with a summary of the contributions and future work.

Notation: In this paper, lowercase, bold lowercase and bold uppercase letters stand for scalars, column vectors and matrices, respectively. When using the mutual information operator, $\mathcal{I}(.;.)$, bold uppercase in the sub-scripts refers to random vectors instead of their realizations. The operations $(\cdot)^T$, $(\cdot)^*$ and $(\cdot)^H$ denote transpose, conjugate, and conjugate transpose, respectively. The operation diag$(\cdot)$ outputs a block diagonal matrix with the input matrices/vectors as the diagonal blocks. The operator vec$(\cdot)$ transforms a matrix into a vector by concatenating its columns. $\mathbf{I}_i$ corresponds to the identity matrix of size i, $\mathbf{1}_{i\times j}$ denotes the $i \times j$ all-ones matrix, and $\mathbf{0}_{i\times j}$ denotes the $i \times j$ all-zeros matrix. In this paper, a randomly chosen matrix corresponds to a realization of a random matrix whose elements are driven from a continuous probability distribution function.

2 System Model

Let us consider K single-antenna users transmitting to an M-antenna BS through a narrow-band channel. The $M \times 1$ received complex vector, $\boldsymbol{y}$, can be expressed as

$$\boldsymbol{y} = \boldsymbol{H}\boldsymbol{s} + \boldsymbol{n}, \tag{1}$$

where $\boldsymbol{H}$ is the channel matrix of dimension $M \times K$, $\boldsymbol{s}$ is the $K \times 1$ vector of symbols transmitted by the users, and $\boldsymbol{n}$ is a zero-mean complex white Gaussian noise vector with sample variance N_0. The M antennas are divided into panels of N antennas; $M/N = P$ is thus restricted to integer values. Each panel, $p \in \{1, \ldots, P\}$, multiplies the received vector, $\boldsymbol{y}_p = [y_{(p-1)N+1} \ \cdots \ y_{pN}]$, by an $L \times N$ matrix, $\boldsymbol{W}_p^H$. The aggregated outputs are combined through a fixed $T \times LP$ matrix, $\boldsymbol{A}^H$. The resulting vector is forwarded to a CPU, which can apply further processing. For our analysis, we will assume that the CPU can multiply the incoming matrix by a $K \times T$ matrix $\boldsymbol{X}^H$ to be able to express the equivalent matrix in the form of already known linear equalizers. However, our main interest is to maximize the information rate at which the users transmit to the CPU, so the last step is not required for the analysis since it will not increase this information rate (recall the data-processing inequality [25]). Also, we define the previous matrices using conjugate transpose so as to ease upcoming notation. Fig. 1 shows a block diagram of the general framework under study.

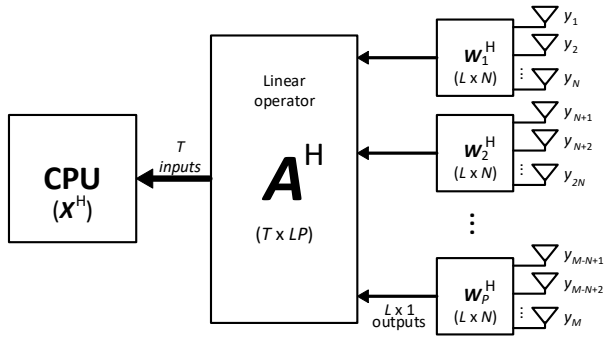

Figure 1: General framework considered in this paper.

The post-processed vector can be expressed as

$$\boldsymbol{z} = \boldsymbol{X}^H \boldsymbol{A}^H \boldsymbol{W}^H \boldsymbol{y}, \tag{2}$$

where $\boldsymbol{W}$ is an $M \times LP$ block diagonal matrix of the form

$$\boldsymbol{W} = \operatorname{diag}\left(\boldsymbol{W}_1, \boldsymbol{W}_2, \ldots, \boldsymbol{W}_P\right). \tag{3}$$

We assume that the matrices $\boldsymbol{W}_p$, and $\boldsymbol{X}$ can be tuned for every channel realization, while the matrix $\boldsymbol{A}$ is fixed. We can interpret $\boldsymbol{A}$ as the matrix associated to a hardware combining network that can be predesigned, but it cannot be changed once deployed. Table 1 shows a classification of the different system parameters considered within our framework.

For tractability we assume that the channel matrix, $\boldsymbol{H}$, is perfectly available at the BS. Thus, we can obtain $\boldsymbol{W}_p$, and $\boldsymbol{X}$ as a function of said matrix. However, the consequences of having an error in the estimation of $\boldsymbol{H}$ due to imperfect CSI would not be enhanced by the framework under study. In fact, the information-loss associated to having imperfect CSI within our framework would not differ from the case of having imperfect CSI in a typical centralized architecture. The reason is that we could still apply an approximation of the spatially-MF within our framework using the imperfectly estimated channel matrix, as we will be able to understand from the upcoming analysis.

For a fixed $\boldsymbol{A}$, we are interested in maximizing the information rate at which the users can transmit, i.e., we would like to solve the maximization problem

$$\underset{\boldsymbol{X}, \{\boldsymbol{W}_p\}_{p=1}^P}{\text{maximize}} \quad \mathcal{I}_{\boldsymbol{Z},\boldsymbol{S}}(\boldsymbol{z}; \boldsymbol{s}). \tag{4}$$

More specifically, we will explore the cases where the maximization results in

Table 1: System parameters

Given parameters M, K	Trade-off parameters L, T, N, P
Tunable parameters $\boldsymbol{W}$, $\boldsymbol{X}$	Parameters fixed by design $\boldsymbol{A}$

$\mathcal{I}_{\boldsymbol{Z},\boldsymbol{S}}(\boldsymbol{z},\boldsymbol{s}) = \mathcal{I}_{\boldsymbol{Y},\boldsymbol{S}}(\boldsymbol{y},\boldsymbol{s})$. From the data-processing inequality [25] we have

$$\begin{aligned} \mathcal{I}_{\boldsymbol{Z},\boldsymbol{S}}(\boldsymbol{z};\boldsymbol{s}) &\leq \mathcal{I}_{\boldsymbol{Y},\boldsymbol{S}}(\boldsymbol{A}^H\boldsymbol{W}^H\boldsymbol{y};\boldsymbol{s}) \\ &\leq \mathcal{I}_{\boldsymbol{Y},\boldsymbol{S}}(\boldsymbol{y};\boldsymbol{s}). \end{aligned} \tag{5}$$

This means that the application of $\boldsymbol{X}^H$ at the CPU cannot possibly increase the information rate and, as we mentioned before, it is just a manipulation to adapt the dimensions. Furthermore, assuming $\boldsymbol{s} \sim \mathcal{CN}(\boldsymbol{0}_{K\times 1}, P_s\mathbf{I}_K)$ so that the mutual information is maximized (and thus coincides with the capacity), we have [26]

$$\mathcal{I}_{\boldsymbol{Y},\boldsymbol{S}}(\boldsymbol{y};\boldsymbol{s}) = \log\det\left(\mathbf{I}_M + \frac{P_s}{N_0}\boldsymbol{H}\boldsymbol{H}^H\right). \tag{6}$$

Therefore, we can state that, if we are able to achieve

$$\mathcal{I}_{\boldsymbol{Z},\boldsymbol{S}}(\boldsymbol{z};\boldsymbol{s}) = \mathcal{I}_{\boldsymbol{Y},\boldsymbol{S}}(\boldsymbol{y};\boldsymbol{s}), \tag{7}$$

the information rate is maximized and the equivalent processing is information-lossless.

One of the main scopes of this paper is to study the conditions, in terms of constraints on the system parameters, for our framework to be able to perform information-lossless processing. The following lemma will be helpful.

Lemma 1 *Considering the presented framework, the equality*

$$\mathcal{I}_{\boldsymbol{Z},\boldsymbol{S}}(\boldsymbol{z};\boldsymbol{s}) = \log\det\left(\mathbf{I}_M + \frac{P_s}{N_0}\boldsymbol{H}\boldsymbol{H}^H\right), \tag{8}$$

is fulfilled if and only if we can find a $\boldsymbol{W}$ *and* $\boldsymbol{X}$ *such that*

$$\boldsymbol{W}\boldsymbol{A}\boldsymbol{X} = \boldsymbol{H}. \tag{9}$$

Proof Let $R(\boldsymbol{y})$ be any linear sufficient statistic for $\boldsymbol{s}$ of dimension K (which means that it is information-lossless [25]). Then, there exists a full-rank $K \times K$ matrix $\widetilde{\boldsymbol{X}}$ such that

$$R(\boldsymbol{y}) = \widetilde{\boldsymbol{X}}\boldsymbol{H}^H\boldsymbol{y}. \tag{10}$$

Therefore, we have that $\boldsymbol{X}^H\boldsymbol{A}^H\boldsymbol{W}^H\boldsymbol{y}$ is a sufficient statistic if and only if

$$\boldsymbol{X}^H\boldsymbol{A}^H\boldsymbol{W}^H\boldsymbol{y} = \widetilde{\boldsymbol{X}}\boldsymbol{H}^H\boldsymbol{y}, \tag{11}$$

which leads to

$$\widetilde{\boldsymbol{X}}^{-1}\boldsymbol{X}^H\boldsymbol{A}^H\boldsymbol{W}^H = \boldsymbol{H}^H, \tag{12}$$

but since $\widetilde{\boldsymbol{X}}^{-1}$ can be absorbed by $\boldsymbol{X}$, we have

$$\boldsymbol{X}^H\boldsymbol{A}^H\boldsymbol{W}^H = \boldsymbol{H}^H, \tag{13}$$

which proves the lemma by taking the conjugate transpose. □

Lemma 1 gives an important result to understand when the maximization in (4) achieves information-lossless processing. This lemma will be the basis in Section 3 for solving the maximization problem (4) whenever information-lossless processing is available within our framework. Note that (13) would correspond to applying MF within our framework, which is well known to be an information-lossless transformation if optimum processing is applied thereafter.

2.1 Notes on the Downlink Scenario

Throughout this paper we focus on the uplink scenario for improved clarity. However, this work can straightforwardly be extended to a downlink scenario. We next provide a few details.

Let us assume channel reciprocity, which eases notation and remarks the equivalence with the uplink scenario.[2] This means that, given the uplink equation (1), the corresponding downlink equation for the vector received by the users is as follows

$$\boldsymbol{y}_{\mathrm{d}} = \boldsymbol{H}^T\boldsymbol{z}_{\mathrm{d}} + \boldsymbol{n}_{\mathrm{d}}, \tag{14}$$

where $\boldsymbol{y}_{\mathrm{d}}$ is now a $K \times 1$ vector with entries associated to the complex baseband signal seen by each user, $\boldsymbol{z}_{\mathrm{d}}$ is the $M \times 1$ precoded vector sent by the antennas, and $\boldsymbol{n}_{\mathrm{d}}$ is the corresponding noise vector. We assume that the same framework as in Fig. 1 applies for the downlink, but changing the arrows from left to right. This implies that the linear operators (including the combining module) are assumed to be able to use inputs as outputs, and vice versa. The precoded vector would then be defined as

$$\boldsymbol{z}_{\mathrm{d}} = \boldsymbol{W}^*\boldsymbol{A}^*\boldsymbol{X}^*\boldsymbol{s}_{\mathrm{d}}, \tag{15}$$

where $\boldsymbol{s}_{\mathrm{d}}$ is now a $K \times 1$ vector with complex entries associated to the signals intended for each user. In this case, Lemma 1 does not apply unless we assume

[2] In case of non-reciprocity, the presented framework would still be valid as long as the base station has access to the downlink channel matrix.

that the users can collaborate with each other. However, we can achieve lossless precoding with respect to standard centralized linear precoding schemes, since we can still apply typical precoding schemes within our framework such as MF, ZF or MMSE. Furthermore, with the assumption of channel reciprocity in place, the $\boldsymbol{W}$ matrices could be kept fixed from the uplink processing ($\boldsymbol{A}$ is still fixed by design) and $\boldsymbol{X}$ can be adapted to apply the desired precoding scheme. In the case of non-reciprocity of the channel, both $\boldsymbol{X}$ and $\boldsymbol{W}$ have to be recomputed for applying the desired precoding based on the downlink channel.

2.2 Previously Studied Architectures within our Framework

There are several multi-antenna architectures that could be represented within our framework, which further motivates our study. In this case, what we mean with "represent an architecture within our framework" is that there is a combination of design variables within our framework that gives the same processing. The most obvious architecture that fulfills this is a typical centralized M-antenna architecture, e.g., centralized massive MIMO systems. In this case all the antennas are directly connected to a CPU, which corresponds to having one antenna per panel, and all antennas connected directly to the CPU, i.e., $N = 1$, $L = 1$, $\boldsymbol{W}_p = 1$ (scalar), $T = M$, $\boldsymbol{A} = \mathbf{I}_M$. This architecture is depicted in Fig. 2 (left).

Another architecture that can be represented within our framework is the decentralized massive MIMO architecture from [18]. In this case, there is also one antenna per panel, but antenna m multiplies its input by the $K \times 1$ local channel vector, $\boldsymbol{h}_m$, and the result is summed over all the antennas so that the size of the vector transmitted to the CPU coincides with the number of users, K. Thus, this architecture can be represented within our framework by setting $N = 1$, $L = K$, $\boldsymbol{W}_p = \boldsymbol{h}_p$ (vector), $T = K$, $\boldsymbol{A} = [\mathbf{I}_K \, \mathbf{I}_K \, \ldots \, \mathbf{I}_K]^T$, which corresponds to MF if no $\boldsymbol{X}$ is applied at the CPU. This architecture is depicted in Fig. 2 (right). In [18] it is claimed that, for a system to be decentralized, the volume of data transmitted to the CPU during the data phase should not scale with M. However, the proposed solution reduces this scaling to K by increasing the number of multiplications/outputs per antenna to K, which increases the decentralized processing complexity. Our framework allows us to freely adjust these parameters.

Comparing the two architectures from Fig. 2, where in both cases information-lossless processing can be applied, we immediately identify a trade-off between the number of connections to the CPU and the number of outputs per antenna panel as depicted in Fig. 3 (left). Note that, in this case, we have a single antenna per panel, i.e., $N = 1$. In our framework, these two quantities, which are traded-off against each other, correspond to T and L, respectively. We can

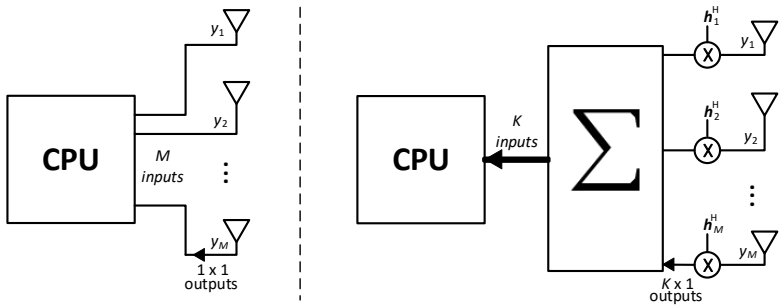

Figure 2: Architecture of centralized massive MIMO (left), and decentralized massive MIMO from [18] (right).

also see the trade-off in terms of multiplications per antenna as in Fig. 3 (right), which can lead to a fairer comparison if we consider panels with more than 1 antenna. The main reason is that, for $N > 1$, the number of outputs can be maintained [27], but the complexity still increases due to a higher number of multiplications.

If we look into other decentralized architectures, such as the ones presented in [17], [19]–[21], [27], we can also represent them within our framework and identify the trade-off between inputs to the CPU and multiplications/outputs per panel (in these cases the trade-off may not lead to information-lossless processing). For example, the architectures from [19]–[21] would all lead to the decentralized point in the plots from Fig. 3 since they all apply $K \times 1$ filters in each antenna during the data phase and generate K outputs per panel during the data phase ($N = 1$ in these architectures). The same is true in [27] if we consider outputs per panel, although if we look at multiplications per panel we should scale the number of outputs by the number of antennas per panel, $N > 1$. Note that, even though [27] presents two different architectures with different level of decentralization, within our framework they lead to the same value of the trade-off; the only difference is that in the fully-decentralized architecture $\boldsymbol{X}$ would not be applied. In [17], however, we would not be able to represent the fully-decentralized architecture within our framework since detection is performed before reaching the CPU, while our framework only considers complex baseband processing.

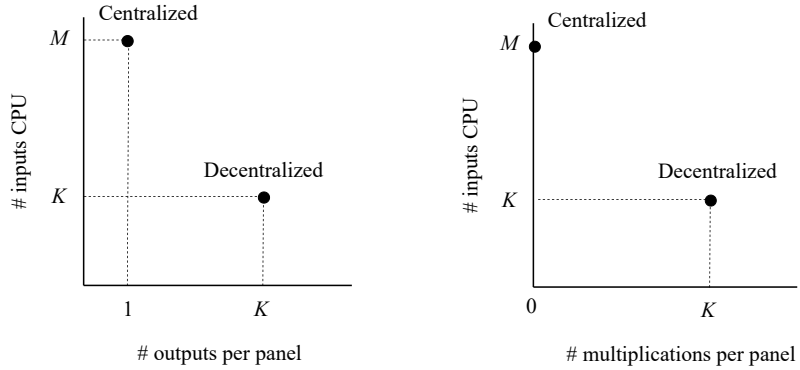

Figure 3: Number of inputs to the CPU (related to T) v.s. number of outputs (left)/number of multiplications (right) per antenna (related to L) for the architectures depicted in Fig. 2. Available literature does not address the behavior in between 1 and K outputs per antenna.

3 WAX Decomposition

Given an arbitrary $M \times K$ matrix, $\boldsymbol{H}$, and a fixed $LP \times T$ matrix, $\boldsymbol{A}$, we define the WAX decomposition of $\boldsymbol{H}$, whenever it exists, as

$$\boldsymbol{H} = \boldsymbol{W}\boldsymbol{A}\boldsymbol{X}. \tag{16}$$

This decomposition relates directly to Lemma 1, i.e., $\boldsymbol{W}$ has the structure defined in (3) and $\boldsymbol{X}$ is a $T \times K$ matrix. Furthermore, the existence of this matrix decomposition for any channel realization would assure that our framework can apply information-lossless processing.

The next lemma will allow us to restrict our study to the case where $N = L$ since this case can span a major part of the general problem through some manipulation.

Lemma 2 *Assume M/L and L/N are integer valued. Consider some fixed $T \times K$ matrix $\boldsymbol{X}$, an $M \times K$ matrix $\boldsymbol{H}$, an $M \times T$ matrix $\widetilde{\boldsymbol{A}}$, and an $LP \times T$ matrix $\boldsymbol{A} = \boldsymbol{T}_{L,N}\widetilde{\boldsymbol{A}}$, with*

$$\boldsymbol{T}_{L,N} = \mathbf{I}_{\frac{M}{L}} \otimes \left(\mathbf{1}_{\frac{L}{N} \times 1} \otimes \mathbf{I}_L\right). \tag{17}$$

Then, the statement

$$\exists \boldsymbol{W} \,:\, \boldsymbol{H} = \boldsymbol{W}\boldsymbol{A}\boldsymbol{X}, \tag{18}$$

where $\boldsymbol{W}$ *is defined as in* (3)*, is true if and only if*

$$\exists \widetilde{\boldsymbol{W}} \,:\, \boldsymbol{H} = \widetilde{\boldsymbol{W}} \widetilde{\boldsymbol{A}} \boldsymbol{X}, \tag{19}$$

where $\widetilde{\boldsymbol{W}} = \mathrm{diag}(\widetilde{\boldsymbol{W}}_1, \ldots, \widetilde{\boldsymbol{W}}_{M/L})$*, and* $\widetilde{\boldsymbol{W}}_p$ *are* $L \times L$ *matrices* $\forall p$*, i.e.,* $\widetilde{\boldsymbol{W}}$ *has the same structure as* (3) *for* $N = L$*.*

Proof The right implication can be immediately seen by choosing $\widetilde{\boldsymbol{W}} = \boldsymbol{W}\boldsymbol{T}_{L,N}$ and noticing that this matrix already has the required structure.

For the left implication it is enough to check that, for any $\widetilde{\boldsymbol{W}}$, there exists some $\boldsymbol{W}$ that fulfills $\boldsymbol{W}\boldsymbol{T}_{L,N} = \widetilde{\boldsymbol{W}}$, both $\boldsymbol{W}$ and $\widetilde{\boldsymbol{W}}$ with their corresponding structure. In this case, there is no linear transformation that gets $\boldsymbol{W}$ from $\widetilde{\boldsymbol{W}}$, but we can construct it as follows. Let us take $\widehat{\boldsymbol{W}} = \widetilde{\boldsymbol{W}}\boldsymbol{T}_{L,M}$, with $\boldsymbol{T}_{L,M} = [\mathbf{I}_L, \ldots, \mathbf{I}_L]^T$. We can then select the diagonal blocks of $\boldsymbol{W}$ to be $\boldsymbol{W}_p = [\widehat{\boldsymbol{w}}_{(p-1)N+1}^T, \ldots, \widehat{\boldsymbol{w}}_{(p-1)N}^T]^T$, where $\widehat{\boldsymbol{w}}_m$, $m = \{1, \ldots, M\}$, are the rows of $\widehat{\boldsymbol{W}}$. Thus, there is a one-to-one mapping between all possible $\widetilde{\boldsymbol{W}}$ and $\boldsymbol{W}$ that fulfills $\boldsymbol{W}\boldsymbol{T}_{L,N} = \widetilde{\boldsymbol{W}}$. □

Lemma 2 also implies that, whenever the assumptions apply, the trade-off between the number of outputs per panel and the number of inputs to the CPU required (L and T, respectively) does not depend on the number of antennas per panel (N). However, the number of multiplications per panel would scale with N. An important constraint of Lemma 2 is that we need to have $L \geq N$, which can be easily checked to be a requirement for having information-lossless processing within our framework unless $L = K$ (leading to the trivial solution of setting $\boldsymbol{W}_p$ as the local MFs).

The rest of this paper assumes $N = L$, unless otherwise stated, due to the intrinsic generality of this case. This means that $\boldsymbol{W}$ in (16) is a square $M \times M$ block diagonal matrix given by (3), with $P = M/L$, and containing square $L \times L$ blocks. The physical implication of this restriction is that all the panels in Fig. 1 have the same number of antennas and outputs. However, as seen in the proof of Lemma 2, we can construct almost any other case from the square case by applying some transformations, with the only limitation that M/L and L/N must evaluate to integer values, as well as that $\boldsymbol{A}$ must be constructed using a specific structure. For simplicity, we will use the same notation as in the general case (16), but considering the new restriction on the dimensions.

3.1 Solving WAX

Let us assume for now that there exists the WAX decomposition of $\boldsymbol{H}$, we later investigate when this is the case. We provide next a step-by-step solution for practical computation of (16), i.e., for obtaining the matrices $\boldsymbol{W}$ and $\boldsymbol{X}$ in (16) based on the current channel realization, $\boldsymbol{H}$, and the fixed combining network,

$\boldsymbol{A}$. This step-by-step solution will also be useful to set the ground for our main result on the applicability of WAX decomposition.

Let us express $\boldsymbol{H} = [\boldsymbol{H}_1^T \, \boldsymbol{H}_2^T \, \dots \boldsymbol{H}_P^T]^T$ and $\boldsymbol{A} = [\boldsymbol{A}_1^T \, \boldsymbol{A}_2^T \, \dots \boldsymbol{A}_P^T]^T$, where $\boldsymbol{H}_p$ and $\boldsymbol{A}_p$ $\forall p \in \{1, \dots, P\}$ are $L \times K$ and $L \times T$ blocks, respectively. The following lemma will be useful.

Lemma 3 *For all matrices* $\boldsymbol{H}$ *satisfying* $\text{rank}(\boldsymbol{H}_n) = L$ *there exists a block diagonal matrix* $\boldsymbol{W}$ *and a matrix* $\boldsymbol{X}$ *such that* $\boldsymbol{WAX} = \boldsymbol{H}$ *if and only if there exists a block diagonal invertible matrix* $\hat{\boldsymbol{W}}$ *with the same form as* $\boldsymbol{W}$ *that fulfills* $\boldsymbol{AX} - \hat{\boldsymbol{W}}\boldsymbol{H} = \boldsymbol{0}_{M \times K}$.

Proof Assume existence of a block diagonal matrix $\boldsymbol{W}$ and a matrix $\boldsymbol{X}$ such that $\boldsymbol{WAX} = \boldsymbol{H}$. This is equivalent to

$$\boldsymbol{W}_p \boldsymbol{A}_p \boldsymbol{X} = \boldsymbol{H}_p, \; 1 \leq p \leq P.$$

Since, by assumption, $\text{rank}(\boldsymbol{H}_p) = L$, it follows that $\text{rank}(\boldsymbol{W}_p) = L \quad \forall p$, making the matrix $\boldsymbol{W}$ invertible.

The reverse statement is trivial; if an invertible $\hat{\boldsymbol{W}}$ exists, then we can set $\boldsymbol{W} = \hat{\boldsymbol{W}}^{-1}$. □

For a randomly chosen $\boldsymbol{H}$, the condition $\text{rank}(\boldsymbol{H}_p) = L$ holds with probability 1. We can then compute the WAX decomposition by invoking Lemma 3, which yields the linear system

$$\boldsymbol{AX} - \boldsymbol{W}^{-1}\boldsymbol{H} = \boldsymbol{0}_{M \times K}. \tag{20}$$

Using the vectorization operator we get an equivalent linear system of equations

$$\boldsymbol{Bu} = \boldsymbol{0}_{MK \times 1}, \tag{21}$$

where $\boldsymbol{u}$ corresponds to the $(TK + ML) \times 1$ vector of unknowns,

$$\boldsymbol{u} = \begin{bmatrix} \text{vec}(\boldsymbol{X}) \\ \text{vec}(\boldsymbol{W}_1) \\ \vdots \\ \text{vec}(\boldsymbol{W}_P) \end{bmatrix}, \tag{22}$$

and $\boldsymbol{B}$ is an $MK \times (TK + ML)$ block matrix of the form $\boldsymbol{B} = [\boldsymbol{B}_1 \; \boldsymbol{B}_2]$ resulting from the vectorization operation, with

$$\boldsymbol{B}_1 = \mathbf{I}_K \otimes \boldsymbol{A}, \quad \boldsymbol{B}_2 = -(\boldsymbol{H}^{\mathrm{T}} \otimes \mathbf{I}_M)\mathbf{P}. \tag{23}$$

$\mathbf{P}$ is an $M^2 \times ML$ block matrix composed of identity matrices, $\boldsymbol{I}_L$, separated by rows of zeros so as to disregard the zeros in $\text{vec}(\boldsymbol{W})$. The solution to (21) can

be found by setting $\boldsymbol{u}$ to be any vector in the null-space of $\boldsymbol{B}$, which will always be non-zero if condition (24) is met (as will be seen shortly). Then, we can obtain the corresponding $\boldsymbol{W}^{-1}$ and $\boldsymbol{X}$ from $\boldsymbol{u}$ through inverse vectorization, and we should check that the resulting $\boldsymbol{W}^{-1}$ is full rank so that we can obtain $\boldsymbol{W}$ by taking the matrix inverse. Thus, the complexity of performing the WAX decomposition using the provided method is equivalent to that of finding the null-space of an $MK \times (TK + ML)$ matrix, and inverting P matrices of dimension $L \times L$.

We have now set the ground for presenting our main result on the applicability of WAX decomposition, which is established in the following theorem.

Theorem 1 *Assuming $N = L$, which implies that $P = M/L$ must evaluate to an integer value, fulfilling the inequality*

$$T > \max\left(M\frac{K-L}{K}, K-1\right) \tag{24}$$

assures that, given a fixed randomly chosen $\boldsymbol{A} \in \mathbb{C}^{M\times T}$, a randomly chosen $\boldsymbol{H} \in \mathbb{C}^{M\times K}$ will admit a decomposition of the form (16) *with probability 1.*

Proof See Appendix A. □

An immediate result of Theorem 1 is that, since we are only interested in having $L \leq K$ due to its practical implications (otherwise there is no dimensionality reduction compared to local MF from Fig. 2 right side), then we have $T \geq L$ since $T \geq K$. The case where Theorem 1 is not fulfilled is considered in Section 6.

For a randomly chosen $\boldsymbol{A}$, $\boldsymbol{W}^{-1}$ is full rank with probability 1, but note that some specific $\boldsymbol{A}$ matrices may lead to rank deficient $\boldsymbol{W}^{-1}$ even if (24) is met. That is, for a poorly chosen matrix $\boldsymbol{A}$, the WAX decomposition of a matrix $\boldsymbol{H}$ cannot be performed. In what follows next we study conditions on $\boldsymbol{A}$ in order for the WAX decomposition to be feasible.

3.2 Studying Validity of Matrix $\boldsymbol{A}$

While Theorem 1 states that any randomly chosen $\boldsymbol{A}$ works for WAX decomposition, we are, from a practical perspective, interested in $\boldsymbol{A}$ matrices having simple forms (providing low computational complexity); for example, sparse matrices with elements in the set $\{0, 1\}$. This would significantly simplify the combining network. However, for such a matrix, Theorem 1 no longer applies. Therefore, it is of importance to investigate the exceptions to Theorem 1.[3]

[3]Note that, in the general case where $N \neq L$, selecting $\boldsymbol{A}$ as in Lemma 2 maintains the overall sparsity properties of $\tilde{\boldsymbol{A}}$ since the transformation $\boldsymbol{T}_{L,N}$ just replicates the matrix $\tilde{\boldsymbol{A}}$ in different positions, filling the rest with 0s.

Definition 1 *We consider* $\boldsymbol{A}$ *to be valid for WAX decomposition* (16) *if the set of matrices* $\boldsymbol{H}$ *that does not admit such a decomposition has measure 0. This is equivalent as saying that the probability of a randomly chosen* $\boldsymbol{H}$ *admitting WAX decomposition for a valid* $\boldsymbol{A}$ *is 1.*

The following theorem will be useful to check if an $\boldsymbol{A}$ matrix is valid or not.

Theorem 2 *Consider a fixed* $M \times T$ *matrix* $\boldsymbol{A}$*, where* T *fulfills* (24)*, and a randomly chosen* $\boldsymbol{H} \in \mathbb{C}^{M \times K}$*, such that* $\boldsymbol{B} = [\boldsymbol{B}_1 \ \boldsymbol{B}_2]$ *from* (23) *is full-rank. If the specific* $\boldsymbol{H}$ *admits WAX decomposition (*(16) *with* $N = L$*) for the given* $\boldsymbol{A}$*, then* $\boldsymbol{A}$ *will be valid for WAX decomposition with probability 1, i.e., any other randomly chosen* $\boldsymbol{H}$ *will admit WAX decomposition for the same* $\boldsymbol{A}$ *with probability 1.*

Proof The proof is a side-result from the proof of Theorem 1 in Appendix A. We just have to notice that the determinant of $\widetilde{\boldsymbol{W}}_p$ still fulfills (37) if $\boldsymbol{A}$ is fixed, so it is enough if we can find an $\boldsymbol{H}$ that gives $\det(\widetilde{\boldsymbol{W}}_p) \neq 0$ so that the determinant is 0 only for a countable set of $\boldsymbol{H}$ matrices. □

The main contribution of Theorem 2 is that we can know if an $\boldsymbol{A}$ matrix is valid or not simply by trying to perform WAX decomposition of a single randomly chosen $\boldsymbol{H}$ using that $\boldsymbol{A}$. Theorem 2 will be widely used for our simulation results since it is our main result on the validity of $\boldsymbol{A}$. An essentially equivalent statement to that of Theorem 2 is to say that, for a given matrix $\boldsymbol{A}$, WAX decomposition of a randomly chosen matrix $\boldsymbol{H}$ is possible with probability either 1 or 0.

The following lemma states a necessary condition for $\boldsymbol{A}$ to be valid.

Lemma 4 *Let* $\widehat{\boldsymbol{A}}$ *be an* $FL \times T$ *submatrix of* $\boldsymbol{A}$ *formed by selecting* F *out of the* P *blocks of size* $L \times T$ *that conform* $\boldsymbol{A}$*,* $\{\boldsymbol{A}_1, \ldots, \boldsymbol{A}_P\}$*. If* $\boldsymbol{A}$ *is valid, then*

$$\operatorname{rank}(\widehat{\boldsymbol{A}}) \geq \min(FL, K). \tag{25}$$

Proof Let $\widehat{\boldsymbol{H}}$ be an $FL \times K$ submatrix of $\boldsymbol{H}$ formed by the F respective $L \times K$ blocks of $\boldsymbol{H}$, and $\widehat{\boldsymbol{W}}$ an $FL \times FL$ block diagonal matrix with the F respective $L \times L$ blocks from $\boldsymbol{W}$ as diagonal elements. If $\boldsymbol{A}$ is valid we can obtain $\widehat{\boldsymbol{W}}$ and $\boldsymbol{X}$ such that $\widehat{\boldsymbol{W}}\widehat{\boldsymbol{A}}\boldsymbol{X} = \widehat{\boldsymbol{H}}$ holds for any $\widehat{\boldsymbol{H}}$ except those in a set of measure 0. For a randomly chosen $\boldsymbol{H}$, $\operatorname{rank}(\widehat{\boldsymbol{H}}) = \min(FL, K)$ with probability 1. Since

$$\operatorname{rank}(\widehat{\boldsymbol{W}}\widehat{\boldsymbol{A}}\boldsymbol{X}) \leq \min\left(\operatorname{rank}(\widehat{\boldsymbol{W}}), \operatorname{rank}(\widehat{\boldsymbol{A}}), \operatorname{rank}(\boldsymbol{X})\right),$$

condition (25) must be fulfilled. □

A further necessary condition for $\boldsymbol{A}$ to be valid is given in Lemma 5.

Lemma 5 *Let $\boldsymbol{A}_0$ be a submatrix of $\boldsymbol{A}$ formed by selecting R rows from $\boldsymbol{A}$, where all rows are in different blocks $\boldsymbol{A}_p$. If $\boldsymbol{A}$ is valid, then*

$$\operatorname{rank}(\boldsymbol{A}_0) > R\frac{K-L}{K}$$

Proof See Appendix B. □

We point out that, since $\boldsymbol{A}$ is an $M \times T$ matrix, $\operatorname{rank}(\boldsymbol{A}_0)$ cannot exceed T. However, with $T > M(K-L)/K$, it is guaranteed that $R\frac{K-L}{K} < T$.

An immediate consequence of Lemma 5 is that a block $\boldsymbol{A}_p$ cannot be repeated arbitrarily often in $\boldsymbol{A}$. In addition, any block $\boldsymbol{A}_p$ must have rank L (see Lemma 4). Repeating the block $\boldsymbol{A}_p$ r times in $\boldsymbol{A}$, and selecting $\boldsymbol{A}_0$ as the same row within each of these r blocks yields,

$$1 > r\frac{K-L}{K},$$

which implies $r < \frac{K}{K-L}$. Whenever $L \leq K/2$, $r = 1$ so that each block $\boldsymbol{A}_p$ can only occur once in $\boldsymbol{A}$.

Appendix C includes another, less intuitive, necessary condition for $\boldsymbol{A}$ to be valid. Despite extensive efforts, we have not been able to establish sufficient conditions for having a valid $\boldsymbol{A}$. The provided necessary conditions might not be helpful in generating valid $\boldsymbol{A}$ matrices, but they constitute initial progress on the matter. Thus, the problem of establishing sufficient conditions for valid $\boldsymbol{A}$ matrices remains open.

4 Finding Sparse $\boldsymbol{A}$ Matrices

Let us keep restricting ourselves to the case where $N = L$ due to the generality of this case. Recall, however, that the transformation (17), which allows considering other N values, maintains the overall sparsity properties of $\boldsymbol{A}$ (although the percentage of 1s can decrease since 0s are being padded). As we have mentioned previously, from an implementation point of view, it is desirable to have $\boldsymbol{A}$ as a sparse matrix of 1s and 0s with as few 1s as possible. The main reason is the direct relation between the number of 1s in $\boldsymbol{A}$ and the number of sum operations required to implement such a combining matrix. Recall that we can view $\boldsymbol{A}$ as the matrix associated to a predesigned hardware combining module, which could be intuitively implemented through a network of sum modules.

In the previous section, we provided some necessary conditions on matrix $\boldsymbol{A}$ for the WAX decomposition to be applicable. However, after extensive research on the matter, we have not been able to find sufficient conditions for having a valid $\boldsymbol{A}$. This motivates the need of simulation results to further understand

the limits on the sparsity of $\boldsymbol{A}$. Nevertheless, we will support these simulations with a simple theoretical bound that allows us to gain better understanding of how sparse $\boldsymbol{A}$ may be.

From Lemma 4, we can say that each $L \times T$ block $\boldsymbol{A}_p$ $p \in \{1, \ldots, P\}$, has to be of rank L. If we put it together with Lemma 5 we can say that a valid $\boldsymbol{A}$ has a maximum of

$$r_{\max} = \left\lceil \frac{K}{K-L} - 1 \right\rceil \tag{26}$$

equal $\boldsymbol{A}_p$ blocks. Therefore, if we aim at $\boldsymbol{A}$ matrices of 1s and 0s with the minimum number of 1s, we can lower bound the number of 1s through the following lemma.

Lemma 6 *Given a valid $\boldsymbol{A} \in \{1,0\}^{M \times T}$, the number of 1s in $\boldsymbol{A}$, which incidentally coincides with its squared Frobenius norm, can be lower bounded by*

$$\|\boldsymbol{A}\|_{\mathrm{F}}^2 \geq \sum_{k=1}^{Q-1} r_{\max}(k-Q)\binom{T}{k} + QM, \tag{27}$$

where Q is obtained by

$$Q = \arg\min_{q} \sum_{k=1}^{q} r_{\max}\binom{T}{k} \geq M. \tag{28}$$

Proof Let us impose the restriction that every row in $\boldsymbol{A}$ can be repeated a maximum of $r_{\max}$ times, as suggested by Lemma 5, where the restriction of selecting the rows from different blocks can be relaxed since we are interested in a lower bound. Each row of $\boldsymbol{A}$ must have at least a 1 at some location, otherwise, considering $L \leq T$, a row of only 0s would result in an $\boldsymbol{A}_p$ block with rank lower than L (contradicting Lemma 4). Therefore, we can bound the number of 1s in $\boldsymbol{A}$ by considering all possible combinations of rows having a single 1, each of which could be repeated a maximum of $r_{\max}$ times. Then, we can do the same for rows having 2 1s, and go on until we have enough rows to fill the M rows of $\boldsymbol{A}$. Straightforward combinatorics result in the statements in the lemma. □

Even though the lower bound presented in Lemma 6 might look a bit hard to compute at first sight, for reasonable values of the design variables ($M \leq 3r_{\max}T$), it is enough to consider only rows with up to two 1s to have enough rows for filling $\boldsymbol{A}$, i.e., $Q \leq 2$.

Figs. 4 and 5 show the minimum percentage of 1s required to have a valid $\boldsymbol{A}$ through numerical optimization, as well as the theoretical lower bound from

Lemma 6, with respect to $100/T_{\text{opt}}$. The optimum T, T_{opt}, is computed as

$$T_{\text{opt}} = \max\left(\left\lfloor M\frac{K-L}{K}+1\right\rfloor, K\right), \tag{29}$$

which corresponds to the minimum integer T that fulfills Theorem 1. The reason for having $100/T_{\text{opt}}$ is that it corresponds to a trivial lower bound in the percentage of 1s, i.e., if we have a single 1 per row. We can see that the relation between the minimum percentage of 1s and $100/T_{\text{opt}}$ is close to linear. In Fig. 4, K is fixed and L is changed, while in Fig. 5 it is the other way around. Although our initial intention was not to provide a tight bound to the numerical simulation, we can note that the obtained percentage of 1s for valid $\boldsymbol{A}$ matrices is in general close to the lower bound computed given by Lemma 6 (within $\pm 3\%$ error in the plots).

The algorithm for computing the minimum percentage of 1s consists of selecting $\boldsymbol{A}$ by adding 1s at random positions, with some constraints related to Lemma 4, until a valid $\boldsymbol{A}$ has been found. Then, we reduce through exhaustive search the number of 1s in $\boldsymbol{A}$ as much as possible while maintaining its validity. The validity of $\boldsymbol{A}$ is evaluated by considering Theorem 2.

Table 2 shows the minimum number of 1s for having a valid $\boldsymbol{A}$ considering different values of K and L (recall $L \leq K$ for information-lossless processing). The same algorithm as for Figs. 4 and 5 is employed, and T is also selected to be T_{opt} from (29). We can see that, even though from Figs. 4 and 5 the percentage of 1s increases with L and decreases with K, for the total number of 1s it is the other way around, i.e., it increases with K and decreases with L. This is because the size of $\boldsymbol{A}$ increases at a higher rate when T is increased. However, if we implement $\boldsymbol{A}$ using sum modules with only two inputs, we would need to subtract T to the number of 1s in $\boldsymbol{A}$, since a single 1 in a column of $\boldsymbol{A}$ would not require any sum module. Table 3 shows the minimum number of 2-input sum modules required to have a valid $\boldsymbol{A}$, i.e., the values of this table correspond to the values of Table 2 subtracting the respective T value to each entry. As we can see, the number of sum modules required does not vary considerably with K and L, and it remains in the order of M.

Fig. 6 shows the percentage of valid $\boldsymbol{A}$ matrices for different percentage of 1s, where the 1s are placed at random positions with the only restriction that they have at least a 1 per row and per column. The algorithm employed consists of generating a big number of random $\boldsymbol{A}$ matrices with the corresponding percentage of 1s (while fulfilling a simple restriction related to Lemma 4 with $F = 1$), and checking what percentage of them are valid (Theorem 2 comes in handy here too). The different curves correspond to the same parameter combinations as Fig. 5, where we can find the minimum percentage of 1s that apply to the different values of K. As we can see, finding an $\boldsymbol{A}$ attaining a percentage of 1s slightly higher than the optimum one ($+10\%$) is not that dif-

L/K	1	2	3	4	5	6	7
1	60	89	98	102	104	105	108
2	-	60	78	89	94	98	102
3	-	-	60	72	80	89	91
4	-	-	-	60	68	78	84
5	-	-	-	-	60	65	72
6	-	-	-	-	-	60	66

Table 2: Minimum number of 1s required to have a valid $\boldsymbol{A}$ for $M = 60$, $T = T_{\text{opt}}$

L/K	1	2	3	4	5	6	7
1	59	58	57	56	55	54	56
2	-	58	57	58	57	57	59
3	-	-	57	56	55	58	56
4	-	-	-	56	55	57	58
5	-	-	-	-	55	54	54
6	-	-	-	-	-	54	57

Table 3: Minimum number of 2-input sum modules required to implement a valid $\boldsymbol{A}$ for $M = 60$, $T = T_{\text{opt}}$

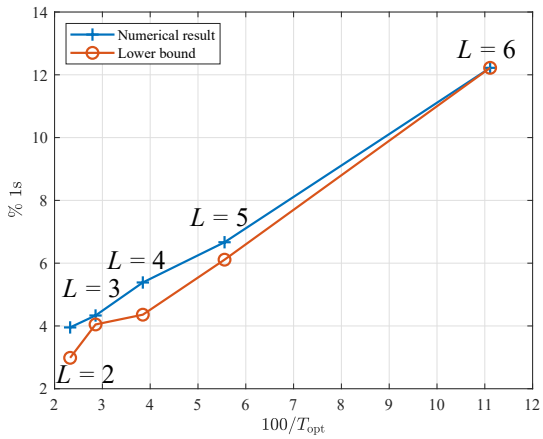

Figure 4: Minimum percentage of 1s required for a valid $\boldsymbol{A} \in \{0,1\}^{M\times T}$ with respect to $100/T_{\text{opt}}$ for $M = 60$, $K = 7$, $L = \{2,3,4,5,6\}$ $(N = L)$.

ficult since we can just put 1s at random positions and, with high probability (around 80% in the case of $K = 4$), this $\boldsymbol{A}$ will be valid.

5 Discussion and Examples

As mentioned previously, one of the goals of this paper is to find the trade-off between the different system parameters required for the equivalent processing to be information-lossless. An interesting case is when $N = 1$, since it relates directly to the trade-off between the centralized and decentralized architectures shown in Fig. 2. Assuming that our framework is equipped with a valid matrix $\boldsymbol{A}$, the trade-off between L and T comes directly from condition (24). We can select T as T_{opt} from (29), as can be seen in Fig. 7.

It is interesting to observe that we reach a reduction compared with the centralized architecture also for $L = 1$. To elaborate a bit further, we observe that with $L = 1$, the number of CPU inputs becomes $T = T_{\max} \triangleq \lfloor M - \frac{M}{K} + 1 \rfloor$. This reduction comes about since we have allowed the antennas to perform multiplications, which leads to a reduction in the number of CPU inputs from M to, at most, $T_{\max}$. The centralized architecture, illustrated in the left part of Fig. 2, has the same number of outputs per antenna, namely 1, but does not perform any multiplications. Therefore, the CPU must operate with $T = M$. If we let L_{mult} denote the number of multiplications per antenna, the centralized

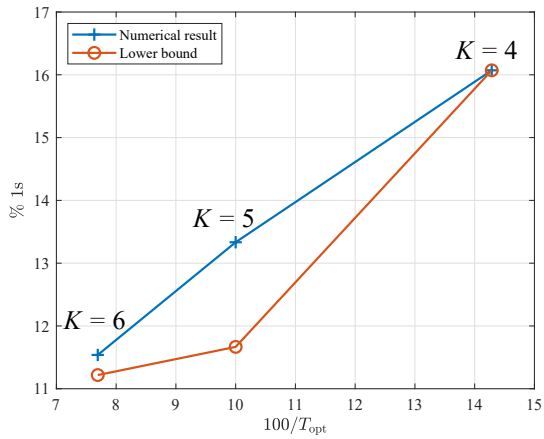

Figure 5: Minimum percentage of 1s required for a valid $\boldsymbol{A} \in \{0,1\}^{M\times T}$ with respect to $100/T_{\text{opt}}$ for $M = 24$, $K = \{6, 5, 4\}$, $L = 3$ ($N = L$).

architecture corresponds to $L_{\text{mult}} = 0$, and we can select T as

$$T = \begin{cases} M & L_{\text{mult}} = 0 \\ \max\left(\left\lfloor M\frac{K-L_{\text{mult}}}{K} + 1\right\rfloor, K\right) & L_{\text{mult}} > 0. \end{cases}$$

This is conceptually illustrated in the right part of Fig. 7.

We conclude this section with a few examples.

Example 1 *Assume a design with a CPU limited to* $T \leq 50$ *inputs, and antenna panels with* $L = 2$ *outputs. We now consider how many antennas and users (*M *and* K*, respectively) can be handled by the system. From* (24)*, we have* $50 > M\frac{K-2}{K}$ *implying that*

$$50\frac{K}{K-2} > M.$$

To maximize the left hand side, excluding the special case $K = L = 2$ *(which allows for an unlimited number of antennas), we set* $K = 3$ *and obtain* $M < 150$ *so that we can at most use* 149 *antennas. Differently put, if we choose to equip the base station with 149 antennas, we can at most serve* $K = 3$ *users. With 150+ antennas, only 2 users can be served. Setting* $K = 4$*, yields that at most 99 antennas can be used.*

We next provide two numerical examples of the WAX decomposition. The first one is meant to illustrate that it is indeed possible to obtain valid sparse matrices $\boldsymbol{A}$ comprising only elements in the set $\{0, 1\}$.

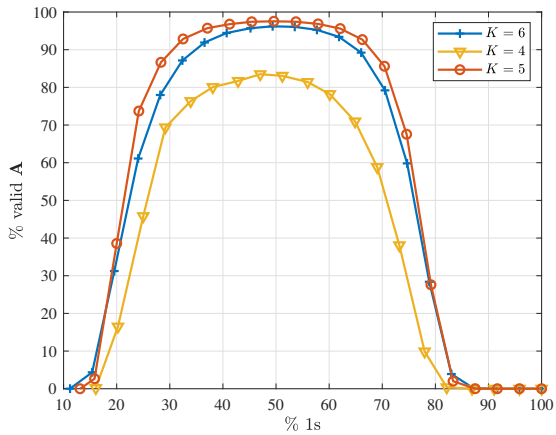

Figure 6: Percentage of valid $\boldsymbol{A} \in \{0,1\}^{M\times T}$ with 1s at random positions with respect to the percentage of 1s for $M = 24$, $L = 3$ (N=L).

Example 2 *Let $M = 100$, $N = 4$, $P = 25$, $K = 10$, and $L = 4$. From Theorem 1, we have that $T > 100 \times 0.6 = 60$, so we take $T = 61$. It can be numerically verified that the matrix*

$$\boldsymbol{A} = \left[\begin{array}{c|c|c} \multicolumn{3}{c}{\boldsymbol{I}_{61}} \\ \hline & \multicolumn{2}{c}{\boldsymbol{I}_{22}} \\ \cline{2-3} & & \boldsymbol{I}_5 \\ \boldsymbol{I}_{39} & \boldsymbol{I}_{17} & \boldsymbol{I}_5 \\ & & \boldsymbol{I}_5 \\ \hline & & \boldsymbol{I}_2 \quad \boldsymbol{I}_2 \quad \boldsymbol{0}_{2\times 1} \end{array}\right] \tag{30}$$

is valid. We designed this $\boldsymbol{A}$ by aiming at a minimum number of non-zero elements, while satisfying both Lemma 4 and Lemma 5. It can be verified that $\boldsymbol{A}$ has 158 ones and 5942 zeros. Thus, merely 2.6% of $\boldsymbol{A}$ is non-zero.

Our next example is providing the reader with a graphical illustration of the WAX decomposition.

Example 3 *Let $M = 8$, $N = 2$, $P = 4$, $K = 5$, and $L = 2$. Thus, $T > 4.8$, so we select $T = 5$. In this case, the number of variables and the number of equations associated to the linear system* (20) *is $TK + ML = 41$ and $MK = 40$, respectively; thus, we have precisely one more variable than equations. A particular example of the WAX decomposition for the given parameters is shown in* (31)*. The strength of the WAX decomposition is that, for any $\boldsymbol{H}$, except for those in a set of measure 0, the matrix $\boldsymbol{A}$ can be kept as it is while only $\boldsymbol{W}$ and $\boldsymbol{X}$ need to change.*

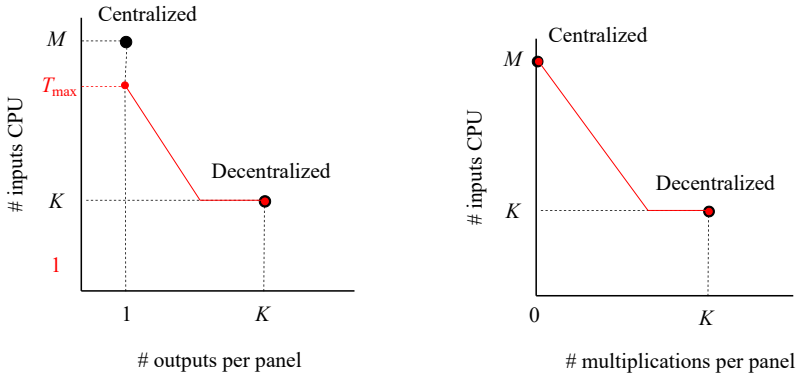

Figure 7: Number of inputs to the CPU (related to T) v.s. number of outputs (left)/number of multiplications (right) per antenna (related to L).

6 Information-Loss without WAX Decomposition

Throughout the previous sections of the paper we have focused on performing information-lossless processing within our framework, i.e., we have focused on the cases where the maximization (4) leads to $\mathcal{I}_{\boldsymbol{Z},\boldsymbol{S}}(\boldsymbol{z};\boldsymbol{s}) = \mathcal{I}_{\boldsymbol{Y},\boldsymbol{S}}(\boldsymbol{y};\boldsymbol{s})$. We have defined the WAX decomposition, which allows performing information-lossless processing within our framework. Theorem 1 sets the main constraints on the system dimensions for WAX decomposition, and equivalently information-lossless processing, to be possible within our framework. However, it is of great interest to know the information-loss produced when WAX decomposition is not possible, i.e., we would like to solve (4) when Theorem 1 is not satisfied.

Solving (4) is a research challenge in itself which might lead to future work

$$\underbrace{\begin{bmatrix} 1 & -1 & 0 & 0 & 0 & 0 & 0 & 0 \\ 2 & 1 & 0 & 0 & 0 & 0 & 0 & 0 \\ 0 & 0 & 1 & 1 & 0 & 0 & 0 & 0 \\ 0 & 0 & 0 & -1 & 0 & 0 & 0 & 0 \\ 0 & 0 & 0 & 0 & 2 & 1 & 0 & 0 \\ 0 & 0 & 0 & 0 & 2 & -1 & 0 & 0 \\ 0 & 0 & 0 & 0 & 0 & 0 & 2 & -1 \\ 0 & 0 & 0 & 0 & 0 & 0 & 2 & 2 \end{bmatrix}}_{\boldsymbol{W}} \underbrace{\begin{bmatrix} 1 & 0 & 0 & 0 & 0 \\ 0 & 1 & 0 & 0 & 0 \\ 0 & 0 & 1 & 0 & 0 \\ 0 & 0 & 0 & 1 & 0 \\ 0 & 0 & 0 & 0 & 1 \\ 1 & 0 & 0 & 1 & 1 \\ 0 & 1 & 0 & 1 & 1 \\ 0 & 0 & 1 & 1 & 1 \end{bmatrix}}_{\boldsymbol{A}} \underbrace{\begin{bmatrix} -2 & -1 & -1 & 2 & 2 \\ 1 & -2 & -1 & 1 & 2 \\ 1 & -1 & -2 & -1 & -2 \\ 0 & 2 & 0 & -1 & 0 \\ 0 & -1 & 2 & 1 & -2 \end{bmatrix}}_{\boldsymbol{X}} = \underbrace{\begin{bmatrix} -3 & 1 & 0 & 1 & 0 \\ -2 & -4 & -3 & 5 & 6 \\ 1 & 1 & -2 & -2 & -2 \\ 0 & -2 & 0 & 1 & 0 \\ -2 & -2 & 5 & 4 & -4 \\ 2 & -2 & 3 & 0 & -4 \\ 1 & -2 & 2 & 3 & 4 \\ 4 & -2 & 2 & 0 & -8 \end{bmatrix}}_{\boldsymbol{H}} \tag{31}$$

on the topic. In this section we will present initial ideas, as well as numerical results using standard optimization methods, to get an overall understanding of the information-losses that are induced when having lower T than the minimum required from Theorem 1. We will again focus on the general case where $N = L$, and we will only consider randomly chosen $\boldsymbol{A}$ and $\boldsymbol{H}$ matrices.

6.1 Approximate MF

A simple first approach, intuitively related to how we compute WAX decomposition, is to work on the minimization problem

$$\begin{aligned} \underset{\boldsymbol{X},\{\hat{\boldsymbol{W}}_p\}_{p=1}^{P}}{\text{minimize}} \quad & \|\boldsymbol{A}\boldsymbol{X} - \hat{\boldsymbol{W}}\boldsymbol{H}\|_{\mathrm{F}}^2, \\ \text{s.t.} \quad & \operatorname{rank}(\hat{\boldsymbol{W}}_p) = L, \, \forall p \\ & \|\boldsymbol{X}\| + \|\hat{\boldsymbol{W}}\| = c, \end{aligned} \tag{32}$$

where $\hat{\boldsymbol{W}}$ has the same structure as (3) for $N = L$ and $P = M/L$, and the actual matrix $\boldsymbol{W}$ to be used in our framework would be obtained as $\boldsymbol{W} = \hat{\boldsymbol{W}}^{-1}$. The last constraint in (32) ensures a non-zero solution, where the scalar c can be any non-zero real value.[4] The minimization (32) leads to the WAX decomposition when Theorem 1 applies. This means that we could solve both problems using the same approach, and thus, without altering the overall complexity. In case (24) is fulfilled, (32) would give 0, and the solution would also solve the maximization (4), which is not true in general.

Solving (32) can be seen as applying approximate MF within our framework. This minimization can be found in closed-form when $L \leq \min(T, K)$ as we will now prove. Let us rewrite the norm as

$$\|\boldsymbol{A}\boldsymbol{X} - \hat{\boldsymbol{W}}\boldsymbol{H}\|_{\mathrm{F}}^2 = \sum_{p=1}^{P} \|\boldsymbol{A}_p\boldsymbol{X} - \hat{\boldsymbol{W}}_p\boldsymbol{H}_p\|_{\mathrm{F}}^2. \tag{33}$$

Assuming the optimum $\boldsymbol{X}$ has been fixed, we would have $\hat{\boldsymbol{W}}_p = \boldsymbol{A}_p\boldsymbol{X}\boldsymbol{H}_p^{\dagger}$ ($\boldsymbol{H}_p^{\dagger}$ being the right pseudo-inverse of $\boldsymbol{H}_p$), which is of rank $\min(T, K, L)$ when $\boldsymbol{A}$ and $\boldsymbol{H}$ are randomly chosen. We can restrict ourselves to $L \leq \min(T, K)$ due to its previously mentioned practical interest. In this case, (32) is solved by considering the equivalent linear system from (21)

$$\|\boldsymbol{A}\boldsymbol{X} - \hat{\boldsymbol{W}}\boldsymbol{H}\|_{\mathrm{F}}^2 = \boldsymbol{u}^H\boldsymbol{B}^H\boldsymbol{B}\boldsymbol{u}. \tag{34}$$

[4] Note that, when applying $\boldsymbol{W} = \hat{\boldsymbol{W}}^{-1}$, the multiplication associated to (2) will cancel out any common scaling of $\hat{\boldsymbol{W}}$ and $\boldsymbol{X}$.

The vector $\boldsymbol{u}$ corresponds to the entries of matrices $\boldsymbol{X}$ and $\hat{\boldsymbol{W}}$, so the constraint on the norms of $\hat{\boldsymbol{W}}$ and $\boldsymbol{X}$ corresponds to an arbitrary norm constraint on $\boldsymbol{u}$. With this in mind, the solution to the minimization problem is obtained by setting $\boldsymbol{u}$ to be the eigenvector associated to the lowest eigenvalue of $\boldsymbol{B}^H\boldsymbol{B}$. If the conditions for WAX were fulfilled, the lowest eigenvalue of $\boldsymbol{B}^H\boldsymbol{B}$ would be 0, which would lead to the information-lossless solution.

6.2 Antenna Selection

Another practical approach that would give a lower bound to the maximum $\mathcal{I}_{\boldsymbol{Z},\boldsymbol{S}}(z,s)$ from (4) is to consider antenna selection so as to reduce M until Theorem 1 is satisfied. Note that this approach is valid only when $T \geq K$, which was not the case with the previous approach. Furthermore, for $N > 1$, the antenna selection would correspond to panel selection since we need an integer number of panels, which means we can only reduce N antennas at a time.

How to optimally make the panel selection is also a research problem in itself, but we limit our results to simple selection where the panels having the highest local channel matrix norms are the ones being used.

6.3 Numerical Results

Definition 2 *Let us define the relative rate for our framework as*

$$\mathbb{E}_{\boldsymbol{A},\boldsymbol{H}}\left(\frac{\mathcal{I}_{\boldsymbol{Z},\boldsymbol{S}}(z,s)}{\mathcal{I}_{\boldsymbol{Y},\boldsymbol{S}}(y,s)}\right), \tag{35}$$

where $\boldsymbol{A}$ and $\boldsymbol{H}$ are standard IID Gaussian random matrices.

Figs. 8 and 9 show the average relative rates, which have been optimized using norm minimization (32) and panel selection. We have also included as a comparison the average relative rate obtained by standard brute force numerical optimization using the result from (32) as starting point. This numerical optimization can give us a hint of what average relative rates could be achieved if more clever optimization approaches were considered. In the plots, we have considered the range of L and T values not accepting a WAX decomposition according to Theorem 1. Fig. 8 shows that when we reduce T below T_{opt} the performance gets slowly degraded, so the system would still be able to work at acceptable rates even if we cannot perform WAX decomposition. In the case of Fig. 9, reducing L below L_{opt},[5] attains a steeper loss, but the degradation is still reasonable. We can also see that the norm minimization associated to (32) presents a considerable loss with respect to the numerical optimization,

[5] L_{opt} can be obtained from Theorem 1 as a converse of T_{opt}.

but it can still serve as a simple auxiliary method that allows our framework to keep serving users under conditions where WAX is not possible, e.g., if the number of users increase. In fact, (32) corresponds to the WAX decomposition when the parameters allow it, so that no further processing would be needed in such a system.

Panel selection, can perform better than the norm minimization in some cases, but the limitation of having to disregard full panels makes it perform slightly worse for most values of T in Fig. 8. Furthermore, this method is slightly less versatile than norm minimization since it is not available for all possible values of T, as can be seen in Fig. 8. However, we can note that $T < K$ intuitively translates into having to discard the data from certain users, which could potentially be considered in more complex antenna selection schemes.

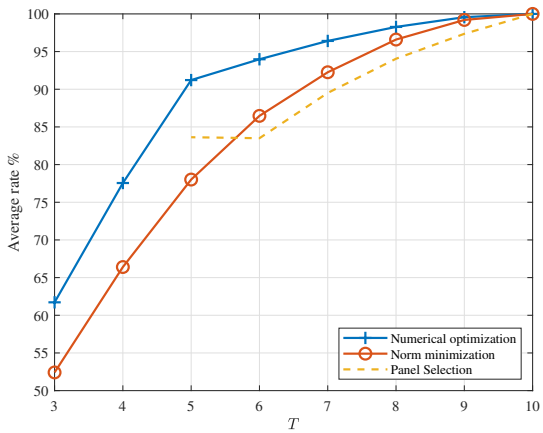

Figure 8: Average relative rate (in percentage), $\mathcal{I}_{\boldsymbol{Z},\boldsymbol{S}}(z,s)/\mathcal{I}_{\boldsymbol{Y},\boldsymbol{S}}(y,z)$, with $\boldsymbol{A}$ and $\boldsymbol{H}$ having IID Gaussian entries, for $M = 24$, $K = 5$, $L = 3$, $T_{\text{opt}} = 10$.

7 Conclusions

We have introduced a general framework that allows the exploitation of the trade-off between complexity (number of multiplications/outputs per panel) and level of decentralization (connections to CPU) in multi-antenna architectures. We have presented the WAX decomposition, a matrix decomposition that achieves information-lossless processing within our framework under some restrictions. Said restrictions also describe the trade-off between number of multiplications/outputs per panel and number of connections to the CPU if we consider only information-lossless processing. Furthermore, we have studied the problem of finding simple combining networks ($\boldsymbol{A}$ matrices) that admit WAX

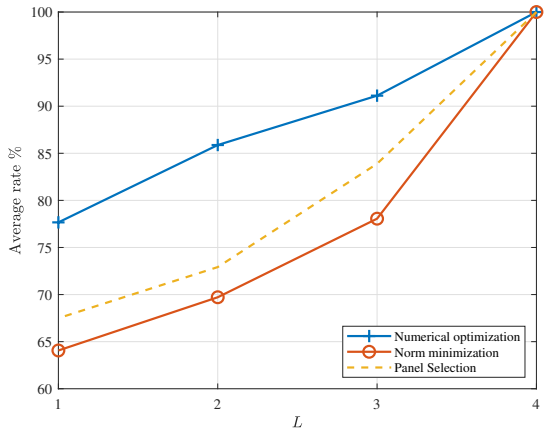

Figure 9: Average relative rate (in percentage), $\mathcal{I}_{\boldsymbol{Z},\boldsymbol{S}}(z,s)/\mathcal{I}_{\boldsymbol{Y},\boldsymbol{S}}(y,z)$, with $\boldsymbol{A}$ and $\boldsymbol{H}$ having IID Gaussian entries, for $M=24$, $K=5$, $T=5$, $L_{\text{opt}}=4$.

decomposition within our framework. Finally, we have broadly studied the information-loss produced when the system parameters lead to non-availability of the WAX decomposition.

Future work could include a deeper study on the cases where WAX decomposition is not available and information-lossy processing has to be applied. This same line would include the design of efficient algorithms and analytical solutions to optimize the achievable information rates. Furthermore, finding sufficient conditions for the combining network (i.e., $\boldsymbol{A}$) to be valid for WAX decomposition still remains unresolved. Other lines of work could include narrowing the study to some of the exceptions that we have not covered such as when the parameters are not divisible, etc.

Appendix A: Proof of Theorem 1

We first make the observation that the rank of $\boldsymbol{A}$ cannot be lower than the rank of $\boldsymbol{H}$. The rank of a randomly chosen $\boldsymbol{A}$ is $\min(M,T)$ with probability 1. Assuming that $M \geq K$, this implies $T \geq K$, expressed as $T > \max(\cdot, K-1)$ in the statement.

We next provide a lemma that will be useful.

Lemma 7 *Let $\boldsymbol{W}$ and $\hat{\boldsymbol{W}}$ be two matrices of the same form as $\boldsymbol{W}$ in (3) with $N=L$ (i.e., they are block diagonal matrices where the blocks are $L \times L$ matrices). If $\boldsymbol{A}\boldsymbol{X} = \hat{\boldsymbol{W}}\boldsymbol{H}$ is solvable such that $\det(\hat{\boldsymbol{W}}_p) > 0$, $1 \leq p \leq P$, then $\boldsymbol{W}\boldsymbol{A}\boldsymbol{X} = \boldsymbol{H}$ is solvable.*

Proof Suppose $\boldsymbol{AX} = \hat{\boldsymbol{W}}^H \boldsymbol{H}$ is solvable such that $\det(\hat{\boldsymbol{W}}_p) > 0,\ 1 \leq p \leq P$. This implies that $\hat{\boldsymbol{W}}^{-1}$ exists. Thus,

$$\hat{\boldsymbol{W}}^{-1} \boldsymbol{AX} = \boldsymbol{H}.$$

The lemma follows by observing that $\hat{\boldsymbol{W}}^{-1}$ is of the same form as $\boldsymbol{W}$, so we can take $\boldsymbol{W} = \hat{\boldsymbol{W}}^{-1}$. □

Let us now study $\boldsymbol{AX} = \hat{\boldsymbol{W}}\boldsymbol{H}$. Said matrix equation specifies MT linear equations in $TK + ML$ variables, and hence, it is solvable if $T > M(K-L)/K$, as can be seen from the vectorized version in (21). It remains to show that for randomly chosen $\boldsymbol{A}$ and $\boldsymbol{H}$, the solution satisfies $\det(\hat{\boldsymbol{W}}_p) > 0,\ 1 \leq p \leq P$. Let us define $\mathcal{V}$ as the set of admissible solutions, i.e.,

$$\begin{aligned} \mathcal{V} = \{\boldsymbol{A}, \boldsymbol{H} \,|\, \exists \hat{\boldsymbol{W}}, \boldsymbol{X} : \boldsymbol{AX} = \hat{\boldsymbol{W}}\boldsymbol{H}, \\ \det(\hat{\boldsymbol{W}}_p) \neq 0, \forall p, \det(\boldsymbol{B}\boldsymbol{B}^H) \neq 0\}, \end{aligned} \tag{36}$$

where $\boldsymbol{B} = [\boldsymbol{B}_1 \boldsymbol{B}_2]$ is again the matrix associated to the equivalent linear system (21), which is given by (23). Assuming that $\boldsymbol{B}$ is full-rank, the solution to $\boldsymbol{AX} = \hat{\boldsymbol{W}}\boldsymbol{H}$ depends on $F = TK + ML - MK$ free variables, here denoted by $\{z_f\}$. The solution $\{\hat{\boldsymbol{W}}\}_{i,j}$ is a linear combination of the free variables $\{z_f\}$ where the weights depend on $\boldsymbol{A}$ and $\boldsymbol{H}$, i.e.,

$$\{\hat{\boldsymbol{W}}_p\}_{i,j} = \sum_{f=1}^{F} c_{p,i,j,f}(\boldsymbol{A}, \boldsymbol{H}) z_f.$$

Note that the number of free variables, F, can be increased if $\boldsymbol{B}$ is not full-rank (leading to a different polynomial expression), that is why we are only interested in the solutions giving a full-rank $\boldsymbol{B}$, i.e., $\det(\boldsymbol{B}\boldsymbol{B}^H) \neq 0$. Thus, the following lemma will come in handy.

Lemma 8 *Given randomly chosen matrices $\boldsymbol{H}$ and $\boldsymbol{A}$, the matrix $\boldsymbol{B} = [\boldsymbol{B}_1 \boldsymbol{B}_2]$ ($\boldsymbol{B}_1$ and $\boldsymbol{B}_2$ are defined as in* (23)*) fulfills* $\det(\boldsymbol{B}\boldsymbol{B}^H) \neq 0$ *with probability 1.*

Proof We can define the determinant $\det(\boldsymbol{B}\boldsymbol{B}^H)$ as a polynomial expression of the form

$$\det(\boldsymbol{B}\boldsymbol{B}^H) = \sum_g b_g(\boldsymbol{A}, \boldsymbol{H}) \prod_{i,j,l,k} \{\boldsymbol{H}\}_{i,j}^{h_{i,j,g}} \{\boldsymbol{A}\}_{l,k}^{a_{l,k,g}}.$$

This polynomial expression will evaluate to 0 only for a countable set (which thus attains probability 0) of $\boldsymbol{A}$ and $\boldsymbol{H}$ matrices if we can find at least an $\boldsymbol{A}$

and an $\boldsymbol{H}$ such that $\det(\boldsymbol{B}\boldsymbol{B}^H) \neq 0$. One example of this is when $\boldsymbol{A}$ is chosen randomly and we have $\{\boldsymbol{H}\}_{i,j} = \{\boldsymbol{A}\}_{i,j}$, $i \in \{1, \dots M\}$, $j \in \{1, \dots, K\}$. □

A similar reasoning to the one used in the proof of Lemma 8 can be applied to show that for randomly chosen $\boldsymbol{A}$ and $\boldsymbol{H}$ we have $\hat{\boldsymbol{W}} \neq 0$ with probability 1. The determinant $\det(\hat{\boldsymbol{W}}_p)$ can be written as a polynomial combination of the previous $\{\hat{\boldsymbol{W}}_p\}_{i,j}$. Thus we can express it as

$$\det(\hat{\boldsymbol{W}}_p) = \sum_{g=1}^{G} \tilde{c}_g(\boldsymbol{A}, \boldsymbol{H}) \prod_{f=1}^{F} z_f^{q_{g,f}}, \tag{37}$$

for some G, with $\sum_{f=1}^{F} q_{g,f} = P$, $\forall g$. Thus, the only possibility for having $\det(\hat{\boldsymbol{W}}_p) = 0$ is if the coefficients are zero, i.e., $\tilde{c}_g(\boldsymbol{A}, \boldsymbol{H}) = 0$, $1 \leq g \leq G$. However, the coefficients $\tilde{c}_g(\boldsymbol{A}, \boldsymbol{H})$ are rational expressions of the entries in $\boldsymbol{A}$ and $\boldsymbol{H}$. This means that, in order to have $\tilde{c}_g(\boldsymbol{A}, \boldsymbol{H}) = 0$, a polynomial multivariate expression of the entries in $\boldsymbol{A}$ and $\boldsymbol{H}$ must be 0. Again, this can only happen at most in a countable set of $\boldsymbol{A}$ and $\boldsymbol{H}$ as long as we find an $\boldsymbol{A}$ and an $\boldsymbol{H}$ such that $\det(\hat{\boldsymbol{W}}_p)$, $\forall p$, while still assuring that $\boldsymbol{B}$ is full-rank so that F remains fixed. The same example as in the proof of Lemma 8, i.e., randomly chosen $\boldsymbol{A}$ and $\{\boldsymbol{H}\}_{i,j} = \{\boldsymbol{A}\}_{i,j}$, $i \in \{1, \dots M\}$, $j \in \{1, \dots, K\}$, gives the trivial solution $\hat{\boldsymbol{W}} = \mathbf{I}_M$, and thus fulfills both conditions. Therefore, we have proved that a randomly chosen $\boldsymbol{A}$ and $\boldsymbol{H}$ will be in the set $\mathcal{V}$ with probability 1.

Appendix B: Proof of Lemma 5

From the structure of $\boldsymbol{B}_1$ in (23), we observe that a particular row of $\boldsymbol{A}$ appears exactly in K rows of $\boldsymbol{B}$. Let us denote $\boldsymbol{B}_0$ as the submatrix of $\boldsymbol{B}$ formed by all rows in $\boldsymbol{B}$ where the rows of $\boldsymbol{A}_0$ appear. Clearly, to satisfy (21), we must in particular satisfy $\boldsymbol{B}_0\boldsymbol{u} = \mathbf{0}_{RK\times 1}$. Now, $\boldsymbol{B}_0$ reads

$$\boldsymbol{B}_0 = \left[\boldsymbol{I}_K \otimes \boldsymbol{A}_0 \;\; \widehat{\boldsymbol{H}}_0\right],$$

where $\widehat{\boldsymbol{H}}_0$ is formed from $\boldsymbol{H}$ as follows: Let $\iota(r)$ denote the block $\boldsymbol{H}_{\iota(r)}$ where the rth row in $\boldsymbol{A}_0$ is taken from. Let $\boldsymbol{H}_0 = \left[\boldsymbol{H}_{\iota(1)}^T \; \boldsymbol{H}_{\iota(2)^T} \; \dots \; \boldsymbol{H}_{\iota(R)}^T\right]^T$, and let $\mathbb{III}(\ell)$ be an $R \times L$ matrix with a single entry equal to 1 at row ℓ and column $(\iota(\ell) \bmod L) + 1$, and all other equal to 0. Then,

$$\begin{aligned}\widehat{\boldsymbol{H}}_0 \;\; = \;\; \Big[&\mathbf{0}_{\mathcal{D}_0} \;\; \boldsymbol{H}_{\iota(1)}^H \otimes \mathbb{III}(1) \;\; \mathbf{0}_{\mathcal{D}_1} \;\; \boldsymbol{H}_{\iota(2)}^H \otimes \mathbb{III}(2) \\ &\dots \;\; \mathbf{0}_{\mathcal{D}_{R-1}} \;\; \boldsymbol{H}_{\iota(R)}^H \otimes \mathbb{III}(R) \;\; \mathbf{0}_{\mathcal{D}_R}\Big]\end{aligned} \tag{38}$$

where we have used the shorthand notation

$$\mathcal{D}_k = RK \times (\iota(k+1) - \iota(k))L^2,$$
$$\iota(0) \triangleq 1, \quad \iota(R+1) \triangleq M/L.$$

To study the null space of $\boldsymbol{B}_0$ we may just as well study the null space of $(\boldsymbol{I}_K \otimes \boldsymbol{Q}_0^H)\boldsymbol{B}_0$, where $\boldsymbol{Q}_0\boldsymbol{R}_0 = \boldsymbol{A}_0$ is the QR decomposition of $\boldsymbol{A}_0$. We have,

$$(\boldsymbol{I}_K \otimes \boldsymbol{Q}_0^H)\boldsymbol{B}_0 = \left[\boldsymbol{I}_K \otimes \boldsymbol{R}_0 \;\; (\boldsymbol{I}_K \otimes \boldsymbol{Q}_0^H)\widehat{\boldsymbol{H}}_0\right]. \tag{39}$$

Let $\kappa = \operatorname{rank}(\boldsymbol{A}_0)$. The matrix $\boldsymbol{I}_K \otimes \boldsymbol{R}_0$ consequently has $K(R-\kappa)$ all-zero rows.

If we extract said all-zero rows, we obtain,

$$\left[\boldsymbol{0}_{K(R-\kappa)\times TK} \; \boldsymbol{P}(\boldsymbol{I}_K \otimes \boldsymbol{Q}_0^H)\widehat{\boldsymbol{H}}_0\right]\begin{bmatrix}\operatorname{vec}(\boldsymbol{X})\\ \operatorname{vec}(\boldsymbol{W}_1)\\ \vdots \\ \operatorname{vec}(\boldsymbol{W}_P)\end{bmatrix} = \boldsymbol{0}_{K(R-\kappa)\times 1}$$

where $\boldsymbol{P}$ is a $K(R-\kappa) \times KR$ matrix that extracts the rows where $\boldsymbol{I}_K \otimes \boldsymbol{R}_0$ is all-zero. This implies that we can discard $\boldsymbol{X}$ so that we equivalently obtain

$$\boldsymbol{P}(\boldsymbol{I}_K \otimes \boldsymbol{Q}_0^H)\widehat{\boldsymbol{H}}_0 \begin{bmatrix}\operatorname{vec}(\boldsymbol{W}_1)\\ \vdots \\ \operatorname{vec}(\boldsymbol{W}_P)\end{bmatrix} = \boldsymbol{0}_{K(R-\kappa)\times 1}. \tag{40}$$

We next note that, due to the many all-zero columns in $\widehat{\boldsymbol{H}}_0$ (represented by the terms $\boldsymbol{0}_{\mathcal{D}_k}$ in (38)), not all the $\boldsymbol{W}_p$ matrices matter. In fact, it can be straightforwardly verified that (40) is equivalent to

$$\boldsymbol{P}(\boldsymbol{I}_K \otimes \boldsymbol{Q}_0^H)\bar{\boldsymbol{H}}_0 \begin{bmatrix}\boldsymbol{w}_{\iota(1)}\\ \vdots \\ \boldsymbol{w}_{\iota(R)}\end{bmatrix} = \boldsymbol{0}_{K(R-\kappa)\times ML}, \tag{41}$$

where $\boldsymbol{w}_m$ is the $1 \times L$ vector formed from extracting the entries at the mth row of $\boldsymbol{W}$ that are allowed to take non-zero values, and

$$\bar{\boldsymbol{H}}_0 = \left[\boldsymbol{H}_{\iota(1)}^H \otimes \mathbb{I}(1) \;\; \boldsymbol{H}_{\iota(2)}^H \otimes \mathbb{I}(2) \;\; \ldots \;\; \boldsymbol{H}_{\iota(R)}^H \otimes \mathbb{I}(R)\right], \tag{42}$$

where $\mathbb{I}(\ell)$ is the non-zero column of $\mathbb{III}(\ell)$.

For randomly chosen $\boldsymbol{H}$, the matrix $\boldsymbol{P}(\boldsymbol{I}_K \otimes \boldsymbol{Q}_0^H)\bar{\boldsymbol{H}}_0$ is full rank with

probability 1. Therefore, (42) only has a non-trivial solution whenever the number of unknowns is larger than the number of equations, i.e., whenever, $RL > K(R-\kappa)$. Consequently,

$$\kappa > R\frac{K-L}{K}.$$

Appendix C: Necessary condition for $\boldsymbol{A}$

As per previous results, a matrix $\boldsymbol{H}$ can, with probability 1, be decomposed as $\boldsymbol{H} = \boldsymbol{W}\boldsymbol{A}\boldsymbol{X}$ if and only if there exists a full rank matrix $\hat{\boldsymbol{W}}$ such that $\boldsymbol{A}\boldsymbol{X} = \hat{\boldsymbol{W}}\boldsymbol{H}$. We are now interested in establishing necessary conditions for the matrix $\boldsymbol{A}$ so that this is possible. Let $\boldsymbol{A}_{\mathcal{S}}$ denote a submatrix of $\boldsymbol{A}$ comprising an arbitrary selection of rows in $\boldsymbol{A}$ with $\operatorname{rank}(\boldsymbol{A}_{\mathcal{S}}) = r$. An immediate consequence is that $\operatorname{rank}(\boldsymbol{A}_{\mathcal{S}}\boldsymbol{X}) \leq r$. Assuming that $\boldsymbol{H} = \boldsymbol{W}\boldsymbol{A}\boldsymbol{X}$ holds, $\operatorname{rank}\left(\hat{\boldsymbol{W}}_{\mathcal{S}}\boldsymbol{H}\right) = \operatorname{rank}(\boldsymbol{A}_{\mathcal{S}}\boldsymbol{X})$, where $\hat{\boldsymbol{W}}_{\mathcal{S}}$ is a submatrix of $\hat{\boldsymbol{W}}$ comprising rows corresponding to those in $\boldsymbol{A}_{\mathcal{S}}$. On the other hand, if no $\hat{\boldsymbol{W}}_{\mathcal{S}}$ exists such that $\operatorname{rank}\left(\hat{\boldsymbol{W}}_{\mathcal{S}}\boldsymbol{H}\right) \leq r$, we can infer that $\boldsymbol{A}$ does not allow for a WAX decomposition, i.e., there are no matrices $\boldsymbol{W}$ and $\boldsymbol{X}$ such that $\boldsymbol{H} = \boldsymbol{W}\boldsymbol{A}\boldsymbol{X}$. Therefore, a necessary condition on $\boldsymbol{A}$ for the existence of a WAX decomposition is

$$\operatorname{rank}(\boldsymbol{A}_{\mathcal{S}}) \geq \min_{\hat{\boldsymbol{W}}_{\mathcal{S}} \in \mathcal{W}} \operatorname{rank}\left(\hat{\boldsymbol{W}}_{\mathcal{S}}\boldsymbol{H}\right), \quad \forall \mathcal{S}, \tag{43}$$

where we will define the set $\mathcal{W}$ after having introduced further notation. The matrix $\boldsymbol{A}$ contains M rows, and since L divides M, $\boldsymbol{A}$ contains $P = M/L$ blocks of L rows. Let the $1 \times P$ vector $\boldsymbol{a}$ denote the number of rows in $\boldsymbol{A}_{\mathcal{S}}$ taken from the pth block in $\boldsymbol{A}$, and let $\boldsymbol{A}_{\mathcal{S},p}$ and $\hat{\boldsymbol{W}}_{\mathcal{S},p}$ be the $a_p \times T$ and $a_p \times M$ submatrices of $\boldsymbol{A}_{\mathcal{S}}$ and $\hat{\boldsymbol{W}}_{\mathcal{S}}$, respectively, formed from these a_p rows. With that, $\mathcal{W}$ is the set containing all block-diagonal matrices where the pth block is of dimensions $a_p \times K$ and has rank a_p (the latter is needed to ensure that the overall matrix $\hat{W}$ is invertible).

We are now ready to study (43). Suppose that the minimum of (43) is r. Since $\hat{\boldsymbol{W}}_{\mathcal{S}}\boldsymbol{H}$ has dimensions $(\sum_p a_p) \times K$ this implies that the null-space of $\hat{\boldsymbol{W}}_{\mathcal{S}}\boldsymbol{H}$ has dimension $K - r$. Thus, if $\operatorname{rank}\left(\hat{\boldsymbol{W}}_{\mathcal{S}}\boldsymbol{H}\right) = r$, there must exist a $K \times (K-r)$ matrix $\boldsymbol{N}$ such that $\hat{\boldsymbol{W}}_{\mathcal{S}}\boldsymbol{H}\boldsymbol{N} = \boldsymbol{0}$. Recalling that $\hat{\boldsymbol{W}}_{\mathcal{S}}$ is block-diagonal with each block being of dimension $a_p \times L$ and having rank a_p, it follows that

$$\operatorname{rank}(\boldsymbol{H}_p\boldsymbol{N}) \leq L - a_p \tag{44}$$

where $\boldsymbol{H}_p$ is of dimension $L \times K$ and $\boldsymbol{H} = [\boldsymbol{H}_1^{\mathrm{H}} \ \cdots \ \boldsymbol{H}_P^{\mathrm{H}}]^{\mathrm{H}}$. Thus, if we want

to solve the minimization in (43), we have the equivalent problem of finding the maximum possible number of columns in the matrix $\boldsymbol{N}$ so that it is full rank and $\text{rank}\,(\boldsymbol{H}_p\boldsymbol{N}) \leq L - a_p,\ p = 1 \ldots P$.

We next define the rank-profile of a matrix $\boldsymbol{N}$ as a matrix $\boldsymbol{J}$ whose (b,p)th element is given by

$$J_{b,p} = \text{rank}\,(\boldsymbol{H}_p\boldsymbol{N}_{1:b}) - \text{rank}\,(\boldsymbol{H}_p\boldsymbol{N}_{1:b-1}),$$

and where $\boldsymbol{N}_{1:b}$ denotes columns $1, 2, \ldots, b$ of $\boldsymbol{N}$. We remark that $J_{b,p} \in \{0,1\}$, and that $\boldsymbol{J}$ depends on $\boldsymbol{H}$, although our notation does not indicate this dependency. In the following lemma, we characterize the admissible rank-profiles.

Lemma 9 *There exists a full rank matrix $\boldsymbol{N}$ containing B columns such that $\text{rank}\,(\boldsymbol{H}_p\boldsymbol{N}) \leq L - a_p$ if and only if the rank-profile matrix $\boldsymbol{J}$ satisfies*

$$K - Ld_{<L}(\bar{\boldsymbol{a}}) + \sum_{b'=1}^{b-1}\sum_{p=1}^{P} J_{b',p} + \sum_{p=1}^{P} J_{b,p}\left(L - \sum_{b'=1}^{b-1} J_{b',p}\right) \geq b, \qquad 1 \leq b \leq B,$$

$$\sum_{b=1}^{B} J_{b,p} \leq \bar{a}_p, \quad 1 \leq p \leq P,$$

where $d_{<L}(\cdot)$ denotes the number of elements of its argument that are less than L, and $\bar{a}_p = L - a_p$.

Proof We first note that if $a_p = 0$ for any p, then the condition in (44) is trivially satisfied for any $\boldsymbol{N}$ so we can without loss of generality assume that $a_p > 0,\ \forall p$. From the definition of $J_{b,p}$ if follows that $\text{rank}\,(\boldsymbol{H}_p\boldsymbol{N}) = \sum_{b=1}^{B} J_{b,p}$; thus, the second set of conditions in the lemma is trivial.

Consider now a specific value b. If $J_{b,p} = 0$, it follows that column b of $\boldsymbol{N}$, $\boldsymbol{n}_b$ is restricted to

$$\boldsymbol{n}_b \in \mathcal{I}_{b,p} = \mathcal{N}(\boldsymbol{H}_p) \cup \text{span}\left(\boldsymbol{H}_p^{+}\boldsymbol{H}_p\boldsymbol{N}_{1:b-1}\right),$$

while $J_{b,p} = 1$ does not restrict $\boldsymbol{n}_b$ so that $\boldsymbol{n}_b \in \mathcal{I}_{b,p} = \mathbb{C}^K$. By inspection, it can be seen that the dimensionality of $\mathcal{I}_{b,p}$ can be written as

$$\dim(\mathcal{I}_{b,p}) = K(1 - J_{b,p}) + J_{b,p}\left(K - L + \sum_{b'=1}^{b-1} J_{b,p}\right).$$

Altogether, we have that

$$\boldsymbol{n}_b \in \bigcap_{p=1}^{P} \mathcal{I}_{b,p}.$$

The dimensionality of the intersection satisfies

$$\dim\left(\bigcap_{p=1}^{P} \mathcal{I}_{b,p}\right) = \sum_{p=1}^{P} \dim(\mathcal{I}_{b,p}) - (P-1)K.$$

This dimensionality must be at least b, since there are already $b-1$ vectors in $\boldsymbol{N}_{1:b-1}$ in the same space, and the rank of $\boldsymbol{N}_{1:b}$ must be full for all b. By manipulation, the statement of the lemma can be obtained. □

Altogether, a necessary condition on $\boldsymbol{A}$ is that the rank of any submatrix $\boldsymbol{A}_{\mathcal{S}}$ satisfies $\text{rank}\,(\boldsymbol{A}_{\mathcal{S}}) \geq K - B_{\mathcal{S}}$, where $B_{\mathcal{S}}$ is the largest integer B that satisfies the conditions specified in Lemma 9; note that the vector $\boldsymbol{a}$ in the conditions depends on $\mathcal{S}$. It can be seen from Lemma 9 that finding the largest integer B that satisfies the conditions is a non-linear (quadratic) integer problem and we have not been able to solve it in closed form.

References

[1] J. G. Andrews, S. Buzzi, W. Choi, *et al.*, "What will 5G be?" *IEEE Journal on Selected Areas in Communications*, vol. 32, no. 6, pp. 1065–1082, 2014.

[2] Z. Pi and F. Khan, "An introduction to millimeter-wave mobile broadband systems," *IEEE Communications Magazine*, vol. 49, no. 6, pp. 101–107, 2011.

[3] T. L. Marzetta, "Noncooperative cellular wireless with unlimited numbers of base station antennas," *IEEE Transactions on Wireless Communications*, vol. 9, no. 11, pp. 3590–3600, 2010.

[4] F. Rusek, D. Persson, B. K. Lau, *et al.*, "Scaling up MIMO: Opportunities and challenges with very large arrays," *IEEE Signal Processing Magazine*, vol. 30, no. 1, pp. 40–60, 2013.

[5] S. Hu, F. Rusek, and O. Edfors, "Beyond massive MIMO: The potential of data transmission with large intelligent surfaces," *IEEE Transactions on Signal Processing*, vol. 66, no. 10, pp. 2746–2758, 2018.

[6] S. Malkowsky *et al.*, "The world's first real-time testbed for massive MIMO: Design, implementation, and validation," *IEEE Access*, vol. 5, pp. 9073–9088, 2017.

[7] C. Shepard *et al.*, "Argos: Practical many-antenna base stations," in *Proceedings of the 18th Annual International Conference on Mobile Computing and Networking (Mobicom)*, Istanbul, Turkey, 2012, pp. 53–64.

[8] Q. Yang, X. Li, H. Yao, *et al.*, "Bigstation: Enabling scalable real-time signal processing in large MU-MIMO systems," in *ACM SIGCOMM'13*, ACM, 2013, pp. 399–410.

[9] J. V. Alegría and F. Rusek, "Achievable rate with correlated hardware impairments in large intelligent surfaces," in *2019 IEEE 8th International Workshop on Computational Advances in Multi-Sensor Adaptive Processing (CAMSAP)*, 2019, pp. 559–563.

[10] H. Q. Ngo, A. Ashikhmin, H. Yang, E. G. Larsson, and T. L. Marzetta, "Cell-free massive MIMO versus small cells," *IEEE Transactions on Wireless Communications*, vol. 16, no. 3, pp. 1834–1850, 2017.

[11] E. Björnson and L. Sanguinetti, "Scalable cell-free massive MIMO systems," *IEEE Transactions on Communications*, vol. 68, no. 7, pp. 4247–4261, 2020.

[12] J. Zhang, E. Björnson, M. Matthaiou, D. W. K. Ng, H. Yang, and D. J. Love, "Prospective multiple antenna technologies for beyond 5G," *IEEE Journal on Selected Areas in Communications*, vol. 38, no. 8, pp. 1637–1660, 2020.

[13] Q. Wu and R. Zhang, "Intelligent reflecting surface enhanced wireless network via joint active and passive beamforming," *IEEE Transactions on Wireless Communications*, vol. 18, no. 11, pp. 5394–5409, 2019.

[14] J. Chen, Y. C. Liang, Y. Pei, and H. Guo, "Intelligent reflecting surface: A programmable wireless environment for physical layer security," *IEEE Access*, vol. 7, pp. 82 599–82 612, 2019.

[15] K. Li, R. R. Sharan, Y. Chen, T. Goldstein, J. R. Cavallaro, and C. Studer, "Decentralized baseband processing for massive MU-MIMO systems," *IEEE Journal on Emerging and Selected Topics in Circuits and Systems*, vol. 7, no. 4, pp. 491–507, 2017.

[16] E. Bertilsson, O. Gustafsson, and E. G. Larsson, "A scalable architecture for massive MIMO base stations using distributed processing," in *2016 50th Asilomar Conference on Signals, Systems and Computers*, 2016, pp. 864–868.

[17] K. Li, J. McNaney, C. Tarver, *et al.*, "Design trade-offs for decentralized baseband processing in massive MU-MIMO systems," in *2019 53rd Asilomar Conference on Signals, Systems, and Computers*, 2019, pp. 906–912.

[18] J. R. Sánchez, J. Vidal Alegría, and F. Rusek, "Decentralized massive MIMO systems: Is there anything to be discussed?" In *2019 IEEE International Symposium on Information Theory (ISIT)*, 2019, pp. 787–791.

[19] M. Sarajlic, F. Rusek, J. R. Sanchez, L. Liu, and O. Edfors, "Fully decentralized approximate zero-forcing precoding for massive MIMO systems," *IEEE Wireless Communications Letters*, pp. 1–1, 2019.

[20] J. Rodríguez Sánchez, F. Rusek, O. Edfors, M. Sarajlić, and L. Liu, "Decentralized massive MIMO processing exploring Daisy-chain architecture and recursive algorithms," *IEEE Transactions on Signal Processing*, vol. 68, pp. 687–700, 2020.

[21] J. Vidal Alegría, J. R. Sánchez, F. Rusek, L. Liu, and O. Edfors, "Decentralized equalizer construction for large intelligent surfaces," in *2019 IEEE 90th Vehicular Technology Conference (VTC2019-Fall)*, 2019, pp. 1–6.

[22] Z. Zhang, H. Li, Y. Dong, X. Wang, and X. Dai, "Decentralized signal detection via expectation propagation algorithm for uplink massive MIMO systems," *IEEE Transactions on Vehicular Technology*, pp. 1–1, 2020.

[23] A. Amiri, C. N. Manchón, and E. de Carvalho, "Uncoordinated and decentralized processing in extra-large MIMO arrays," *IEEE Wireless Communications Letters*, vol. 11, no. 1, pp. 81–85, 2022.

[24] J. V. Alegría, F. Rusek, J. R. Sánchez, and O. Edfors, "Trade-offs in quasi-decentralized massive MIMO," in *2020 IEEE International Conference on Communications Workshops (ICC Workshops)*, 2020, pp. 1–6.

[25] T. M. Cover and J. A. Thomas, *Elements of Information Theory (Wiley Series in Telecommunications and Signal Processing)*. USA: Wiley-Interscience, 2006.

[26] A. Paulraj, R. Nabar, and D. Gore, *Introduction to Space-Time Wireless Communications*, 1st. USA: Cambridge University Press, 2008.

[27] C. Jeon, K. Li, J. R. Cavallaro, and C. Studer, "Decentralized equalization with feedforward architectures for massive MU-MIMO," *IEEE Transactions on Signal Processing*, vol. 67, no. 17, pp. 4418–4432, 2019.

Paper III

Cell-free Massive MIMO: Exploiting the WAX decomposition

Cell-free massive MIMO consists of a large set of distributed APs serving a number of users. The APs can be far from each other, and they can also have a big number of antennas. Thus, decentralized architectures have to be considered so as to reduce the interconnection bandwidth to a CPU and make the system scalable. On the other hand, the APs in a heterogeneous network might have limited processing capabilities and fully-decentralized processing may not be available. In a recent paper, a trade-off between level of decentralization and decentralized processing complexity has been identified. Furthermore, a novel matrix decomposition—the WAX decomposition—which, if applicable to the channel matrix, allows for exploitation of said trade-off without loss of information. The results on WAX decomposition are only available for random channel matrices without specific structures, while in a cell-free massive MIMO scenario the channel can have sparse structures. In this work, we study the applicability of WAX decomposition to cell-free massive MIMO with its implications to the above-mentioned trade-off.

©2022 IEEE. Reprinted, with permission, from
J. Vidal Alegría, J. Huang, F. Rusek,
"Cell-free Massive MIMO: Exploiting the WAX decomposition,"
in *Proc. IEEE ICASSP2022*, Singapore, Singapore, 2022, pp. 5393-5397.

1 Introduction

Cell-free massive MIMO [1]–[4] is currently gaining importance as an alternative to cell-based massive MIMO systems. The idea is to have a large number of distributed APs which jointly serve a number of user equipments (UEs) within the same time-frequency resource. This idea directly relates to the concept of distributed LIS, where the APs would correspond to LIS panels [5]–[7].

Cell-free massive MIMO scenarios depend on a great number of distributed APs. Thus, the availability of decentralized processing capabilities at the APs is crucial to reduce the interconnection bandwidth between the APs and a CPU. There is extensive research on decentralized approaches for large multi-antenna systems [6], [8]–[12]. In these approaches, part of the processing is performed at the antenna-end (or panel-end), so that a CPU does not need to gather all the channel information and perform all the processing tasks. However, in future heterogeneous networks, the processing capabilities of the cell-free APs might be limited due to the use of cheap equipment easily deployable and scalable.

In [13] an information-lossless trade-off between level of decentralization (inputs to a CPU) and decentralized processing capabilities (multiplications per antenna) is identified, together with a framework that allows the exploitation of said trade-off. [13] also introduces the WAX decomposition, which is a novel matrix decomposition that, if applicable to the channel matrix, allows for information-lossless processing within the framework studied. However, the conditions for the applicability of WAX decomposition, which define the previously mentioned trade-off, are only given for a randomly chosen channel matrix with probability 1, leaving some gaps in the case of channel matrices with some specific structure.

The current work aims at closing some gaps from [13] by considering the application of WAX decomposition to cell-free massive MIMO channels, where the sparsity of the channel can be problematic. We have adapted the framework from [13] to a cell-free massive MIMO scenario, which consists of a set of APs with an arbitrary number of antennas serving several users. Our findings show that the sparsity of the cell-free massive MIMO channel can degrade the trade-off presented in [13] under some parameter configurations, but WAX decomposition can still offer a viable solution for applying information-lossless processing in a cell-free massive MIMO scenario with limited processing capabilities at the APs.

The rest of the paper is organized as follows. The system model is presented in Section 2 together with some background on the previous results on WAX decomposition. Section 3 presents new results on the applicability of WAX decomposition for cell-free massive MIMO scenarios. In Section 4, numerical results are given showing the implications of the new results on the WAX decomposition trade-off in cell-free massive MIMO. Section 5 concludes the paper with some final remarks.

Notation: In this paper, lowercase, bold lowercase and bold uppercase letters stand for scalars, column vectors and matrices, respectively. When using the mutual information operator, $\mathcal{I}(.;.)$, bold uppercase in the sub-scripts refers to random vectors instead of their realizations. The operations $(\cdot)^{\mathrm{T}}$, $(\cdot)^*$ and $(\cdot)^{\mathrm{H}}$ denote transpose, conjugate, and conjugate transpose, respectively. The operation diag$(\cdot)$ outputs a block diagonal matrix with the input matrices as the diagonal blocks. The operation $\|\cdot\|_1$ denotes L^1-norm. $\mathbf{0}_{i\times j}$ denotes the $i \times j$ all-zeros matrix. In this paper, a randomly chosen matrix corresponds to a realization of a random matrix whose elements are independently drawn from a continuous probability distribution function.

2 System Model

Let us consider the uplink of a cell-free network of P APs serving K single-antenna users. Each AP is equipped with N antennas, such that the total number of antennas is $M = PN$. The aggregated $M \times 1$ received complex vector, $\boldsymbol{y}$, can be expressed as

$$\boldsymbol{y} = \boldsymbol{H}\boldsymbol{s} + \boldsymbol{n}, \tag{1}$$

where $\boldsymbol{H}$ is an $M \times K$ channel matrix, $\boldsymbol{s}$ is the $K \times 1$ vector of symbols transmitted by the users, and $\boldsymbol{n}$ is a zero-mean complex white Gaussian noise vector with sample variance N_0.

In cell-free massive MIMO scenarios the APs can be physically situated far from each other. Therefore, each AP might only see a small subset of the users, while each user can still be seen by several APs. The implication of such a scenario is thus that the matrix $\boldsymbol{H}$ would become a sparse matrix having 0s at the positions associated to hidden users. Furthermore, in a rich scattering environment the entries associated to non-hidden users can be assumed to be IID complex Gaussian (Rayleigh fading).

Let us consider the framework presented in Fig. 1 so that each AP only needs to apply $L \times L$ filters to each of the N_L groups of L antennas, i.e., AP i applies $\boldsymbol{W}_{ij}^{\mathrm{H}}$ to the jth L-group. Note that $N_{\mathrm{L}} = N/L$ should evaluate to an integer. We can thus identify L as the number of multiplications per antenna, which corresponds to the trade-off parameter associated to decentralized processing capabilities. The outputs from the APs are then combined through a $T \times M$ fixed combining module, $\boldsymbol{A}^H$, which reduces the dimensions of the data to T. The resulting T entries would be the inputs to the CPU, which corresponds to the trade-off parameter associated to level of decentralization. An equivalent framework would be to consider that each antenna in an AP multiplies its received signals by L numbers and the corresponding sums would be applied in the combining module; however, this framework would scale by L the number

of outputs per AP.

$$\boldsymbol{z} = \boldsymbol{X}^{\mathrm{H}} \boldsymbol{A}^{\mathrm{H}} \boldsymbol{W}^{\mathrm{H}} \boldsymbol{y}, \tag{2}$$

where $\boldsymbol{W}$ is an $M \times M$ block diagonal matrix of the form

$$\boldsymbol{W} = \mathrm{diag}\left(\boldsymbol{W}_{11}, \ldots, \boldsymbol{W}_{1N_{\mathrm{L}}}, \boldsymbol{W}_{21}, \ldots, \boldsymbol{W}_{PN_{\mathrm{L}}}\right). \tag{3}$$

The matrices $\boldsymbol{W}$ and $\boldsymbol{X}$ can be recalculated for every channel realization, while the matrix $\boldsymbol{A}$ remains unchanged once the system is deployed (think of it as a fixed hardware combining module). The framework under study is represented in Fig. 1.

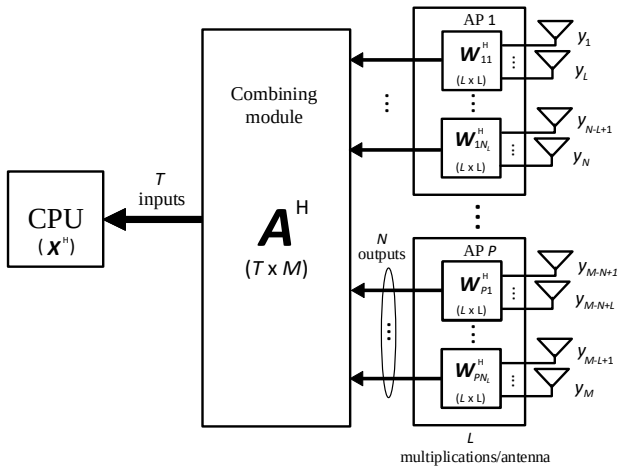

Figure 1: Framework used in this paper during the data phase.

The framework under study allows for the exploitation of the trade-off between the number of multiplications per antenna, associated to L, and the number of inputs to the CPU, associated to T. Said trade-off, which can be seen as a trade-off between decentralized processing complexity and level of decentralization, was identified in [13], which considers an equivalent version of the framework under study.

We constrain the information rate at which the users can transmit to the BS, i.e., $I_{\boldsymbol{Z},\boldsymbol{S}}(\boldsymbol{z}, \boldsymbol{s})$, or, correspondingly[6], $I_{\boldsymbol{Y},\boldsymbol{S}}(\boldsymbol{A}^{\mathrm{H}}\boldsymbol{W}^{\mathrm{H}}\boldsymbol{y}, \boldsymbol{s})$ to be lossless. Thus, $I_{\boldsymbol{Y},\boldsymbol{S}}(\boldsymbol{A}^{\mathrm{H}}\boldsymbol{W}^{\mathrm{H}}\boldsymbol{y}, \boldsymbol{s}) = I_{\boldsymbol{Y},\boldsymbol{S}}(\boldsymbol{y}, \boldsymbol{s})$.

[6]Note that $\boldsymbol{X}$ cannot possibly increase the maximum information rate at which the users can transmit (recall data-processing inequality [14]).

2.1 Background

As we mentioned earlier, the architecture considered in this paper is based on the framework presented in [13], where important results are shown that will be the required for our analysis. From [13, Lemma 1], the framework under study can achieve information lossless processing if and only if we can decompose the channel matrix $\boldsymbol{H}$ into the so called WAX decomposition

$$\boldsymbol{H} = \boldsymbol{W}\boldsymbol{A}\boldsymbol{X}, \tag{4}$$

where $\boldsymbol{W}$, $\boldsymbol{A}$ and $\boldsymbol{X}$ correspond to the matrices from (2), i.e., $\boldsymbol{A}$ is fixed by design while $\boldsymbol{W}$ and $\boldsymbol{X}$ can be tuned to $\boldsymbol{H}$. Note that selecting $\boldsymbol{W}$ and $\boldsymbol{X}$ in (2) such that (4) is fulfilled leads to information-lossless processing within our framework. The main result of the applicability of WAX decomposition is given in [13, Theorem 1], which states that, for a randomly chosen $\boldsymbol{A} \in \mathbb{C}^{M\times T}$, a randomly chosen $\boldsymbol{H} \in \mathbb{C}^{M\times K}$ admits WAX decomposition with probability 1 if

$$T > \max\left(M\frac{K-L}{K}, K-1\right). \tag{5}$$

3 WAX Decomposition for Sparse Channels

Much of the WAX theory, including methods for practical computation of the constituent matrices $\boldsymbol{W}$ and $\boldsymbol{X}$, is underpinned by [13, Lemma 3]. However, for sparse channels, an important assumption of [13, Lemma 3] is not fulfilled. Let $\boldsymbol{H} = [\boldsymbol{H}_{11}^{\mathrm{T}}\ \boldsymbol{H}_{12}^{\mathrm{T}}\ \ldots\ \boldsymbol{H}_{PN_{\mathrm{L}}}^{\mathrm{T}}]^{\mathrm{T}}$, where we used notation from (3), and $\boldsymbol{H}_{pn}$ is an $L \times K$ submatrix of $\boldsymbol{H}$. For [13, Lemma 3] to hold it should be assumed that $\mathrm{rank}(\boldsymbol{H}_{pn}) = L$, $\forall p, n$. However, in the current scenario, it could very well happen that a certain panel sees far less UEs than L, so $\mathrm{rank}(\boldsymbol{H}_{pn}) = L$ cannot be guaranteed. Wherefore, [13, Lemma 3] needs to be generalized, which we do next.

Lemma 10 ([13, Lemma 3] for sparse channels) *For all matrices $\boldsymbol{H}$ satisfying $\mathrm{rank}(\boldsymbol{H}_{pn}) = \min(k_{pn}, L)$, where k_{pn} can be seen as the number of non-zero columns in $\boldsymbol{H}_{pn}$, there exists a block diagonal matrix $\boldsymbol{W}$ and a matrix $\boldsymbol{X}$ such that $\boldsymbol{W}\boldsymbol{A}\boldsymbol{X} = \boldsymbol{H}$, if and only if, there exists a block diagonal invertible matrix $\hat{\boldsymbol{W}}$ with the same form as $\boldsymbol{W}$ such that $\boldsymbol{A}\boldsymbol{X} - \hat{\boldsymbol{W}}\boldsymbol{H} = \boldsymbol{0}_{M\times K}$.*

Proof The *if* part is trivial. If an invertible matrix $\hat{\boldsymbol{W}}$ exists, then we can set $\boldsymbol{W} = \hat{\boldsymbol{W}}^{-1}$. To prove the *only if* part, assume that $\boldsymbol{W}\boldsymbol{A}\boldsymbol{X} = \boldsymbol{H}$. Specifically,

$$\boldsymbol{W}_{pn}\boldsymbol{A}_{pn}\boldsymbol{X} = \boldsymbol{H}_{pn},\ \forall p, n.$$

Let us now focus on indices p, n where $\text{rank}(\boldsymbol{H}_{pn}) = k_{pn} < L$, as rank L blocks are treated in [13, Lemma 3]. Let $\boldsymbol{X}_{pn}$ be the columns of $\boldsymbol{X}$ corresponding to the k_{pn} nonzero columns of $\boldsymbol{H}_{pn}$. Then, $\boldsymbol{A}_{pn}\boldsymbol{X}_{pn}$ is an $L \times k_{pn}$ matrix whose rank must be k_{pn}. Moreover, $\text{rank}(\boldsymbol{W}_{pn}) \geq k_{pn}$. Being a full rank matrix, the left nullspace of $\boldsymbol{A}_{pn}\boldsymbol{X}_{pn}$ has dimensionality of precisely $L - k_{pn}$, i.e., there exists a full rank $(L-k_{pn}) \times L$ matrix $\boldsymbol{N}_{pn}$ such that $\boldsymbol{N}_{pn}\boldsymbol{A}_{pn}\boldsymbol{X}_{pn} = \boldsymbol{0}_{(L-k_{pn})\times k_{pn}}$. Decompose $\boldsymbol{W}_{pn}$ as $\boldsymbol{W}_{pn} = \tilde{\boldsymbol{W}}_{pn} + \boldsymbol{Z}_{pn}\boldsymbol{N}_{pn}$, where $\tilde{\boldsymbol{W}}_{pn}\boldsymbol{N}_{pn} = \boldsymbol{0}_{L\times k_{pn}}$ and $\boldsymbol{Z}_{pn}$ is $L \times (L - k_{pn})$. We have,

$$\begin{aligned}\boldsymbol{W}_{pn}\boldsymbol{A}_{pn}\boldsymbol{X} &= (\tilde{\boldsymbol{W}}_{pn} + \boldsymbol{Z}_{pn}\boldsymbol{N}_{pn})\boldsymbol{A}_{pn}\boldsymbol{X} \\ &= \tilde{\boldsymbol{W}}_{pn}\boldsymbol{A}_{pn}\boldsymbol{X} \\ &= \boldsymbol{H}_{pn}.\end{aligned}$$

Therefore, it follows that $\text{rank}(\tilde{\boldsymbol{W}}_{pn}) = k_{pn}$, but $\boldsymbol{W}_{pn}$ is constructed from $\tilde{\boldsymbol{W}}_{pn}$ by adding a rank $L - k_{pn}$ matrix that is orthogonal to $\tilde{\boldsymbol{W}}_{pn}$, which directly implies that there exists a full rank solution $\boldsymbol{W}_{pn}$ whenever a solution exists. Specifically, this implies that there exists a full rank $\boldsymbol{W}$ that solves $\boldsymbol{W}\boldsymbol{A}\boldsymbol{X} = \boldsymbol{H}$ whenever a solution exists. But this implies that we can set $\hat{\boldsymbol{W}} = \boldsymbol{W}^{-1}$, which concludes the proof. □

3.1 2 APs Scenario

In order to get an understanding of how to deal with WAX decomposition in the case of sparse channel matrices, let us first take a look at a simplified scenario where there are only 2 APs. Assume that K_1 users are only seen by AP 1, K_2 users are only seen by AP 2s, and K_3 users are seen by both APs. Without any loss of generality, we can express the channel matrix for this scenario as

$$\boldsymbol{H} = \begin{pmatrix} \boldsymbol{H}_{11} & \boldsymbol{0}_{N\times K_2} & \boldsymbol{H}_{13} \\ \boldsymbol{0}_{N\times K_1} & \boldsymbol{H}_{22} & \boldsymbol{H}_{23} \end{pmatrix}, \tag{6}$$

where $\boldsymbol{H}_{13}$ and $\boldsymbol{H}_{23}$ correspond to the $N \times K_3$ channel matrices from the shared users to AP 1 and AP 2, respectively, while $\boldsymbol{H}_{11}$ and $\boldsymbol{H}_{22}$ correspond to the $N \times K_1$ and $N \times K_2$ channel matrices from the non-shared users to AP 1 and AP 2, respectively. Note that any permutation of the columns of $\boldsymbol{H}$ only corresponds to a re-indexing of the user IDs[7]. Incidentally, the structure of $\boldsymbol{H}$ corresponds to the structure of the matrices being decomposed in the WAX modules from the binary tree architecture presented in [7], which only considered (4) as a first limit to the dimension reduction. Thus, the results we

[7]Such a permutation can be applied by multiplying $\boldsymbol{H}$ from the right with an invertible matrix, which, in fact, could be absorbed by $\boldsymbol{X}$ in its WAX decomposition

obtain in this subsection have direct implications in the dimension reduction that can be achieved by such architecture.

Let us express the WAX decomposition (4) of (6) as

$$\boldsymbol{H} = \begin{pmatrix} \boldsymbol{W}_1 & \boldsymbol{0}_{N\times N} \\ \boldsymbol{0}_{N\times N} & \boldsymbol{W}_2 \end{pmatrix} \begin{pmatrix} \boldsymbol{A}_1 \\ \boldsymbol{A}_2 \end{pmatrix} \begin{pmatrix} \boldsymbol{X}_1 & \boldsymbol{X}_2 & \boldsymbol{X}_3 \end{pmatrix}, \tag{7}$$

where $\boldsymbol{W}_1$ and $\boldsymbol{W}_2$ are the two $N \times N$ blocks of $\boldsymbol{W}$, which are also formed by $L \times L$ diagonal blocks, $\boldsymbol{A}_1$ and $\boldsymbol{A}_2$ are the two $N \times T$ row blocks of $\boldsymbol{A}$, and $\boldsymbol{X}_1$, $\boldsymbol{X}_2$, and $\boldsymbol{X}_3$ are the $T \times K_1$, $T \times K_2$, and K_3 column blocks of $\boldsymbol{X}$. Assume that the non-zero blocks of $\boldsymbol{H}$ are randomly chosen matrices (e.g., IID complex Gaussian), and so is the $\boldsymbol{A}$ matrix from the WAX decomposition.

From Lemma 10 we assure that the existence of solution to $\boldsymbol{WAX} = \boldsymbol{H}$ is equivalent to the existence of solution to $\boldsymbol{AX} = \boldsymbol{W}^{-1}\boldsymbol{H}$ with full-rank $\boldsymbol{W}^{-1}$. Let us thus focus on the equivalent problem

$$\boldsymbol{AX} = \boldsymbol{W}^{-1}\boldsymbol{H}, \tag{8}$$

for full-rank $\boldsymbol{W}^{-1}$. If (5) is fulfilled, (8) will have a non-zero solution for $\boldsymbol{X}$ and $\boldsymbol{W}^{-1}$, but it remains to assure full-rank $\boldsymbol{W}^{-1}$. Considering the structure of $\boldsymbol{H}$, we can translate (7) into the following set of equations

$$\boldsymbol{A}_1\boldsymbol{X}_1 = \boldsymbol{W}_1^{-1}\boldsymbol{H}_{11}, \tag{9a}$$

$$\boldsymbol{A}_1\boldsymbol{X}_2 = \boldsymbol{0}_{N\times K_2}, \tag{9b}$$

$$\boldsymbol{A}_1\boldsymbol{X}_3 = \boldsymbol{W}_1^{-1}\boldsymbol{H}_{13}, \tag{9c}$$

$$\boldsymbol{A}_2\boldsymbol{X}_1 = \boldsymbol{0}_{N\times K_1}, \tag{9d}$$

$$\boldsymbol{A}_2\boldsymbol{X}_2 = \boldsymbol{W}_2^{-1}\boldsymbol{H}_{22}, \tag{9e}$$

$$\boldsymbol{A}_2\boldsymbol{X}_3 = \boldsymbol{W}_2^{-1}\boldsymbol{H}_{23}, \tag{9f}$$

where $\boldsymbol{W}_1^{-1}$ and $\boldsymbol{W}_2^{-1}$ are now restricted to be full-rank matrices. In order for (9b) and (9d) to hold $\boldsymbol{X}_1$ and $\boldsymbol{X}_2$ must be in the null-space of $\boldsymbol{A}_2$ and $\boldsymbol{A}_1$, respectively. Since $\boldsymbol{A}$ is randomly chosen, $\boldsymbol{A}_1$ and $\boldsymbol{A}_2$ will be full rank with probability 1. We thus have

$$\boldsymbol{X}_1 = \boldsymbol{N}_2\widetilde{\boldsymbol{X}}_1, \quad \boldsymbol{N}_2 = \mathcal{N}\{\boldsymbol{A}_2\}, \tag{10a}$$

$$\boldsymbol{X}_2 = \boldsymbol{N}_1\widetilde{\boldsymbol{X}}_2, \quad \boldsymbol{N}_1 = \mathcal{N}\{\boldsymbol{A}_1\}, \tag{10b}$$

where $\boldsymbol{N}_1$ and $\boldsymbol{N}_2$ are the $T \times (T-N)$ matrices conforming the null-spaces of $\boldsymbol{A}_1$ and $\boldsymbol{A}_2$, respectively. We can now rewrite the set of equations (9) as

$$\boldsymbol{A}_1\boldsymbol{N}_2\widetilde{\boldsymbol{X}}_1 = \boldsymbol{W}_1^{-1}\boldsymbol{H}_{11}, \tag{11a}$$

$$\boldsymbol{A}_1\boldsymbol{X}_3 = \boldsymbol{W}_1^{-1}\boldsymbol{H}_{13}, \tag{11b}$$

$$\boldsymbol{A}_2\boldsymbol{N}_1\widetilde{\boldsymbol{X}}_2 = \boldsymbol{W}_2^{-1}\boldsymbol{H}_{22}. \tag{11c}$$

$$\boldsymbol{A}_2\boldsymbol{X}_3 = \boldsymbol{W}_2^{-1}\boldsymbol{H}_{23}, \tag{11d}$$

Let us rewrite (11a) and (11c) as

$$\widetilde{\boldsymbol{A}}_1\widetilde{\boldsymbol{X}}_1 = \boldsymbol{W}_1^{-1}\boldsymbol{H}_{11}, \tag{12a}$$

$$\widetilde{\boldsymbol{A}}_2\widetilde{\boldsymbol{X}}_2 = \boldsymbol{W}_2^{-1}\boldsymbol{H}_{22}, \tag{12b}$$

where $\widetilde{\boldsymbol{A}}_1$ and $\widetilde{\boldsymbol{A}}_2$ can be seen as two $N \times (T-N)$-sized randomly chosen matrices, since they are computed as a product of a randomly chosen matrix with the null-space of another randomly chosen matrix. Equations (12a) and (12b) can be transformed into linear equations by vectorizing. Thus, in order have non-zero solution the following conditions should be fulfilled

$$(T-N) > \max\left(N\frac{K_1-L}{K_1}, K_1-1\right), \tag{13a}$$

$$(T-N) > \max\left(N\frac{K_2-L}{K_2}, K_2-1\right). \tag{13b}$$

Furthermore, the set of $\boldsymbol{W}_1^{-1}$ and $\boldsymbol{W}_2^{-1}$ matrices solving (12a) and (12b) will be full-rank except for a subset of measure 0.[8]On the other hand, if (5) is fulfilled, (11b) and (11d) will have at least one solution randomly situated in the continuous set of $\boldsymbol{W}_1^{-1}$ and $\boldsymbol{W}_2^{-1}$ that solve (12a) and (12b).[8] Therefore, a matrix $\boldsymbol{H}$ selected as in (6) admits WAX decomposition with probability 1 for randomly chosen $\boldsymbol{A}$ if and only if the conditions (5), (13a), and (13b) are jointly fulfilled.

3.2 Extension to Any Number of APs

Let us consider now the general case with P APs. The channel matrix for this scenario can be now expressed as

$$\boldsymbol{H} = \begin{bmatrix} b_{11}\boldsymbol{H}_{11} & b_{12}\boldsymbol{H}_{12} & \cdots & b_{1C}\boldsymbol{H}_{1C} \\ b_{21}\boldsymbol{H}_{21} & b_{22}\boldsymbol{H}_{22} & \cdots & b_{2C}\boldsymbol{H}_{1C} \\ \vdots & \vdots & \ddots & \vdots \\ b_{P1}\boldsymbol{H}_{P1} & b_{P2}\boldsymbol{H}_{P2} & \cdots & b_{PC}\boldsymbol{H}_{PC} \end{bmatrix}, \tag{14}$$

[8]For further understanding see [13, Proof of Theorem 1]

where $C = 2^P - 1$, $\boldsymbol{b}_j = (b_{1j}b_{2j}\cdots b_{Pj})_2$ is the binary expansion of j, and $\boldsymbol{H}_{ij}$ are randomly chosen matrices (e.g., IID complex Gaussian entries) of dimensions $N \times K_j$.[9] It can thus be noted that selecting $\boldsymbol{H}$ as (14) allows us to consider any possible channel matrix within the presented cell-free scenario ($P = 2$ leads to (6)).

Proposition 1 *A matrix $\boldsymbol{H}$ selected as* (14) *admits WAX decomposition with probability 1 for randomly chosen $\boldsymbol{A}$ if and only if the set of conditions*

$$T - (P - \|\boldsymbol{b}_j\|_1)\, N > \max\left(\|\boldsymbol{b}_j\|_1 N \frac{K_j - L}{K_j}, K_j - 1\right), \forall j, \tag{15}$$

together with (5) *are jointly fulfilled.*

Proof *The proof follows from direct extension of the arguments used in the 2 APs scenario. We should note that the jth column block of $\boldsymbol{H}$ has $\|\boldsymbol{b}_j\|_1$ randomly chosen blocks of size $N \times K_j$, and $P - \|\boldsymbol{b}_j\|_1$ blocks with $\boldsymbol{0}_{N\times K_j}$.* □

The previous proposition states the conditions of existence of WAX decomposition for cell-free massive MIMO channels within the considered framework. This poses an important advancement in the definition and exploitation of the trade-off between processing complexity at the APs and level of decentralization of the system.

4 Numerical Results

We next present some results on the impact of cell-free massive MIMO sparse channels on the WAX decomposition trade-off. We define

$$T_{\text{WAX}} = \max\left(\left\lfloor M\frac{K-L}{K} + 1\right\rfloor, K\right),$$

which corresponds to the minimum T that can be used to fulfill (5), i.e., the trade-off for non-sparse channels.

Fig. 2 shows how T is degraded with respect to T_{WAX} in the 2 APs case as we increase $K_1 = K_2$, i.e. the number users seen by only one of the APs. From Fig. 2 (left) we can see that increasing L, N and K at the same rate degrades the trade-off by shifting the curves towards the left (faster sensitivity to unseen users), but it seems to converge. Fig. 2 (right) indicates that decreasing the total number of users K also degrades the trade-off by shifting the curves to the left, decreasing the antennas per panel N degrades the trade-off only by increasing the slope, while increasing the multiplications per antenna L degrades trade-off by both shifting to the left and increasing the slope.

[9] Note that the K_j values are also allowed to be 0.

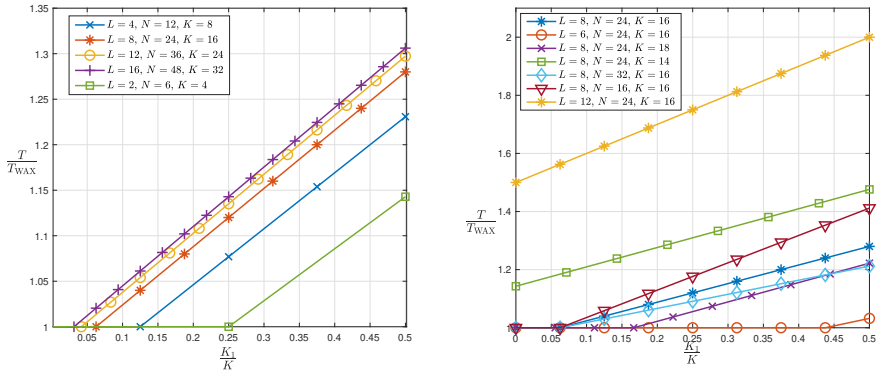

Figure 2: APs scenario with $K_2 = K_1$. Plot of T/T_{WAX} with respect to K/K_1.

In Fig. 3 we can see how the sparsity degrades the trade-off in a more general scenario. For the simulation we have drawn the number of panels seen by each user, n, from a discrete distribution with $p_n = a/n^q$, where a is a constant for normalization purposes, and the n APs are randomly selected with equal probabilities (i.e., select uniformly $\boldsymbol{b}_j$ such that $\|\boldsymbol{b}_j\| = n$). Thus, variable q can be related to the sparsity level since a bigger value of it means that each user will see less panels with more probability. From the plot, we can also see that increasing the total number of users K decreases the impact of sparsity on the trade-off. Increasing the number of panels further, degrades the trade-off since it increases the inherent sparsity. We should note that having $q = 0$ still incurs a degradation of the trade-off since in this case a row of $\boldsymbol{H}$ would have any number of zero blocks (between 1 and P) with equal probability, i.e., $q = 0$ is not equivalent to having no sparsity.

5 Conclusions

We have extended the application of the WAX decomposition to a cell-free massive MIMO scenario with sparse channel matrix. We have found a new set of conditions that limit the information-lossless trade-off between multiplications per antenna and number of input to a CPU in the case of channel sparsity. Our numerical results confirm that the trade-off presented in [13] is degraded as the sparsity of the channel increases.

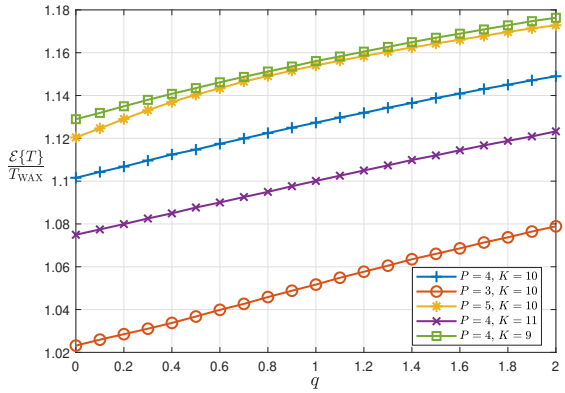

Figure 3: Average T/T_{WAX} with respect to sparsity factor q. $L = 2$ and $N = 16$.

References

[1] H. Q. Ngo, A. Ashikhmin, H. Yang, E. G. Larsson, and T. L. Marzetta, "Cell-free massive MIMO versus small cells," *IEEE Transactions on Wireless Communications*, vol. 16, no. 3, pp. 1834–1850, 2017.

[2] J. Zhang, S. Chen, Y. Lin, J. Zheng, B. Ai, and L. Hanzo, "Cell-free massive MIMO: A new next-generation paradigm," *IEEE Access*, vol. 7, pp. 99 878–99 888, 2019.

[3] S. Buzzi and C. D'Andrea, "Cell-free massive MIMO: User-centric approach," *IEEE Wireless Communications Letters*, vol. 6, no. 6, pp. 706–709, 2017.

[4] E. Björnson and L. Sanguinetti, "Scalable cell-free massive MIMO systems," *IEEE Transactions on Communications*, vol. 68, no. 7, pp. 4247–4261, 2020.

[5] S. Hu, K. Chitti, F. Rusek, and O. Edfors, "User assignment with distributed large intelligent surface (LIS) systems," in *2018 IEEE 29th Annual International Symposium on Personal, Indoor and Mobile Radio Communications (PIMRC)*, 2018, pp. 1–6.

[6] J. Vidal Alegría, J. R. Sánchez, F. Rusek, L. Liu, and O. Edfors, "Decentralized equalizer construction for large intelligent surfaces," in *2019 IEEE 90th Vehicular Technology Conference (VTC2019-Fall)*, 2019, pp. 1–6.

[7] J. V. Alegría, F. Rusek, J. R. Sánchez, and O. Edfors, "Modular binary tree architecture for distributed large intelligent surface," in *ICASSP*

2021 - 2021 IEEE International Conference on Acoustics, Speech and Signal Processing (ICASSP), 2021, pp. 4565–4569.

[8] K. Li, R. R. Sharan, Y. Chen, T. Goldstein, J. R. Cavallaro, and C. Studer, "Decentralized baseband processing for massive MU-MIMO systems," *IEEE Journal on Emerging and Selected Topics in Circuits and Systems*, vol. 7, no. 4, pp. 491–507, 2017.

[9] E. Bertilsson, O. Gustafsson, and E. G. Larsson, "A scalable architecture for massive MIMO base stations using distributed processing," in *2016 50th Asilomar Conference on Signals, Systems and Computers*, 2016, pp. 864–868.

[10] J. R. Sánchez, J. Vidal Alegría, and F. Rusek, "Decentralized massive MIMO systems: Is there anything to be discussed?" In *2019 IEEE International Symposium on Information Theory (ISIT)*, 2019, pp. 787–791.

[11] J. Rodríguez Sánchez, F. Rusek, O. Edfors, M. Sarajlić, and L. Liu, "Decentralized massive MIMO processing exploring Daisy-chain architecture and recursive algorithms," *IEEE Transactions on Signal Processing*, vol. 68, pp. 687–700, 2020.

[12] A. Amiri, S. Rezaie, C. N. Manchón, and E. de Carvalho, "Distributed receiver processing for extra-large MIMO arrays: A message passing approach," *IEEE Transactions on Wireless Communications*, vol. 21, no. 4, pp. 2654–2667, 2022.

[13] J. V. Alegría, F. Rusek, and O. Edfors, "Trade-offs in decentralized multi-antenna architectures: The wax decomposition," *IEEE Transactions on Signal Processing*, vol. 69, pp. 3627–3641, 2021.

[14] T. M. Cover and J. A. Thomas, *Elements of Information Theory (Wiley Series in Telecommunications and Signal Processing)*. USA: Wiley-Interscience, 2006.

Paper IV

Impact of Quantization in Decentralized Processing for Large Multi-Antenna Architectures

The demand for an increased number of antennas at base stations is driving research on decentralized processing schemes aimed at reducing the information volume that has to be transferred to, and processed at, a CPU. Some of these schemes can reduce the dimensions of the data while achieving information-lossless processing with respect to centralized architectures. However, little is known about the impact of quantization in these decentralized schemes. Moreover, it is unclear if an information-lossless reduction of dimensions directly corresponds to a reduction in the bit-rate that has to be transmitted to the CPU after quantization. This paper studies how quantization affects the performance of decentralized processing. Bit rates after quantization of a received vector (in a centralized scheme) are contrasted with bit rates after quantization of post-processed vectors using various information-lossless dimension reductions that can potentially be applied in decentralized schemes.

©2022 IEEE. Reprinted, with permission, from
J. Vidal Alegría, F. Rusek, A. Lozano,
"Impact of Quantization in Decentralized Processing for Large Multi-Antenna Architectures,"
in *Proc. 56th Asilomar Conf. on Signals, Syst., Comput.*, Pacific Grove, CA, USA, 2022, pp. 1351-1356.

1 Introduction

An important benefit of decentralized processing in large multi-antenna architectures is to reduce the amount of information transferred to a CPU. In [1], a generalized architecture is proposed that enables a trade-off between the complexity of information-lossless[10] decentralized processing, measured in number of multiplications per antenna, and the level of decentralization, measured in number of connections to a CPU. Other decentralized processing schemes, such as those in [2] or [3], [4], consider decentralized application of MRC or approximate ZF, where the amount of data that has to be transferred to the CPU scales with the number of users and not the number of antennas at the BS.

The results in [1]–[4] assume infinite precision for every signal vector from the antennas to the CPU. In emerging scenarios of interest, however, it is desirable to consider low-resolution quantizers to reduce cost and energy consumption [5]. If we consider coarse quantization, while still seeking information-lossless processing, it is not clear whether a reduction in the connections to a CPU directly translates to a lower information transfer to said CPU. If we want to transmit the same bit rate from a set of users through a lower number of inputs to a CPU than a centralized architecture, do we need to compensate by increasing the quantization precision? Then, is there a benefit in reducing the inputs to a CPU? These questions motivate the present work.

The effect of quantization on the information transfer to a CPU in decentralized processing schemes is examined. Fig. 1 shows a rough comparison between centralized and decentralized architectures. The upper part of Fig. 1 has already been studied and its information-lossless trade-off between complexity of decentralized processing and inputs to CPU has been characterized [1]. However, it is unclear if this trade-off is upheld once quantization comes into play. In [6] a distributed Karhunen-Loève solution is presented that falls within the information-lossy regime of the top-right corner of Fig. 1 and also touches the bottom-right corner. However, the framework considered in [6] does not fall within the scope of this paper since it only considers lossy dimensionality reductions of Gaussian random vectors. Other works such as [7] or [8] study similar problems that could fall in the information-lossy regime of the top-right corner of Fig. 1; however, quantization is ignored in these works. Hence, a proper characterization of the dimensionality reductions with quantization (bottom-right corner of Fig. 1) remains largely unexplored.

Notation: Lowercase, bold lowercase and bold uppercase letters stand for scalars, column vectors and matrices, respectively. The operations $(\cdot)^{\mathrm{T}}$, $(\cdot)^*$ and $(\cdot)^{\mathrm{H}}$ denote transpose, conjugate, and conjugate transpose, respectively. $\mathcal{I}(\cdot;\cdot)$ and $\mathbb{E}\{\cdot\}$ denote mutual information and expectation, respectively. Given two

[10] By *information-lossless processing* we mean that the mutual information between the processed signal and the transmitted signal is equal to that between the received signal and the transmitted signal, i.e., we can achieve the same user rates as in centralized processing.

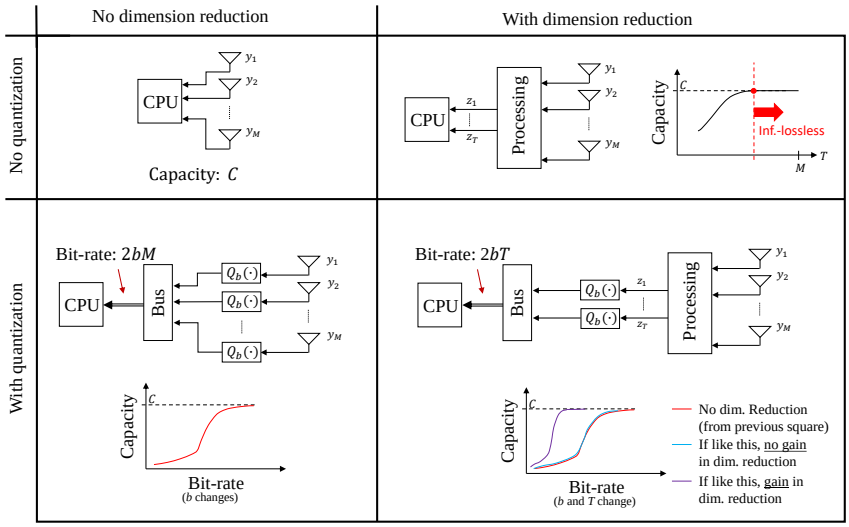

Figure 1: Centralized and decentralized architectures, with or without quantization losses.

random vectors $\boldsymbol{x}$ and $\boldsymbol{y}$, $\boldsymbol{R}_{\boldsymbol{xy}} = \mathbb{E}\left\{\boldsymbol{x}\boldsymbol{y}^{\mathrm{H}}\right\}$ is the correlation matrix between them. $P_X(\cdot)$ corresponds to PMF of a discrete random variable X, and $p_Y(\cdot)$ corresponds to PDF of a continuous random variable Y. $\Re\{\cdot\}$ and $\Im\{\cdot\}$ denote real and imaginary part, respectively. The operation $\mathrm{diag}(\cdot)$ when applied to a matrix gives the same matrix with zeros in the off-diagonal elements; when applied to a set of scalars/blocks, it outputs a matrix with said scalars/blocks along the main diagonal. $\mathcal{Q}(.)$ corresponds to the Q-function. The notation $[\boldsymbol{A}]_{i:j,\ell:k}$ denotes a matrix formed by rows i to j and columns ℓ to k of $\boldsymbol{A}$ (absence of one such index indicates that the included rows start/end corresponds to the first/last row/column of $\boldsymbol{A}$, respectively).

2 System Model

Assume K users transmitting to a BS with M receive antennas, $M > K$. The complex baseband received vector for one narrowband subcarrier is given by

$$\boldsymbol{y} = \boldsymbol{H}\boldsymbol{x} + \boldsymbol{n}, \tag{1}$$

where $\boldsymbol{x}$ is the $K \times 1$ vector of transmitted symbols, $\boldsymbol{H}$ is the $M \times K$ channel matrix, perfectly known by the receiver, and $\boldsymbol{n} \sim \mathcal{N}_{\mathbb{C}}(\boldsymbol{0}_{M\times 1}, N_0\boldsymbol{I}_M)$ is the noise vector. The capacity-achieving signal distribution is $\boldsymbol{x} \sim \mathcal{N}_{\mathbb{C}}(\boldsymbol{0}_{K\times 1}, E_{\mathrm{s}}\boldsymbol{I}_K)$ [9].

We consider information-lossless dimension reductions such as the ones presented in [1], [2], [10], which can be applied in a decentralized fashion before forwarding the data to a CPU. Thus, we have the $T \times 1$ post-processed vector

$$\boldsymbol{z} = \boldsymbol{F}\boldsymbol{y}, \tag{2}$$

where $\boldsymbol{F}$ is a $T \times M$ information-lossless processing transformation with $T < M$. Thus, conditioned on $\boldsymbol{H}$ and $\boldsymbol{F}$, $\boldsymbol{z} \sim \mathcal{N}_{\mathbb{C}}(\boldsymbol{0}_{M\times 1}, \boldsymbol{R}_{\boldsymbol{zz}})$ with

$$\boldsymbol{R}_{\boldsymbol{zz}} = E_{\mathrm{s}}\boldsymbol{F}\boldsymbol{H}\boldsymbol{H}^{\mathrm{H}}\boldsymbol{F}^{\mathrm{H}} + N_0\boldsymbol{F}\boldsymbol{F}^{\mathrm{H}}. \tag{3}$$

Since we restrict $\boldsymbol{F}$ to be information-lossless, $\boldsymbol{z}$ must contain the same information about $\boldsymbol{x}$ as $\boldsymbol{y}$, i.e., $\mathcal{I}(\boldsymbol{z};\boldsymbol{x}) = \mathcal{I}(\boldsymbol{y};\boldsymbol{x})$. An especially interesting structure for $\boldsymbol{F}$ is given by

$$\boldsymbol{F} = \boldsymbol{\Lambda}_{\boldsymbol{F}}\,[\boldsymbol{U}]^{\mathrm{H}}_{:,1:T} \tag{4}$$

where $\boldsymbol{\Lambda}_{\boldsymbol{F}}$ is an arbitrary $T \times T$ diagonal matrix and $\boldsymbol{U}$ is the $M \times M$ matrix of left singular vectors of $\boldsymbol{H}$. Such $\boldsymbol{F}$ corresponds to a Karhunen-Loève transform of $\boldsymbol{z}$, i.e., it leads to uncorrelated (and thus independent given their jointly Gaussian distribution) entries of $\boldsymbol{z}$. For such $\boldsymbol{F}$,

$$\boldsymbol{R}_{\boldsymbol{zz}} = E_{\mathrm{s}}\boldsymbol{\Lambda}^2_{\boldsymbol{F}}[\boldsymbol{\Lambda}_{\boldsymbol{H}}]_{1:T,1:T} + N_0\boldsymbol{\Lambda}^2_{\boldsymbol{F}}, \tag{5}$$

where $\boldsymbol{\Lambda}_{\boldsymbol{H}}$ is a diagonal matrix with the ordered eigenvalues of $\boldsymbol{H}\boldsymbol{H}^{\mathrm{H}}$, so the last $M - K$ eigenvalues are zero. With (4), vector quantization can be disregarded in favor of scalar quantization, since the entries of $\boldsymbol{z}$ are independent. Furthermore, selecting

$$\boldsymbol{\Lambda}_{\boldsymbol{F}} = \sqrt{\beta}\left(E_{\mathrm{s}}[\boldsymbol{\Lambda}_{\boldsymbol{H}}]_{1:T,1:T} + N_0\boldsymbol{I}_T\right)^{-1/2} \tag{6}$$

leads to $\boldsymbol{R}_{\boldsymbol{zz}} = \beta\boldsymbol{I}_T$, i.e., the entries of $\boldsymbol{z}$ are not only independent, but also identically distributed (IID). Then, there is no loss in having the same quantization process for each entry of $\boldsymbol{z}$.

These structures for $\boldsymbol{F}$ entail a certain loss of generality; however, we are most interested in understanding the relation between the dimension of the post-processed data and the corresponding bit rate to a CPU for a given user. In this regard, these structures fundamentally capture the essence of the problem since they correspond to information-lossless transformations where the output dimensions can be arbitrarily selected by setting T between M and K.

3 Quantization

As a first step towards understanding the effect of quantization in decentralized processing schemes, we consider that $\boldsymbol{F}$ can be implemented with full

precision and in a decentralized fashion. Quantization is then applied to the post-processed vector, giving

$$\boldsymbol{z}_{\mathrm{Q}} = Q_b\left(\boldsymbol{z}\right), \tag{7}$$

where $Q_b(\cdot)$ represents a b-bit scalar quantization, with independent equal quantization parameters for the in-phase and quadrature components at each entry of $\boldsymbol{z}$. We can thus write

$$z_{\mathrm{Q}t} = Q_b\big(\Re\{z_t\}\big) + \jmath\, Q_b\big(\Im\{z_t\}\big), \tag{8}$$

where $z_{\mathrm{Q}t}$ is the tth entry of $\boldsymbol{z}_{\mathrm{Q}}$, for $t = 1, \ldots, T$. The system model is depicted in Fig. 2 (right).

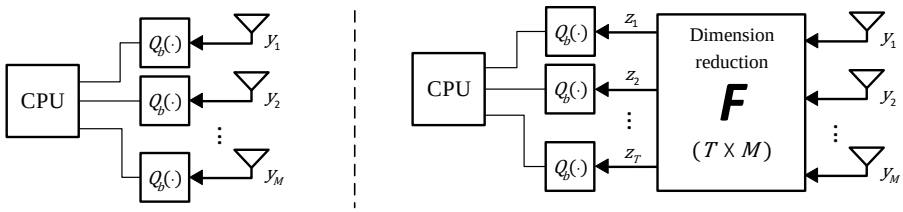

Figure 2: Quantization for centralized architecture (left) v.s. quantization after dimension reduction (right).

For the quantization process, we define the set of thresholds

$$\mathcal{T} = \{\tau_1, \tau_2, \ldots, \tau_{2^b+1}\}, \tag{9}$$

with $\tau_1 = -\infty$ and $\tau_{2^b+1} = \infty$, and the set of labels

$$\mathcal{L} = \{\lambda_1, \lambda_2, \ldots, \lambda_{2^b}\}. \tag{10}$$

Then, if

$$\Re\{z_t\} \in (\tau_k, \tau_{k+1}] \text{ and } \Im\{z_t\} \in (\tau_\ell, \tau_{\ell+1}] \tag{11}$$

the tth entry of the quantized vector equals

$$z_{\mathrm{Q}t} = \lambda_k + \jmath\lambda_\ell. \tag{12}$$

The sets of thresholds and labels, $\mathcal{T}$ and $\mathcal{L}$, are computed using the Lloyd-Max algorithm [11], [12]. The obtained optimum thresholds and labels, which minimize the mean-square error, approximately fulfill the conditions [12, Eqs.

5 and 6]

$$\tau_i = \frac{\lambda_i + \lambda_{i-1}}{2}, \qquad i = 2, \ldots, 2^b \tag{13a}$$

$$\lambda_j = \frac{\int_{\tau_j}^{\tau_{j+1}} z\, p_Z(z) dz}{\int_{\tau_j}^{\tau_{j+1}} p_Z(z) dz}, \tag{13b}$$

where $p_Z(\cdot)$ is the PDF of the variable being quantized. Condition (13b) corresponds to selecting each label as the conditional mean of the quantized variable given the interval it belongs to. Considering equal quantization for the in-phase and quadrature components of each entry of $\boldsymbol{z}$, we need to define $p_Z(\cdot)$ such that it reflects all the involved distributions. However, $\Re\{z_t\}$ and $\Im\{z_t\}$ are IID, so we only need to consider the distribution of either of them for each entry z_t. We have $\Re\{z_t\}, \Im\{z_t\} \sim \mathcal{N}(0, \sigma_{z_t}^2/2)$, where $\sigma_{z_t}^2$ is the variance of z_t, given by the tth diagonal entry of $\boldsymbol{R}_{\boldsymbol{zz}}$ in (3). A meaningful distribution $p_Z(z)$ equally reflecting all entries of $\boldsymbol{z}$ is

$$p_Z(z) = \frac{1}{T} \sum_{t=1}^{T} \frac{\exp\left(-z^2/\sigma_{z_t}^2\right)}{\sqrt{\pi \sigma_{z_t}^2}}, \tag{14}$$

which corresponds to a Gaussian mixture of the entries of $\boldsymbol{z}$. With (4) and (6), $p_Z(\cdot)$ returns a pure Gaussian distribution that perfectly represents the in-phase and quadrature components of every entry of $\boldsymbol{z}$. Note that, if quantization parameters are not adapted to the channel realization, $p_Z(\cdot)$ should also account for the random nature of $\boldsymbol{H}$ (which may affect $\sigma_{z_t}^2$). Assuming that the quantization function can be tuned in every coherence interval, and that $\boldsymbol{H}$ is available to the quantization process, we can obtain the optimum labels from (13b) using (14), namely

$$\lambda_i = \frac{\sum_{t=1}^{T} \sigma_{z_t} \left(\exp(-\tau_i^2/\sigma_{z_t}^2) - \exp(-\tau_{i+1}^2/\sigma_{z_t}^2)\right)}{2\sqrt{\pi} \sum_{t=1}^{T} \left(\mathcal{Q}(\sqrt{2}\tau_i/\sigma_{z_t}) - \mathcal{Q}(\sqrt{2}\tau_{i+1}/\sigma_{z_t})\right)}. \tag{15}$$

The Max-Lloyd algorithm is then applied by iterating the two conditions in (13) until convergence.

As a benchmark, we consider the centralized case where the received vector $\boldsymbol{y}$ is directly quantized and sent to the CPU as described in Fig. 2 (left). In this case,

$$\boldsymbol{y}_{\mathrm{Q}} = Q_b(\boldsymbol{y}), \tag{16}$$

where the quantization process is equivalent to the one defined for $\boldsymbol{z}$. In fact, we can think of this case as being the same as earlier for $T = M$ and $\boldsymbol{F} = \boldsymbol{I}_M$. Furthermore, we will assume that square transformations $\boldsymbol{F}$, i.e., which

maintain the dimensions, still fall withing the centralized case.

We are interested in determining $\mathcal{I}(\boldsymbol{z}_{\mathrm{Q}};\boldsymbol{x})$ and $\mathcal{I}(\boldsymbol{y}_{\mathrm{Q}};\boldsymbol{x})$ and comparing them under different quantization precisions. The goal is to understand if an information-lossless reduction of dimensions also translates to a reduction in the information transfer to a CPU while $\mathcal{I}(\boldsymbol{z}_{\mathrm{Q}};\boldsymbol{x}) \approx \mathcal{I}(\boldsymbol{y}_{\mathrm{Q}};\boldsymbol{x})$. We would also like to understand, for different values of T (inputs to the CPU), the relation between the user rate $\mathcal{I}(\boldsymbol{z}_{\mathrm{Q}};\boldsymbol{x})$ and the rate that needs to be transmitted to the CPU given by

$$R_{\mathrm{CPU}} = 2bT. \tag{17}$$

4 Bussgang Decomposition

Applying the Bussgang decomposition [13]

$$\boldsymbol{z}_{\mathrm{Q}} = \boldsymbol{B}\boldsymbol{z} + \boldsymbol{\eta}, \tag{18}$$

where $\boldsymbol{\eta}$ is a random vector with unknown distribution uncorrelated with $\boldsymbol{y}$ (and with $\boldsymbol{x}$ and $\boldsymbol{n}$), and with covariance

$$\boldsymbol{R}_{\boldsymbol{\eta}\boldsymbol{\eta}} = \boldsymbol{R}_{\boldsymbol{z}_{\mathrm{Q}}\boldsymbol{z}_{\mathrm{Q}}} - \boldsymbol{R}_{\boldsymbol{z}_{\mathrm{Q}}\boldsymbol{z}}\boldsymbol{R}_{\boldsymbol{z}\boldsymbol{z}}^{-1}\boldsymbol{R}_{\boldsymbol{z}\boldsymbol{z}_{\mathrm{Q}}} \tag{19}$$

while $\boldsymbol{B}$, known as the Bussgang gain matrix, corresponds to the LMMSE estimator of $\boldsymbol{z}_{\mathrm{Q}}$ from $\boldsymbol{z}$,

$$\boldsymbol{B} = \boldsymbol{R}_{\boldsymbol{z}_{\mathrm{Q}}\boldsymbol{z}}\boldsymbol{R}_{\boldsymbol{z}\boldsymbol{z}}^{-1}. \tag{20}$$

Since we have entry-wise quantization, the Bussgang gain matrix can be expressed as [13]

$$\boldsymbol{B} = \mathrm{diag}(d_1, d_2, \ldots, d_T) \tag{21}$$

with $d_t = \mathbb{E}\{z_{\mathrm{Q}t}z_t^*\}/\mathbb{E}\{|z_t|^2\}$. From the derivations in [14],

$$d_t = \sum_{i=1}^{2^b} \frac{\lambda_i}{\sqrt{\pi\sigma_{z_t}^2}} \left(\exp\left(-\frac{\tau_i^2}{\sigma_{z_t}^2} \right) - \exp\left(-\frac{\tau_{i+1}^2}{\sigma_{z_t}^2} \right) \right), \tag{22}$$

where $\sigma_{z_t}^2 = \mathbb{E}\{|z_t|^2\}$ is the tth diagonal entry of $\boldsymbol{R}_{\boldsymbol{z}\boldsymbol{z}}$. Note that $\boldsymbol{R}_{\boldsymbol{z}_{\mathrm{Q}}\boldsymbol{z}}$ can be then obtained from (20). Thus, to have a full statistical characterization of (18) up to second-order moments (the distribution of $\boldsymbol{\eta}$ is unknown) it remains to characterize $\boldsymbol{R}_{\boldsymbol{z}_{\mathrm{Q}}\boldsymbol{z}_{\mathrm{Q}}}$ in (19), as well as the bias

$$\mathbb{E}\{\boldsymbol{\eta}\} = \mathbb{E}\{\boldsymbol{z}_Q\} - \mathbb{E}\{\boldsymbol{z}\} \tag{23a}$$

$$= \mathbb{E}\{\boldsymbol{z}_Q\}. \tag{23b}$$

Said bias is given by

$$\mathbb{E}\{z_{\mathrm{Q}t}\} = \mathbb{E}\big\{Q_b\big(\Re\{z_t\}\big) + \jmath\, Q_b\big(\Im\{z_t\}\big)\big\} \tag{24a}$$
$$= (1+\jmath)\,\mathbb{E}\big\{Q_b\big(\Re\{z_t\}\big)\big\} \tag{24b}$$
$$= (1+\jmath)\int_{-\infty}^{\infty} \frac{Q_b(z)}{\sqrt{\pi\sigma_{z_t}^2}} \exp\left(-\frac{z^2}{\sigma_{z_t}^2}\right) \tag{24c}$$
$$= (1+\jmath)\sum_{i=1}^{2^b} \lambda_i \left(\mathcal{Q}\left(\frac{\sqrt{2}\tau_i}{\sigma_{z_t}}\right) - \mathcal{Q}\left(\frac{\sqrt{2}\tau_{i+1}}{\sigma_{z_t}}\right)\right), \tag{24d}$$

where we have considered that the real and imaginary parts of z_t are CPU Gaussian conditioned on the channel realization. However, the Max-Lloyd quantization will approximately lead to (13), which, due to the symmetry of the resulting thresholds, together with the symmetry of the distribution of $\boldsymbol{z}$ around $\mathbf{0}$, gives

$$\mathbb{E}\{\boldsymbol{z}_{\mathrm{Q}}\} \approx \mathbf{0}. \tag{25}$$

Thus, unbiased quantization can be assumed, which greatly simplifies the notation.[11]

4.1 Characterization of $\boldsymbol{R}_{\boldsymbol{z}_{\mathrm{Q}}\boldsymbol{z}_{\mathrm{Q}}}$

The diagonal entries of $\boldsymbol{R}_{\boldsymbol{z}_{\mathrm{Q}}\boldsymbol{z}_{\mathrm{Q}}}$ can be characterized as

$$[\boldsymbol{R}_{\boldsymbol{z}_{\mathrm{Q}}\boldsymbol{z}_{\mathrm{Q}}}]_{t,t} = \mathbb{E}\{|\boldsymbol{z}_{\mathrm{Q}t}|^2\} - |\mathbb{E}\{\boldsymbol{z}_{\mathrm{Q}t}\}|^2 \tag{26}$$

where

$$\mathbb{E}\{|\boldsymbol{z}_{\mathrm{Q}t}|^2\} = \mathbb{E}\Big\{Q_b\left(\Re\{z_t\}\right)^2 + Q_b\left(\Im\{z_t\}\right)^2\Big\} \tag{27a}$$
$$= 2\,\mathbb{E}\Big\{Q_b\left(\Re\{z_t\}\right)^2\Big\} \tag{27b}$$
$$= 2\int_{-\infty}^{\infty} \frac{Q_b(z)^2}{\sqrt{\pi\sigma_{z_t}^2}} \exp\left(-\frac{z^2}{\sigma_{z_t}^2}\right) \mathrm{d}z \tag{27c}$$
$$= 2\sum_{i=1}^{2^b} \lambda_i^2 \left(\mathcal{Q}\left(\frac{\sqrt{2}\tau_i}{\sigma_{z_t}}\right) - \mathcal{Q}\left(\frac{\sqrt{2}\tau_{i+1}}{\sigma_{z_t}}\right)\right). \tag{27d}$$

The off-diagonal entries of $\boldsymbol{R}_{\boldsymbol{z}_{\mathrm{Q}}\boldsymbol{z}_{\mathrm{Q}}}$ lead to integrals that cannot be expressed by means of Q-functions. However, in [15] it can be seen that the correlation of the quantization distortion, i.e., the off diagonal entries of $\boldsymbol{R}_{\boldsymbol{\eta}\boldsymbol{\eta}}$, is negligible

[11] For other quantization approaches, unbiased quantization can also be assumed since the bias is fully characterized from (24) and it can thus be removed after reconstruction.

for ADC resolutions over 6 bits. Moreover, the number of users considered in [15] for the previous statement is only $K = 2$, while the correlation of the quantization distortion at ADC resolutions below 6 bits also decreases with the number of users. Thus, we can approximate $\boldsymbol{R}_{\boldsymbol{\eta\eta}}$ as a diagonal matrix, with the consideration that this approximation is more accurate as the number of users and quantization bits increase. With said approximation,

$$\boldsymbol{R}_{\boldsymbol{\eta\eta}} \approx \operatorname{diag}\big(\boldsymbol{R}_{\boldsymbol{z}_{\mathrm{Q}}\boldsymbol{z}_{\mathrm{Q}}}\big) - \operatorname{diag}\big(\boldsymbol{R}_{\boldsymbol{z}_{\mathrm{Q}}\boldsymbol{z}}\boldsymbol{R}_{\boldsymbol{z}\boldsymbol{z}}^{-1}\boldsymbol{R}_{\boldsymbol{z}\boldsymbol{z}_{\mathrm{Q}}}\big). \tag{28}$$

On the other hand, if $\boldsymbol{R}_{\boldsymbol{zz}}$ is considered to be diagonal, which is the case when $\boldsymbol{F}$ is given by (4), the non-diagonal entries of $\boldsymbol{R}_{\boldsymbol{z}_{\mathrm{Q}}\boldsymbol{z}_{\mathrm{Q}}}$ are zero since

$$\begin{aligned}
\mathbb{E}\{\boldsymbol{z}_{\mathrm{Q}t}^{*}\boldsymbol{z}_{\mathrm{Q}\ell}\} &= 2\,\mathbb{E}\big\{Q_b\big(\Re\{z_t\}\big)Q_b\big(\Re\{z_l\}\big)\big\} && \text{(29a)}\\
&= 2\int_{-\infty}^{\infty}\int_{-\infty}^{\infty}\frac{Q_b(z_1)Q_b(z_2)}{\sqrt{\pi^2\sigma_{z_t}^2\sigma_{z_l}^2}} \\
&\quad\cdot\exp\!\left(-\frac{z_1^2}{\sigma_{z_t}^2}-\frac{z_2^2}{\sigma_{z_l}^2}\right)\mathrm{d}z_1\mathrm{d}z_2 && \text{(29b)}\\
&= \mathbb{E}\{\boldsymbol{z}_{\mathrm{Q}t}\}^{*}\mathbb{E}\{\boldsymbol{z}_{\mathrm{Q}\ell}\} \approx \boldsymbol{0}, && \text{(29c)}
\end{aligned}$$

where, again, the real and imaginary parts of z_t $\forall t$ have been taken to be IID Gaussian. Thus, given (4),

$$\begin{aligned}
\boldsymbol{R}_{\boldsymbol{\eta\eta}} &= \boldsymbol{R}_{\boldsymbol{z}_{\mathrm{Q}}\boldsymbol{z}_{\mathrm{Q}}} - \boldsymbol{R}_{\boldsymbol{z}_{\mathrm{Q}}\boldsymbol{z}}\boldsymbol{R}_{\boldsymbol{z}\boldsymbol{z}}^{-1}\boldsymbol{R}_{\boldsymbol{z}\boldsymbol{z}_{\mathrm{Q}}} \\
&= \operatorname{diag}\big(\boldsymbol{R}_{\boldsymbol{z}_{\mathrm{Q}}\boldsymbol{z}_{\mathrm{Q}}}\big) - \operatorname{diag}\big(\boldsymbol{R}_{\boldsymbol{z}_{\mathrm{Q}}\boldsymbol{z}}\boldsymbol{R}_{\boldsymbol{z}\boldsymbol{z}}^{-1}\boldsymbol{R}_{\boldsymbol{z}\boldsymbol{z}_{\mathrm{Q}}}\big),
\end{aligned} \tag{30}$$

where we have also considered that $\boldsymbol{R}_{\boldsymbol{z}_{\mathrm{Q}}\boldsymbol{z}}$ (and hence $\boldsymbol{R}_{\boldsymbol{z}\boldsymbol{z}_{\mathrm{Q}}}$) is also diagonal whenever $\boldsymbol{R}_{\boldsymbol{zz}}$ is diagonal, since it can be obtained from (20) as a product of diagonal matrices. Therefore, whenever $\boldsymbol{F}$ fulfills (4), we have a perfect characterization of (18) up to second moments.

5 Achievable Rates

5.1 Gaussian Lower Bound

Given the condition $\mathbb{E}\{\boldsymbol{x}\boldsymbol{\eta}^{\mathrm{H}}\} = 0$, assured by the Bussgang decomposition, we can lower-bound $\mathcal{I}(\boldsymbol{z}_{\mathrm{Q}};\boldsymbol{x})$ by replacing $\boldsymbol{\eta}$ in (18) by a Gaussian-distributed vector with equal covariance and independent of $\boldsymbol{x}$ [16]. This gives

$$\widetilde{\boldsymbol{z}}_{\mathrm{Q}} = \boldsymbol{B}\boldsymbol{z} + \widetilde{\boldsymbol{\eta}}, \tag{31}$$

where $\widetilde{\boldsymbol{\eta}} \sim \mathcal{N}_{\mathbb{C}}(\mathbf{0}_{T\times 1}, \boldsymbol{R}_{\boldsymbol{\eta}\boldsymbol{\eta}})$ with $\boldsymbol{R}_{\boldsymbol{\eta}\boldsymbol{\eta}}$ approximated by (28). Then, (31) can be rewritten as an equivalent Gaussian MIMO channel

$$\widetilde{\boldsymbol{z}}_{\mathrm{Q}} = \widetilde{\boldsymbol{H}}\boldsymbol{x} + \widetilde{\boldsymbol{n}}, \tag{32}$$

where the equivalent channel is

$$\widetilde{\boldsymbol{H}} = \boldsymbol{B}\boldsymbol{F}\boldsymbol{H}, \tag{33}$$

and $\widetilde{\boldsymbol{n}} \sim \mathcal{N}_{\mathbb{C}}(\mathbf{0}_{T\times 1}, \boldsymbol{R}_{\widetilde{\boldsymbol{n}}\widetilde{\boldsymbol{n}}})$ with covariance

$$\boldsymbol{R}_{\widetilde{\boldsymbol{n}}\widetilde{\boldsymbol{n}}} = N_0 \boldsymbol{B}\boldsymbol{F}\boldsymbol{F}^{\mathrm{H}}\boldsymbol{B}^{\mathrm{H}} + \boldsymbol{R}_{\boldsymbol{\eta}\boldsymbol{\eta}}. \tag{34}$$

For the channel in (32), the mutual information is

$$\mathcal{I}(\widetilde{\boldsymbol{z}}_{\mathrm{Q}}; \boldsymbol{x}) = \log\det\left(\boldsymbol{I}_T + E_s \boldsymbol{R}_{\widetilde{\boldsymbol{n}}\widetilde{\boldsymbol{n}}}^{-1} \widetilde{\boldsymbol{H}}\widetilde{\boldsymbol{H}}^{\mathrm{H}}\right), \tag{35}$$

which in fact coincides with the capacity for MIMO channel having correlated noise and equal power allocation among users [17]. Note that $\mathcal{I}(\boldsymbol{z}_{\mathrm{Q}}; \boldsymbol{x}) \geq \mathcal{I}(\widetilde{\boldsymbol{z}}_{\mathrm{Q}}; \boldsymbol{x})$, so (35) will also be achievable in the considered framework.

5.2 Mismatched Receiver

The approximation taken in (19) assumes $\boldsymbol{R}_{\boldsymbol{\eta}\boldsymbol{\eta}}$ to be diagonal, while in our framework this can only be assured whenever $\boldsymbol{F}$ is selected as (4). This may give, in some cases, rates that are not necessarily achievable. To evaluate the validity of the approximation we will compare the previous rates with the achievable rates obtained when operating under a mismatched receiver which assumes $\boldsymbol{R}_{\boldsymbol{\eta}\boldsymbol{\eta}}$ to be diagonal.

The achievable rate $I_q(\boldsymbol{z}_{\mathrm{Q}}, \boldsymbol{x})$ of a receiver operating under a mismatched decoding rule, i.e., assuming an input-output relation $q(\boldsymbol{z}_{\mathrm{Q}}|\boldsymbol{x})$ instead of the real conditional probability mass function $P_{\boldsymbol{z}_{\mathrm{Q}}|\boldsymbol{x}}(\boldsymbol{z}_{\mathrm{Q}}|\boldsymbol{x})$, is lower bounded by [18]

$$\begin{aligned} I_q(\boldsymbol{z}_{\mathrm{Q}}, \boldsymbol{x}) &\leq I_{\mathrm{LB},q} \\ &\triangleq -\mathbb{E}_{\boldsymbol{z}_{\mathrm{Q}}}\{\log q(\boldsymbol{z}_{\mathrm{Q}})\} + \mathbb{E}_{\boldsymbol{z}_{\mathrm{Q}},\boldsymbol{x}}\{\log q(\boldsymbol{z}_{\mathrm{Q}}|\boldsymbol{x})\}, \end{aligned} \tag{36}$$

where the expectation is over the true distribution of $\boldsymbol{z}_{\mathrm{Q}}$ (and $\boldsymbol{x}$), and we have

$$q(\boldsymbol{z}_{\mathrm{Q}}) = \int_{-\infty}^{\infty} p_{\boldsymbol{X}}(x) q(\boldsymbol{z}_{\mathrm{Q}}|\boldsymbol{x}) d\boldsymbol{x}. \tag{37}$$

Note that $I_{\mathrm{LB},q}$ is itself a lower bound for $\mathcal{I}(\boldsymbol{z}_{\mathrm{Q}}; \boldsymbol{x})$, since operating under a mismatched receiver can only reduce the information rate.

Let us have

$$q(\boldsymbol{z}_{\mathrm{Q}}|\boldsymbol{x}) = \frac{\exp\big(-(\boldsymbol{z}_{\mathrm{Q}} - \boldsymbol{B}\boldsymbol{F}\boldsymbol{x})^{\mathrm{H}}\boldsymbol{R}_{\widetilde{\boldsymbol{n}}\widetilde{\boldsymbol{n}}}^{-1}(\boldsymbol{z}_{\mathrm{Q}} - \boldsymbol{B}\boldsymbol{F}\boldsymbol{x})\big)}{\pi^{T}\det(\boldsymbol{R}_{\widetilde{\boldsymbol{n}}\widetilde{\boldsymbol{n}}})}, \tag{38}$$

where $\boldsymbol{R}_{\widetilde{\boldsymbol{n}}\widetilde{\boldsymbol{n}}}$ is given in (34) with $\boldsymbol{R}_{\boldsymbol{\eta}\boldsymbol{\eta}}$ approximated by (28). The function $q(\boldsymbol{z}_{\mathrm{Q}}|\boldsymbol{x})$ corresponds to a valid PDF describing (31), which is mismatched with respect to the true PMF $P_{\boldsymbol{Z}_{\mathrm{Q}}|\boldsymbol{X}}(\boldsymbol{z}_{\mathrm{Q}}|\boldsymbol{x})$ describing (18). We then have

$$q(\boldsymbol{z}_{\mathrm{Q}}) = \frac{\exp\Big(-\boldsymbol{z}_{\mathrm{Q}}^{\mathrm{H}}\boldsymbol{R}_{\widetilde{\boldsymbol{z}}_{\mathrm{Q}}\widetilde{\boldsymbol{z}}_{\mathrm{Q}}}^{-1}\boldsymbol{z}_{\mathrm{Q}}\Big)}{\pi^{T}\det(\boldsymbol{R}_{\widetilde{\boldsymbol{z}}_{\mathrm{Q}}\widetilde{\boldsymbol{z}}_{\mathrm{Q}}})}. \tag{39}$$

The achievable bound $I_{\mathrm{LB},q}$ can then be computed from (36) through Monte-Carlo simulations. This is not as efficient as computing the rates from (35), but it will be useful for assessing the approximation error of considering (19).

6 Numerical Results

Fig. 3 shows the achievable rates using the Gaussian lower bound (35) for different values of T when $\boldsymbol{F}$ is given by (4) with (6). The rates have been averaged over 10^3 realizations of an CPU Rayleigh fading channel. In this case the quantization process is optimum in terms of MSE since all entries of $\boldsymbol{z}$ are CPU. In Fig. 3 (left) we can see that the achievable rates with respect to the number of quantization bits are almost independent of T, so that we can potentially achieve a perfect dimension reduction which does not sacrifice performance. This way, the rates that need to be transmitted to the CPU can be linearly related to T, as can be seen in Fig. 3 (right). However, this is trivially understood by the fact that selecting $\boldsymbol{F}$ as (4) with (6) leads to the last $K - T$ components of $\boldsymbol{z}$ consist of pure noise. Future works may consider including an extra unitary matrix multiplying from the left in $\boldsymbol{F}$ in order to spread more wisely the signal power throughout the components of $\boldsymbol{z}$.

In Fig. 4 achievable rates for different strategies of constructing $\boldsymbol{F}$ are shown. When $\boldsymbol{F}$ is not given by (4) with (6), the Gaussian lower bound (35) requires the approximation (28). In order to assess the approximation error we have also included the mismatched receiver achievable rates when the decoder assumes (38), or equivalently (28), as true. This leads to the achievable lower bound (36) which has been evaluated through Monte-Carlo simulations, using 10^4 realizations of $\boldsymbol{z}_{\mathrm{Q}}$ (and $\boldsymbol{x}$). Again, we have averaged all rates over 10^3 CPU Rayleigh fading channel realizations. From Fig. 4 (left), we can see that when $\boldsymbol{F}$ is given by (4) with (6), which is only included at $T = M/2$ since for any other $T \geq K$ it will be equal (as previously discussed), the mismatched receiver bound coincides with the Gaussian bound. However, any other selection of $\boldsymbol{F}$

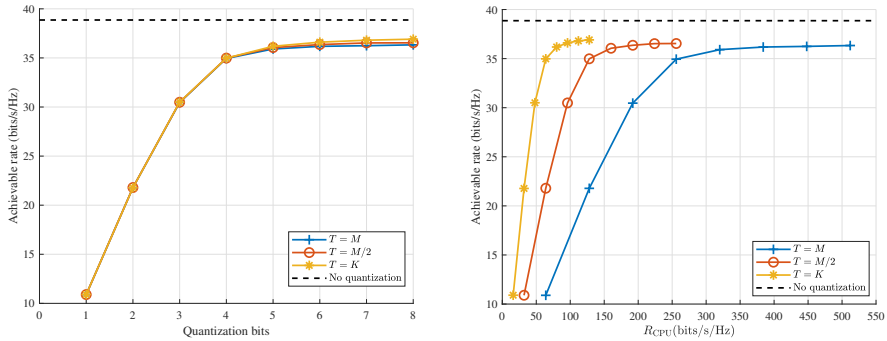

Figure 3: Achievable sum rates versus quantization bits (left) and CPU rate (right) for $M = 32$ antennas, $K = 8$ users, $E_s = 1$, $N_0 = 1$.

shows a mismatch between the two rates, in which case we should trust the curve for the mismatched receiver (dashed) since it will always give a true lower bound without approximation error. We can see that choosing $\boldsymbol{F}$ as the MRC or ZF equalization matrices leads to a worse performance than choosing (4) and (6). On the other hand, any selection of the dimension reduction matrix $\boldsymbol{F}$ seems to have a loss with respect to the centralized case without dimension reduction (i.e., $\boldsymbol{F} = \boldsymbol{I}_M$). Anyhow, dimension reduction still allows for a decrease in the CPU rate with respect to the centralized case for given achievable rate, as seen in Fig. 4 (right).

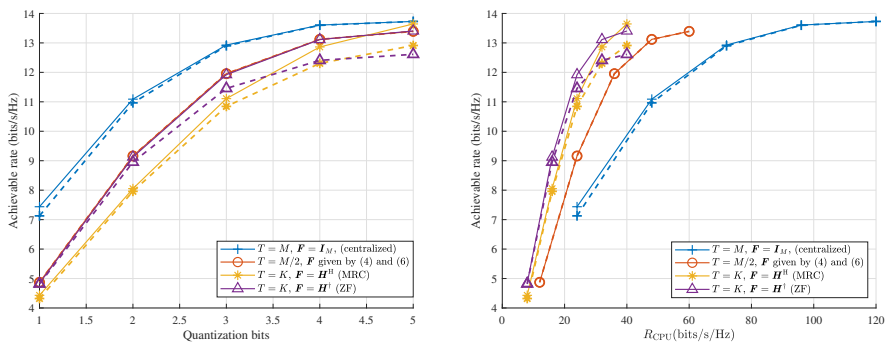

Figure 4: Achievable sum rates versus quantization bits (left) and CPU rate (right) for $M = 12$ antennas, $K = 4$ users, $E_s = 1$, $N_0 = 1$. Dashed lines denote mismatched achievable rates from (36), while solid lines denote Gaussian achievable rates from (35) using the approximation (28).

7 Conclusion

We have characterized the achievable rates for quantized post-processed vectors obtained from information-lossless dimension reductions of the received vectors. The focus of this work is to consider dimension reductions that can be applied through decentralized schemes. Our results suggest that decentralized dimension reduction allows for a reduction in the rates that have to be transmitted to a CPU for a given user rate. However, the selection of said dimension reduction clearly affects the resulting user rates, which may incur in a minor loss with respect centralized schemes where the received vectors are directly quantized. Future work may explore how to define decentralized dimension reductions for improved performance after quantization.

Acknowledgment

This work was supported by the European Research Council under the H2020 Framework Programme/ERC grant agreement 694974, by the ICREA Academia program, and by the UPF-Fractus Chair on Tech Transfer and 6G.

References

[1] J. V. Alegría, F. Rusek, and O. Edfors, "Trade-offs in decentralized multi-antenna architectures: The wax decomposition," *IEEE Transactions on Signal Processing*, vol. 69, pp. 3627–3641, 2021.

[2] J. R. Sánchez, J. Vidal Alegría, and F. Rusek, "Decentralized massive MIMO systems: Is there anything to be discussed?" In *2019 IEEE International Symposium on Information Theory (ISIT)*, 2019, pp. 787–791.

[3] J. Rodríguez Sánchez, F. Rusek, O. Edfors, M. Sarajlić, and L. Liu, "Decentralized massive MIMO processing exploring Daisy-chain architecture and recursive algorithms," *IEEE Transactions on Signal Processing*, vol. 68, pp. 687–700, 2020.

[4] J. Vidal Alegría, J. R. Sánchez, F. Rusek, L. Liu, and O. Edfors, "Decentralized equalizer construction for large intelligent surfaces," in *2019 IEEE 90th Vehicular Technology Conference (VTC2019-Fall)*, 2019, pp. 1–6.

[5] S. Moon, I.-S. Kim, D. Kam, D.-W. Jee, J. Choi, and Y. Lee, "Massive MIMO systems with low-resolution ADCs: Baseband energy consumption vs. symbol detection performance," *IEEE Access*, vol. 7, pp. 6650–6660, 2019.

[6] M. Gastpar, P. L. Dragotti, and M. Vetterli, "The distributed Karhunen–Loève transform," *IEEE Transactions on Information Theory*, vol. 52, no. 12, pp. 5177–5196, 2006.

[7] F. Wiffen, W. H. Chin, and A. Doufexi, "Distributed dimension reduction for distributed massive MIMO c-ran with finite fronthaul capacity," in *2021 55th Asilomar Conference on Signals, Systems, and Computers*, 2021, pp. 1228–1236.

[8] J. Rodríguez Sánchez, F. Rusek, O. Edfors, and L. Liu, "Distributed and scalable uplink processing for LIS: Algorithm, architecture, and design trade-offs," *IEEE Transactions on Signal Processing*, vol. 70, pp. 2639–2653, 2022.

[9] R. W. Heath Jr and A. Lozano, *Foundations of MIMO communication*. Cambridge University Press, 2018.

[10] J. Vidal Alegría, F. Rusek, J. Rodríguez Sánchez, and O. Edfors, "Modular binary tree architecture for distributed large intelligent surface," in *ICASSP 2021 - 2021 IEEE International Conference on Acoustics, Speech and Signal Processing (ICASSP)*, 2021, pp. 4565–4569.

[11] S. Lloyd, "Least squares quantization in PCM," *IEEE Transactions on Information Theory*, vol. 28, no. 2, pp. 129–137, 1982.

[12] J. Max, "Quantizing for minimum distortion," *IRE Transactions on Information Theory*, vol. 6, no. 1, pp. 7–12, 1960.

[13] O. T. Demir and E. Bjornson, "The Bussgang decomposition of nonlinear systems: Basic theory and MIMO extensions [lecture notes]," *IEEE Signal Processing Magazine*, vol. 38, no. 1, pp. 131–136, 2021.

[14] S. Jacobsson, G. Durisi, M. Coldrey, U. Gustavsson, and C. Studer, "Throughput analysis of massive MIMO uplink with low-resolution ADCs," *IEEE Transactions on Wireless Communications*, vol. 16, no. 6, pp. 4038–4051, 2017.

[15] E. Björnson, L. Sanguinetti, and J. Hoydis, "Hardware distortion correlation has negligible impact on UL massive MIMO spectral efficiency," *IEEE Transactions on Communications*, vol. 67, no. 2, pp. 1085–1098, 2019.

[16] B. Hassibi and B. Hochwald, "How much training is needed in multiple-antenna wireless links?" *IEEE Transactions on Information Theory*, vol. 49, no. 4, pp. 951–963, 2003.

[17] L. Schumacher, K. Pedersen, and P. Mogensen, "From antenna spacings to theoretical capacities - guidelines for simulating MIMO systems," in *The 13th IEEE International Symposium on Personal, Indoor and Mobile Radio Communications*, vol. 2, 2002, 587–592 vol.2.

[18] D. Arnold, H.-A. Loeliger, P. Vontobel, A. Kavcic, and W. Zeng, "Simulation-based computation of information rates for channels with memory," *IEEE Transactions on Information Theory*, vol. 52, no. 8, pp. 3498–3508, 2006.

[19] A. Mezghani and J. Nossek, "Capacity lower bound of MIMO channels with output quantization and correlated noise," in *Proc. IEEE Int. Symp. Inf. Theory (ISIT)*, 2012.

Paper V

Channel Orthogonalization with Reconfigurable Surfaces

Orthogonal MU-MIMO channels allow for optimum performance with simplified precoding/equalization, and they achieve maximum multiplexing gain which is shared fairly among users. RIS constitutes a promising cost-efficient solution to improve the wireless channel, since they consist of passive reflecting elements able to adjust the phases of the incoming waves. However, it is still widely unclear how these surfaces can improve spatial-multiplexing. In fact, the common RIS model cannot achieve perfect orthogonalization of MU-MIMO channels with a reasonable number of elements. Furthermore, efficient channel estimation algorithms for RIS, which are key for taking advantage of its benefits, are still a matter of research. We study two types of RSs, namely ARIS and FRIS, with extended capabilities over RIS. We show how these RSs allow for perfect channel orthogonalization, and, by minimizing the applied power, we show that they can potentially be implemented without the need of amplification. We also present an efficient channel estimation method for each of them that allows the BS to select the desired propagation channel.

©2022 IEEE. Reprinted, with permission, from
J. Vidal Alegría, F. Rusek,
"Channel Orthogonalization with Reconfigurable Surfaces,"
in *Proc. IEEE GLOBECOM-Wkshps 2022.*, Rio de Janeiro, Brazil, 2022, pp. 37-42.

1 Introduction

MU-MIMO [1], has become a standard solution for BS implementation in 5G networks. After the first commercial deployments of Massive MIMO [2], [3], its large scale counterpart, MU-MIMO is now a mature technology that allows multiplexing UEs in the spatial domain. However, the ability to exploit multiplexing gains with MU-MIMO depends on the conditions of the wireless propagation channels.

RIS has emerged as a promising enabling technology towards future generation networks [3]–[5]. Also known as IRS, this technology works as a passive reflector which can adjust the propagation environment in a power and cost-efficient manner. The reflected waves at the RIS can be redirected to create constructive interference and increase the received signal, leading to impressive gains in energy efficiency [6], [7].

Previous work has also considered RIS for improving spatial multiplexing in MIMO settings. For example, [8] uses RIS for improving the rank of a single-user MIMO channel. RIS has also been considered for maximizing the user rates in different settings [9], [10]. However, most of the previous results rely on the availability of channel state information at the BS, while channel estimation in RIS scenarios becomes extremely challenging [5] due to its limited capabilities and large number of elements.

In this work, we study two alternatives to RIS, namely ARIS and FRIS, for orthogonalizing MU-MIMO channels. To the best of our knowledge, the available research has not considered the fundamental problem of using RSs for obtaining orthogonal MIMO channels, while this is of essential interest since it leads to full-multiplexing gain with fair user sharing (same channel power per UE) [11]. Furthermore, for these channels, optimal processing at the base station is achieved by simple MRT/MRC. We present a channel estimation method for each RS that allows the BS to select its own channel by computing and sending the RS configuration with a reduced number of pilots. We also show that these RSs can be realized without the need for amplification by minimizing the required power.

The rest of the paper is organized as follows. Section 2 describes the system model, and defines the different RSs capabilities. Section 3 describes how to achieve perfectly orthogonal channels with RSs. In Section 4, we present the channel estimation processes for configuring the RSs. Section 5 the power minimization setting. Section 6 gives numerical results. The paper is concluded in Section 7.

2 System Model

Let us consider an uplink MU-MIMO scenario where K UEs are transmitting to an M-antenna BS, with $M > K$, through a narrow-band channel with the aid of an N-element RS. The $M \times 1$ received complex vector, $\boldsymbol{y}$, can be expressed as

$$\boldsymbol{y} = \boldsymbol{H}\boldsymbol{s} + \boldsymbol{n}, \tag{1}$$

where $\boldsymbol{H}$ is the $M \times K$ channel matrix, $\boldsymbol{s}$ is the $K \times 1$ vector of symbols transmitted by the UEs, with $\mathbb{E}(|s_k|^2) = E_s \ \forall k$, and $\boldsymbol{n} \sim \mathcal{CN}(\mathbf{0}_{M\times 1}, N_0\mathbf{I}_M)$ is the noise vector. Considering that there exists a direct channel, as well as a reflected channel through the RS, we can express the channel matrix as

$$\boldsymbol{H} = \boldsymbol{H}_0 + \boldsymbol{H}_1\boldsymbol{\Theta}\boldsymbol{H}_2, \tag{2}$$

where $\boldsymbol{H}_0$ corresponds to the $M \times K$ direct channel between the BS and the UEs, $\boldsymbol{H}_1$ and $\boldsymbol{H}_2$ correspond to the $M \times N$ channel between the BS and the RS and the $N \times K$ channel between the RS and the UEs, respectively, and $\boldsymbol{\Theta}$ is the reflection matrix applied at the RS.

In the literature, it is common to restrict the RS to have phase shifting capabilities. This corresponds to the widely known concept of RIS where

$$\boldsymbol{\Theta}_{\text{RIS}} = \text{diag}\left(\exp(j\theta_1), \ldots, \exp(j\theta_N)\right). \tag{3}$$

In this paper, however, we propose two RS technologies where said restriction is relaxed, and we compare them in the task of orthogonalizing the channel matrix.

Let us consider an RS, here referred to as ARIS, whose elements can also adjust amplitude. The corresponding reflection matrix is then defined by

$$\boldsymbol{\Theta}_{\text{ARIS}} = \text{diag}\left(\alpha_1, \ldots, \alpha_N\right), \quad \alpha_i \in \mathbb{C} \ \ \forall i. \tag{4}$$

Note that the restriction of having each α_i of amplitude 1 is here relaxed. The idea of adding amplification to a RIS has already been considered in the literature, and some of the hardware implications to realize these systems are given in [12], [13]. However, one of our goals is to restrict the power of these surfaces so that they can still be implemented without the need for active amplification.

We also consider an RS, here referred to as FRIS, whose reflection matrix is a complete matrix. Thus, we have

$$\boldsymbol{\Theta}_{\text{FRIS}} \in \mathbb{C}^{N\times N}. \tag{5}$$

In this work, we will not elaborate on the challenges of realizing such a RS. However, we can think of architectures based on vector modulators such that

the matrix multiplication can be performed by an analog combiner as in [14], although, if future technology allows it, fully-digital implementations would be desirable so that processing is done per sub-carrier.

3 Channel Orthogonalization

The main goal of employing RSs is to adjust the propagation channel to make it more beneficial in some metric, e.g., array gain, channel capacity, multiplexing gain, etc. Within the considered framework, orthogonal channels[12] are channels whose columns are constructed from unitary matrices, i.e., $\boldsymbol{H} = \sqrt{\beta}\widetilde{\boldsymbol{U}}$, where

$$\widetilde{\boldsymbol{U}} = \boldsymbol{U} \begin{bmatrix} \mathbf{I}_K \\ \mathbf{0}_{(M-K)\times K} \end{bmatrix}, \tag{6}$$

and $\boldsymbol{U} \in \mathcal{U}(M)$ ($M \times M$ unitary). Note the slight abuse of notation so that $\sqrt{\beta}$ corresponds to the singular values of the orthogonal channel. We then have

$$\boldsymbol{H}^{\mathrm{H}}\boldsymbol{H} = \beta \mathbf{I}_K. \tag{7}$$

Since the early research on MIMO systems, orthogonal channels were found to be desirable for several reasons [11]:

- Full multiplexing gain is available since all eigenvalues of the channel matrix are non-zero.
- Waterfilling algorithms are not required for maximizing capacity since all eigenvalues of the channel are equal.
- In the case of MU-MIMO, the users are served fairly since the different spatial streams have equal power.
- Simple linear equalization or precoding, namely MRC or MRT, achieves optimum performance, since it can exploit the orthogonal paths of the channel without the need for UE cooperation in MU-MIMO.

We next show how to construct $\boldsymbol{\Theta}$, for the case of ARIS and FRIS, so that the resulting channel (2) is orthogonal.

3.1 ARIS

We are interested in finding $\alpha_1, \ldots, \alpha_N$ such that

$$\boldsymbol{H}_0 + \boldsymbol{H}_1 \boldsymbol{\Theta}_{\mathrm{ARIS}} \boldsymbol{H}_2 = \sqrt{\beta}\widetilde{\boldsymbol{U}}, \tag{8}$$

[12] A more accurate term would be unitary channels due to the complex nature of the channel matrix.

Let us define

$$\boldsymbol{H}_1 = \left[\boldsymbol{h}_{11}, \ldots, \boldsymbol{h}_{1N}\right], \quad \boldsymbol{H}_2 = \left[\boldsymbol{h}_{21}, \ldots, \boldsymbol{h}_{2N}\right]^{\mathrm{T}},$$

where $\boldsymbol{h}_{1i}$ corresponds to column i of $\boldsymbol{H}_1$ and $\boldsymbol{h}_{2i}^{\mathrm{T}}$ corresponds to row i of $\boldsymbol{H}_2$. We can then rewrite (8) as

$$\sum_{i=1}^{N} \alpha_i \boldsymbol{h}_{1i} \boldsymbol{h}_{2i}^{\mathrm{T}} = \sqrt{\beta}\widetilde{\boldsymbol{U}} - \boldsymbol{H}_0. \tag{9}$$

By noting that (9) is a linear equation in the vector $\boldsymbol{\alpha} = \left[\alpha_1, \ldots, \alpha_N\right]^{\mathrm{T}}$, we can use the vectorization operation to reach

$$\boldsymbol{\mathcal{H}}_{12}\boldsymbol{\alpha} = \mathrm{vec}\left(\sqrt{\beta}\widetilde{\boldsymbol{U}} - \boldsymbol{H}_0\right), \tag{10}$$

where $\boldsymbol{\mathcal{H}}_{12} = \left[\mathrm{vec}(\boldsymbol{h}_{11}\boldsymbol{h}_{21}^{\mathrm{T}}) \quad \ldots \quad \mathrm{vec}(\boldsymbol{h}_{1N}\boldsymbol{h}_{2N}^{\mathrm{T}})\right]$, which corresponds to an $MK \times N$ matrix. Assuming $\boldsymbol{\mathcal{H}}_{12}$ is full-rank, (10) leads to an orthogonalization requirement for ARIS, namely $N \geq MK$. We would then solve (10) by

$$\boldsymbol{\alpha} = \boldsymbol{\mathcal{H}}_{12}^{\dagger}\mathrm{vec}\left(\sqrt{\beta}\widetilde{\boldsymbol{U}} - \boldsymbol{H}_0\right), \tag{11}$$

where $\boldsymbol{\mathcal{H}}_{12}^{\dagger}$ is the right pseudo-inverse[13] of $\boldsymbol{\mathcal{H}}_{12}$. Note that for obtaining $\boldsymbol{\alpha}$ we have not used the fact that the desired channel should be orthogonal. In fact, we could generate any channel matrix if we substitute $\sqrt{\beta}\widetilde{\boldsymbol{U}}$ in (11) by the desired channel.

3.2 FRIS

We are interested in finding a full-matrix $\boldsymbol{\Theta}_{\mathrm{FRIS}}$ such that

$$\boldsymbol{H}_0 + \boldsymbol{H}_1\boldsymbol{\Theta}_{\mathrm{FRIS}}\boldsymbol{H}_2 = \sqrt{\beta}\widetilde{\boldsymbol{U}}. \tag{12}$$

Assuming $\boldsymbol{H}_1$ and $\boldsymbol{H}_2$ are full-rank, we can select the reflection matrix as $\boldsymbol{\Theta}_{\mathrm{FRIS}} = \boldsymbol{H}_1^{\dagger}\boldsymbol{B}\boldsymbol{H}_2^{\dagger}$, where $\boldsymbol{H}_1^{\dagger}$ is the right pseudo-inverse of $\boldsymbol{H}_1$, $\boldsymbol{H}_2^{\dagger}$ is the left pseudo-inverse of $\boldsymbol{H}_2$, and $\boldsymbol{B}$ is an $M \times K$ matrix to be selected. This removes, with minimum power, the effect of $\boldsymbol{H}_1$ and $\boldsymbol{H}_2$ on the overall channel, and gives the orthogonalization requirement for FRIS $N \geq \min(M, K)$, which,

[13]Note that, although we can generate different right pseudo-inverses by adding matrices in the null-space of $\boldsymbol{\mathcal{H}}_{12}$, the common expression for right pseudo-inverse $\boldsymbol{\mathcal{H}}_{12}^{\dagger} = \boldsymbol{\mathcal{H}}_{12}^{\mathrm{H}}(\boldsymbol{\mathcal{H}}_{12}\boldsymbol{\mathcal{H}}_{12}^{\mathrm{H}})^{-1}$ minimizes the norm of $\boldsymbol{\alpha}$ for the given $\widetilde{\boldsymbol{U}}$ and β, which is most desirable in this work.

given $M > K$, leads to $N \geq M$. We then get

$$\boldsymbol{\Theta}_{\text{FRIS}} = \boldsymbol{H}_1^{\dagger} \left(\sqrt{\beta} \widetilde{\boldsymbol{U}} - \boldsymbol{H}_0 \right) \boldsymbol{H}_2^{\dagger}. \tag{13}$$

As happened with ARIS, we can also generate a non-orthogonal channel matrix by substituting $\sqrt{\beta}\widetilde{\boldsymbol{U}}$ in (13) with any other channel matrix.

3.3 RIS Baseline

Achieving perfect channel orthogonalization is generally not possible if we consider the widely studied RIS model (3). In case there existed a solution, it would come from finding a vector $\boldsymbol{\alpha}$ in (11) such that $|\alpha_n|^2 = 1 \; \forall n$. Obtaining said solution would correspond to finding a combination of $\widetilde{\boldsymbol{U}}$ (from a subspace of the unitary matrices), β, and a vector in the null-space of $\boldsymbol{\mathcal{H}}_{12}$ leading to a solution of (10) with $|\alpha_n|^2 = 1 \; \forall n$. This problem seems analytically intractable, so we can only restrict ourselves to approximate solutions by numerical optimization. Since our goal is channel orthogonalization, we can find approximate solutions by numerical minimization of

$$\min_{\theta_1,\ldots,\theta_N} \kappa(\boldsymbol{H}_0 + \boldsymbol{H}_1 \boldsymbol{\Theta}_{\text{RIS}} \boldsymbol{H}_2), \tag{14}$$

where $\kappa(\cdot)$ is the condition number of a matrix, given by the division between its maximum and minimum singular value, i.e., $\kappa(\cdot) = \sigma_{\max}(\cdot)/\sigma_{\min}(\cdot)$. Note that $\kappa(\cdot) \geq 1$, with equality only for orthogonal matrices. Thus, by minimizing it we would achieve a channel as close as possible to orthogonal, which will be used as a baseline approach.

4 Channel Estimation and RS Configuration

In this section, we propose two techniques (one for ARIS and one for FRIS) for estimating the channel and RS configuration at the BS. The idea is that, since it is desirable for RSs to have limited energy consumption[15], [16], and thus limited computation capabilities, we propose to leave most of the task of channel estimation and RS weight computation to the BS. For the sake of simplicity, we assume that each channel estimation step works perfectly. Proposing more specific channel estimation methods and characterizing the estimation errors is left as future work.

4.1 ARIS Configuration

We start by proposing a method to configure the ARIS and obtain the desired channel. The main goal is to estimate the necessary channel information at the

BS to be able to compute $\boldsymbol{\alpha}$ given by (11). Since the channel matrix can be arbitrarily chosen by selecting $\sqrt{\beta}\widetilde{\boldsymbol{U}}$ in (11) (recall it needs not be orthogonal), we can assume that it is the BS itself that selects the desired channel so that it does not need to further estimate it. The following steps describe the method for finding the ARIS configuration at the BS:

Estimation of $\boldsymbol{H}_0$

First, the ARIS fixes $\boldsymbol{\alpha} = \mathbf{0}_{N\times 1}$, and the UEs send K orthogonal pilots. The received symbols over K slots would be then given by the $M \times K$ matrix

$$\boldsymbol{Y}_1 = \boldsymbol{H}_0\boldsymbol{P} + \boldsymbol{N}_1, \tag{15}$$

where $\boldsymbol{P}$ is the previously known pilot matrix, which can be fixed to, e.g., $\boldsymbol{P} = \mathbf{I}_K$, and $\boldsymbol{N}_1$ is the noise matrix with IID entries $n_{ij} \sim \mathcal{CN}(0, N_0)$. From (15) we can directly estimate $\boldsymbol{H}_0$ using state-of-the art channel estimation methods.

Estimation of $\boldsymbol{\mathcal{H}}_{12}$

Since the effect of $\boldsymbol{H}_1$ and $\boldsymbol{H}_2$ for the selection of $\boldsymbol{\alpha}$ only comes through $\boldsymbol{\mathcal{H}}_{12}$, it is enough to estimate said matrix, whose columns are given by

$$[\boldsymbol{\mathcal{H}}_{12}]_{:,n} = \mathrm{vec}(\boldsymbol{h}_{1n}\boldsymbol{h}_{2n}^{\mathrm{T}}). \tag{16}$$

Let us assume that the ARIS is configured such that for a given n we have $\alpha_n = 1$ and $\alpha_i = 0$ for $i \neq n$. Transmitting K orthogonal pilots from the UEs would then lead to

$$\boldsymbol{Y}_{2n} = \boldsymbol{H}_0\boldsymbol{P} + \boldsymbol{h}_{1n}\boldsymbol{h}_{2n}^{\mathrm{T}}\boldsymbol{P} + \boldsymbol{N}_{2n}, \tag{17}$$

where $\boldsymbol{P}$ and $\boldsymbol{N}_{2n}$ are defined as before. Assuming we already know $\boldsymbol{H}_0$ from the previous step, we can cancel it at the BS, leading to

$$\widetilde{\boldsymbol{Y}}_{2n} = \boldsymbol{h}_{1n}\boldsymbol{h}_{2n}^{\mathrm{T}}\boldsymbol{P} + \widetilde{\boldsymbol{N}}_{2n}, \tag{18}$$

where $\widetilde{\boldsymbol{N}}_{2n}$ would include the estimation error from the previous step, which could lead to correlated entries. From (18) we can estimate $\boldsymbol{h}_{1n}\boldsymbol{h}_{2n}^{\mathrm{T}}$ using state-of-the-art estimation methods, which, after vectorizing, would give the estimate of the nth column of $\boldsymbol{\mathcal{H}}_{12}$ given in (16). If we iteratively perform this estimation step for $n = 1, \ldots, N$, i.e., setting to 1 each element of the ARIS at a time, the BS would construct a full estimate of $\boldsymbol{\mathcal{H}}_{12}$.

Computation and forwarding of $\boldsymbol{\alpha}$

Once the BS has estimated $\boldsymbol{H}_0$ and $\boldsymbol{\mathcal{H}}_{12}$ it can select its desired channel, which in our case corresponds to $\sqrt{\beta}\widetilde{\boldsymbol{U}}$, and compute $\boldsymbol{\alpha}$ using (11). The BS should then forward $\boldsymbol{\alpha}$ to the ARIS so that it can be configured to create the desired channel, which is already known at the BS.

The proposed method allows to configure the ARIS to generate any channel matrix by using a total of $(N+1)K$ pilot slots. This corresponds to a notable decrease with respect to estimating $\boldsymbol{H}_0$, $\boldsymbol{H}_1$, and $\boldsymbol{H}_2$ independently, which would at least require $MK+N(M+K)$ slots, or even more for practical methods such as in [17] for RIS. Moreover, since the BS selects its desired channel, it can directly use it for equalization/precoding purposes. Also, form the restriction of the channels to be orthogonal, optimum equalization/precoding would be achieved through simple MRC/MRT, i.e., multiplying the conjugate transpose of the channel matrix at the BS.

4.2 FRIS Configuration

If we inspect (13), we note that we need an estimate of both $\boldsymbol{H}_1$ and $\boldsymbol{H}_2$ to be able to compute the corresponding FRIS configuration, so an efficient method such as the the one for ARIS may not be available. Let us thus consider that the FRIS can transmit pilots through each of its elements. Although this might not be desirable in practice, the concept of FRIS is not yet well-established in contemporary literature, so we use this assumption as a first step towards defining the operation of such RSs. Coming up with more elaborate methods to avoid the requirement of sending pilots from the FRIS will be considered in future work. The following steps describe the proposed method for FRIS configuration:

Estimation of $\boldsymbol{H}_0$

In the initial step the FRIS would fix $\boldsymbol{\Theta}_{ARIS} = \boldsymbol{0}_{N\times N}$, and the UEs would send pilots to perform the channel estimation of $\boldsymbol{H}_0$ as in the ARIS case.

Estimation of $\boldsymbol{H}_1$

In the case of FRIS we need to have an estimate of $\boldsymbol{H}_1$ and $\boldsymbol{H}_2$ to compute their pseudo-inverses in (13). With the assumption that the FRIS has the ability to send pilots through each of its elements, the FRIS would send N orthogonal pilots leading to the received matrix at the BS

$$\boldsymbol{Y}_2 = \boldsymbol{H}_1\boldsymbol{P}_{\text{FRIS}} + \boldsymbol{N}_2, \tag{19}$$

where $\boldsymbol{P}_{\text{FRIS}}$ is the $N \times N$ known pilot matrix, which can be set to $\mathbf{I}_N$. From (19), the BS can estimate $\boldsymbol{H}_1$ using state-of-the-art estimation methods.

Estimation of $\boldsymbol{H}_2$

Let the FRIS fix alternatively each group of M elements to 1, i.e., at instant n we select

$$\boldsymbol{\Theta}_{\text{FRIS}} = \text{diag}(\begin{bmatrix}\mathbf{0}_{1\times(n-1)M} & \mathbf{1}_{1\times M} & \mathbf{0}_{1\times(N-nM)}\end{bmatrix}), \tag{20}$$

and we send K orthogonal pilots from the UEs. The BS would then receive

$$\boldsymbol{Y}_{3n} = \boldsymbol{H}_0\boldsymbol{P} + \boldsymbol{H}_{1,\text{sq}}(n)\boldsymbol{H}_{2,\text{sq}}(n)\boldsymbol{P} + \boldsymbol{N}_3, \tag{21}$$

where $\boldsymbol{H}_{1,sq}(n)$ is the $M \times M$ matrix formed by the columns $(n-1)M+1$ to nM of $\boldsymbol{H}_1$, $\boldsymbol{H}_{2,sq}(n)$ is the $M \times K$ matrix formed by rows $(n-1)M+1$ to nM of $\boldsymbol{H}_2$, and $\boldsymbol{N}_3$ and $\boldsymbol{P}$ are the noise and pilot matrix, respectively. Assuming $\boldsymbol{H}_{1,sq}(n)$ is full-rank $\forall n$, we can get an estimate of $\boldsymbol{H}_{2,sq}(n)$ applying state-of-the-art estimation methods to

$$\widetilde{\boldsymbol{Y}}_{3n} = \widehat{\boldsymbol{H}}_{1,\text{sq}}^{-1}(n)(\boldsymbol{H}_{1,\text{sq}}(n)\boldsymbol{H}_{2,\text{sq}}(n)\boldsymbol{P} + \boldsymbol{N}_3), \tag{22}$$

where $\widehat{\boldsymbol{H}}_{1,\text{sq}}(n)$ is the estimate of $\boldsymbol{H}_{1,\text{sq}}(n)$ from the previous stage. In the last instant, given by $n = \lceil N/M \rceil$, nM might exceed N, so everything should be cropped to N in (22), and we would change the inverse for the left pseudo-inverse of the cropped $\widehat{\boldsymbol{H}}_1$. Note that the assumption of having $\boldsymbol{H}_{1,\text{sq}}(n)$ of rank M $\forall n$ is a bit more restrictive than the requirement of solvability of (12), where only the whole matrix $\boldsymbol{H}_1$ should be rank M. However, in case some $\boldsymbol{H}_{1,\text{sq}}(n)$ are ill-conditioned, which can be known at the BS from the estimate of $\boldsymbol{H}_1$, we could think of alternative solutions, e.g., selecting groups of M linearly independent rows. In the worst case, we could also fix a smaller number of 1s in the FRIS and use the pseudo-inverse instead of inverse of the resulting cropped $\boldsymbol{H}_1$, but this would require larger number of pilot slots.

Computation and forwarding of $\boldsymbol{\Theta}_{\text{FRIS}}$

As a final step, the BS would select the desired channel ($\sqrt{\beta}\widetilde{\boldsymbol{U}}$) and compute the FRIS configuration, $\boldsymbol{\Theta}_{\text{FRIS}}$, using (13) with the estimates of $\boldsymbol{H}_0$, $\boldsymbol{H}_1$, and $\boldsymbol{H}_2$. The BS would then forward $\boldsymbol{\Theta}_{\text{FRIS}}$ to the FRIS, which would then apply it.

The proposed method allows the BS to configure the FRIS for inducing some desired channel, in this case orthogonal, by employing a total of $(1 + \lceil N/M \rceil)\, K + N$ pilots, where N of them would correspond to pilots sent from the FRIS. For a moderate number of users, this leads to a notable decrease

with respect to the ARIS method, which requires $(N+1)K$ pilots. Furthermore, we should note that the required N for FRIS can also be remarkably smaller than for ARIS. A summary of the orthogonalization conditions for each RS can be found in Table 1.

5 RS Power Constraints

In this section we study the problem of reducing the power requirements for the RS configurations achieving channel orthogonality. As shown in Table 1, we define the power of the different RS settings as the squared Frobenius norm of the reflection matrix $\boldsymbol{\Theta}$, which corresponds to the sum power throughout its entries. Let us then assume that each RS can operate without amplification as long as the average power per RS element is no greater than 1 (RIS achieves this with equality), which translates to $\|\boldsymbol{\Theta}\|_{\text{fro}}^2 \leq N$. Note that, ideally, each RS element should have power no greater than 1, which will be considered in the extended version of the paper.

Another factor to consider is the power of the resulting orthogonal subchannels of $\boldsymbol{H} = \sqrt{\beta}\widetilde{\boldsymbol{U}}$. Said power, given by β (orthogonal channels have all eigenvalues equal), would be linearly related to the post-processed SNR per UE (after MRC/MRT), $\eta = \beta E_s/N_0$, where we have assumed that the RS does not introduce extra noise.[14] Recall that, from the orthogonality of the channel, there is no interference between UEs and all UEs have the same post-processed SNR. Thus, for a limited RS power, we would ideally like to have a large β so as to increase the capacity per UE .

5.1 ARIS

The ARIS sum power required for having $\boldsymbol{H} = \sqrt{\beta}\widetilde{\boldsymbol{U}}$ is given by (see Table 1)

$$P_{\text{A}}(\beta, \widetilde{\boldsymbol{U}}) = \beta g_1(\widetilde{\boldsymbol{U}}) - 2\sqrt{\beta} f_1(\widetilde{\boldsymbol{U}}) + c_1, \tag{23}$$

where $f_1(\widetilde{\boldsymbol{U}}) = \mathfrak{Re}\left\{\text{vec}(\widetilde{\boldsymbol{U}})^{\text{H}} \boldsymbol{G}_{12}^{-1} \text{vec}(\boldsymbol{H}_0)\right\}$, $g_1(\widetilde{\boldsymbol{U}}) = \text{vec}(\widetilde{\boldsymbol{U}})^{\text{H}} \boldsymbol{G}_{12}^{-1} \text{vec}(\widetilde{\boldsymbol{U}})$, and $c_1 = \text{vec}(\boldsymbol{H}_0)^{\text{H}} \boldsymbol{G}_{12}^{-1} \text{vec}(\boldsymbol{H}_0)$, with $\boldsymbol{G}_{12} = \boldsymbol{\mathcal{H}}_{12} \boldsymbol{\mathcal{H}}_{12}^{\text{H}}$. Equation (23) comes from substituting (11) in the ARIS power expression from Table 1 and operating. Let us first focus on obtaining the minimum ARIS power for achieving an orthogonal channel. We can immediately note that the existence of the direct channel $\boldsymbol{H}_0$ is responsible for requiring a minimum power to be able to orthogonalize the channel with ARIS. In the absence of $\boldsymbol{H}_0$ ($c_1 = f_1(\widetilde{\boldsymbol{U}}) = 0$), $P_{\text{A}}(\beta, \widetilde{\boldsymbol{U}})$ can be made arbitrarily small by lowering β, i.e., sacrificing SNR;

[14] RSs with amplification might suffer from noise enhancement similar to that of zero-forzing (ZF) equalizers. A thorough characterization of it may be considered in future work.

therefore, channel orthogonalization would be achievable without the need for amplification. Let us then assume $\boldsymbol{H}_0$ is present. Note that the BS has freedom in selecting $\widetilde{\boldsymbol{U}}$ and β. We can then obtain the minimum power required for orthogonalization with ARIS by solving

$$\begin{aligned} P_{\mathrm{A,min}} = \min_{\beta,\widetilde{\boldsymbol{U}}} \;& P_{\mathrm{A}}(\beta,\widetilde{\boldsymbol{U}}) \\ \text{s.t. } & \widetilde{\boldsymbol{U}}^{\mathrm{H}}\widetilde{\boldsymbol{U}} = \mathbf{I}_K. \end{aligned} \tag{24}$$

Differentiating $P_{\mathrm{A}}(\beta,\widetilde{\boldsymbol{U}})$ over β and equalling to 0 gives us the minimum β

$$\beta_{\mathrm{o1}} = \left(\frac{f_1(\widetilde{\boldsymbol{U}})}{g_1(\widetilde{\boldsymbol{U}})}\right)^2. \tag{25}$$

We can then substitute β_{o1} in (23) to get $P_{\mathrm{A}}(\beta_{\mathrm{o1}},\widetilde{\boldsymbol{U}})$, which can then be minimized using gradient descent within the unitary space. In order to improve accuracy of the optimization, we consider optimization over the geodesics of the unitary space as proposed in [18]. Thus, we need to obtain the Euclidean gradient by differentiating $P_{\mathrm{A}}(\beta_*,\widetilde{\boldsymbol{U}})$ over $\boldsymbol{U}^*$ (recall (6)), and use it for algorithm in [18, Table II], which includes Armijo line-search for better convergence. We get

$$\begin{aligned} \frac{\partial P_{\mathrm{A}}(\beta_{\mathrm{o1}},\widetilde{\boldsymbol{U}})}{\partial \widetilde{\boldsymbol{U}}^*} = \frac{b}{g_1^2(\widetilde{\boldsymbol{U}})}\mathrm{vec}^{-1}\Big(& -f_1^2(\widetilde{\boldsymbol{U}})\boldsymbol{G}_{12}^{-1}\mathrm{vec}(\widetilde{\boldsymbol{U}}) \\ & + f_1(\widetilde{\boldsymbol{U}})g_1(\widetilde{\boldsymbol{U}})\boldsymbol{G}_{12}^{-1}\mathrm{vec}(\boldsymbol{H}_0)\Big), \end{aligned} \tag{26}$$

where $b = 1 - 2\mathrm{sign}\Big(f_1(\widetilde{\boldsymbol{U}})\Big)$. Note that, for differentiating over $\boldsymbol{U}^*$ instead of $\widetilde{\boldsymbol{U}}^*$, we would just complete (26) with zeros, since the corresponding extra columns of $\boldsymbol{U}$ have no bearing on $P_{\mathrm{A}}(\beta_{\mathrm{o1}},\widetilde{\boldsymbol{U}})$. Once we have obtained $P_{\mathrm{A,min}}$, any other ARIS sum power above it can be achieved from (23) by solving a second order equation over $\sqrt{\beta}$. Note that for every different β there may be a new optimal $\widetilde{\boldsymbol{U}}$, i.e., different from the one solving (24), which minimizes the resulting power. Alternatives of (24) will be studied in the extended version.

5.2 FRIS

The FRIS sum power giving $\boldsymbol{H} = \sqrt{\beta}\widetilde{\boldsymbol{U}}$ corresponds to

$$P_{\mathrm{F}} = \beta g_2(\widetilde{\boldsymbol{U}}) - 2\sqrt{\beta}f_2(\widetilde{\boldsymbol{U}}) + c_2, \tag{27}$$

	ARIS	**FRIS**	**RIS**
Minimum N for orthogonalization	MK	$\min(M,K)$	-
Number of pilots	$(N+1)K$	$\left(1+\lceil\frac{N}{M}\rceil\right)K+N$	$> MK+N(M+K)$ [17]
RS sum power	$\|\Theta_{\text{ARIS}}\|_{\text{fro}}^2=\boldsymbol{\alpha}^{\text{H}}\boldsymbol{\alpha}$	$\|\Theta_{\text{FRIS}}\|_{\text{fro}}^2=\text{tr}(\Theta_{\text{FRIS}}^{\text{H}}\Theta_{\text{FRIS}})$	$\|\Theta_{\text{RIS}}\|_{\text{fro}}^2=N$

Table 1: Orthogonalization conditions for different RSs.

where we defined $f_2(\widetilde{\boldsymbol{U}})=\mathfrak{Re}\left\{\text{tr}(\boldsymbol{G}_2^{-1}\widetilde{\boldsymbol{U}}^{\text{H}}\boldsymbol{G}_1^{-1}\boldsymbol{H}_0)\right\}$, $g_2(\widetilde{\boldsymbol{U}})=\text{tr}(\boldsymbol{G}_2^{-1}\widetilde{\boldsymbol{U}}^{\text{H}}\boldsymbol{G}_1^{-1}\widetilde{\boldsymbol{U}})$, $c_2=\text{tr}(\boldsymbol{G}_2^{-1}\boldsymbol{H}_0^{\text{H}}\boldsymbol{G}_1^{-1}\boldsymbol{H}_0)$, with $\boldsymbol{G}_1=\boldsymbol{H}_1\boldsymbol{H}_1^{\text{H}}$ and $\boldsymbol{G}_2=\boldsymbol{H}_2^{\text{H}}\boldsymbol{H}_2$. We can use the same reasoning as in the case for ARIS throughout the different steps. Let us thus focus on solving

$$\begin{aligned} P_{\text{F,min}}= \min_{\beta,\widetilde{\boldsymbol{U}}} \quad & P_{\text{F}}(\beta,\widetilde{\boldsymbol{U}}) \\ \text{s.t.} \quad & \widetilde{\boldsymbol{U}}^{\text{H}}\widetilde{\boldsymbol{U}}=\mathbf{I}_K. \end{aligned} \tag{28}$$

Proceeding as in the previous case we can get

$$\beta_{\text{o2}}=\left(\frac{f_2(\widetilde{\boldsymbol{U}})}{g_2(\widetilde{\boldsymbol{U}})}\right)^2, \tag{29}$$

which leads to the euclidean gradient to be used for minimizing over $\widetilde{\boldsymbol{U}}$ using [18, Table II],

$$\begin{aligned} \frac{\partial P_{\text{F}}(\beta_{\text{o1}},\widetilde{\boldsymbol{U}})}{\partial\widetilde{\boldsymbol{U}}^*}=\frac{b}{g_2^2(\widetilde{\boldsymbol{U}})}\Big(&-f_2^2(\widetilde{\boldsymbol{U}})\boldsymbol{G}_1^{-1}\widetilde{\boldsymbol{U}}^{\text{H}}\boldsymbol{G}_2^{-1} \\ &+g_2(\widetilde{\boldsymbol{U}})f_2(\widetilde{\boldsymbol{U}})\boldsymbol{G}_1^{-1}\boldsymbol{H}_0\boldsymbol{G}_2^{-1}\Big), \end{aligned} \tag{30}$$

where $b=1-2\text{sign}\left(f_2(\widetilde{\boldsymbol{U}})\right)$.

6 Numerical Results

For the numerical results, we have tried to solve the optimization problems defined in (24) and (28). Finding closed form results for said problems is in general intractable due the constraint in $\widetilde{\boldsymbol{U}}$, which should live in a subspace of the unitary matrices. However, good local solutions can be found by using gradient descent along the geodesics, as proposed in [18]. We cannot assure that the obtained results reach absolute minima, but, since our main goal is to check if the proposed RS technologies can be realized without amplification, local minima may be enough for our purpose. We have thus implemented [18,

Table II] with the Euclidean gradients defined in (26) and (30) to find the minimum power required for perfect channel orthongonalization using ARIS and FRIS, respectively.

In Fig. 1 we can see the minimum average RS power per element, $P_{\mathrm{RS,avg}} = P_{\{\mathrm{A,F}\},\mathrm{min}}/N$, and the resulting channel gain per UE, equal to β for all UEs from the orthogonal restriction, with respect to the normalized power of the direct channel, E_0. Since we are most interested in the power relation between the direct and reflected channels, we have used normalized IID Rayleigh fading channels with $\|\boldsymbol{H}_0\|_{\mathrm{Fro}}^2 = E_0 MK$, $\|\boldsymbol{H}_1\|_{\mathrm{Fro}}^2 = MN$, $\|\boldsymbol{H}_2\|_{\mathrm{Fro}}^2 = NK$. Other channel models will be considered in future work, but we may note from the analytical results that ill-conditioned channels are most harmful in the RS-reflected paths. Fig. 1 (left) shows that in most practical scenarios (direct links with power below 100 times the reflected one), the minimum average power for channel orthogonalization, with both ARIS and FRIS, can be smaller than that of RIS, so these surfaces could potentially be implemented without amplification. The resulting channel gains for these minimized powers have analogous linear relation with E_0, still impressive since they even outperform RIS, which has been numerically optimized for channel orthogonalization using (14).[15] However, the results for RIS may be far from optimum due to the difficulty of such task, and the analytical intractability. Finding more suitable optimization formulations for channel orthogonalization with RIS should be further studied. A important thing to note is that the channel gains in Fig. 1 are achieved with RS power dependent on E_0, and generally below that of RIS. If we increase the respective gains until all RS powers are equal to that of RIS, the resulting channel gains, which are plotted in Fig. 2, are even more impressive, especially for FRIS, which can get 10 times better channel gains than ARIS with a lower number of elements. In fact, there is room for improvement by further optimization of $\widetilde{\boldsymbol{U}}$, as previously discussed.

7 Conclusions

We have presented the concepts of FRIS and ARIS, two alternative RS technologies with relaxed restrictions over RIS. We have obtained analytical results for FRIS and ARIS configurations that achieve perfect channel orthogonalization. We proposed a channel estimation method for each RS technology at the BS, which selects the desired channel and forwards the corresponding RS configuration. We have also showed that these RS can perform channel orthogonalization without the need of amplification by minimizing over the unitary space. The achieved channel gains, which are fairly distributed among users

[15] For the RIS, since perfect orthogonality may not be reachable, we plotted the average channel gain and minimum channel gain per UE.

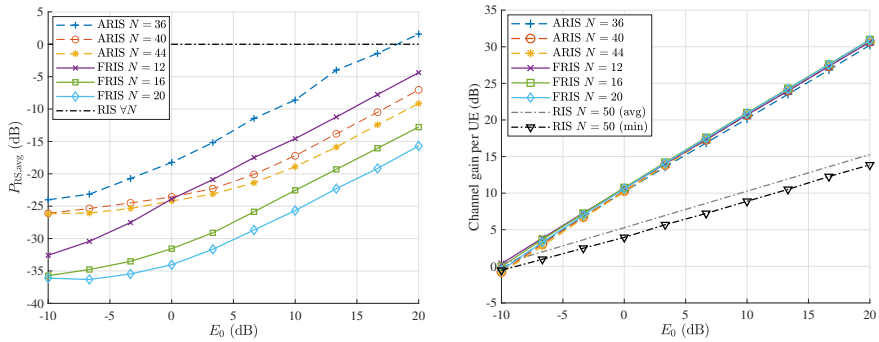

Figure 1: Minimum average RS power per element (left) and resulting minimum channel gain per UE with respect to normalized gain of the direct channel.

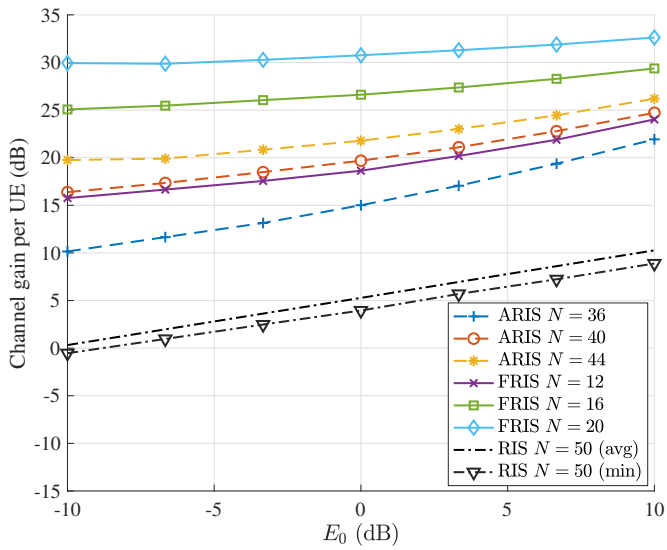

Figure 2: Channel gain per UE for unit average RS power per element with respect to normalized gain of the direct channel.

from the orthogonalization, remark the benefits of adding more processing capabilities at the RSs.

References

[1] N. Jindal, "MIMO broadcast channels with finite-rate feedback," *IEEE Transactions on Information Theory*, vol. 52, no. 11, pp. 5045–5060, 2006.

[2] T. L. Marzetta, "Noncooperative cellular wireless with unlimited numbers of base station antennas," *IEEE Transactions on Wireless Communications*, vol. 9, no. 11, pp. 3590–3600, 2010.

[3] E. Björnson, L. Sanguinetti, H. Wymeersch, J. Hoydis, and T. L. Marzetta, "Massive MIMO is a reality—what is next?: Five promising research directions for antenna arrays," *Digital Signal Processing*, vol. 94, pp. 3–20, 2019, Special Issue on Source Localization in Massive MIMO.

[4] E. Basar, M. Di Renzo, J. De Rosny, M. Debbah, M.-S. Alouini, and R. Zhang, "Wireless communications through reconfigurable intelligent surfaces," *IEEE Access*, vol. 7, pp. 116 753–116 773, 2019.

[5] C. Huang, S. Hu, G. C. Alexandropoulos, *et al.*, "Holographic MIMO surfaces for 6G wireless networks: Opportunities, challenges, and trends," *IEEE Wireless Communications*, vol. 27, no. 5, pp. 118–125, 2020.

[6] Q. Wu and R. Zhang, "Intelligent reflecting surface enhanced wireless network via joint active and passive beamforming," *IEEE Transactions on Wireless Communications*, vol. 18, no. 11, pp. 5394–5409, 2019.

[7] C. Huang, A. Zappone, G. C. Alexandropoulos, M. Debbah, and C. Yuen, "Reconfigurable intelligent surfaces for energy efficiency in wireless communication," *IEEE Transactions on Wireless Communications*, vol. 18, no. 8, pp. 4157–4170, 2019.

[8] O. Ozdogan, E. Björnson, and E. G. Larsson, "Using intelligent reflecting surfaces for rank improvement in MIMO communications," in *ICASSP 2020 - 2020 IEEE International Conference on Acoustics, Speech and Signal Processing (ICASSP)*, 2020, pp. 9160–9164.

[9] H. Guo, Y.-C. Liang, J. Chen, and E. G. Larsson, "Weighted sum-rate maximization for reconfigurable intelligent surface aided wireless networks," *IEEE Transactions on Wireless Communications*, vol. 19, no. 5, pp. 3064–3076, 2020.

[10] Y. Zhang, C. Zhong, Z. Zhang, and W. Lu, "Sum rate optimization for two way communications with intelligent reflecting surface," *IEEE Communications Letters*, vol. 24, no. 5, pp. 1090–1094, 2020.

[11] A. Paulraj, R. Nabar, and D. Gore, *Introduction to Space-Time Wireless Communications*, 1st. USA: Cambridge University Press, 2008.

[12] R. A. Tasci, F. Kilinc, E. Basar, and G. C. Alexandropoulos, "A new RIS architecture with a single power amplifier: Energy efficiency and error performance analysis," *IEEE Access*, vol. 10, pp. 44 804–44 815, 2022.

[13] R. Long, Y.-C. Liang, Y. Pei, and E. G. Larsson, "Active reconfigurable intelligent surface-aided wireless communications," *IEEE Transactions on Wireless Communications*, vol. 20, no. 8, pp. 4962–4975, 2021.

[14] T. Zirtiloglu, N. Shlezinger, Y. C. Eldar, and R. Tugce Yazicigil, "Power-efficient hybrid MIMO receiver with task-specific beamforming using low-resolution ADCs," in *ICASSP 2022 - 2022 IEEE International Conference on Acoustics, Speech and Signal Processing (ICASSP)*, 2022, pp. 5338–5342.

[15] M. Di Renzo, K. Ntontin, J. Song, *et al.*, "Reconfigurable intelligent surfaces vs. relaying: Differences, similarities, and performance comparison," *IEEE Open Journal of the Communications Society*, vol. 1, pp. 798–807, 2020.

[16] Y. Liu, X. Liu, X. Mu, *et al.*, "Reconfigurable intelligent surfaces: Principles and opportunities," *IEEE Communications Surveys & Tutorials*, vol. 23, no. 3, pp. 1546–1577, 2021.

[17] M. Joham, H. Gao, and W. Utschick, "Estimation of channels in systems with intelligent reflecting surfaces," in *ICASSP 2022 - 2022 IEEE International Conference on Acoustics, Speech and Signal Processing (ICASSP)*, 2022, pp. 5368–5372.

[18] T. E. Abrudan, J. Eriksson, and V. Koivunen, "Steepest descent algorithms for optimization under unitary matrix constraint," *IEEE Transactions on Signal Processing*, vol. 56, no. 3, pp. 1134–1147, 2008.

Paper VI

Trade-offs in Decentralized Multi-Antenna Architectures: Sparse Combining Modules for WAX Decomposition

With the increase in the number of antennas at BS, centralized multi-antenna architectures have encountered scalability problems from excessive interconnection bandwidth to the CPU, as well as increased processing complexity. Thus, research efforts have been directed towards finding decentralized receiver architectures where a part of the processing is performed at the antenna end (or close to it). A recent paper put forth an information-lossless trade-off between level of decentralization (inputs to CPU) and decentralized processing complexity (multiplications per antenna). This trade-off was obtained by studying a newly defined matrix decomposition–the WAX decomposition–which is directly related to the information-lossless processing that should to be applied in a general framework to exploit the trade-off. The general framework consists of three stages: a set of decentralized filters, a linear combining module, and a processing matrix applied at the CPU; these three stages are linear transformations which can be identified with the three constituent matrices of the WAX decomposition. The previous work was unable to provide explicit constructions for linear combining modules which are valid for WAX decomposition, while it remarked the importance of these modules being sparse with 1s and 0s so they could be efficiently implemented using hardware accelerators. In this work we present a number of constructions, as well as possible variations of them, for effectively defining linear combining modules which can be used in the WAX decomposition. Furthermore, we show how these structures facilitate decentralized calculation of the WAX decomposition for applying information-lossless processing in architectures with an arbitrary level of decentralization.

J. Vidal Alegría, F. Rusek,
"Trade-offs in Decentralized Multi-Antenna Architectures: Sparse Combining Modules for WAX Decomposition,"
submitted to *IEEE Trans. Signal Process.* (second review).

1 Introduction

Multi-antenna architectures constitute a mature technology which keeps developing to improve wireless communication links. Their main benefits include increased data rates and reliability due to the exploitation of space-division multiplexing and diversity. Current research on multi-antenna architectures is trending towards scaling up the number of antennas in order to further increase spectral efficiency and spatial resolution. This trend can be seen, e.g., in massive MIMO [1], [2] and LIS [3], where massive MIMO considers BSs with hundreds of antennas, while LIS goes beyond by considering whole walls of electromagnetically active material.

Several prototypes of massive MIMO have been developed and tested [4]–[6]. In the prototypes from [4], [6], centralized processing results in scalability issues due to the increased data-rates between the antennas and the CPU, which scales with the number of antennas. These issues become even more concerning in LIS, where practical deployments are expected to include a number of antennas at least an order of magnitude greater than massive MIMO [7].[16] Cell-free massive MIMO[9]–[12] is also likely to suffer from scalability issues due to the large number of access points (APs) distributed throughout large geographical areas. Our system model will consider a general multi-antenna architecture which can be generalized to more specific applications, e.g., the ones previously mentioned.

Decentralized pre-processing of the received signals at the antenna end (or nearby) allows to reduce the dimension of the data that needs to be transmitted to a CPU[13]–[15]. In the recent years, there has been a trend towards considering more decentralized architectures [13]–[23] in order to cope with scalability issues arising in large-scale multi-antenna architectures. The literature on decentralized massive MIMO includes a number of solutions, ranging from fully-decentralized architectures [16], [19]–[21], where CSI does not have to be available at the CPU, to partially decentralized architectures, where some of the processing tasks are distributed, but neither full [17], [23], nor partial CSI [13] is available at the CPU. We can also find decentralized solutions tailored for other large-scale multi-antenna systems such as for cell-free massive MIMO [10], [24], or for extra-large scale MIMO (XL-MIMO) [23], [25], which can be seen as a system with a number of antennas in the regime of massive MIMO where the antenna array is deployed throughout a large surface such that spatial non-stationarities appear [26].

In [27], an information-lossless trade-off between the number of connections to a CPU and number of multiplications per antenna is presented.[17] To this

[16] Discrete surfaces approximate continuous ones when sampling is dense enough [3], [8].

[17] Information-lossless here means that the mutual information between the post-processed and the user data is equal to the mutual information between the received data and the user data.

end, a general framework is considered which can accommodate classical centralized processing architectures, decentralized architectures such as [13], as well as a wide range of intermediate architectures. Unlike [18], where a system-level trade-off between different decentralized architectures, algorithms, and data precision is studied, [27] gives a fundamental trade-off between level of decentralization and decentralized processing complexity. The information-lossy regime of said trade-off is considered in [7], [14], while we restrict our work to the information-lossless regime. Hence, the results from [14], [16]–[23], [25] lie essentially outside the scope of our work since they rely on the usage of linear equalizers which incur information-losses before symbol detection, and/or they focus on the symbol detection problem, which we disregard in this work. Furthermore, most of these works focus on the implementation of solutions as decentralized as possible, while our aim is to understand the trade-offs arising when we can have different levels of decentralization. Thus, we consider the general framework from [27], which corresponds to a generic architecture useful in the analysis of the information-lossless regime of decentralized linear equalization. Note that BER is not a suitable metric for judging the results presented in this work,[18] while channel capacity is perfectly achievable under this framework.

The WAX decomposition, as originally introduced in [27], is a matrix decomposition which has direct correspondence with the information-lossless linear processing to be applied in an architecture with an arbitrary level of decentralization. It thus allows to characterize the information-lossless trade-off between level of decentralization and decentralized processing complexity. The idea is to decompose the channel matrix into the product of a (block-diagonal) decentralized processing matrix $\boldsymbol{W}$, a linear combining module $\boldsymbol{A}$, and a CPU processing matrix $\boldsymbol{X}$. In [27, Theorem 1], the requirements for the existence of the WAX decomposition are only proved for randomly chosen channel matrices and using fixed randomly chosen combining modules $\boldsymbol{A}$ (for definition of "randomly chosen" see *Notation*). In [12], the applicability of the WAX decomposition is generalized to sparse channel matrices, showing that channel sparsity can degrade the trade-off given in [27]. On the other hand, [27] remarks the importance of employing a simple sparse combining matrix $\boldsymbol{A}$ with 1s and 0s, so that it could be efficiently implemented through hardware modules, i.e., generalizing the trivial combining modules from purely decentralized architectures (e.g., the sum module from [13]) or common centralized architectures (i.e., an identity module). However, [27] only presents necessary conditions for an $\boldsymbol{A}$ to be valid for WAX decomposition.

The current paper is a continuation of the work presented in [27], and it further extends the results from [30]. Thus, our aim is to fill some of the gaps

[18] BER can be made arbitrarily small when operating at rates below capacity [28] with marginal loss when considering practical channel coding methods, e.g., LDPC [29].

from [27] by presenting a set of constructions for $\boldsymbol{A}$ which consist of sparse structures of 1s and 0s,[19] and which can be proved valid for WAX decomposition under different parameter settings. The proven existence of these constructions strengthens the practicality of the WAX decomposition for the exploitation of the trade-off between level of decentralization and decentralized processing complexity from [27]. Furthermore, we exploit the structure of said $\boldsymbol{A}$ matrices to define a decentralized scheme for computing the information-lossless decentralized filters without the need of aggregating the full CSI at any single point. We also extend [27, Theorem 1] by proving the converse (only if) statement for arbitrary combining modules, thus showing that the information-lossless trade-off studied [27] is of fundamental nature and it is not possible to operate without loss beyond it. The list of contributions are summarized next:

- We prove that there exists no combining module, $\boldsymbol{A}$, attaining a less-restrictive information-lossless trade-off than the one obtained in [27, Theorem 1], which was only proved for randomly chosen $\boldsymbol{A}$.
- We present an equivalent formulation of the WAX decomposition which describes the information-lossless regime without the need of taking into account any processing at the CPU. This was already included in [30].
- We present 3 sparse structures for $\boldsymbol{A}$ and prove their validity for WAX decomposition. Only one of these structures was included in [30]. The new structures allow for more freedom in the exploitation without loss of the achievable trade-off, which corresponds to a novel generalization of the trade-off from [27] with marginal loss.
- We present two transformations for $\boldsymbol{A}$ that maintain its validity. One of them was included in [30].
- We present a general algorithm to construct a matrix $\boldsymbol{A}$ that allows for the exploitation of the achievable trade-off for any set of system parameters. Unfortunately, we were unable to formally prove the validity of the $\boldsymbol{A}$ matrices constructed using said algorithm.
- We present a decentralized scheme for computing the information-lossless decentralized filters which generalizes the one included in [30] to the new $\boldsymbol{A}$ structures presented in this work.

The rest of the paper is organized as follows. Section 2 presents the system model and discusses the relevant background from [27]. Section 3 presents the main theoretical results, including the converse of [27, Theorem 1], and the equivalent formulation of the WAX decomposition. In Section 4, we discuss different ways of constructing a valid combining matrix $\boldsymbol{A}$. Section 5 describes

[19] This condition is slightly relaxed in degenerate cases as will be discussed.

the decentralized scheme for computing the decentralized filters considering the valid $\boldsymbol{A}$ structures. In Section 5, we present some examples as well as a discussion of the previous results. Finally, Section 7 concludes the paper.

Notation: In this paper, lowercase, bold lowercase and bold uppercase letters stand for scalars, column vectors and matrices, respectively. When using the mutual information operator, $I(\cdot;\cdot)$, bold uppercase sub-scripts refer to random vectors instead of their realizations. The operations $(\cdot)^{\mathrm{T}}$, $(\cdot)^*$ and $(\cdot)^{\mathrm{H}}$ denote transpose, conjugate, and conjugate transpose, respectively. The operation $(\cdot)^\dagger$ denotes Moore-Penrose inverse. The operation $\mathrm{diag}(\cdot,\ldots,\cdot)$ outputs a block diagonal matrix with the input matrices as the diagonal blocks. $\boldsymbol{A}\otimes\boldsymbol{B}$ denotes the Kronecker product between matrices $\boldsymbol{A}$ and $\boldsymbol{B}$. $\mathbf{I}_i$ corresponds to the identity matrix of size i, $\mathbf{1}_{i\times j}$ denotes the $i\times j$ all-ones matrix, and $\mathbf{0}_{i\times j}$ denotes the $i\times j$ all-zeros matrix (absence of one such index indicates that the matrix is square). The notation $[\boldsymbol{A}]_{i:j,\ell:k}$ denotes a matrix formed by rows i to j and columns ℓ to k of $\boldsymbol{A}$ (as in Python vector notation, absence of one or more indexes indicates that start/end of the included rows or columns corresponds to the first/last row or column of $\boldsymbol{A}$, respectively). In this paper, a randomly chosen matrix corresponds to a realization of a random matrix where any submatrix of it is full-rank with probability 1, e.g., a realization of an IID Gaussian matrix.

2 System Model

Let us consider K single-antenna users transmitting to an M-antenna BS, with $M > K$, through a narrow-band channel. The $M\times 1$ received complex baseband vector can be expressed as

$$\boldsymbol{y} = \boldsymbol{H}\boldsymbol{s} + \boldsymbol{n}, \tag{1}$$

where $\boldsymbol{H}$ is the $M \times K$ channel matrix, $\boldsymbol{s}$ is the $K \times 1$ vector of symbols transmitted by the users, and $\boldsymbol{n}$ is a zero-mean complex white Gaussian noise vector with sample variance N_0. The M antennas are divided into M_{P} groups (or panels) with L antennas (M/L evaluates to an integer). Thus, we can express the channel matrix as $\boldsymbol{H} = [\boldsymbol{H}_1^{\mathrm{T}}\, \boldsymbol{H}_2^{\mathrm{T}}\, \ldots\, \boldsymbol{H}_{M_{\mathrm{P}}}^{\mathrm{T}}]^{\mathrm{T}}$ where $\boldsymbol{H}_m$ corresponds to the $L \times K$ local channel matrix seen by panel p, for $p \in \{1,\ldots,M_{\mathrm{P}}\}$. Each panel multiplies the received vector by an $L\times L$ matrix, $\boldsymbol{W}_m^{\mathrm{H}}$ $m \in \{1,\ldots,M_{\mathrm{P}}\}$, thus generating L outputs,[20] $L \leq K$. The aggregated outputs are combined through a fixed $T \times M$ matrix, $\boldsymbol{A}^{\mathrm{H}}$, $T \leq M$. We can view $\boldsymbol{A}^{\mathrm{H}}$ as a hardware combining module which can be predesigned, but is fixed once deployed. The resulting vector is forwarded to a CPU, which can apply further processing.

[20] From [27], the restriction of having the same number of antennas and outputs in each panel can be relaxed through an equivalent transformation without constraining the validity of our analysis.

In order be able to relate the resulting linear processing to common strategies, e.g., MRC, ZF, MMSE, etc, we assume that the processing at the CPU can be given by a matrix multiplication with a $K \times T$ matrix $\boldsymbol{X}^{\mathrm{H}}$ (see [27] for further details). The post-processed vector is then given by

$$\boldsymbol{z} = \boldsymbol{X}^{\mathrm{H}} \boldsymbol{A}^{\mathrm{H}} \boldsymbol{W}^{\mathrm{H}} \boldsymbol{y}, \tag{2}$$

where $\boldsymbol{W}$ is an $M \times M$ block diagonal matrix of the form

$$\boldsymbol{W} = \mathrm{diag}\left(\boldsymbol{W}_1, \boldsymbol{W}_2, \ldots, \boldsymbol{W}_{M_{\mathrm{P}}}\right). \tag{3}$$

The matrices $\boldsymbol{W}$ and $\boldsymbol{X}$ can be recalculated for every channel realization, while the matrix $\boldsymbol{A}$ remains unchanged once the system is deployed (we can think of it as a fixed hardware combining module). The framework under study is represented in Fig. 1. Note that, during the whole uplink transmission, information is only flowing from the antennas towards the CPU, unlike message passing approaches like [22], [23], [25]. This means that there is no extra delay with respect to common centralized architectures, apart from the delay associated to the computation of the decentralized filters which is only done once per coherence interval.

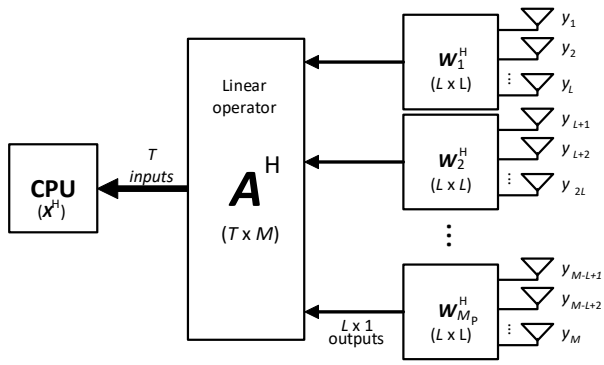

Figure 1: Framework considered in this paper during an uplink transmission.

The main challenge of the current framework is to maximize the information rate at which the users can transmit to the BS, i.e., $I_{\boldsymbol{Z},\boldsymbol{S}}(\boldsymbol{z};\boldsymbol{s})$, or, correspondingly,[21] $I_{\boldsymbol{Y},\boldsymbol{S}}(\boldsymbol{A}^{\mathrm{H}}\boldsymbol{W}^{\mathrm{H}}\boldsymbol{y};\boldsymbol{s})$. In this paper we will aim at applying information lossless processing, where $I_{\boldsymbol{Y},\boldsymbol{S}}(\boldsymbol{A}^{\mathrm{H}}\boldsymbol{W}^{\mathrm{H}}\boldsymbol{y};\boldsymbol{s}) = I_{\boldsymbol{Y},\boldsymbol{S}}(\boldsymbol{y};\boldsymbol{s})$. Note that the ap-

[21] Note that $\boldsymbol{X}$ cannot possibly increase the maximum information rate at which the users can transmit (recall data-processing inequality [28]). The main purpose of it is to be able to consider specific linear receiver schemes, e.g., ZF, MF, etc.

plication of $\boldsymbol{X}$ is not strictly necessary since it cannot possibly increase the information rate.

The framework under study allows for an information-lossless trade-off between the number of multiplications per antenna, L, and the number of inputs to the CPU, T. Said trade-off was identified in [27], where initial results are presented. In the present work we aim at presenting new results that allow for practical exploitation of the trade-off.

Having the number of antennas per panel equal to the multiplications per antenna, both given by L in this work, might seem like unnecessarily restrictive. In [27], the number of antennas per panel considered was an arbitrary number N, leading to $\boldsymbol{W}_m$ matrices of size $N \times L$. However, the most important results in said paper consider the case $N = L$ due to its intrinsic generality in the information-lossless scenario. Note that, in order to achieve information-lossless processing, we require $N \leq L$, while if N divides L, [27, Lemma 2] shows that there is a direct mapping to the case where $N = L$. Furthermore, from a practical perspective, minimum interconnection bandwidth (i.e., outputs per panel) in the information-lossless case is achieved for $N = L$. Considering all the above, we find it reasonable to focus on the case where the number of antennas per panel coincides with the number of outputs per panel as in the presented framework. However, it would be straightforward to consider panels formed by several of these groups of L antennas as in [12].

The framework discussed so far shows how the system operates during the data phase, where the users are transmitting data within one coherence block, so the corresponding $\boldsymbol{W}$ and $\boldsymbol{X}$ matrices have already been calculated for the current channel realization $\boldsymbol{H}$. In this work we also focus on what is being done during the training phase. Specifically, we want to find decentralized schemes to compute the information-lossless decentralized filters to be applied.[22] Since the application of $\boldsymbol{X}$ at the CPU cannot possibly increase mutual information (as previously discussed), we restrict our problem to proposing a decentralized scheme that allows us to compute the equalizer that each panel has to apply, i.e., $\boldsymbol{W}_m$ $\forall m$, such that the overall processing is information-lossless. In this way, the data arriving at the CPU will contain the same amount of information from the users as in the centralized case. As we will see, the structure of $\boldsymbol{A}$ plays a big role in how the decentralized computation of $\boldsymbol{W}$ can be performed. Thus, we will explore how certain structures for $\boldsymbol{A}$ allow the definition of decentralized schemes for obtaining $\boldsymbol{W}_m$ at each panel.

[22] By decentralized here we mean that each panel has access to its local channel, $\boldsymbol{H}_m$ and it can share some reduced data with a number of other panels to find the processing to be applied.

2.1 Background

As we mentioned earlier, the system model considered in this work was already studied in [27], where we can find important results which will be required for our analysis. From [27, Lemma 1], the framework under study can achieve information lossless processing if and only if we can decompose the channel matrix $\boldsymbol{H}$ into the so called WAX decomposition

$$\boldsymbol{H} = \boldsymbol{W}\boldsymbol{A}\boldsymbol{X}, \tag{4}$$

where $\boldsymbol{W}$, $\boldsymbol{A}$ and $\boldsymbol{X}$ correspond to the matrices from (2), i.e., $\boldsymbol{A}$ is fixed by design while $\boldsymbol{W}$ and $\boldsymbol{X}$ can be tuned to $\boldsymbol{H}$. Note that, according to [27, Lemma 1], selecting $\boldsymbol{W}$ and $\boldsymbol{X}$ in (2) such that (4) is fulfilled leads to information-lossless processing within our framework. The main result of the applicability of WAX decomposition is given in [27, Theorem 1], which states that, for a fixed randomly chosen $\boldsymbol{A} \in \mathbb{C}^{M\times T}$, a randomly chosen $\boldsymbol{H} \in \mathbb{C}^{M\times K}$ admits WAX decomposition with probability 1 if

$$T > \max\left(M\frac{K-L}{K}, K-1\right). \tag{5}$$

An alternative formulation of (5), can be given by considering the restriction on the other trade-off parameter, L. This results in

$$L > K\frac{M-T}{M}, \tag{6}$$

where we restrict ourselves to the regime $T \geq K$ where there exists an information-lossless trade-off between T and L (for $T < K$ there would be information-loss no matter the value of L). Defining $T_{\mathrm{P}} = T/L$ we have

$$L > K\frac{M_{\mathrm{P}}-T_{\mathrm{P}}}{M_{\mathrm{P}}}, \tag{7}$$

which is more significant for the current work as we will see.

In this paper, however, we will explore specific structures for $\boldsymbol{A}$ matrices and prove their validity for WAX decomposition. We consider the same definition as in [27, Definition 1] for the validity of $\boldsymbol{A}$, i.e., a randomly chosen $\boldsymbol{H}$ admits WAX decomposition with probability 1 for a valid $\boldsymbol{A}$. Note that [27] only provides necessary conditions for valid $\boldsymbol{A}$ matrices which are not randomly chosen, as well as a method to test if a specific $\boldsymbol{A}$ matrix is valid for some fixed dimensions (not generalizable). It is one of our desires to find structures for $\boldsymbol{A}$ that allow for a trade-off between L and T as close as possible to (7) (for $T \geq K$).

3 New Results on the WAX Decomposition

3.1 The Necessary Information-Lossless Trade-off

In[27, Theorem 1], the condition (5) for the existence of WAX decomposition was only proved for a randomly chosen $\boldsymbol{A}$. However, it is unclear if there exist any other selection of $\boldsymbol{A}$ that may attain a better trade-off than the one defined in (5). The following theorem shows that (5) is not only a sufficient condition for the existence of the WAX decomposition, but also a necessary condition.

Theorem 3 *Let $\boldsymbol{A}$ be an arbitrary $M \times T$, and $\boldsymbol{H}$ be an $M \times K$ randomly chosen matrix. The WAX decomposition of $\boldsymbol{H}$, given by* (5)*, can only exists if* (5) *is satisfied. Furthermore, $\boldsymbol{A}$ should be of rank T to be able to attain* (5)*.*

Proof *See Appendix A.* □

Theorem 3 states that the fundamental trade-off between the number of multiplications per antenna (L), and the number of inputs to the CPU (T), is ultimately governed by (5) (or its alternative formulations). For the rest of the paper we assume $M \geq T \geq K$, which is the regime where the information-lossless trade-off between L and T applies.

3.2 The Equivalent Formulation of the WAX Decomposition

Let us divide $\boldsymbol{A}$ into two blocks

$$\boldsymbol{A} = \begin{bmatrix} \boldsymbol{A}_{\mathrm{T}} \\ \boldsymbol{A}_{\mathrm{B}} \end{bmatrix}, \tag{8}$$

where $\boldsymbol{A}_{\mathrm{T}}$ is a $T \times T$ matrix corresponding to the top part of $\boldsymbol{A}$, and $\boldsymbol{A}_{\mathrm{B}}$ is the $(M-T) \times T$ matrix corresponding to the bottom part of $\boldsymbol{A}$. We next provide a theorem corresponding to an equivalent formulation of the WAX decomposition.

Theorem 4 *Assume that $T_{\mathrm{P}} = T/L$ evaluates to an integer value, and that $\boldsymbol{A}_{\mathrm{T}}$ is full-rank. Then, the WAX decomposition of some $M \times K$ matrix $\boldsymbol{H}$, given by* (4)*, exists if and only if we can find a full-rank $\boldsymbol{W}$ (corresponding to* (3)*) such that*

$$\boldsymbol{B}^T \boldsymbol{W}^{-1} \boldsymbol{H} = \boldsymbol{0}_{(M-T)\times K}, \tag{9}$$

where the matrix $\boldsymbol{B}$ is defined as

$$\boldsymbol{B} = \begin{bmatrix} \boldsymbol{A}_B \boldsymbol{A}_T^{-1} & -\mathbf{I}_{M-T} \end{bmatrix}^T.$$

Proof *Let us assume* $\boldsymbol{W}$ *in* (4) *to be full-rank; correspondingly,* $\boldsymbol{W}_m$ *are also full-rank* $\forall m$*. Note that, considering [27, Lemma 3], the WAX decomposition of a randomly chosen* $\boldsymbol{H}$ *exists if and only if then there exists a full-rank* $\boldsymbol{W}$ *that achieves said decomposition. From* (4) *we can get*

$$\boldsymbol{X} = \boldsymbol{A}_{\mathrm{T}}^{-1}\mathrm{diag}\left(\boldsymbol{W}_1, \boldsymbol{W}_2, \ldots, \boldsymbol{W}_{T_{\mathrm{P}}}\right)^{-1} \begin{bmatrix} \boldsymbol{H}_1 \\ \boldsymbol{H}_2 \\ \vdots \\ \boldsymbol{H}_{T_{\mathrm{P}}} \end{bmatrix}, \tag{10}$$

where $\boldsymbol{A}_{\mathrm{T}}$ *is full-rank by assumption. On the other hand, selecting* $\boldsymbol{X}$ *as in* (10) *implies that, in order to fulfill* (4)*, we only need to fulfill*

$$\boldsymbol{W}\boldsymbol{A}_B\boldsymbol{X} = \begin{bmatrix} \boldsymbol{H}_{T_{\mathrm{P}}+1} \\ \boldsymbol{H}_{T_{\mathrm{P}}+2} \\ \vdots \\ \boldsymbol{H}_{M_{\mathrm{P}}} \end{bmatrix}. \tag{11}$$

If we substitute (10) *in* (11) *and do some simple matrix manipulations we get* (9)*.* □

We should note that the assumptions taken in Theorem 4 are not as restrictive as they seem. In fact, they are fairly reasonable within our framework:

- If L is small with respect to T, restricting $T_{\mathrm{P}} = T/L$ to integers will only have a minor effect on the achievable optimum trade-off between T and L from (5). For arbitrary T this restriction can translate to an increase of $T - L\lfloor T/L \rfloor < L$ CPU inputs. Furthermore, in the optimum trade-off regime we have $0 \leq L \leq K$ and $K \leq T \leq M$, so L is small with respect to T throughout much of the trade-off, specially as M grows large.

- Having full-rank $\boldsymbol{A}_{\mathrm{T}}$ can be relaxed by re-indexing the diagonal blocks of $\boldsymbol{W}$, i.e., only a submatrix formed by T_{P} out of the M_{P} horizontal blocks of dimensions $L \times T$ in $\boldsymbol{A}$ should be full-rank. Moreover, from Theorem 1, $\boldsymbol{A}$ should be of rank T to attain (5), so a $T \times T$ submatrix of it should be full-rank.

Therefore, we will keep these assumptions throughout the rest of the paper.

The importance of Theorem 4 resides in the fact that it provides an alternative formulation of the WAX decomposition without any need to consider $\boldsymbol{X}$. Since the WAX decomposition allows for information-lossless processing within the framework under study (see [27]), the new formulation, given in (9), will also assure information-lossless processing. Thus, we can see (9) as

the restriction on the $\boldsymbol{W}_m$ matrices $\forall m$ in order to achieve information-lossless processing until the CPU is reached (under the assumptions of Theorem 4).

Another important implication of Theorem 4 is that we can construct a valid $\boldsymbol{A}$ matrix by selecting $\boldsymbol{A}_{\mathrm{B}}\boldsymbol{A}_{\mathrm{T}}^{-1}$ such that there exists a $\boldsymbol{W}$ that satisfies (11) for any randomly chosen $\boldsymbol{H}$ (except those in a zero-probability set). We can thus note that we have full freedom in selecting $\boldsymbol{A}_{\mathrm{T}}$ (as long as it is full-rank) since this matrix can be compensated through a full-rank transformation on $\boldsymbol{A}_{\mathrm{B}}$.

Throughout the rest of the paper, we will focus on the study of $\boldsymbol{A}$ matrices formed as

$$\boldsymbol{A} = \widetilde{\boldsymbol{A}} \otimes \mathbf{I}_L, \tag{12}$$

where $\widetilde{\boldsymbol{A}}$ is now an $M_{\mathrm{P}} \times T_{\mathrm{P}}$ matrix. Even though it may seem like an unnecessary restriction, (12) is in fact a desirable construction for a number of reasons:

- Any $\boldsymbol{A}$ matrix resulting from (12) will be inherently sparse since it would have a minimum of $(M - M_{\mathrm{P}})T$ zeros out of its MT elements.
- The combining module resulting from (12) has a simple hardware implementation since it only requires to scale and phase-shift the aggregated output of each panel before combining it with other panels. In fact, our goal is to eliminate the scaling and phase-shifting so that only sum modules are required.
- The equivalent formulation of the WAX decomposition (9) can simplify greatly through (12), as will be apparent in Corollary 1. Hence, it will lead to increased mathematical tractability, allowing to prove the validity of some interesting $\boldsymbol{A}$ structures.

The main concern that can raise from fixing (12) is that we may sacrifice achievability of the optimum trade-off (7), which is defined for randomly chosen $\boldsymbol{A}$. However, if we are able to reach a bound arbitrarily close to (7) we could conclude that there is no loss associated to (12).

Given (12), it becomes natural to extend the definition from [27, Definition 1] and talk about valid $\widetilde{\boldsymbol{A}}$ matrices for WAX decomposition. Considering (8), we can now write

$$\begin{aligned} \boldsymbol{A}_{\mathrm{T}} &= \widetilde{\boldsymbol{A}}_{\mathrm{T}} \otimes \boldsymbol{I}_L, \\ \boldsymbol{A}_{\mathrm{B}} &= \widetilde{\boldsymbol{A}}_{\mathrm{B}} \otimes \boldsymbol{I}_L, \end{aligned} \tag{13}$$

where $\widetilde{\boldsymbol{A}}_{\mathrm{T}}$ and $\widetilde{\boldsymbol{A}}_{\mathrm{B}}$ are matrices of dimensions $T_{\mathrm{P}} \times T_{\mathrm{P}}$ and $(M_{\mathrm{P}} - T_{\mathrm{P}}) \times T_{\mathrm{P}}$, respectively. In order to simplify upcoming notation, let us define

$$\Phi = M_{\mathrm{P}} - T_{\mathrm{P}}. \tag{14}$$

The next corollary comes as a direct consequence of Theorem 4 whenever we have (12).

Corollary 1 *Assume that* $\boldsymbol{A}$ *is of the form* (12)*, and that* $\widetilde{\boldsymbol{A}}_T$ *is full rank. If we define the matrix*

$$\widetilde{\boldsymbol{B}} = \begin{bmatrix} \widetilde{\boldsymbol{A}}_B \widetilde{\boldsymbol{A}}_T^{-1} & -\mathbf{I}_{M_\mathrm{P}-T_\mathrm{P}} \end{bmatrix}^\mathrm{T}, \tag{15}$$

the WAX decomposition of some $M \times K$ *matrix* $\boldsymbol{H}$*, given by* (4)*, exists if and only if we can find full-rank* $\boldsymbol{W}_m$ *matrices such that*

$$\begin{bmatrix} \boldsymbol{W}_1^{-1} & \boldsymbol{W}_2^{-1} & \dots & \boldsymbol{W}_{M_\mathrm{P}}^{-1} \end{bmatrix} \begin{bmatrix} \tilde{\boldsymbol{b}}_1^\mathrm{T} \otimes \boldsymbol{H}_1 \\ \tilde{\boldsymbol{b}}_2^\mathrm{T} \otimes \boldsymbol{H}_2 \\ \vdots \\ \tilde{\boldsymbol{b}}_{M_\mathrm{P}}^\mathrm{T} \otimes \boldsymbol{H}_{M_\mathrm{P}} \end{bmatrix} = \mathbf{0}_{L \times K\Phi}, \tag{16}$$

where $\tilde{\boldsymbol{b}}_m^\mathrm{T}$*, for* $m = 1, \dots, M_\mathrm{P}$*, correspond to the rows of* $\widetilde{\boldsymbol{B}}$*. A more compact notation for* (16) *is achieved by considering the face-splitting product,* $(\cdot) \bullet (\cdot)$*, which corresponds to a special case of the Khatri-Rao product dividing the left matrix into its rows, i.e.,*

$$\begin{bmatrix} \boldsymbol{W}_1^{-1} & \boldsymbol{W}_2^{-1} & \dots & \boldsymbol{W}_{M_\mathrm{P}}^{-1} \end{bmatrix} \left(\widetilde{\boldsymbol{B}} \bullet \boldsymbol{H} \right) = \mathbf{0}_{L \times K\Phi}. \tag{17}$$

Proof *Let us take Theorem 4 and substitute* (13) *in* (9)*. Simple matrix manipulation leads to* (16)*.* □

Corollary 1 provides a new formulation of the WAX decomposition, now taking into account (12). The main benefit of this new formulation is that the diagonal blocks of $\boldsymbol{W}^{-1}$ come in the form of a block row matrix instead of a block diagonal matrix, which will simplify the tasks of proving valid $\widetilde{\boldsymbol{A}}$ structures. As happened for $\boldsymbol{A}$, we can note that the validity of $\widetilde{\boldsymbol{A}}$ for WAX decomposition depends only on $\widetilde{\boldsymbol{B}}$, i.e., the product $\widetilde{\boldsymbol{A}}_\mathrm{B} \widetilde{\boldsymbol{A}}_\mathrm{T}^{-1}$ will determine the validity of $\widetilde{\boldsymbol{A}}$. Our next goal is to come up with clever ways of constructing the product $\widetilde{\boldsymbol{A}}_\mathrm{B} \widetilde{\boldsymbol{A}}_\mathrm{T}^{-1}$ which can lead to valid $\widetilde{\boldsymbol{A}}$.

4 Constructing Valid $\widetilde{\boldsymbol{A}}$ Matrices

4.1 Transforming $\widetilde{\boldsymbol{A}}$ while Maintaining Validity

Taking into account the results from the previous section, we will start by stating some transformations on $\widetilde{\boldsymbol{A}}$ that maintain its validity for WAX decomposition. These may be useful for proving the validity of specific constructions for $\widetilde{\boldsymbol{A}}$, or for generating new $\widetilde{\boldsymbol{A}}$ structures from those that can be proved valid.

Proposition 2 *Assume a valid $\widetilde{\boldsymbol{A}}$ for WAX decomposition. If we construct $\widetilde{\boldsymbol{A}}' = \widetilde{\boldsymbol{A}}\boldsymbol{\Theta}$, where $\boldsymbol{\Theta}$ can be any $T_\mathrm{P} \times T_\mathrm{P}$ full-rank matrix, $\widetilde{\boldsymbol{A}}'$ is also valid for WAX decomposition.*

Proof *Considering* (15) *we have that*

$$\begin{aligned}\widetilde{\boldsymbol{B}}' &= \begin{bmatrix}\widetilde{\boldsymbol{A}}'_B \widetilde{\boldsymbol{A}}'^{-1}_T & -\mathbf{I}_\Phi\end{bmatrix}^\mathrm{T} \\ &= \begin{bmatrix}\widetilde{\boldsymbol{A}}_B \boldsymbol{\Theta}\boldsymbol{\Theta}^{-1} \widetilde{\boldsymbol{A}}_T^{-1} & -\mathbf{I}_{M_\mathrm{P}-T_\mathrm{P}}\end{bmatrix}^\mathrm{T}, \\ &= \widetilde{\boldsymbol{B}}.\end{aligned}$$

From Corollary 1 the validity of $\widetilde{\boldsymbol{A}}'$ is only determined by $\widetilde{\boldsymbol{B}}'$, which leads to Proposition 2. □

The previous proposition can be also trivially extended to $\boldsymbol{A}$ if we disregard the restriction (12). This proposition also remarks that the selection of $\widetilde{\boldsymbol{A}}_\mathrm{T}$ does not affect the validity of $\widetilde{\boldsymbol{A}}$ as long as it is full-rank, since it can be compensated by selecting $\boldsymbol{\Theta}$.

Proposition 3 *Assume $\widetilde{\boldsymbol{A}}$ is valid for WAX decomposition. If we construct $\widetilde{\boldsymbol{A}}' = \boldsymbol{P}\widetilde{\boldsymbol{A}}$, where $\boldsymbol{P}$ can be any $M_\mathrm{P} \times M_\mathrm{P}$ permutation matrix, $\widetilde{\boldsymbol{A}}'$ is also valid for WAX decomposition.*

Proof *It is enough to notice that applying a permutation matrix on $\widetilde{\boldsymbol{A}}$ only corresponds to a re-indexing of the $\boldsymbol{W}_m$ matrices in* (3)*, which does not affect the solvability of* (4). □

The previous propositions focused on applying transformations on $\widetilde{\boldsymbol{A}}$ that maintain its validity for WAX decomposition. However, as we will see, one way to explore valid $\widetilde{\boldsymbol{A}}$ matrices is to explore $\widetilde{\boldsymbol{B}}$ matrices of the form (15) that allow us to solve (17). Thus, let us define valid $\widetilde{\boldsymbol{B}}$ for WAX decomposition as such matrices allowing for a solution to (16), i.e., leading to a valid $\boldsymbol{A}$ through (13) and (15).

4.2 Constructing $\widetilde{\boldsymbol{A}}$ from Predesigned $\widetilde{\boldsymbol{B}}$

In Section 3 we noted that properties of $\widetilde{\boldsymbol{B}}$, given by (15), determine the validity of a matrix $\widetilde{\boldsymbol{A}}$. We can thus construct an $\widetilde{\boldsymbol{A}}$ by first specifying a valid $\widetilde{\boldsymbol{B}}$ and then extracting an underlying $\widetilde{\boldsymbol{A}}$. More specifically, we should only define the product $\widetilde{\boldsymbol{A}}_{\mathrm{B}}\widetilde{\boldsymbol{A}}_{\mathrm{T}}^{-1}$ giving a valid $\widetilde{\boldsymbol{B}}$, and then we can extract a valid $\widetilde{\boldsymbol{A}}$ from the possible $\widetilde{\boldsymbol{A}}_{\mathrm{B}}$ and $\widetilde{\boldsymbol{A}}_{\mathrm{T}}$.

If we consider the $\Phi \times T_{\mathrm{P}}$ upper part of $\widetilde{\boldsymbol{B}}$, given by $(\widetilde{\boldsymbol{A}}_{\mathrm{B}}\widetilde{\boldsymbol{A}}_{\mathrm{T}}^{-1})^{\mathrm{T}}$, we can note that we have no loss of generality if we set

$$\widetilde{\boldsymbol{A}}_{\mathrm{T}} = \mathbf{I}_{T_{\mathrm{P}}}, \tag{18}$$

since we can still generate any possible $\widetilde{\boldsymbol{B}}$ of the form (15) by choosing $\widetilde{\boldsymbol{A}}_{\mathrm{B}}$. [23] Any other full-rank $\widetilde{\boldsymbol{A}}_{\mathrm{T}}$ can be selected by considering the transformation in Proposition 2, although said transformation would also change $\widetilde{\boldsymbol{A}}_{\mathrm{B}}$. On the other hand, the physical implication of having (18) is also practically desirable, since this would result in an $\widetilde{\boldsymbol{A}}$ with minimum number of 1s in its first T_{P} rows, i.e., it corresponds to the sparsest possible $\widetilde{\boldsymbol{A}}_{\mathrm{T}}$. The reason is that such $\widetilde{\boldsymbol{A}}_{\mathrm{T}}$ leads, through (12), to an $\boldsymbol{A}$ matrix with a single 1 per row in its first T rows, thus attaining the lower bound from [27, Lemma 6], which corresponds to a lower bound on the number of 1s per row of $\boldsymbol{A}$ for it to be valid. Therefore, in what follows, we consider $\widetilde{\boldsymbol{A}}$ matrices such that (18) is fulfilled. We remark that such selection does not impact the validity of $\widetilde{\boldsymbol{A}}$ since if we can find a valid $\widetilde{\boldsymbol{A}}$ with a different $\widetilde{\boldsymbol{A}}_{\mathrm{T}}$, we can always find a valid $\widetilde{\boldsymbol{A}}'$ with $\widetilde{\boldsymbol{A}}'_{\mathrm{T}} = \mathbf{I}_{T_{\mathrm{P}}}$ by invoking Proposition 2 with $\boldsymbol{\Theta} = \widetilde{\boldsymbol{A}}_{\mathrm{T}}^{-1}$. Thus, (18) should not be seen as a restriction, but a beneficial selection of $\widetilde{\boldsymbol{A}}_{\mathrm{T}}$ achieving maximum sparsity without loss.

The following proposition presents a structure for $\boldsymbol{A}$, taking into account the previous assumptions, which is proved to be valid for WAX decomposition.

Proposition 4 *Assume that* $\boldsymbol{A}$ *is given by* (12)*, with* $\widetilde{\boldsymbol{A}}_{\mathrm{T}} = \mathbf{I}_{T_{\mathrm{P}}}$*, and* $\widetilde{\boldsymbol{A}}_{\mathrm{B}}$ *constructed as*

$$\widetilde{\boldsymbol{A}}_{\mathrm{B}} = \begin{bmatrix} \mathbf{1}_{\Phi\times 1} & \mathbf{0}_{\Phi\times J} & \underbrace{\boldsymbol{I}_{\Phi} \quad \cdots \quad \boldsymbol{I}_{\Phi}}_{Q_1 = \left\lfloor \frac{T_{\mathrm{P}}-1}{\Phi} \right\rfloor} \end{bmatrix}, \tag{19}$$

where $J = T_{\mathrm{P}} - 1 - Q_1\Phi$*, and where*

$$Q_1 = \left\lfloor \frac{T_{\mathrm{P}} - 1}{\Phi} \right\rfloor. \tag{20}$$

[23] Note that with (18), $\widetilde{\boldsymbol{A}}_{\mathrm{B}}$ would directly correspond the top T_{P} rows of $\widetilde{\boldsymbol{B}}$, which are the only ones that can be changed for Corollary 1 to apply.

A randomly chosen matrix $\boldsymbol{H}$ *admits WAX decomposition with probability 1 for the given* $\boldsymbol{A}$ *if*

$$L \geq \frac{K}{1+Q_1}, \tag{21}$$

Furthermore, $\boldsymbol{W}_1$ *(defined in* (3)*) can be fixed to an arbitrary* $L \times L$ *full-rank matrix without affecting the solvability of the WAX decomposition.*

Proof *Selecting* $\widetilde{\boldsymbol{A}}_{\mathrm{T}} = \mathbf{I}_{T_{\mathrm{P}}}$ *and* $\widetilde{\boldsymbol{A}}_{\mathrm{B}}$ *as in* (19) *leads to*

$$\widetilde{\boldsymbol{B}} = \begin{bmatrix} \mathbf{1}_{\Phi\times 1} & \mathbf{0}_{\Phi\times J} & \underbrace{\boldsymbol{I}_\Phi \quad \cdots \quad \boldsymbol{I}_\Phi}_{Q_1} & -\mathbf{I}_\Phi \end{bmatrix}^{\mathrm{T}}.$$

From Corollary 1, we can solve the equivalent formulation of the WAX decomposition, given in (16)*, with the restriction of having full-rank* $\boldsymbol{W}_m$ $\forall m$*. If we invoke* (16)*, we get the set of equations*

$$\boldsymbol{W}_1^{-1}\boldsymbol{H}_1 = \sum_{q=0}^{Q_1+1} \boldsymbol{W}_{J+r+q\Phi}^{-1}\boldsymbol{H}_{J+r+q\Phi}, \quad r = 1,\ldots,\Phi. \tag{22}$$

Note that we have ignored the negative sign associated to the last identity block in $\widetilde{\boldsymbol{B}}$ *since this can be absorbed without loss of generality by the corresponding* $\boldsymbol{H}_m$ *blocks. Let us consider* $\boldsymbol{W}_1$ *to be fixed to an arbitrary* $L \times L$ *full-rank matrix (e.g.,* $\boldsymbol{W}_1 = \mathbf{I}_L$*), since this is the only* $\boldsymbol{W}_m$ *shared in all the* Φ *equations from* (22)*. Note that the selection of* $\boldsymbol{W}_1$*, as long as it is full-rank, does not affect the solvability of* (22) *because this matrix can be absorbed by* $\boldsymbol{H}_1$ *(or by the rest of the* $\boldsymbol{W}_m$ *matrices) without changing its nature. Then, through trivial linear algebra arguments, namely counting equations and variables in the resulting linear system, and assuming randomly chosen* $\boldsymbol{H}$ *(i.e.,* $\boldsymbol{H}_m$ *are also randomly chosen* $\forall m$ *and their sum will reduce rank with probability 0), we can independently solve each of the* Φ *equations whenever* (21) *is fulfilled.* □

The trade-off between T_{P} and L given by (21) can be linked to the optimum trade-off for randomly chosen $\boldsymbol{A}$, given in (7), by assuming that $\Phi = M_{\mathrm{P}} - T_{\mathrm{P}}$ divides $T_{\mathrm{P}} - 1$. In this case we would have,

$$L \geq K\frac{(M_{\mathrm{P}} - T_{\mathrm{P}})}{M_{\mathrm{P}} - 1}, \tag{23}$$

which for $M_{\mathrm{P}} \gg 1$ corresponds approximately to the same bound as in (7) (for small M_{P}, the gap can be linked to the loss of degrees of freedom when fixing $\boldsymbol{W}_1^{-1}$). We can thus conclude that there is essentially no loss in restricting (12). Note that, unlike (23), the optimum trade-off (7) cannot be achieved

with equality, which further promotes the equivalence between (7) and (23). Furthermore, due to the integer nature of the variables under consideration, in most cases, both trade-offs would give the same effective parameter restrictions. Let us thus refer to (23) as the achievable trade-off. The achievable trade-off results from fixing one of the diagonal blocks of $\boldsymbol{W}$ to identity, as in the proof of Proposition 4.

The main restriction of the construction for $\boldsymbol{A}$ considered in Proposition 4 is that the only meaningful points of the achievable trade-off (21) are those where Φ divides $T_{\mathrm{P}} - 1$, since except for those points, there would be an increase in the number of inputs to the CPU, given by $T = LT_{\mathrm{P}}$, without a corresponding decrease in the multiplications per antenna, given by L. This restriction becomes specially concerning when we have $T_{\mathrm{P}} < M_{\mathrm{P}}/2+1$, since in this regime Proposition 4 cannot exploit any trade-off between T (or T_{P}) and L. Thus, the following proposition considers a novel structure for $\boldsymbol{A}$ that allows for exploitation of the trade-off between T and L in the regime $T_{\mathrm{P}} < M_{\mathrm{P}}/2+1$.

Proposition 5 *Let $\boldsymbol{A}$ be given by (12), with $\widetilde{\boldsymbol{A}}_{\mathrm{T}} = \mathbf{I}_{T_{\mathrm{P}}}$, and $\widetilde{\boldsymbol{A}}_{\mathrm{B}}$ constructed as*

$$\widetilde{\boldsymbol{A}}_{\mathrm{B}} = \begin{bmatrix} \alpha_1 \mathbf{1}_{(T_{\mathrm{P}}-1)\times 1} & \mathbf{I}_{T_{\mathrm{P}}-1} \\ \vdots & \vdots \\ \alpha_{Q_2-1}\mathbf{1}_{(T_{\mathrm{P}}-1)\times 1} & \mathbf{I}_{T_{\mathrm{P}}-1} \\ \alpha_{Q_2}\mathbf{1}_{\Pi\times 1} & [\mathbf{I}_{T_{\mathrm{P}}-1}]_{1:\Pi,:} \end{bmatrix}, \tag{24}$$

where $\Pi = \Phi - (Q_2 - 1)(T_{\mathrm{P}} - 1)$, i.e., the last column block is cropped to fit the dimensions, and where

$$Q_2 = \left\lceil \frac{\Phi}{T_{\mathrm{P}} - 1} \right\rceil. \tag{25}$$

Furthermore, $\alpha_i \in \mathbb{C}\backslash\{0\}$ can be arbitrarily selected as long as

$$\alpha_i = \alpha_j \iff i = j,\ \forall i, j \in \{1, \ldots, Q_2\}.$$

A randomly chosen matrix $\boldsymbol{H}$ admits WAX decomposition with probability 1 for the given $\boldsymbol{A}$ if

$$L \geq \frac{K}{1 + \frac{1}{Q_2}}. \tag{26}$$

Moreover, $\boldsymbol{W}_1$ (defined in (3)) can be fixed to an arbitrary $L \times L$ full-rank matrix without affecting the solvability of the WAX decomposition.

Proof *See Appendix B* □

If we assume values of M_{P} and T_{P} such that (25) gives an integer without the need of the ceiling operator, the trade-off in (26) leads again to (23). However,

with the $\boldsymbol{A}$ structure given in Proposition 5 we can now select parameters that allow to exploit the trade-off in the regime $T_{\mathrm{P}} < M_{\mathrm{P}}/2 + 1$. The following proposition presents a structure for $\boldsymbol{A}$ which can be seen as combination of the structures from Propositions 4 and 5, and which allows more freedom in the exploitation of the achievable trade-off in the regime $T_{\mathrm{P}} \geq M_{\mathrm{P}}/2 + 1$.

Proposition 6 *Let $\boldsymbol{A}$ be given by (12), with $\widetilde{\boldsymbol{A}}_{\mathrm{T}} = \mathbf{I}_{T_{\mathrm{P}}}$, and $\widetilde{\boldsymbol{A}}_{\mathrm{B}}$ constructed as*

$$\widetilde{\boldsymbol{A}}_{\mathrm{B}} = \left[\mathbf{1}_{\Phi \times 1} \quad \left[\mathbf{1}_{Q_2 \times 1} \otimes \mathbf{I}_J \right]_{1:\Phi,:} \quad \underbrace{\boldsymbol{I}_\Phi \quad \cdots \quad \boldsymbol{I}_\Phi}_{Q_1} \right], \tag{27}$$

where $Q_1 \geq 1$ and J are defined in Proposition 4, while Q_2 is now given by

$$Q_2 = \left\lceil \frac{\Phi}{J} \right\rceil. \tag{28}$$

A randomly chosen matrix $\boldsymbol{H}$ admits WAX decomposition with probability 1 for the given $\boldsymbol{A}$ if

$$L \geq \frac{K}{1 + Q_1 + \frac{1}{Q_2}}. \tag{29}$$

Moreover, $\boldsymbol{W}_1$ (defined in (3)) can be fixed to an arbitrary $L \times L$ full-rank matrix without affecting the solvability of the WAX decomposition.

Proof *See Appendix C* □

Note that for $Q_1 = 0$, the previous structure degenerates to the case from Proposition 5, where some elements from the first column of $\widetilde{\boldsymbol{A}}_{\mathrm{B}}$ should be changed to fulfill the additional α_i requirements. Furthermore, for $J = 0$ (i.e., Φ divides $T_{\mathrm{P}} - 1$) the previous structure leads directly to the one presented in Proposition 4.

As happened in the previous cases, we can still reach the achievable trade-off (23) whenever we have parameters such that Q_2 in (28) evaluates to an integer value without the need of the ceiling operator. However, we can also reach it if we have parameters such that Q_1 evaluates to an integer value without the floor operation, since this would lead to $J = 0$ and Q_2 would tend to infinity, so we could remove it altogether. Thus, the structure from Proposition 6 has a looser requirement so as to reach the achievable trade-off in the regime $T_{\mathrm{P}} \geq M_{\mathrm{P}}/2 + 1$ as compared to structure from Proposition 4, where Q_1 had to evaluate to an integer value without the floor operation. Thus, the $\boldsymbol{A}$ structure defined in Proposition 6 allows for a broader selection of parameters leading to the achievable trade-off (23), hence increasing the freedom in the exploitation of said trade-off.

Algorithm 3 Generalized $\widetilde{\boldsymbol{A}}_{\mathrm{B}}$ for WAX decomposition.

Require: M_{P}, T_{P}

Ensure: $\widetilde{\boldsymbol{A}}_{\mathrm{B}}$

Initialize:

$\left[\widetilde{\boldsymbol{A}}_{\mathrm{B}}\right]_{1,:} = \left[\alpha_1, \ldots, \alpha_\Phi\right]^T$

$R_{\mathrm{row}} = T_{\mathrm{P}} - 1,\ R_{\mathrm{col}} = \Phi,\ i = 0,\ i_{\mathrm{row}} = 1,\ i_{\mathrm{col}} = 2$

while $R_{\mathrm{col}} > 0$ **and** $R_{\mathrm{row}} > 0$ **do**

$i = i + 1$

if $R_{\mathrm{col}} > R_{\mathrm{row}}$ **then**

$Q_i = \lfloor R_{\mathrm{col}} / R_{\mathrm{row}} \rfloor$

$[\widetilde{\boldsymbol{A}}_{\mathrm{B}}]_{i_{\mathrm{row}}:(i_{\mathrm{row}}+Q_i R_{\mathrm{row}}),i_{\mathrm{col}}:(i_{\mathrm{col}}+Q_i R_{\mathrm{row}})} = \mathbf{1}_{1\times Q_i} \otimes \mathbf{I}_{R_{\mathrm{row}}}$

$R_{\mathrm{col}} = R_{\mathrm{col}} - Q_i \cdot R_{\mathrm{row}}$

$i_{\mathrm{col}} = i_{\mathrm{col}} + Q_i \cdot R_{\mathrm{row}}$

else

$Q_i = \lfloor R_{\mathrm{row}} / R_{\mathrm{col}} \rfloor$

$[\widetilde{\boldsymbol{A}}_{\mathrm{B}}]_{i_{\mathrm{row}}:(i_{\mathrm{row}}+Q_i R_{\mathrm{col}}),i_{\mathrm{col}}:(i_{\mathrm{col}}+Q_i R_{\mathrm{col}})} = \mathbf{1}_{Q_i\times 1} \otimes \mathbf{I}_{R_{\mathrm{col}}}$

$R_{\mathrm{row}} = R_{\mathrm{row}} - Q_i \cdot R_{\mathrm{col}}$

$i_{\mathrm{row}} = i_{\mathrm{row}} + Q_i \cdot R_{\mathrm{col}}$

end if

end while

4.3 General Construction of Valid $\widetilde{\boldsymbol{A}}$

A natural generalization of the structure given in Proposition 6, which already corresponds to a generalization of the structures from Propositions 4 and 5, consists of filling the dimensions of $\widetilde{\boldsymbol{A}}_{\mathrm{B}}$ with full identity matrices, alternating horizontal and vertical allocation until all dimensions are exhausted. This method is presented in Algorithm 3, where the first column of $\widetilde{\boldsymbol{A}}_{\mathrm{B}}$ is given by α_i so that it can accommodate degenerated cases as the one in Proposition 5. The following conjecture aims at generalizing the validity of the structures defined by Algorithm 3.

Conjecture 1 *Let* $\boldsymbol{A}$ *be given by* (12)*, with* $\widetilde{\boldsymbol{A}}_{\mathrm{T}} = \mathbf{I}_{T_{\mathrm{P}}}$*, and* $\widetilde{\boldsymbol{A}}_{\mathrm{B}}$ *constructed through Algorithm 3. A randomly chosen matrix* $\boldsymbol{H}$ *admits WAX decomposition with probability 1 for the given* $\boldsymbol{A}$ *if*

$$L \geq \frac{K}{1 + Q_{\mathrm{tot}}}, \tag{30}$$

where, given Q_i *for* $i = 1, \ldots, N_Q$*, which are defined in Algorithm 3, and* N_Q*, corresponding to the iteration* i *where dimensions are exhausted, we have*

$$Q_{\mathrm{tot}} = Q_1 + \cfrac{1}{Q_2 + \cfrac{1}{\ddots + \cfrac{1}{Q_{N_Q}}}}. \tag{31}$$

Furthermore, in the regime $T_{\mathrm{P}} < M_{\mathrm{P}}/2 + 1$*, the first column of* $\widetilde{\boldsymbol{A}}_{\mathrm{B}}$*, given by* $[\alpha_1, \ldots, \alpha_\Phi]^{\mathrm{T}}$*, should fulfill the same restrictions as in Proposition 5.*

Idea for Proof *We first note that* N_Q *is determined by* T_{P} *and* M_{P} *(as more thoroughly discussed later), with the restriction* $N_Q \in \{1, \ldots, \min(T_{\mathrm{P}} - 1, \Phi)\}$*. Then, for every value of* N_Q *an equation similar to* (47) *can be obtained, which should be proved solvable. However, after extensive work on the matter, a formal proof for general* N_Q *has not been found. We have only been able to test this formula through thorough simulations without encountering a single exception to it. One simulation procedure we employed to check the conjecture was to randomly define a large number of combinations of* K*,* M_{P}*, and* T_{P}*, and for each of these combinations construct an* $\boldsymbol{A}$ *matrix through Algorithm 3 (together with* (12) *and* (18)*) using different values for* L*. Then, considering [27, Theorem 2], we tried to perform WAX decomposition of a randomly chosen* $\boldsymbol{H}$ *(e.g., an IID Gaussian matrix realization), which would either be possible (i.e.,* $\boldsymbol{A}$ *is valid) or not (i.e.,* $\boldsymbol{A}$ *may not be valid). The simulation results led to valid* $\boldsymbol{A}$ *matrices if and only if Conjecture 1 was satisfied.* □

Figure 2 illustrates with an example how Algorithm 3 is used to define the $T_{\mathrm{P}} - 1$ last columns of $\widetilde{\boldsymbol{A}}_{\mathrm{B}}$. We can immediately notice that its iterations are equivalent to the steps of the Euclidean algorithm for finding the GCD between $T_{\mathrm{P}} - 1$ and $\Phi = M_{\mathrm{P}} - T_{\mathrm{P}}$. In fact, we can see that Q_{tot}, given in (31), corresponds to a continued fraction expansion [31] of $(T_{\mathrm{P}} - 1)/\Phi$. Hence, the value for N_{Q}, from Conjecture 1, is equal to the number of steps to calculate $\mathrm{GCD}(T_{\mathrm{P}} - 1, \Phi)$. Furthermore, since T_{P} and M_{P} are restricted to integers, $(T_{\mathrm{P}} - 1)/\Phi$ corresponds to a rational number, so its continued fraction expansion will always be finite [31]. Thus, we can substitute Q_{tot} in (30) by $(T_{\mathrm{P}} - 1)/\Phi$, which gives directly the achievable bound (23). On the other hand, the number

of 1s in the last $T_{\mathrm{P}}-1$ columns of $\widetilde{\boldsymbol{A}}_{\mathrm{B}}$, which gives its sparsity, corresponds to

$$\left\| \left[\widetilde{\boldsymbol{A}}_{\mathrm{B}}\right]_{:,2:T_{\mathrm{P}}} \right\|_{\mathrm{F}}^{2} = \Phi - \mathrm{GCD}(T_{\mathrm{P}}-1, \Phi).$$

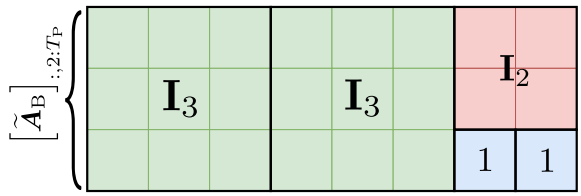

Figure 2: Example of how Algorithm 3 constructs the last $T_{\mathrm{P}}-1$ columns of $\widetilde{\boldsymbol{A}}_{\mathrm{B}}$ for $M_{\mathrm{P}}=12$ and $T_{\mathrm{P}}=9$.

The reader may also note here the direct relation between Conjecture 1 and Propositions 4-6. When $N_{\mathrm{Q}}=1$, i.e., Φ divides $T_{\mathrm{P}}-1$, Conjecture 1 directly corresponds to Proposition 4 (for this case we can choose $\alpha_i=1$). Furthermore, when $N_{\mathrm{Q}}=2$, i.e., $J=T_{\mathrm{P}}-1-Q_1\Phi$ divides Φ, Conjecture 1 leads to either Proposition 5 (in the $T_{\mathrm{P}}<M_{\mathrm{P}}/2+1$ regime) or Proposition 6 (in the $T_{\mathrm{P}}\geq M_{\mathrm{P}}/2+1$ regime, where we can choose $\alpha_i=1, \forall i$). Thus, although we lack a formal proof for Conjecture 1, we may use Algorithm 3 as a general strategy for constructing $\widetilde{\boldsymbol{A}}$ since it merges the previous results whenever they attain the achievable trade-off (23).

Another thing to remark is that, for centralized architectures, where we can identify $T_{\mathrm{P}}=M_{\mathrm{P}}$, our structures degenerate to the trivial $\widetilde{\boldsymbol{A}}=\mathbf{I}_{M_{\mathrm{P}}}$, i.e., the combining module can be disregarded altogether. Moreover, for information-lossless fully-decentralized architectures (e.g., local-MF as in [13]), where we can identify $T_{\mathrm{P}}=1$ (for this case we have $L=K$), our structures degenerate to $\widetilde{\boldsymbol{A}}=\mathbf{1}_{M_{\mathrm{P}}\times 1}$ (taking the case $\alpha_i=1$), i.e., the combining module would correspond to a sum module that combines all the outputs from the decentralized filters. This remarks the relevance of the presented work as a generalization of architectures with an arbitrary level of decentralization, since it allows for a wide range of architectures from centralized to fully-decentralized, and where both extremes can be considered within the same framework.

5 Decentralized Computation of $\boldsymbol{W}$

The structures for $\boldsymbol{A}$ presented in the previous section are not only interesting for their sparsity and validity for WAX decomposition, but we can also use them to create decentralized schemes for computing $\boldsymbol{W}$. As previously discussed, decentralized here means that each panel would find the $\boldsymbol{W}_m$ to be applied, i.e., leading to information-lossless processing, by exchanging reduced data with

the rest of the panels so that the full channel matrix $\boldsymbol{H}$ needs not be collected at any single point. Using the equivalent formulation of the WAX decomposition (9), or (16) with (12), we can find $\boldsymbol{W}_m$ matrices achieving information-lossless processing without having to compute $\boldsymbol{X}$.

The $\boldsymbol{A}$ structures from Propositions 4, 5, and 6, allow the use of a tree-based scheme, such as the one illustrated in Fig. 3 where we have conveniently re-indexed the $\boldsymbol{W}_m$ and $\boldsymbol{H}_m$ matrices to make them general for all three cases. Specifically, we identify now $\boldsymbol{W}_0$ with the original $\boldsymbol{W}_1$ from (3), which is the $\boldsymbol{W}_m$ that can be arbitrarily selected in Propositions 4-6. The tree scheme consists of a reference panel, which is connected through a one-way link to N_1 processing panels, i.e., having a LPU, each of which communicates with a set of N_2 passive panels. For simplicity, the reference panel makes use of the available freedom provided by Propositions 4-6 by fixing $\boldsymbol{W}_0 = \mathbf{I}_L$. This way, $\boldsymbol{W}_0$ has no effect, so the reference panel only needs to share its $L \times K$ local channel matrix $\boldsymbol{H}_0$ with the N_1 processing panels.[24] Each group of N_2 passive panels would share their local channels to their corresponding processing panel, which would then use them to compute all the $\boldsymbol{W}_m$ matrices that have to be applied in its group (including itself). Lastly, the processing panels would send each $\boldsymbol{W}_m$ to the corresponding passive panels in their group so that they can apply them.

In order to understand why the $\boldsymbol{A}$ structures from Propositions 4-6 can make use of the decentralized scheme from Fig. 3, we will refer to the proofs of said propositions. For Proposition 4, we can see that the equivalent formulation of the WAX decomposition can be solved by solving a set of independent equations of the form (22), where the LHS, which is the only part shared in all equations, is associated to the reference panel ($\boldsymbol{W}_1$, here re-indexed to $\boldsymbol{W}_0$, which is later fixed in the proof), and the RHS can be associated to a group of panels of which one would be the processing panel and the rest the passive panels. Each processing panel would only need the $\boldsymbol{H}_m$ matrices of the rest of the panels in the group, as well as the one from the reference panel, to be able to solve its equation, corresponding to one out of the Φ independent equations from (22). For Proposition 5, the reference panel determines the LHS of (38). On the other hand, (38) can be divided into a set of independent equations of the form (39), only sharing $\boldsymbol{H}_0$ (or $\widetilde{\boldsymbol{H}}_0$ in the proof), and each of which can be solved at one processing panel by accumulating the involved $\boldsymbol{H}_m$ matrices. The same is true for Proposition 6 where instead of (39) we would have (47) solved at each processing panel.

Table 1 gives the resulting parameters N_1 and N_2 of the decentralized scheme in Fig.3 for the different structures from Propositions 4-6. Said pa-

[24] $\boldsymbol{W}_0$ can also be fixed to any other full-rank matrix. In that case, either all processing panels have previous knowledge of $\boldsymbol{W}_0$ for their computations, or the reference panel should share the $L \times K$ matrix resulting from the multiplication $\boldsymbol{W}_0^{-1}\boldsymbol{H}_0$ instead of $\boldsymbol{H}_0$ directly. Hence, any selection other than $\boldsymbol{W}_0 = \mathbf{I}_L$ leads to higher computation complexity.

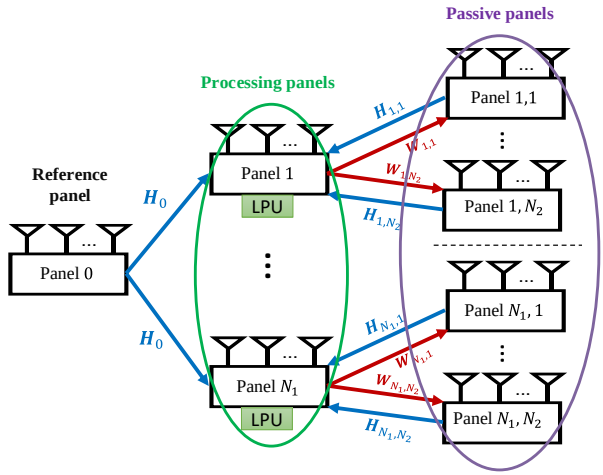

Figure 3: Architecture for decentralized computation of the $\boldsymbol{W}_m$ matrices for the $\widetilde{\boldsymbol{A}}$ given in Propositions 4-6. Blue arrows indicate sharing of local CSI, and red arrows indicate sharing of decentralized filters after computation.

$\boldsymbol{A}$ structure	N_1	N_2
Proposition 4	Φ	Q_1
Proposition 5	$T_{\mathrm{P}}-1$	Q_2 (from (25))
Proposition 6	J	Q_2 (from (28))

Table 1: Decentralized scheme parameters.

rameters are related to the number of independent equations and the number of involved passive panels in each equation, respectively, as explained before. In the case of Propositions 5 and 6, we are assuming that Q_2 evaluates to an integer without the need of the ceiling operator; otherwise, the last group of panels would have a number of passive panels smaller than N_2 due to the cropping of the corresponding equation. Note that, in all cases, several independent equations can be solved at a single processing panel by gathering the corresponding $\boldsymbol{H}_m$ matrices at said panel. Thus, the values of N_1 from Table 1 could be trivially reduced by a corresponding increase in N_2.

To conclude this section, we have shown that, not only can we define architectures with an arbitrary level of decentralization in the data phase (i.e., by employing the framework from Fig. 1), but, during the training phase, and if $\boldsymbol{A}$ is suitably selected, these architectures can be used for computing in a decentralized manner the decentralized processing to be applied (i.e., by considering schemes like the one in Fig. 3).

6 Numerical Results and Examples

In Section 4, we presented some constructions for $\boldsymbol{A}$ that were proved to be valid for WAX decomposition. The current section aims at providing some discussion, as well as useful examples, to further understand the differences of said constructions, and the circumstances under which they reach the achievable trade-off (23).

In Section 4, we discussed the requirements for Propositions 4-6 to achieve (23), namely that either Q_1 or Q_2 should evaluate to an integer without requiring the floor/ceiling operator, respectively. Instead of obtaining Q_1 or Q_2 from T_P and M_P, we can also take them as arbitrary integers, and substitute the resulting K/L in (21), (26), and (29) (after restricting the inequality for the case of equality) to get the ratios K/L that achieve (23) for the structures in Propositions 4, 5, and 6, respectively. The reason is that we can always find a combination of integers M_P and T_P leading to the corresponding Q_1 or Q_2 without the need of the respective floor/ceiling operators. An alternative interpretation of the presented structures is that they are directly defined by a (truncated) continued fraction expansion of the ratio K/L, corresponding to (31). The structure from Algorithm 3 considers the full continued fraction expansion of K/L, the structure from Proposition 4 is given by a fraction expansion of K/L truncated to a single term (Q_1), and the structure from Proposition 6 (which degenerates to the one from Proposition 5 for $Q_1 = 0$) is given by a fraction expansion of K/L truncated to two terms (Q_1 and Q_2). Fig. 4 shows the possible K/L ratios achieving (23) for the $\boldsymbol{A}$ structures from Propositions 4-6. Proposition 5 is the only one having values in the interval $(1, 2)$, associated to the regime $T_\mathrm{P} < M_\mathrm{P}/2 + 1$, as previously mentioned. However, the structure from Proposition 6 would also reach the points from Proposition 5 by selecting the first column of $\widetilde{\boldsymbol{A}}_\mathrm{B}$ as in (24) with $\alpha_i \neq \alpha_j$ for $i \neq j$. Note that, for Proposition 6, the values in the interval [2,3] can be shifted to any other interval [i,i+1] with $i \geq 2$ (which corresponds to increasing Q_1). Any other value for K/L can be obtained by using Algorithm 3, since any positive rational number can be decomposed into a continued fraction of the form (31) [31], while $K/L - 1$ is inherently restricted to positive rational numbers since K and L are restricted to integers, and we have $L \leq K$.

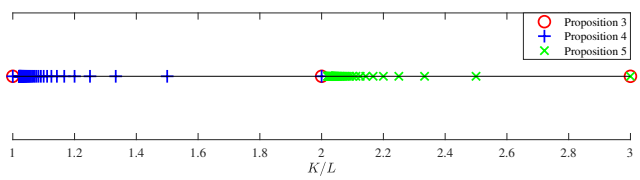

Figure 4: Values of K/L achieving (23) in the interval $[1, 3]$ with the $\boldsymbol{A}$ structures from the different propositions.

As previously discussed, the results presented in this paper lead to conditions that exhibit direct connection to the ratio K/L. However, the main value of the original condition (5), as presented in [27], and which has now been shown to be fundamental due to Theorem 3, is to give a trade-off between L, the number of multiplications per antenna, and T, the required connections to a CPU. It is thus of special interest to outline the explicit relation between T and L in the conditions obtained in this work: (21), (26) and (29), as well as (23), which ultimately governs all the previous conditions (apart from being attained by the structure from Conjecture 1). On the other hand, the achievable trade-off from (23) can be straightforwardly translated into a condition between L and T (instead of T_{P}) if we multiply both the numerator and denominator of the RHS by L. However, there may be points of this trade-off not attainable by the proposed structures, as we will illustrate next.

In Fig. 5 we compare the trade-off between T and L considering the different strategies for constructing $\boldsymbol{A}$. The dashed blue line corresponds to the trade-off defined in (5), which is proved to be attained by randomly chosen $\boldsymbol{A}$ [27, Theorem 1], while Theorem 3 shows that it is also the optimum trade-off. The red line corresponds to the achievable trade-off (23), which can be attained by all the structures presented in this work under favorable parameter combinations. We can see that there is a minor gap between the achievable trade-off and the optimum one, which is mainly noticeable as L grows. This gap can be explained by the exhaustion of degrees of freedom when fixing one $L \times L$ matrix, which clearly grows with L. The rest of the points correspond to the achievable points that can be exploited in practice through the proposed structures. We have used [27, Theorem 2], i.e., by performing WAX decomposition of a randomly chosen $\boldsymbol{H}$, to check that the proposed $\boldsymbol{A}$ structures are valid at these points, thus confirming the theoretical claims from Propositions 4-6, as well as Conjecture 1. The purple triangles correspond to the achievable points with randomly chosen $\boldsymbol{A}$ after considering the integer restriction of the variables T, L, and M_{P}. Hence, these points correspond to the fundamental limits of multi-antenna architectures with an arbitrary level of decentralization, while the main motivation of the current work is to get as close as possible to these points with structured sparse constructions for $\boldsymbol{A}$. The red circles correspond to the $\boldsymbol{A}$ structures defined through Proposition 4, which was already included in the conference version [30]. The remaining points are novel contributions achieved by Propositions 5 and 6, as well as by Conjecture 1. As we can see, the achievable points when constructing $\boldsymbol{A}$ as in Conjecture 1 have minor gap (if any) with respect to the achievable trade-off due to the integer nature of T_{P} from the limitation $T_{\mathrm{P}} = T/L$. As for the other constructions, we see that the achievable points for the constructions from Propositions 5 and 6 get fairly close to the points achieved by Conjecture 1, while the main difference is that they exploit different regimes of the trade-off. We again note that the achievable points from Proposition 4 only allowed for reductions in

the regime $T_{\mathrm{P}} \geq M_{\mathrm{P}}/2 + 1$, which justifies the poor performance in the right part of the plots. These results remark the importance of the novel structures presented in this work for better exploitation of the trade-off between level of decentralization and decentralized complexity.

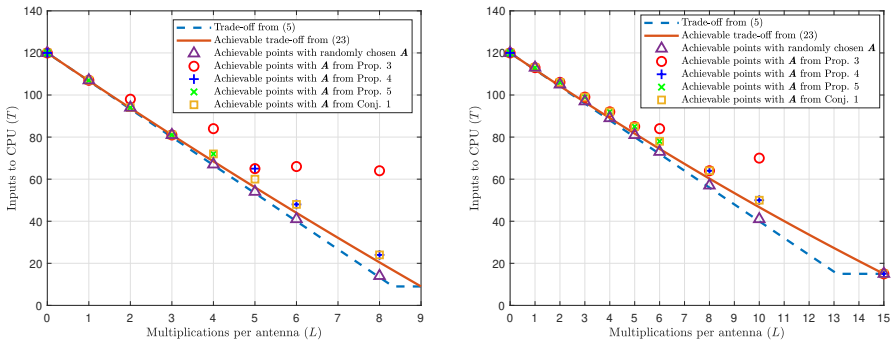

Figure 5: Comparison of fundamental trade-off (5) with achievable trade-off (23) and achievable points with the presented structures. We assume $M = 120$, $K = 9$ (left) and $K = 15$ (right).

The following example illustrates the differences between the presented strategies for constructing $\boldsymbol{A}$. By focusing on the regime $T_{\mathrm{P}} \geq M_{\mathrm{P}}/2 + 1$, we intentionally skip Proposition 5 due to its correspondence with Proposition 6 for $Q_1 = 0$.

Example 4 *Let $T_{\mathrm{P}} = 6$, $M_{\mathrm{P}} = 9$, and $K = 40$. We then have $\Phi = 3$. Let $\boldsymbol{A}_1$, $\boldsymbol{A}_2$, and $\boldsymbol{A}_3$, be $\boldsymbol{A}$ matrices constructed using Propositions 4, 6, and Algorithm 3, respectively. Such matrices are found in* (33)*, where every pair of $\mathbf{I}_L$ matrices in each row block of $\boldsymbol{A}$ can be seen as a sum module which combines the outputs from the two respective panels.*[25] *Note that the structure from Proposition 5 does not apply here since we are not in the regime $T_{\mathrm{P}} < M_{\mathrm{P}}/2+1$. Using Propositions 4, 6, and Conjecture 1, we can find the possible values for L to be*

$$L_1 \geq 20, \qquad L_2 \geq 16, \qquad L_3 \geq 15,$$

respectively. On the other hand, (23) *leads to the restriction $L \geq 15$. Thus, in this case Algorithm 3 gives the only structure reaching the achievable trade-off. However, the structure from Proposition 6 gets considerably closer to it than the one from Proposition 4.*

We next show a practical example of how to use the theory developed in this work for designing a BS with constrained decentralized processing complexity.

[25] We have horizontally flipped $[\widetilde{\boldsymbol{A}}_{\mathrm{B}}]_{:,2:T_{\mathrm{P}}}$ from Algorithm 3, which is possible considering Propositions 2 and 3, to remark its similarity with the other constructions.

Example 5 *Let us have a massive MIMO BS with $M = 64$ antennas serving $K = 10$ users. If we choose an arbitrary number of multiplications per antenna L, we would like to see which methods can be used for constructing a combining module $\boldsymbol{A}$, and what would be their resulting minimum number of inputs to the CPU. Recall that L should be an integer dividing M to be able to group the antennas into $M_{\mathrm{P}} = M/L$ panels. The number of inputs to the CPU is given by $T = T_{\mathrm{P}}L$, where we can find the minimum achievable integer T_{P} from* (23) *by*

$$T_{\mathrm{P,min}} = \left\lceil M_{\mathrm{P}} - \frac{M-L}{K} \right\rceil, \tag{32}$$

which, using Conjecture 1, will always be possible by constructing $\boldsymbol{A}$ through Algorithm 3.

- *Let us have $L = 2$, which gives $M_{\mathrm{P}} = 32$ and the achievable trade-off $T_{\mathrm{P}} \geq 25.8$ leading to $T_{\mathrm{P,min}} = 26$. If we choose to construct $\boldsymbol{A}$ through Proposition 4, we start by using $T_{\mathrm{P}} = T_{\mathrm{P,min}}$ to get $\Phi = 6$ from* (14)*. This gives $Q_1 = 4$ by* (20)*, which leads to the restriction $L \geq 2$. So we get the desired L without the need to increase T_{P}. If we use Proposition 6 this restriction transforms to $L \geq 1.94$. Thus, for this case, due to the integer restrictions, there is no difference in terms of inputs to the CPU of defining $\boldsymbol{A}$ from Propositions 4, 6, or Algorithm 3, since all give $T = 52$. We would recommend Proposition 4 for its simplicity and greater sparsity.*

- *Let us have $L = 4$, which gives $M_{\mathrm{P}} = 16$ leading to $T_{\mathrm{P,min}} = 10$. If we want to construct $\boldsymbol{A}$ through Proposition 4, we proceed as before using first $T_{\mathrm{P}} = T_{\mathrm{P,min}}$ to get $Q_1 = 1$, which leads to $L \geq 5$. In this case the desired L is not possible, so we increase $T_{\mathrm{P}} = T_{\mathrm{P,min}} + 1 = 25$, and calculate again $Q_1 = 2$, which leads to $L \geq 3.33$. This means that in order to use $\boldsymbol{A}$ from Proposition 4 we need $T = 100$ inputs to the CPU. Instead, if we try to construct $\boldsymbol{A}$ from Proposition 6, we start again with $T_{\mathrm{P}} = T_{\mathrm{P,min}}$, leading to $Q_1 = 2$ and $Q_2 = 2$. This gives the restriction $L \geq 4$, which is already fulfilled by the desired one. Thus, using Proposition 6 to define $\boldsymbol{A}$ would require $T = 96$ inputs to the CPU, i.e., there is no loss with respect to the achievable gain, which can also be reached by defining $\boldsymbol{A}$ through Algorithm 3.*

7 Conclusions

We have continued with the work on WAX decomposition by filling some gaps from [27]. We have proved that the trade-off given in [27] is fundamental in the sense that no decentralized system falling withing our general framework can perform beyond it. We have defined an equivalent formulation of the WAX

decomposition without the need of considering the CPU processing matrix $\boldsymbol{X}$. We have used said equivalent formulation to prove some properties that allow to transform the combining matrix $\boldsymbol{A}$ while maintaining its validity. We have also proved the validity of 3 structures for $\boldsymbol{A}$ which lead to an achievable version of the trade-off in [27] under different system parameter settings. An ad hoc method for constructing $\boldsymbol{A}$ such that the achievable trade-off is reached for any system parameter setting is also presented. We have defined a decentralized scheme for obtaining the information-lossless decentralized filters $\boldsymbol{W}_m$ to be applied at different panels without the need to aggregate their CSIs.

Future work can include jointly considering the sparse combining modules $\boldsymbol{A}$ in scenarios where the channel matrix $\boldsymbol{H}$ is also sparse or has rank-deficiencies. More clever decentralized schemes, e.g., those which could be also employed with $\boldsymbol{A}$ matrices constructed through the general ad hoc method from Algorithm 3, could also be explored. It would also be desirable to come up with a formal proof for the validity of the $\boldsymbol{A}$ matrices constructed through the ad hoc method.

Appendix A: Proof of Theorem 1

The necessary condition $T \geq K$, in (5) stated as $T > (K-1)$ due to the integer nature of T, comes trivially by the fact that $\text{rank}(\boldsymbol{WAX}) \leq T$ and $\text{rank}(\boldsymbol{H}) = K$ with probability 1 for randomly chosen $\boldsymbol{H}$. Let us thus assume $T \geq K$. If we invoke [27, Lemma 3], we can conclude that a randomly chosen $\boldsymbol{H}$ admits WAX decomposition if and only if we can find full-rank $\boldsymbol{W}$ solving the linear system

$$\boldsymbol{AX} = \boldsymbol{W}^{-1}\boldsymbol{H}.$$

$$\boldsymbol{A}_1 = \begin{cases} \boldsymbol{A}_\text{T} \begin{cases} \begin{bmatrix} \mathbf{I}_L & \mathbf{0} & \mathbf{0} & \mathbf{0} & \mathbf{0} & \mathbf{0} \\ \mathbf{0} & \mathbf{I}_L & \mathbf{0} & \mathbf{0} & \mathbf{0} & \mathbf{0} \\ \mathbf{0} & \mathbf{0} & \mathbf{I}_L & \mathbf{0} & \mathbf{0} & \mathbf{0} \\ \mathbf{0} & \mathbf{0} & \mathbf{0} & \mathbf{I}_L & \mathbf{0} & \mathbf{0} \\ \mathbf{0} & \mathbf{0} & \mathbf{0} & \mathbf{0} & \mathbf{I}_L & \mathbf{0} \\ \mathbf{0} & \mathbf{0} & \mathbf{0} & \mathbf{0} & \mathbf{0} & \mathbf{I}_L \end{bmatrix} \\ \boldsymbol{A}_\text{B} \begin{bmatrix} \mathbf{I}_L & \mathbf{0} & \mathbf{0} & \mathbf{I}_L & \mathbf{0} & \mathbf{0} \\ \mathbf{I}_L & \mathbf{0} & \mathbf{0} & \mathbf{0} & \mathbf{I}_L & \mathbf{0} \\ \mathbf{I}_L & \mathbf{0} & \mathbf{0} & \mathbf{0} & \mathbf{0} & \mathbf{I}_L \end{bmatrix} \end{cases}, \quad \boldsymbol{A}_2 = \begin{bmatrix} \mathbf{I}_L & \mathbf{0} & \mathbf{0} & \mathbf{0} & \mathbf{0} & \mathbf{0} \\ \mathbf{0} & \mathbf{I}_L & \mathbf{0} & \mathbf{0} & \mathbf{0} & \mathbf{0} \\ \mathbf{0} & \mathbf{0} & \mathbf{I}_L & \mathbf{0} & \mathbf{0} & \mathbf{0} \\ \mathbf{0} & \mathbf{0} & \mathbf{0} & \mathbf{I}_L & \mathbf{0} & \mathbf{0} \\ \mathbf{0} & \mathbf{0} & \mathbf{0} & \mathbf{0} & \mathbf{I}_L & \mathbf{0} \\ \mathbf{0} & \mathbf{0} & \mathbf{0} & \mathbf{0} & \mathbf{0} & \mathbf{I}_L \\ \mathbf{I}_L & \mathbf{I}_L & \mathbf{0} & \mathbf{I}_L & \mathbf{0} & \mathbf{0} \\ \mathbf{I}_L & \mathbf{0} & \mathbf{I}_L & \mathbf{0} & \mathbf{I}_L & \mathbf{0} \\ \mathbf{I}_L & \mathbf{I}_L & \mathbf{0} & \mathbf{0} & \mathbf{0} & \mathbf{I}_L \end{bmatrix}, \quad \boldsymbol{A}_3 = \begin{bmatrix} \mathbf{I}_L & \mathbf{0} & \mathbf{0} & \mathbf{0} & \mathbf{0} & \mathbf{0} \\ \mathbf{0} & \mathbf{I}_L & \mathbf{0} & \mathbf{0} & \mathbf{0} & \mathbf{0} \\ \mathbf{0} & \mathbf{0} & \mathbf{I}_L & \mathbf{0} & \mathbf{0} & \mathbf{0} \\ \mathbf{0} & \mathbf{0} & \mathbf{0} & \mathbf{I}_L & \mathbf{0} & \mathbf{0} \\ \mathbf{0} & \mathbf{0} & \mathbf{0} & \mathbf{0} & \mathbf{I}_L & \mathbf{0} \\ \mathbf{0} & \mathbf{0} & \mathbf{0} & \mathbf{0} & \mathbf{0} & \mathbf{I}_L \\ \mathbf{I}_L & \mathbf{I}_L & \mathbf{0} & \mathbf{I}_L & \mathbf{0} & \mathbf{0} \\ \mathbf{I}_L & \mathbf{0} & \mathbf{I}_L & \mathbf{0} & \mathbf{I}_L & \mathbf{0} \\ \mathbf{I}_L & \mathbf{I}_L & \mathbf{I}_L & \mathbf{0} & \mathbf{0} & \mathbf{I}_L \end{bmatrix} \tag{33}$$

The previous expression can be vectorized as in [27] giving

$$\left[\mathbf{I}_K \otimes \boldsymbol{A} \quad -(\boldsymbol{H}^{\mathrm{T}} \otimes \mathbf{I}_M)\widetilde{\mathbf{I}}_{\boldsymbol{W}}\right] \begin{bmatrix} \mathrm{vec}(\boldsymbol{X}) \\ \mathrm{vec}(\boldsymbol{W}_1) \\ \vdots \\ \mathrm{vec}(\boldsymbol{W}_{M_{\mathrm{P}}}) \end{bmatrix} = \mathbf{0}_{MK\times 1}, \tag{34}$$

where $\widetilde{\mathbf{I}}_{\boldsymbol{W}}$ corresponds to an $M^2 \times ML$ matrix having $\mathbf{I}_L$ blocks separated by blocks of zeros so as to disregard the zeros in $\mathrm{vec}(\boldsymbol{W})$. The rank of the block $\mathbf{I}_K \otimes \boldsymbol{A}$, which multiplies $\mathrm{vec}(\boldsymbol{X})$, is given by

$$\mathrm{rank}(\mathbf{I}_K \otimes \boldsymbol{A}) = KR_{\boldsymbol{A}},$$

where $R_{\boldsymbol{A}} = \mathrm{rank}(\boldsymbol{A})$. If $\mathrm{vec}(\boldsymbol{X})$ is in the null-space of $\mathbf{I}_K \otimes \boldsymbol{A}$, then the vector $[\mathrm{vec}(\boldsymbol{W}_1)^T, \ldots, \mathrm{vec}(\boldsymbol{W}_{M_{\mathrm{P}}})^T]^T$ should be in the null-space of $-(\boldsymbol{H}^{\mathrm{T}} \otimes \mathbf{I}_M)\widetilde{\mathbf{I}}_{\boldsymbol{W}}$ (full-rank with probability 1), leading to a more restrictive condition than (5), $K < L$. Thus, we can remove the subspace of $\mathrm{vec}(\boldsymbol{X})$ that falls in the null-space of $\mathbf{I}_K \otimes \boldsymbol{A}$, which means that can rewrite (34) as

$$\left[\boldsymbol{C} \quad -(\boldsymbol{H}^{\mathrm{T}} \otimes \mathbf{I}_M)\widetilde{\mathbf{I}}_{\boldsymbol{W}}\right] \begin{bmatrix} \tilde{\boldsymbol{x}} \\ \mathrm{vec}(\boldsymbol{W}_1) \\ \vdots \\ \mathrm{vec}(\boldsymbol{W}_{M_{\mathrm{P}}}) \end{bmatrix} = \mathbf{0}_{MK\times 1}, \tag{35}$$

where $\boldsymbol{C}$ is now an $MK \times KR_{\boldsymbol{A}}$. Since $\boldsymbol{H}$ is a randomly chosen matrix, the block $-(\boldsymbol{H}^{\mathrm{T}} \otimes \mathbf{I}_M)\widetilde{\mathbf{I}}_{\boldsymbol{W}}$ adds full-rank to $\boldsymbol{C}$ with probability 1. Hence, the $MK\times(KR_{\boldsymbol{A}}+ML)$ matrix $\left[\boldsymbol{C} \quad -(\boldsymbol{H}^{\mathrm{T}} \otimes \mathbf{I}_M)\widetilde{\mathbf{I}}_{\boldsymbol{W}}\right]$ is full-rank with probability 1, which means that it has non-empty null-space only if

$$MK < KR_{\boldsymbol{A}} + ML. \tag{36}$$

After simple manipulation of (36), and noting that $R_{\boldsymbol{A}} \leq T$, where equality corresponds to $\boldsymbol{A}$ having rank T, we reach the necessary condition (5) .

Appendix B: Proof of Proposition 5

Selecting $\widetilde{\boldsymbol{A}}_{\mathrm{T}} = \mathbf{I}_{T_{\mathrm{P}}}$ and $\widetilde{\boldsymbol{A}}_{\mathrm{B}}$ as in (24) leads to

$$\widetilde{\boldsymbol{B}} = \begin{bmatrix} \alpha_1 \mathbf{1}_{(T_{\mathrm{P}}-1)\times 1} & \mathbf{I}_{T_{\mathrm{P}}-1} & \\ \vdots & \vdots & -\mathbf{I}_{\Phi} \\ \alpha_{Q_2-1}\mathbf{1}_{(T_{\mathrm{P}}-1)\times 1} & \mathbf{I}_{T_{\mathrm{P}}-1} & \\ \alpha_{Q_2}\mathbf{1}_{\Pi\times 1} & [\mathbf{I}_{T_{\mathrm{P}}-1}]_{1:\Pi,:} & \end{bmatrix}^{\mathrm{T}}. \tag{37}$$

If we use Corollary 1, we can substitute $\widetilde{\boldsymbol{B}}$ in the equivalent formulation of the WAX decomposition, given in (17). We then fix $\boldsymbol{W}_1^{-1}$ to some arbitrary full-rank matrix, for simplicity let us have $\boldsymbol{W}_1^{-1} = \mathbf{I}_L$ (any other full rank-matrix can be absorbed by $\boldsymbol{H}_1$ or by the remaining $\boldsymbol{W}_m$'s), so (17) gives

$$\begin{aligned} -\begin{bmatrix}\alpha_1 & \cdots & \alpha_{Q_2}\end{bmatrix} \otimes \boldsymbol{H}_1 = \begin{bmatrix}\boldsymbol{W}_2^{-1} & \cdots & \boldsymbol{W}_{M_{\mathrm{P}}}^{-1}\end{bmatrix} \\ \times \left(\begin{bmatrix} \mathbf{I}_{T_{\mathrm{P}}-1} & \cdots & [\mathbf{I}_{T_{\mathrm{P}}-1}]_{1:\Pi,:} \\ & -\mathbf{I}_{\Phi} & \end{bmatrix} \bullet \begin{bmatrix} \boldsymbol{H}_2 \\ \vdots \\ \boldsymbol{H}_{M_{\mathrm{P}}} \end{bmatrix} \right). \end{aligned} \tag{38}$$

We can notice that the face-splitting product $(.) \bullet (.)$ only substitutes in the left matrix each 1 at row m by $\boldsymbol{H}_m$. Furthermore, (38) corresponds to a series of $T_{\mathrm{P}} - 1$ independent equations of the form

$$\begin{aligned} \begin{bmatrix}\alpha_1 & \cdots & \alpha_{Q_2}\end{bmatrix} \otimes \widehat{\boldsymbol{H}}_0 = \begin{bmatrix}\widehat{\boldsymbol{W}}_1^{-1} & \cdots & \widehat{\boldsymbol{W}}_{Q_2+1}^{-1}\end{bmatrix} \\ \times \begin{bmatrix} \widehat{\boldsymbol{H}}_1 & \widehat{\boldsymbol{H}}_1 & \cdots & \widehat{\boldsymbol{H}}_1 \\ \widehat{\boldsymbol{H}}_2 & \mathbf{0}_{L\times K} & \cdots & \mathbf{0}_{L\times K} \\ \mathbf{0}_{L\times K} & \widehat{\boldsymbol{H}}_3 & \ddots & \vdots \\ \vdots & \ddots & \ddots & \mathbf{0}_{L\times K} \\ \mathbf{0}_{L\times K} & \cdots & \mathbf{0}_{L\times K} & \widehat{\boldsymbol{H}}_{Q_2+1} \end{bmatrix}, \end{aligned} \tag{39}$$

where $\widehat{\boldsymbol{H}}_i$ corresponds to a re-indexing of the respective $\boldsymbol{H}_m$, including a possible change of sign ($\widehat{\boldsymbol{H}}_0 = -\boldsymbol{H}_1$ is the only matrix shared in all equations), so we can think of them as $L \times K$ blocks from a randomly chosen matrix. Note that we may also require the ability to solve a sub-problem of (39) with 1 less column block, i.e., substituting Q_2 by $Q_2 - 1$. This is due to the possibly cropped block in (24) or (38), $[\mathbf{I}_{T_{\mathrm{P}}-1}]_{1:\Pi,:}$, which would lead to $(T_{\mathrm{P}} - 1 - \Pi)$ equations having $Q_2 - 1$ instead of Q_2 column blocks in (39). However, this sub-problem is less restrictive than (24), as we will see.

Let us multiply from the right both sides of (39) by the full rank matrix

$\text{diag}(\widehat{\boldsymbol{V}}_1, \ldots, \widehat{\boldsymbol{V}}_1)$, where $\widehat{\boldsymbol{V}}_1$ is the $K \times K$ right unitary matrix from the singular value decomposition of $\widehat{\boldsymbol{H}}_1$. If we further use the fact that any full-rank block diagonal matrix being multiplied between the $\widehat{\boldsymbol{W}}_m^{-1}$'s and $\widehat{\boldsymbol{H}}_m$'s block matrices in the RHS of (39), as well as any full-rank $L \times L$ matrix that multiplies from the left both sides of (39), can be absorbed by the corresponding $\widehat{\boldsymbol{W}}_m^{-1}$ matrices, we reach

$$\begin{aligned}([\alpha_1 \ \cdots \ \alpha_{Q_2}] \otimes [\mathbf{I}_L \ \widetilde{\boldsymbol{H}}_0]) = \left[\widetilde{\boldsymbol{W}}_1^{-1} \ \ \cdots \ \ \widetilde{\boldsymbol{W}}_{Q_2+1}^{-1}\right] \\ \times \begin{bmatrix} [\mathbf{I}_L \ \mathbf{0}_{L\times(K-L)}] & [\mathbf{I}_L \ \mathbf{0}_{L\times(K-L)}] & \cdots & [\mathbf{I}_L \ \mathbf{0}_{L\times(K-L)}] \\ [\mathbf{I}_L \ \widetilde{\boldsymbol{H}}_2] & \mathbf{0}_{L\times K} & \cdots & \mathbf{0}_{L\times K} \\ \mathbf{0}_{L\times K} & [\mathbf{I}_L \ \widetilde{\boldsymbol{H}}_3] & \ddots & \vdots \\ \vdots & \ddots & \ddots & \mathbf{0}_{L\times K} \\ \mathbf{0}_{L\times K} & \cdots & \mathbf{0}_{L\times K} & [\mathbf{I}_L \ \widetilde{\boldsymbol{H}}_{Q_2+1}] \end{bmatrix},\end{aligned} \tag{40}$$

where $\widetilde{\boldsymbol{H}}_i$, $i \in \{0, 2, \ldots, (Q_2+1)\}$, are now $L \times (K-L)$ blocks from a randomly chosen matrices.[26] Equation (40) corresponds to the system of equations

$$\begin{cases} \widetilde{\boldsymbol{W}}_1^{-1} + \widetilde{\boldsymbol{W}}_{i+1}^{-1} = \alpha_i \mathbf{I}_L \\ \widetilde{\boldsymbol{W}}_{i+1}^{-1} \widetilde{\boldsymbol{H}}_{i+1} = \alpha_i \widetilde{\boldsymbol{H}}_0 \end{cases}, \quad i = 1, \ldots, Q_2. \tag{41}$$

We can now isolate $\widetilde{\boldsymbol{W}}_{i+1}^{-1} = \alpha_i \mathbf{I}_L - \widetilde{\boldsymbol{W}}_1^{-1}$ from the first line of (41), and then substitute it in the second line to reach $\alpha_i \widetilde{\boldsymbol{H}}_{i+1} - \widetilde{\boldsymbol{W}}_1^{-1} \widetilde{\boldsymbol{H}}_{i+1} = \alpha_i \widetilde{\boldsymbol{H}}_0$. After reordering terms and merging the inequalities for $i = 1, \ldots, Q_2$, into matrix notation, we can write

$$\widetilde{\boldsymbol{W}}_1^{-1} \widetilde{\boldsymbol{\mathcal{H}}} = \left[\alpha_1(\widetilde{\boldsymbol{H}}_2 - \widetilde{\boldsymbol{H}}_0) \ \ \cdots \ \ \alpha_{Q_2}(\widetilde{\boldsymbol{H}}_{Q_2+1} - \widetilde{\boldsymbol{H}}_0)\right], \tag{42}$$

where $\widetilde{\boldsymbol{\mathcal{H}}} = \left[\widetilde{\boldsymbol{H}}_2 \ \ \cdots \ \ \widetilde{\boldsymbol{H}}_{Q_2+1}\right]$ gives an $L \times Q_2(K-L)$ randomly chosen matrix, which is thus full-rank with probability 1. The block matrix on the RHS of (42) is also a randomly chosen matrix, and thus full-rank with probability 1, as long as $\alpha_i \neq 0 \ \forall i$. We now note that (42) corresponds to a linear equation solvable for $L \geq Q_2(K-L)$, which directly gives us the condition (26).

It remains to prove that we have a full-rank solution for each $\widetilde{\boldsymbol{W}}_i^{-1}$ (then each corresponding $\boldsymbol{W}_m^{-1}$ would also be full-rank). Solving for $\widetilde{\boldsymbol{W}}_1^{-1}$ in (41)

[26] Note that the multiplication by a common unitary matrix from the right to generate each $\widetilde{\boldsymbol{H}}_i$ can be seen as a common rotation to their original random unitary matrices, thus it does not affect the randomly chosen property

gives the set of solutions

$$\widetilde{\boldsymbol{W}}_1^{-1} = \left[\alpha_1(\widetilde{\boldsymbol{H}}_2 - \widetilde{\boldsymbol{H}}_0)\cdots\alpha_{Q_2}(\widetilde{\boldsymbol{H}}_{Q_2+1} - \widetilde{\boldsymbol{H}}_0)\right]\widetilde{\boldsymbol{\mathcal{H}}}^{\dagger} + \mathbf{N}_{\widetilde{\boldsymbol{\mathcal{H}}}}, \tag{43}$$

where $\mathbf{N}_{\widetilde{\boldsymbol{\mathcal{H}}}}$ can be selected to be any $L \times L$ matrix in the left null-space of $\widetilde{\boldsymbol{\mathcal{H}}}$. Thus, rank$(\mathbf{N}_{\widetilde{\boldsymbol{\mathcal{H}}}}) \leq L - Q_2(K-L)$, and $\mathbf{N}_{\widetilde{\boldsymbol{\mathcal{H}}}}$ would vanish in case of equality in (26) ($\widetilde{\boldsymbol{\mathcal{H}}}$ square). We can now note that the first term in the sum from the RHS of (43) has rank $Q_2(K-L)$ with probability 1. The reason is that it is the multiplication of an $L \times Q_2(K-L)$ matrix with a $Q_2(K-L) \times L$ matrix, so its rank cannot be above $Q_2(K-L)$, while, if we multiply $\widetilde{\boldsymbol{\mathcal{H}}}$ from the right, which cannot increase the rank, we get an $L \times Q_2(K-L)$ randomly chosen matrix (full-rank with probability 1). On the other hand, $\mathbf{N}_{\widetilde{\boldsymbol{\mathcal{H}}}}$ adds its rank to the other term of the sum, since they are in perpendicular spaces (left null-space and row-space are perpendicular). Therefore, by selecting any $\mathbf{N}_{\widetilde{\boldsymbol{\mathcal{H}}}}$ spanning the whole null-space of $\widetilde{\boldsymbol{\mathcal{H}}}$, i.e., having rank $L - Q_2(K-L)$, we get a full-rank $\widetilde{\boldsymbol{W}}_1^{-1}$.

We now show that full-rank solutions for $\widetilde{\boldsymbol{W}}_i^{-1}$, $i > 1$, are also available as long as $\alpha_i \neq \alpha_j$ for $i \neq i$. Substituting $\widetilde{\boldsymbol{W}}_1^{-1}$ from (42) in the first equation of (41) gives a solution for each $\widetilde{\boldsymbol{W}}_i^{-1}$ of the form

$$\begin{aligned}\widetilde{\boldsymbol{W}}_i^{-1} =& \alpha_i \mathbf{I}_L - \mathbf{N}_{\widetilde{\boldsymbol{\mathcal{H}}}} \\ &- \left[\alpha_1(\widetilde{\boldsymbol{H}}_2 - \widetilde{\boldsymbol{H}}_0) \quad \cdots \quad \alpha_{Q_2}(\widetilde{\boldsymbol{H}}_{Q_2+1} - \widetilde{\boldsymbol{H}}_0)\right]\widetilde{\boldsymbol{\mathcal{H}}}^{\dagger}.\end{aligned} \tag{44}$$

Let us define $\tilde{\alpha}_j = \alpha_j - \alpha_i$. We then have

$$\begin{aligned}\widetilde{\boldsymbol{W}}_i^{-1} =& \alpha_i\left(\mathbf{I}_L - \widetilde{\boldsymbol{\mathcal{H}}}\widetilde{\boldsymbol{\mathcal{H}}}^{\dagger}\right) - \mathbf{N}_{\widetilde{\boldsymbol{\mathcal{H}}}} \\ &- \left[\tilde{\alpha_1}\widetilde{\boldsymbol{H}}_2 \quad \cdots \quad \tilde{\alpha}_{Q_2}\widetilde{\boldsymbol{H}}_{Q_2+1}\right]\widetilde{\boldsymbol{\mathcal{H}}}^{\dagger} \\ &+ \left[\alpha_1\widetilde{\boldsymbol{H}}_0 \quad \cdots \quad \alpha_{Q_2}\widetilde{\boldsymbol{H}}_0\right]\widetilde{\boldsymbol{\mathcal{H}}}^{\dagger}.\end{aligned} \tag{45}$$

However, it can be checked that

$$\widetilde{\boldsymbol{\mathcal{H}}}\widetilde{\boldsymbol{\mathcal{H}}}^{\dagger} = \boldsymbol{U}\mathrm{diag}\left(\mathbf{I}_{Q_2(K-L)}, \mathbf{0}_{L-Q_2(K-L)}\right)\boldsymbol{U}^{\mathrm{H}},$$

where $\boldsymbol{U}$ corresponds to the left unitary matrix from the singular value decom-

position of $\widetilde{\boldsymbol{\mathcal{H}}}$. Thus, we get

$$\begin{aligned}\widetilde{\boldsymbol{W}}_i^{-1} = \alpha_i \boldsymbol{U} \mathrm{diag}\left(\mathbf{0}_{Q_2(K-L)}, \mathbf{I}_{L-Q_2(K-L)}\right) \boldsymbol{U}^{\mathrm{H}} - \mathbf{N}_{\widetilde{\boldsymbol{\mathcal{H}}}} \\ - \left[\tilde{\alpha_1}\widetilde{\boldsymbol{H}}_2 \quad \cdots \quad \tilde{\alpha}_{Q_2}\widetilde{\boldsymbol{H}}_{Q_2+1}\right] \widetilde{\boldsymbol{\mathcal{H}}}^{\dagger} \\ + \left[\alpha_1\widetilde{\boldsymbol{H}}_0 \quad \cdots \quad \alpha_{Q_2}\widetilde{\boldsymbol{H}}_0\right] \widetilde{\boldsymbol{\mathcal{H}}}^{\dagger}.\end{aligned} \tag{46}$$

We then note that the first two matrices on the RHS of (46) are both in the null-space of $\widetilde{\boldsymbol{\mathcal{H}}}$, and, since we have freedom in selecting $\mathbf{N}_{\widetilde{\boldsymbol{\mathcal{H}}}}$ as long as it spans the whole null-space, we can choose it so that the rank from the first matrix is not reduced after subtracting. Therefore, the first two matrices will always add rank $L - Q_2(K-L)$ to the last two, which lay in the row-space of $\widetilde{\boldsymbol{\mathcal{H}}}$. On the other hand, after multiplying $\widetilde{\boldsymbol{\mathcal{H}}}$ to the last two matrices in the RHS of (46) we get one matrix of rank $N_{\tilde{\alpha}}(K-L)$, with $N_{\tilde{\alpha}}$ the number of non-zero $\tilde{\alpha}_j$, and one matrix of rank $(K-L)$. Note that $N_{\tilde{\alpha}} \leq (Q_2 - 1)$ since $\tilde{\alpha}_i = 0$ by definition. The sum of the latter two matrices would then be

$$\left[\alpha_1\widetilde{\boldsymbol{H}}_0 - \tilde{\alpha_1}\widetilde{\boldsymbol{H}}_2 \quad \cdots \quad \alpha_i\widetilde{\boldsymbol{H}}_0 \quad \cdots \quad \alpha_{Q_2}\widetilde{\boldsymbol{H}}_0 - \tilde{\alpha}_{Q_2}\widetilde{\boldsymbol{H}}_{Q_2+1}\right].$$

The rank is then[27] $(N_{\tilde{\alpha}} + 1)(K-L)$ so, in order to have (46) full-rank, we need $N_{\tilde{\alpha}} = Q_2 - 1$ for each i, which means all $\tilde{\alpha_j}$ $(j \neq i)$ should be non-zero. Considering $\widetilde{\boldsymbol{W}}_i^{-1}$ $\forall i$, this translates to having $\alpha_i \neq \alpha_j$ for $i \neq j$. Hence, Proposition 5 is proved.

Appendix C: Proof of Proposition 6

Selecting $\widetilde{\boldsymbol{A}}_{\mathrm{T}} = \mathbf{I}_{T_{\mathrm{P}}}$ and $\widetilde{\boldsymbol{A}}_{\mathrm{B}}$ as in (27) leads to

$$\widetilde{\boldsymbol{B}} = \left[\mathbf{1}_{\Phi\times 1} \quad \left[\mathbf{1}_{Q_2\times 1} \otimes \mathbf{I}_J\right]_{1:\Phi,:} \quad \underbrace{\mathbf{I}_\Phi \quad \cdots \quad \mathbf{I}_\Phi}_{Q_1} \quad -\mathbf{I}_\Phi\right]^{\mathrm{T}}.$$

Note the similarity of the previous $\widetilde{\boldsymbol{B}}$ with (37), which for $\alpha_i = 1$ only the Q_1 extra $\mathbf{I}_\Phi$ would be added. Applying similar arguments as in the proof of Proposition 5, which include fixing $\boldsymbol{W}_1$ to an arbitrary full-rank matrix, we can transform the equivalent formulation of the WAX decomposition (17) into

[27] $\widetilde{\boldsymbol{H}}_0$ and $\widetilde{\boldsymbol{H}}_i$ do not destroy rank since they are blocks from a randomly chosen matrix, and they are full-rank with probability 1.

a series of independent equations of the form

$$\mathbf{1}_{1\times Q_2}\otimes\widehat{\boldsymbol{H}}_0=\begin{bmatrix}\widehat{\boldsymbol{W}}_1^{-1} & \cdots & \widehat{\boldsymbol{W}}_{(Q_1+1)Q_2+1}^{-1}\end{bmatrix}\times\begin{bmatrix}\widehat{\boldsymbol{H}}_1 & \cdots & \widehat{\boldsymbol{H}}_1\\ \widehat{\boldsymbol{H}}_2 & & \\ & \ddots & \\ & & \widehat{\boldsymbol{H}}_{Q_2+1}\\ & \vdots & \\ \widehat{\boldsymbol{H}}_{Q_1Q_2+2} & & \\ & \ddots & \\ & & \widehat{\boldsymbol{H}}_{(Q_1+1)Q_2+1}\end{bmatrix},\tag{47}$$

where we have relaxed notation by removing the blocks of zeros. Again, only $\widehat{\boldsymbol{H}}_0$ is shared among the different independent equations. Let us have

$$\widehat{\boldsymbol{H}}_m=\begin{bmatrix}\widehat{\boldsymbol{H}}_{m,\mathrm{sq}} & \widehat{\boldsymbol{H}}_{m,\mathrm{r}}\end{bmatrix},\ m=0,\ldots,(Q_1+1)Q_2+1,$$

where $\widehat{\boldsymbol{H}}_{m,\mathrm{sq}}$ and $\widehat{\boldsymbol{H}}_{m,\mathrm{r}}$ are $L\times L$ and $L\times(K-L)$ blocks from a randomly chosen matrix, respectively. We can then have $\widehat{\boldsymbol{H}}_{1,\mathrm{r}}=\mathbf{0}_{L,(K-L)}$ by absorbing the corresponding right unitary matrix in the rest of $\widehat{\boldsymbol{H}}_m$ as before. We then get the set of equations

$$\begin{cases}\widehat{\boldsymbol{W}}_1^{-1}\widehat{\boldsymbol{H}}_{1,\mathrm{sq}}+\sum_{q=0}^{Q_1}\widehat{\boldsymbol{W}}_{i+1+qQ_2}^{-1}\widehat{\boldsymbol{H}}_{i+1+qQ_2,\mathrm{sq}}=\widehat{\boldsymbol{H}}_{0,\mathrm{sq}}\\ \sum_{q=0}^{Q_1}\widehat{\boldsymbol{W}}_{i+1+qQ_2}^{-1}\widehat{\boldsymbol{H}}_{i+1+qQ_2,\mathrm{r}}=\widehat{\boldsymbol{H}}_{0,\mathrm{r}}\end{cases},\tag{48}$$

where $i=1,\ldots,Q_2$. Let us isolate $\widetilde{\boldsymbol{W}}_{i+1+Q_1Q_2}^{-1}$ in the first equation of (48)

$$\widehat{\boldsymbol{W}}_{i+1+Q_1Q_2}^{-1}=\Bigg(\widehat{\boldsymbol{H}}_{0,\mathrm{sq}}-\widehat{\boldsymbol{W}}_1^{-1}-\sum_{q=0}^{Q_1-1}\widehat{\boldsymbol{W}}_{i+1+qQ_2}^{-1}\widehat{\boldsymbol{H}}_{i+1+qQ_2,\mathrm{sq}}\Bigg)\widehat{\boldsymbol{H}}_{i+1+Q_1Q_2,\mathrm{sq}}^{-1},\tag{49}$$

which, assuming full-rank $\widehat{\boldsymbol{W}}_{i+1+qQ_2}$ for $q<Q_1$, corresponds to a random combination of full-rank matrices, so it will lead to full-rank $\widehat{\boldsymbol{W}}_{i+1+Q_1Q_2}^{-1}$ with probability 1. Substituting in the second equation from (48), absorbing some square randomly chosen matrices (full-rank with probability 1) in the corre-

sponding $\widehat{\boldsymbol{W}}_i$, and renaming blocks, we get

$$\widetilde{\boldsymbol{W}}_1^{-1}\widetilde{\boldsymbol{H}}_{1i} + \sum_{q=0}^{Q_1-1} \widetilde{\boldsymbol{W}}_{i+1+qQ_2}^{-1}\widetilde{\boldsymbol{H}}_{i+1+qQ_2} = \widetilde{\boldsymbol{H}}_0 + \widetilde{\boldsymbol{H}}_{1i}, \tag{50}$$

where all $\widetilde{\boldsymbol{H}}_m$ (or $\widetilde{\boldsymbol{H}}_{mn}$) correspond again to blocks of size $L \times (K-L)$ from a randomly chosen since they come from sums and products of different blocks from a randomly chosen matrix. Multiplying both sides by $\widetilde{\boldsymbol{V}}_{1i}$, where $\widetilde{\boldsymbol{V}}_{1i}^{\mathrm{H}}$ corresponds to the right unitary matrix of $\widetilde{\boldsymbol{H}}_{1i}$, we reach

$$\begin{aligned}\left[\widetilde{\boldsymbol{H}}_{01}+\widetilde{\boldsymbol{H}}_{11} \quad \cdots \quad \widetilde{\boldsymbol{H}}_{0Q_2}+\widetilde{\boldsymbol{H}}_{1Q_2}\right] = \left[\widetilde{\boldsymbol{W}}_1^{-1} \quad \cdots \quad \widetilde{\boldsymbol{W}}_{Q_1Q_2+1}^{-1}\right] \\ \times \begin{bmatrix} \widetilde{\boldsymbol{H}}_{11} & \cdots & \widetilde{\boldsymbol{H}}_{1Q_2} \\ \widetilde{\boldsymbol{H}}_2 & & \\ & \ddots & \\ & & \widetilde{\boldsymbol{H}}_{Q_2+1} \\ & \vdots & \\ \widetilde{\boldsymbol{H}}_{(Q_1-1)Q_2+2} & & \\ & \ddots & \\ & & \widetilde{\boldsymbol{H}}_{Q_1Q_2+1} \end{bmatrix},\end{aligned} \tag{51}$$

where $\widetilde{\boldsymbol{H}}_{0i} = \widetilde{\boldsymbol{H}}_0\widetilde{\boldsymbol{V}}_{1i}$, and $\widetilde{\boldsymbol{H}}_{1i} = [\widetilde{\boldsymbol{H}}_{1i,\mathrm{sq}} \quad \boldsymbol{0}_{L\times(K-2L)}]$. We then reach the following set of equations for $i = 1, \ldots, Q_2$

$$\begin{cases} \widetilde{\boldsymbol{W}}_1^{-1}\widetilde{\boldsymbol{H}}_{1i,\mathrm{sq}} + \sum_{q=0}^{Q_1-1}\widetilde{\boldsymbol{W}}_{i+1+qQ_2}^{-1}\widetilde{\boldsymbol{H}}_{i+1+qQ_2,\mathrm{sq}} = \widetilde{\boldsymbol{H}}_{0i,\mathrm{sq}} \\ \sum_{q=0}^{Q_1-1}\widetilde{\boldsymbol{W}}_{i+1+qQ_2}^{-1}\widetilde{\boldsymbol{H}}_{i+1+qQ_2,\mathrm{r}} = \widetilde{\boldsymbol{H}}_{0i,\mathrm{r}} \end{cases}, \tag{52}$$

where $\widetilde{\boldsymbol{H}}_m = [\widetilde{\boldsymbol{H}}_{m,\mathrm{sq}} \quad \widetilde{\boldsymbol{H}}_{m,\mathrm{r}}]$, with $\widetilde{\boldsymbol{H}}_{m,\mathrm{sq}}$ being square blocks as before. Note that (52) is almost like (48), but the dimensions have been reduced, as well as the number of sum elements, and we have now different $\widetilde{\boldsymbol{H}}_{1i,\mathrm{sq}}$ and $\widetilde{\boldsymbol{H}}_{0i,\mathrm{sq}}$. If we follow the same steps as before, isolating $\widetilde{\boldsymbol{W}}_{i+1+(Q_1-1)Q_2}$ instead, we would reach an expression as (51) with one less diagonal block where each $\widetilde{\boldsymbol{H}}_m$ (still randomly chosen) has reduced the column dimension by L. We can thus

perform these reductions inductively until we reach

$$\begin{bmatrix}(\breve{\boldsymbol{H}}_{01}+\breve{\boldsymbol{H}}_{11}) & \cdots & (\breve{\boldsymbol{H}}_{0Q_2}+\breve{\boldsymbol{H}}_{1Q_2})\end{bmatrix}=\begin{bmatrix}\breve{\boldsymbol{W}}_1^{-1} & \cdots & \breve{\boldsymbol{W}}_{Q_2+1}^{-1}\end{bmatrix} \times \begin{bmatrix}\breve{\boldsymbol{H}}_{11} & \cdots & \breve{\boldsymbol{H}}_{1Q_2} \\ \breve{\boldsymbol{H}}_2 & & \\ & \ddots & \\ & & \breve{\boldsymbol{H}}_{Q_2+1}\end{bmatrix}, \tag{53}$$

where $\breve{\boldsymbol{H}}_{0i}=\breve{\boldsymbol{H}}_0\breve{\boldsymbol{V}}_i$, with $\breve{\boldsymbol{V}}_i$ being a unitary matrix coming from a product of unitary matrices from randomly chosen blocks, $\breve{\boldsymbol{H}}_{1i}=[\breve{\boldsymbol{H}}_{1i,\mathrm{sq}}\ \ \boldsymbol{0}_{L\times(K-(Q_1+1)L)}]$ with $\breve{\boldsymbol{H}}_{1i,\mathrm{sq}}$ randomly chosen, and $\breve{\boldsymbol{H}}_m$ for $m=0,2,\ldots,Q_2+1$ are different $L\times(K-Q_1L)$ randomly chosen blocks. It only remains to show that (53) is solvable with full-rank $\breve{\boldsymbol{W}}_i^{-1}$ for $i=1,\ldots,Q_2+1$. If we compare (53) with (39) we can note that they have the same structure, but the changes in the blocks, which will allow to have $\alpha_i=1$, require a new proof.

Let us now prove that (53) allows for a solution with full-rank $\breve{\boldsymbol{W}}_i^{-1}$ if (29) is fulfilled. By trivial linear algebra, we immediately note that (29) follows from the need to have at least as many rows as columns in the matrix multiplying the RHS of (53), since said matrix will be full-rank with probability 1. We should then check we can have full-rank $\breve{\boldsymbol{W}}_i^{-1}$ given (29). Proceeding as before we express the set of equations

$$\begin{cases}\breve{\boldsymbol{W}}_1^{-1}\breve{\boldsymbol{H}}_{1i,\mathrm{sq}}+\breve{\boldsymbol{W}}_{i+1}^{-1}\breve{\boldsymbol{H}}_{i+1,\mathrm{sq}}=\breve{\boldsymbol{H}}_{01i,\mathrm{sq}} \\ \breve{\boldsymbol{W}}_{i+1}^{-1}\breve{\boldsymbol{H}}_{i+1,\mathrm{r}}=\breve{\boldsymbol{H}}_{0i,\mathrm{r}}\end{cases}, i=1,\ldots,Q_2 \tag{54}$$

with $\breve{\boldsymbol{H}}_m=[\breve{\boldsymbol{H}}_{m,\mathrm{sq}}\ \ \breve{\boldsymbol{H}}_{m,\mathrm{r}}]$, where $\breve{\boldsymbol{H}}_{m,\mathrm{sq}}$ are again square, and $\breve{\boldsymbol{H}}_{01i,\mathrm{sq}}=\breve{\boldsymbol{H}}_{0i,\mathrm{sq}}+\breve{\boldsymbol{H}}_{1i,\mathrm{sq}}$. Isolating $\breve{\boldsymbol{W}}_{i+1}^{-1}$ in the first line of (54), substituting it in the second line, and solving for $\breve{\boldsymbol{W}}_1^{-1}$,[28] we reach

$$\breve{\boldsymbol{W}}_1^{-1}=\breve{\boldsymbol{\mathcal{H}}}\breve{\boldsymbol{\mathcal{H}}}^\dagger+\begin{bmatrix}(\boldsymbol{\Theta}_1-\breve{\boldsymbol{H}}_{0i,\mathrm{r}}) & \cdots & (\boldsymbol{\Theta}_{Q_2}-\breve{\boldsymbol{H}}_{0i,\mathrm{r}})\end{bmatrix}\breve{\boldsymbol{\mathcal{H}}}^\dagger+\mathbf{N}_{\breve{\boldsymbol{\mathcal{H}}}}, \tag{55}$$

where $\boldsymbol{\Theta}_m=\breve{\boldsymbol{H}}_{0m,\mathrm{sq}}\breve{\boldsymbol{H}}_{m+1,\mathrm{sq}}^{-1}\breve{\boldsymbol{H}}_{m+1,\mathrm{r}}$, which has dimensions $L\times(K-Q_1L)$,

[28] Note that reaching from (54) to (55) corresponds to the same set of steps as reaching from (41) to (43) in the proof of Proposition 5, with the only difference that in the first line of (54) each term has an invertible (with probability 1) matrix multiplying from the right.

$\mathbf{N}_{\breve{\boldsymbol{\mathcal{H}}}}$ is an $L \times L$ matrix to be selected from the left null-space of $\breve{\boldsymbol{\mathcal{H}}}$,

$$\breve{\boldsymbol{\mathcal{H}}} = \left[\breve{\boldsymbol{H}}_{11,\mathrm{sq}} \breve{\boldsymbol{H}}_{2,\mathrm{sq}}^{-1} \breve{\boldsymbol{H}}_{2,\mathrm{r}} \quad \cdots \quad \breve{\boldsymbol{H}}_{1Q_2,\mathrm{sq}} \breve{\boldsymbol{H}}_{Q_2+1,\mathrm{sq}}^{-1} \breve{\boldsymbol{H}}_{Q_2+1,\mathrm{r}} \right],$$

and $\breve{\boldsymbol{\mathcal{H}}}^{\dagger}$ is the left pseudo-inverse of $\breve{\boldsymbol{\mathcal{H}}}$. Note that the existence of said pseudo-inverse also leads to the condition (29). By similar arguments as in the proof of Proposition 5, we have a sum between a matrix in the row space of $\breve{\boldsymbol{\mathcal{H}}}$, having rank $Q_2(K - Q_1 L)$ with probability 1, and a matrix free to choose in the left null-space of $\breve{\boldsymbol{\mathcal{H}}}$, so $\breve{\boldsymbol{W}}_1$ is full-rank with probability 1 as long as $\mathbf{N}_{\breve{\boldsymbol{\mathcal{H}}}}$ is selected such that its rows span the whole left null-space of dimension $L - Q_2(K - Q_1 L)$ (with probability 1). We then substitute the expression of $\breve{\boldsymbol{W}}_1^{-1}$ obtained in (55) into the first equation from (54) and get

$$\begin{aligned} \breve{\boldsymbol{W}}_{i+1}^{-1} \breve{\boldsymbol{H}}_{1i,\mathrm{sq}}^{-1} \breve{\boldsymbol{H}}_{i+1,\mathrm{sq}} = \breve{\boldsymbol{H}}_{0i,\mathrm{sq}} + \Big(& \left[\breve{\boldsymbol{H}}_{01,\mathrm{r}} \quad \cdots \quad \breve{\boldsymbol{H}}_{0Q_2,\mathrm{r}} \right] \breve{\boldsymbol{\mathcal{H}}}^{\dagger} \\ & + \mathbf{I}_L - \breve{\boldsymbol{\mathcal{H}}} \breve{\boldsymbol{\mathcal{H}}}^{\dagger} - \mathbf{N}_{\breve{\boldsymbol{\mathcal{H}}}} - \left[\boldsymbol{\Theta}_1 \quad \cdots \quad \boldsymbol{\Theta}_{Q_2} \right] \breve{\boldsymbol{\mathcal{H}}}^{\dagger} \Big) \breve{\boldsymbol{H}}_{1i,\mathrm{sq}}, \end{aligned} \tag{56}$$

where we only need to check that the RHS is full-rank, since multiplying square randomly chosen blocks cannot reduce the rank (with probability 1). Reasoning as in the proof of Proposition 5, $(\mathbf{I}_L - \breve{\boldsymbol{\mathcal{H}}} \breve{\boldsymbol{\mathcal{H}}}^{\dagger})$ is a matrix in the null-space of $\breve{\boldsymbol{\mathcal{H}}}$ which gives rank $L - Q_2(K - Q_1 L)$, and $\mathbf{N}_{\breve{\boldsymbol{\mathcal{H}}}}$ can be selected so as to not destroy said rank. Then, the other two matrices multiplying $\breve{\boldsymbol{\mathcal{H}}}^{\dagger}$ can add the remaining rank. Furthermore, $\breve{\boldsymbol{H}}_{0i,\mathrm{sq}}$ only shares space with $\boldsymbol{\Theta}_i$ (the rest are made of different randomly chosen blocks), so it can at most reduce rank $(K - Q_1 L)$, which would be then compensated with the rank added by $\breve{\boldsymbol{H}}_{0i,\mathrm{r}}$, which does not share randomly chosen blocks with either $\breve{\boldsymbol{H}}_{0i,\mathrm{sq}}$ or $\boldsymbol{\Theta}_i$. Hence, we have proved that we can obtain full-rank $\breve{\boldsymbol{W}}_{i+1}^{-1}$, and this concludes the proof of Proposition 6.

References

[1] T. L. Marzetta, "Noncooperative cellular wireless with unlimited numbers of base station antennas," *IEEE Transactions on Wireless Communications*, vol. 9, no. 11, pp. 3590–3600, 2010.

[2] F. Rusek, D. Persson, B. K. Lau, *et al.*, "Scaling up MIMO: Opportunities and challenges with very large arrays," *IEEE Signal Processing Magazine*, vol. 30, no. 1, pp. 40–60, 2013.

[3] S. Hu, F. Rusek, and O. Edfors, "Beyond massive MIMO: The potential of data transmission with large intelligent surfaces," *IEEE Transactions on Signal Processing*, vol. 66, no. 10, pp. 2746–2758, 2018.

[4] S. Malkowsky *et al.*, "The world's first real-time testbed for massive MIMO: Design, implementation, and validation," *IEEE Access*, vol. 5, pp. 9073–9088, 2017.

[5] C. Shepard *et al.*, "Argos: Practical many-antenna base stations," in *Proceedings of the 18th Annual International Conference on Mobile Computing and Networking (Mobicom)*, Istanbul, Turkey, 2012, pp. 53–64.

[6] Q. Yang, X. Li, H. Yao, *et al.*, "Bigstation: Enabling scalable real-time signal processing in large MU-MIMO systems," in *ACM SIGCOMM'13*, ACM, 2013, pp. 399–410.

[7] J. Rodríguez Sánchez, F. Rusek, O. Edfors, and L. Liu, "Distributed and scalable uplink processing for LIS: Algorithm, architecture, and design trade-offs," *IEEE Transactions on Signal Processing*, vol. 70, pp. 2639–2653, 2022.

[8] A. Pizzo, A. d. J. Torres, L. Sanguinetti, and T. L. Marzetta, "Nyquist sampling and degrees of freedom of electromagnetic fields," *IEEE Transactions on Signal Processing*, vol. 70, pp. 3935–3947, 2022.

[9] H. Q. Ngo, A. Ashikhmin, H. Yang, E. G. Larsson, and T. L. Marzetta, "Cell-free massive MIMO versus small cells," *IEEE Transactions on Wireless Communications*, vol. 16, no. 3, pp. 1834–1850, 2017.

[10] E. Björnson and L. Sanguinetti, "Scalable cell-free massive MIMO systems," *IEEE Transactions on Communications*, vol. 68, no. 7, pp. 4247–4261, 2020.

[11] J. Zhang, E. Björnson, M. Matthaiou, D. W. K. Ng, H. Yang, and D. J. Love, "Prospective multiple antenna technologies for beyond 5G," *IEEE Journal on Selected Areas in Communications*, vol. 38, no. 8, pp. 1637–1660, 2020.

[12] J. Vidal Alegría, J. Huang, and F. Rusek, "Cell-free massive MIMO: Exploiting the WAX decomposition," in *ICASSP 2022 - 2022 IEEE International Conference on Acoustics, Speech and Signal Processing (ICASSP)*, 2022, pp. 5393–5397.

[13] J. R. Sánchez, J. Vidal Alegría, and F. Rusek, "Decentralized massive MIMO systems: Is there anything to be discussed?" In *2019 IEEE International Symposium on Information Theory (ISIT)*, 2019, pp. 787–791.

[14] F. Wiffen, W. H. Chin, and A. Doufexi, "Distributed dimension reduction for distributed massive MIMO C-RAN with finite fronthaul capacity," in *2021 55th Asilomar Conference on Signals, Systems, and Computers*, 2021, pp. 1228–1236.

[15] J. Vidal Alegría, F. Rusek, J. Rodríguez Sánchez, and O. Edfors, "Modular binary tree architecture for distributed large intelligent surface," in *ICASSP 2021 - 2021 IEEE International Conference on Acoustics, Speech and Signal Processing (ICASSP)*, 2021, pp. 4565–4569.

[16] K. Li, R. R. Sharan, Y. Chen, T. Goldstein, J. R. Cavallaro, and C. Studer, "Decentralized baseband processing for massive MU-MIMO systems," *IEEE Journal on Emerging and Selected Topics in Circuits and Systems*, vol. 7, no. 4, pp. 491–507, 2017.

[17] E. Bertilsson, O. Gustafsson, and E. G. Larsson, "A scalable architecture for massive MIMO base stations using distributed processing," in *2016 50th Asilomar Conference on Signals, Systems and Computers*, 2016, pp. 864–868.

[18] K. Li, J. McNaney, C. Tarver, *et al.*, "Design trade-offs for decentralized baseband processing in massive MU-MIMO systems," in *2019 53rd Asilomar Conference on Signals, Systems, and Computers*, 2019, pp. 906–912.

[19] M. Sarajlic, F. Rusek, J. R. Sanchez, L. Liu, and O. Edfors, "Fully decentralized approximate zero-forcing precoding for massive MIMO systems," *IEEE Wireless Communications Letters*, pp. 1–1, 2019.

[20] J. Rodríguez Sánchez, F. Rusek, O. Edfors, M. Sarajlić, and L. Liu, "Decentralized massive MIMO processing exploring Daisy-chain architecture and recursive algorithms," *IEEE Transactions on Signal Processing*, vol. 68, pp. 687–700, 2020.

[21] J. Vidal Alegría, J. R. Sánchez, F. Rusek, L. Liu, and O. Edfors, "Decentralized equalizer construction for large intelligent surfaces," in *2019 IEEE 90th Vehicular Technology Conference (VTC2019-Fall)*, 2019, pp. 1–6.

[22] Z. Zhang, H. Li, Y. Dong, X. Wang, and X. Dai, "Decentralized signal detection via expectation propagation algorithm for uplink massive MIMO systems," *IEEE Transactions on Vehicular Technology*, pp. 1–1, 2020.

[23] A. Amiri, S. Rezaie, C. N. Manchón, and E. de Carvalho, "Distributed receiver processing for extra-large MIMO arrays: A message passing approach," *IEEE Transactions on Wireless Communications*, vol. 21, no. 4, pp. 2654–2667, 2022.

[24] F. Riera-Palou and G. Femenias, "Decentralization issues in cell-free massive MIMO networks with zero-forcing precoding," in *2019 57th Annual Allerton Conference on Communication, Control, and Computing (Allerton)*, 2019, pp. 521–527.

[25] A. Amiri, C. N. Manchón, and E. de Carvalho, "Uncoordinated and decentralized processing in extra-large MIMO arrays," *IEEE Wireless Communications Letters*, vol. 11, no. 1, pp. 81–85, 2022.

[26] E. D. Carvalho, A. Ali, A. Amiri, M. Angjelichinoski, and R. W. Heath, "Non-stationarities in extra-large-scale massive MIMO," *IEEE Wireless Communications*, vol. 27, no. 4, pp. 74–80, 2020.

[27] J. V. Alegría, F. Rusek, and O. Edfors, "Trade-offs in decentralized multi-antenna architectures: The wax decomposition," *IEEE Transactions on Signal Processing*, vol. 69, pp. 3627–3641, 2021.

[28] T. M. Cover and J. A. Thomas, *Elements of Information Theory (Wiley Series in Telecommunications and Signal Processing)*. USA: Wiley-Interscience, 2006.

[29] D. J. MacKay and R. M. Neal, "Near shannon limit performance of low density parity check codes," *Electronics letters*, vol. 33, no. 6, pp. 457–458, 1997.

[30] J. Vidal Alegría and F. Rusek, "Enabling decentralized computation of the WAX decomposition," in *ICC 2022 - IEEE International Conference on Communications*, 2022, pp. 1–6.

[31] G. H. Hardy and E. M. Wright, *An Introduction to the Theory of Numbers*, Fourth. Oxford, 1975.

Paper VII

Increased Multiplexing Gain with Reconfigurable Surfaces: Simultaneous Channel Orthogonalization and Information Embedding

RS has been shown to be an effective solution for improving wireless communication links in general MU-MIMO setting. Current research efforts have been largely directed towards the study of RIS, which corresponds to an RS made of passive reconfigurable elements with only phase shifting capabilities. RIS constitutes a cost- and energy- efficient solution for increased beamforming gain since it allows to generate constructive interference towards desired directions, e.g., towards a BS. However, in many situations, multiplexing gain may have greater impact on the achievable transmission rates and number of simultaneously connected devices, while RIS has only been able to achieve minor improvements in this aspect. Recent work has proposed the use of alternative RS technologies, namely ARIS and FRIS, to achieve perfect orthogonalization of MU-MIMO channels, thus allowing for maximum multiplexing gain at reduced complexity. In this work we consider the use of ARIS and FRIS for simultaneously orthogonalizing a MU-MIMO channel, while embedding extra information in the orthogonalized channel. We show that the resulting achievable rates allow for full exploitation of the degrees of freedom in a MU-MIMO system with excess of BS antennas.

J. Vidal Alegría, J. Vieira, F. Rusek,
"Increased Multiplexing Gain with Reconfigurable Surfaces: Simultaneous Channel Orthogonalization and Information Embedding."
submitted to *IEEE GLOBECOM 2023*

1 Introduction

Massive MIMO [1] constitutes one of the main state-of-the-art solutions for BS implementation in 5G networks and beyond[2], [3]. This technology corresponds to an evolution of the traditional MU-MIMO [4] where the number of antennas at the BS grows large, leading to increased spatial resolution for effectively multiplexing UEs in the spatial domain [1], [5].

Commercial deployments of massive MIMO are already available [2], confirming the potential and maturity of this technology. Thus, the research community is now directing efforts towards exploring new disruptive technologies beyond massive MIMO. These technologies include LIS [6], which correspond to the natural evolution of massive MIMO by considering BSs consisting of whole walls covered with electromagnetially active material,[29] or RIS [7], [8], which consider surfaces made of passive elements with tunable reflecting coefficients, thus offering some control over propagation channel between two communication ends. This work considers some RS technologies, initially proposed in [9], which lie in between the concepts of LIS and RIS, but which are mainly inspired by RIS since they are used to adjust the propagation channel, i.e., they are not a BS technology like LIS.

Also known as IRS, RIS constitutes an attractive enabling technology for 6G [10] due to it cost- and energy-efficient implementation, which can still lead to important improvements in link connectivity [7], [8]. Much of the work on RIS rely on exploiting its impressive power scaling laws [8], which is a result of the increased beamforming gain associated to redirecting the reflected waves towards the intended directions. However, RIS has also been considered for improving multiplexing capabilities either directly, e.g., by improving the rank of the single-user MIMO system [11], or indirectly, e.g., by maximizing sum-rates in different settings [12], [13]. Moreover, in [9], two alternative RS technologies, namely ARIS and FRIS, are considered in a MU-MIMO scenario to achieve perfect channel orthogonalization without the need for RS amplification, i.e., leading to perfect multiplexing of UEs at the BS with reduced complexity. This work builds upon the results from [9], since we use the proposed RS technologies to achieve perfect channel orthogonalization while embedding information in the process.

The use of RIS as a low-complexity energy-efficient transmitter has also been considered in various works, with interesting proposals on how the RIS can modulate information [8]. These proposals combine the concept of symbiotic radio [14], where backscatter devices passively modulate information on incoming waves, with the RIS paradigm. For example, in [15], index-modulation is proposed for embedding information from the RIS to both modulated and

[29] As discussed in [6], practical implementations of LIS may consist of discrete antenna arrays, i.e., giving a sampled version of the continuous LIS.

unmodulated carrier signals, while in [16] an 8-PSK modulation is practically implemented using RIS.

On the other hand, it is also possible to use the RIS for simultaneously improving a communication link while embedding its own information. Some examples include [17], where a solution is proposed for employing RIS to achieve beamforming gains to a UE while transmitting information to the BS by turning on/off some of its elements—thus sacrificing RIS beamforming performance—or [18], which studies the capacity of a RIS-assisted single-user MIMO communication where the RIS selects its reflecting states from a predesigned codebook to embed information. However, the literature has failed to characterize the achievable multiplexing gain when using RS technologies for allowing effective multiplexing of UEs while simultaneously embedding information in the channels. To this end, we consider the RS technologies proposed in [9], ARIS and FRIS, to study an extra RS-to-BS communication link simultaneous to the UEs-to-BS over a MU-MIMO channel orthogonalized by the RS. We show that we can achieve maximum multiplexing gains, i.e., scaling with the total number of BS antennas, even when there is a large excess of BS antennas with respect to UEs.

The rest of the paper is organized as follows. Section 2 presents the system model, together with some background on how to achieve channel orthogonalization with ARIS and FRIS. In Section 3 we derive the achievable rates for simultaneous UE-BS and RS-BS communication with orthogonalized channels. Section 4 presents the derivation of the multiplexing gain associated to the achievable rates. Finally, Section 6 concludes the paper.

2 System model

Let us consider an uplink MU-MIMO scenario where K single-antenna UEs are transmitting to an M-antenna BS, with $M > K$, through a narrow-band channel with the aid of an RS with N reconfigurable elements, $N \gg M$. The $M \times 1$ received complex vector, $\boldsymbol{y}$, can be expressed as

$$\boldsymbol{y} = \boldsymbol{H}\boldsymbol{s} + \boldsymbol{n}, \tag{1}$$

where $\boldsymbol{H}$ is the $M \times K$ channel matrix, $\boldsymbol{s}$ is the $K \times 1$ vector of symbols transmitted by the users, and $\boldsymbol{n}$ is a zero-mean complex white Gaussian noise vector with sample variance N_0.[30] Considering that there exists a direct channel as well as a reflected channel through the RS, we can express the channel matrix as

$$\boldsymbol{H} = \boldsymbol{H}_0 + \boldsymbol{H}_1 \boldsymbol{\Theta} \boldsymbol{H}_2, \tag{2}$$

[30] We assume that the RS does not add correlated noise since it may not require relevant amplification [9].

where $\boldsymbol{H}_0$ corresponds to the $M \times K$ direct channel from the BS to the UEs, $\boldsymbol{H}_1$ and $\boldsymbol{H}_2$ correspond to the $M \times N$ channel from the BS to the RS and the $N \times K$ channel from the RS to the UEs, respectively, and $\boldsymbol{\Theta}$ is the matrix of reflection coefficients at the RS.

2.1 Background

We consider two types of RS systems proposed in [9], namely ARIS and FRIS, which give the reflection matrices

$$\boldsymbol{\Theta}_{\text{ARIS}} = \text{diag}\left(\alpha_1, \ldots, \alpha_N\right), \quad \alpha_i \in \mathbb{C} \ \ \forall i, \tag{3}$$

$$\boldsymbol{\Theta}_{\text{FRIS}} \in \mathbb{C}^{N \times N}. \tag{4}$$

Note the increased requirement in processing capabilities with respect to the widely studied RIS, which is typically modeled as an ARIS with the additional restriction $|\alpha_i|^2 = 1 \ \forall i$.

In [9] it is shown that both ARIS and FRIS can create a perfectly orthogonal channel, which is given by

$$\boldsymbol{H} = \sqrt{\beta}\widetilde{\boldsymbol{U}}, \tag{5}$$

where we restrict $\widetilde{\boldsymbol{U}}^{\text{H}}\widetilde{\boldsymbol{U}} = \mathbf{I}_K$. Equivalently, we can express

$$\widetilde{\boldsymbol{U}} = \boldsymbol{U}\begin{bmatrix} \mathbf{I}_K \\ \mathbf{0}_{(M-K)\times K} \end{bmatrix}, \tag{6}$$

where $\boldsymbol{U}$ is an $M \times M$ unitary matrix. Note that we do not lose generality in (6) by disregarding the multiplication from the right of another unitary matrix since said matrix could be absorbed by the first K rows of $\boldsymbol{U}$, leading to another unitary matrix.

From [9], we can obtain the desired orthogonal channel matrix $\boldsymbol{H} = \sqrt{\beta}\widetilde{\boldsymbol{U}}$ by selecting the reflection coefficients of the ARIS as

$$\boldsymbol{\alpha} = \boldsymbol{\mathcal{H}}_{12}^{\dagger}\text{vec}\left(\sqrt{\beta}\widetilde{\boldsymbol{U}} - \boldsymbol{H}_0\right), \tag{7}$$

where $\boldsymbol{\mathcal{H}}_{12}^{\dagger}$ corresponds to the right pseudo-inverse of the $MK \times N$ matrix $\boldsymbol{\mathcal{H}}_{12} = \left[\text{vec}(\boldsymbol{h}_{11}\boldsymbol{h}_{21}^{\text{T}}) \ \ \ldots \ \ \text{vec}(\boldsymbol{h}_{1N}\boldsymbol{h}_{2N}^{\text{T}})\right]$. The existence of $\boldsymbol{\mathcal{H}}_{12}^{\dagger}$ gives the conditions $N > MK$, together with full-rank $\boldsymbol{\mathcal{H}}_{12}$, for appropiate operation of the ARIS. For the FRIS, the same channel would be achieved by selecting the reflection matrix as

$$\boldsymbol{\Theta}_{\text{FRIS}} = \boldsymbol{H}_1^{\dagger}\left(\sqrt{\beta}\widetilde{\boldsymbol{U}} - \boldsymbol{H}_0\right)\boldsymbol{H}_2^{\dagger}, \tag{8}$$

where $\boldsymbol{H}_1^\dagger$ is the right pseudo-inverse of $\boldsymbol{H}_1$ and $\boldsymbol{H}_2^\dagger$ is the left pseudo-inverse of $\boldsymbol{H}_2$. The existence of $\boldsymbol{H}_1^\dagger$ and $\boldsymbol{H}_2^\dagger$ gives the conditions $N > \min(M, K)$, together with full-rank $\boldsymbol{H}_1$ and $\boldsymbol{H}_2$, for appropriate operation of the FRIS. Note that we can also achieve any arbitrary channel using ARIS or FRIS by substituting $\sqrt{\beta}\widetilde{\boldsymbol{U}}$ in (7) or (8) with the desired channel matrix, respectively. However, this work restricts to the case where the desired channel is given by (5) due to the beneficial properties of orthogonal channels in MU-MIMO [9], [19].

3 Achievable rates for simultaneous RS-plus-UEs transmission

In Section 2, we show that ARIS and FRIS can be configured so as to generate arbitrary channel matrices. Let us, however, maintain the channel orthogonality constraint, i.e., $\boldsymbol{H}$ is restricted to (5) with $\widetilde{\boldsymbol{U}}$ given in (6), since this corresponds to the most desirable channel structure for spatially multiplexing the UEs at reduced complexity, as discussed in [9]. Note that we still have freedom in selecting $\boldsymbol{U}$ as long as it is unitary. We propose to use this freedom for embedding extra information at the RS, hence opening a new communication link between the RS and the BS which comes at essentially no cost.

In order to understand the potential of embedding extra information in the RS, we will compute $\mathcal{I}\big(\boldsymbol{y}; \boldsymbol{s}, \widetilde{\boldsymbol{U}}\big)$, i.e., the mutual information between the received vector, and the RS and UEs symbols for some input distribution. This corresponds to the rate at which the RS and the UEs can simultaneously transmit information to the BS over an orthogonalized channel. However, assuming that there is no cooperation between the UEs and the RS, the information that can be transmitted by the UEs is upper bounded by $\mathcal{I}\big(\boldsymbol{y}; \boldsymbol{s}|\widetilde{\boldsymbol{U}}\big)$, i.e., the mutual information of the corresponding orthogonal MIMO channel with perfect-CSI, so $\mathcal{I}\big(\boldsymbol{y}; \boldsymbol{s}, \widetilde{\boldsymbol{U}}\big)$ would correspond the achievable sum-rate for the UEs-plus-RS data. From the chain rule of mutual information we have

$$\mathcal{I}\big(\boldsymbol{y}; \boldsymbol{s}, \widetilde{\boldsymbol{U}}\big) = \mathcal{I}\big(\boldsymbol{y}; \widetilde{\boldsymbol{U}}\big) + \mathcal{I}\big(\boldsymbol{y}; \boldsymbol{s}|\widetilde{\boldsymbol{U}}\big), \tag{9}$$

so we can always have a non-negative information gain, given by $\mathcal{I}\big(\boldsymbol{y}; \widetilde{\boldsymbol{U}}\big)$, with respect to the baseline for common MIMO systems, corresponding to $\mathcal{I}\big(\boldsymbol{y}; \boldsymbol{s}|\widetilde{\boldsymbol{U}}\big)$. An interpretation of (9) is that we can embed information at the RS by making use of the freedom to select $\widetilde{\boldsymbol{U}}$, which can then be extracted from $\boldsymbol{y}$ with arbitrarily small error as long as the respective information rate is below $\mathcal{I}\big(\boldsymbol{y}; \widetilde{\boldsymbol{U}}\big)$ [20].[31] Assuming the UEs transmit Gaussian symbols,

[31] Changing the variable order in the chain rule from (9) gives $\mathcal{I}\big(\boldsymbol{y}; \boldsymbol{s}, \widetilde{\boldsymbol{U}}\big) = \mathcal{I}\big(\boldsymbol{y}; \boldsymbol{s}\big) + \mathcal{I}\big(\boldsymbol{y}; \widetilde{\boldsymbol{U}}|\boldsymbol{s}\big)$, which means that we could sacrifice UE rate to achieve maximum RS rate,

$\boldsymbol{s} \sim \mathcal{CN}(\mathbf{0}_{K\times 1}, E_s\mathbf{I}_K)$, which corresponds to the input distribution achieving capacity for the perfect-CSI case, $\mathcal{I}\big(\boldsymbol{y};\boldsymbol{s}|\widetilde{\boldsymbol{U}}\big)$ is maximized and leads to the famous log-det formula [19], which for the orthogonal channel is given by

$$\mathcal{I}\big(\boldsymbol{y};\boldsymbol{s}|\widetilde{\boldsymbol{U}}\big) = K\log\left(1+\frac{\beta E_s}{N_0}\right). \tag{10}$$

It would then remain to compute $\mathcal{I}\big(\boldsymbol{y};\widetilde{\boldsymbol{U}}\big)$, which can be expressed as

$$\mathcal{I}\big(\boldsymbol{y};\widetilde{\boldsymbol{U}}\big) = \mathfrak{h}(\boldsymbol{y}) - \mathfrak{h}\big(\boldsymbol{y}|\widetilde{\boldsymbol{U}}\big). \tag{11}$$

The conditional differential entropy $\mathfrak{h}\big(\boldsymbol{y}|\widetilde{\boldsymbol{U}}\big)$ is well defined since we have $\boldsymbol{y}|\widetilde{\boldsymbol{U}} \sim \mathcal{CN}\big(\mathbf{0}_{M\times 1}, \beta E_s\widetilde{\boldsymbol{U}}\widetilde{\boldsymbol{U}}^{\mathrm{H}} + N_0\mathbf{I}_M\big)$, which gives

$$\begin{aligned}\mathfrak{h}\big(\boldsymbol{y}|\widetilde{\boldsymbol{U}}\big) =& \log\det\Big(\pi\exp(1)\big(\beta E_s\widetilde{\boldsymbol{U}}\widetilde{\boldsymbol{U}}^{\mathrm{H}} + N_0\mathbf{I}_M\big)\Big)\\ =& K\log\left(\pi\exp(1)(\beta E_s + N_0)\right)\\ &+ (M-K)\log\left(\pi\exp(1)N_0\right),\end{aligned} \tag{12}$$

where we have used (6) and extracted the unitary matrix from the determinant to reach the final simplified expression. On the other hand, $\mathfrak{h}(\boldsymbol{y})$ is given by

$$\mathfrak{h}(\boldsymbol{y}) = -\mathbb{E}\{\log(p(\boldsymbol{y}))\}, \tag{13}$$

which may be computed through Monte-Carlo simulations by averaging over random realizations of $\boldsymbol{y}$. However, in order to compute (13) we first need to specify an input distribution for $\widetilde{\boldsymbol{U}}$ and then characterize $p(\boldsymbol{y})$, the corresponding probability distribution function (PDF) of $\boldsymbol{y}$ from said input distribution of $\widetilde{\boldsymbol{U}}$. The most meaningful input distribution for $\widetilde{\boldsymbol{U}}$ is for it to be isotropically distributed in the unitary subspace where it lies, i.e., $\widetilde{\boldsymbol{U}}$ would be constructed by (6) with $\boldsymbol{U}$ uniformly distributed in the unitary space $\mathcal{U}(M)$. Furthermore, works like [21] motivate the use of isotropically distributed random matrices since they achieve capacity under Rayleigh fading scenarios, while our work considers the multiplication of the information transmitting orthogonal channel with a Gaussian vector, which is the vector equivalent of a Rayleigh fading channel. The following proposition gives the expression for $p(\boldsymbol{y})$ with isotropically distributed $\widetilde{\boldsymbol{U}}$.

Proposition 7 *Let $\boldsymbol{y}$ be the $M\times 1$ random vector from* (1)*, where we have $\boldsymbol{s} \sim \mathcal{CN}(\mathbf{0}_{K\times 1}, E_s\mathbf{I}_K)$, and $\boldsymbol{n} \sim \mathcal{CN}(\mathbf{0}_{M\times 1}, N_0\mathbf{I}_M)$. Assume $\boldsymbol{H}$ is given by*

$\mathcal{I}\big(\boldsymbol{y};\widetilde{\boldsymbol{U}}|\boldsymbol{s}\big)$. However, this has lower practicality since the UEs are likely have more information to transfer.

(5), *where* $\widetilde{\boldsymbol{U}}$ *is defined in* (6) *for an isotropically distributed random unitary matrix* $\boldsymbol{U}$. *We can then express the PDF of* $\boldsymbol{y}$ *as*

$$p(\boldsymbol{y}) = \exp\left(-\frac{\|\boldsymbol{y}\|^2}{N_0}\right) \frac{(M-1)!}{(-1)^{K(M-K)}\big(\pi(\beta E_s + N_0)\big)^K} \times \frac{\det(\boldsymbol{Z})}{(\pi N_0)^{M-K}(-\gamma\|\boldsymbol{y}\|^2)^{M-1} \prod_{k=1}^{K-1} k! \prod_{n=1}^{M-K-1} n!}, \tag{14}$$

where $\gamma = \frac{\beta E_s}{N_0(\beta E_s + N_0)}$, *and* $\boldsymbol{Z}$ *is an* $M \times M$ *matrix whose* (i,j)*th entry is given by*

$$[\boldsymbol{Z}]_{i,j} = \begin{cases} (\gamma\|\boldsymbol{y}\|^2)^{j-1}\exp(\gamma\|\boldsymbol{y}\|^2), & j \le K,\ i = 1 \\ (\gamma\|\boldsymbol{y}\|^2)^{\tilde{j}-1}, & K < j \le M,\ i = 1 \\ \frac{(\tilde{i}-1)!}{(\tilde{i}-j)!}, & j \le K,\ \tilde{i} \ge j \\ (\tilde{i}-1)!, & K < j \le M,\ \tilde{i} = \tilde{j} \\ 0, & \text{otherwise,} \end{cases} \tag{15}$$

with $\tilde{j} = j - K$, *and* $\tilde{i} = i - 1$.

Proof *See Appendix A* □

Using Proposition 7 we can substitute $p(\boldsymbol{y})$, given by (14), into (13), and compute the expected value through Monte-Carlo simulations to obtain $\mathfrak{h}(\boldsymbol{y})$. This way we can characterize $\mathcal{I}\big(\boldsymbol{y};\widetilde{\boldsymbol{U}}\big)$, hence characterizing the potential of simultaneous RS-BS and UEs-to-BS communication through orthogonalized MU-MIMO channels.

4 Increased multiplexing gain

In the previous section we reached a closed-form expression for $p(\boldsymbol{y})$, i.e., the PDF of the received vector $\boldsymbol{y}$ for an orthogonal channel with isotropically distributed $\widetilde{\boldsymbol{U}}$. The obtained $p(\boldsymbol{y})$ is fairly complex, so finding a closed-form expression for $\mathcal{I}\big(\boldsymbol{y};\boldsymbol{s},\widetilde{\boldsymbol{U}}\big)$ becomes extremely challenging. However, we may simplify this expression by considering the asymptotic regime, which may allow the characterization of the multiplexing gain achieved by such a system. Let us thus focus on the high-SNR regime, i.e., $\frac{E_s}{N_0} \to \infty$. The following proposition gives the multiplexing gain associated to (9).

Proposition 8 *Let us have the same input distribution assumptions as in Proposition 7 such that* $\boldsymbol{y}$ *is distributed according to the respective* $p(\boldsymbol{y})$. *The*

multiplexing gain associated to $\mathcal{I}\big(\boldsymbol{y};\widetilde{\boldsymbol{U}}\big)$*, i.e., the asymptotic pre-log factor for* $\frac{E_s}{N_0} \to \infty$*, is given by* $(M-K)$*. Furthermore, the overall multiplexing gain associated to* $\mathcal{I}\big(\boldsymbol{y};\boldsymbol{s},\widetilde{\boldsymbol{U}}\big)$ *is given by* M*.*

Proof *Without loss of generality, let us consider the high-SNR regime* $\frac{E_s}{N_0} \to \infty$ *by having fixed* E_s *and* $N_0 \to 0$*. We can then find the following limit*

$$\lim_{N_0\to 0} p(\boldsymbol{y}) = \frac{(M-1)!\|\boldsymbol{y}\|^{2(K-M)}}{(-1)^{(K+1)M-K^2-1}(\beta E_s)^K} \times \frac{\det(\tilde{\boldsymbol{Z}})}{\pi^M \prod_{k=1}^{K} k! \prod_{n=1}^{M-K-1} n!}, \tag{16}$$

where the last $M-1$ *rows of* $\tilde{\boldsymbol{Z}}$ *coincide with* $\boldsymbol{Z}$ *from* (15)*, while* $[\tilde{\boldsymbol{Z}}]_{1,j} = \delta_{jK}$*, i.e., it is independent of* $\|\boldsymbol{y}\|^2$*. Thus, we can use it in* (13) *to find the limit*

$$\lim_{N_0\to 0} \mathfrak{h}(\boldsymbol{y}) = (M-K)\log(\beta E_s) + K\log(\beta E_s) + c_1, \tag{17}$$

where c_1 *is a constant independent of* E_s*, and thus of SNR. We can then plug* (17) *into* (11)*, which using* (12) *leads to*

$$\mathcal{I}\big(\boldsymbol{y};\widetilde{\boldsymbol{U}}\big)\Big|_{N_0\to 0} = (M-K)\log\Big(\frac{\beta E_s}{N_0} + c_2\Big) + c_3, \tag{18}$$

where c_2 *and* c_3 *are fixed constants independent of the SNR. The pre-log factor in* (18) *gives the multiplexing gain achieved by the RS-to-BS data transmission. By summing it to the pre-log factor* K *from* (10)*, i.e., considering* (9)*, we obtain the overall multiplexing gain* M*. A more detailed proof may be included in the extended version, e.g., with extra steps to reach expressions like* (16)*.* □

Proposition 8 shows that the considered RSs can exploit the available degrees of freedom for transmitting to the BS while a simultaneous UEs-to-BS communication is established through a desirable orthogonal channel. Furthermore, the total multiplexing gain of such a communication scheme is maximum, i.e., we could potentially transmit a number of information streams equal to the total number of BS antennas, thus taking full advantage of systems with a large excess of BS antennas, e.g., massive MIMO, LIS, cell-free massive MIMO.

5 Numerical results

In Fig. 1 are shown the achievable UEs-plus-RS sum-rates, given by $\mathcal{I}\big(\boldsymbol{y};\boldsymbol{s},\widetilde{\boldsymbol{U}}\big)$ with isotropically distributed $\widetilde{\boldsymbol{U}}$, for different values for M. These rates have

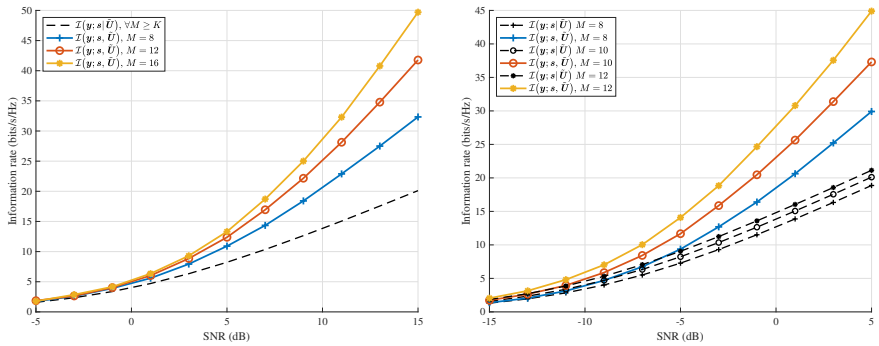

Figure 1: Information rates with $K = 4$ UEs, and channel gain $\beta = 1$ (left) and $\beta = M$ (right).

been computed using (9), (10) and (11), where $\mathfrak{h}(\boldsymbol{y})$ has been computed through Mote-Carlo simulations considering (13) with $p(\boldsymbol{y})$ given by Proposition 7. As baseline, we may take the UEs sum rate for perfect CSI knowledge with an orthogonal channel, corresponding to $\mathcal{I}\big(\boldsymbol{y};,\boldsymbol{s}|\widetilde{\boldsymbol{U}}\big)$, i.e., given in closed-form by (10). Note that, since we consider perfectly orthogonal channels $\widetilde{\boldsymbol{U}}$, the UE sum rate can be shared equally among UEs without interference. In Fig. 1 (left) we ignore the possible array gains by fixing $\beta = 1$, hence the lack of dependency on M of $\mathcal{I}\big(\boldsymbol{y};,\boldsymbol{s}|\widetilde{\boldsymbol{U}}\big)$, while in Fig. 1 (right) we have $\beta = M$ to account for the respective array gain. Considering (9), the gap between $\mathcal{I}\big(\boldsymbol{y};\boldsymbol{s},\widetilde{\boldsymbol{U}}\big)$ and $\mathcal{I}\big(\boldsymbol{y};\boldsymbol{s}|\widetilde{\boldsymbol{U}}\big)$ corresponds to $\mathcal{I}\big(\boldsymbol{y};\widetilde{\boldsymbol{U}}\big)$, i.e., the achievable rate at which the the RS can communicate with the BS while allowing maximum transmission rate for the UEs. The results show that the extra link between the RS and the BS can exploit the $M - K$ degrees of freedom of the channel to increase the overall multiplexing gain of the transmission, which seems to scale with M instead of with K as for common MU-MIMO uplink transmissions [19]. Thus, these numerical results confirm the asymptotic study from the previous section.

6 Conclusions

We have considered the use of two RS technologies, namely ARIS and FRIS, for simultaneous communication of UEs and RS data to a MU-MIMO BS. The main advantage of these RS technologies is that they can achieve perfectly orthogonal channels, thus allowing for perfect multiplexing of UEs in the spatial domain at reduced complexity. We have proposed employing the freedom in the desirable channel selection, which should only fulfill the orthogonality constraint, to embed extra information from the RS to the BS at essentially

no cost. We have computed the mutual information of such a framework, and showed that the resulting multiplexing gain allows to exploit all the available degrees of freedom from the excess of BS antennas.

Appendix A: Proof of Proposition 7

Given (1), using straightforward probabilistic identities, we can express the PDF of $\boldsymbol{y}$ as

$$p(\boldsymbol{y}) = \mathbb{E}_{\boldsymbol{H}} \left\{ \int_{\boldsymbol{s}\in\mathbb{C}^K} p(\boldsymbol{y}|\boldsymbol{H},\boldsymbol{s}) p(\boldsymbol{s}) d\boldsymbol{s} \right\}. \tag{19}$$

Considering the assumptions $\boldsymbol{s} \sim \mathcal{CN}(\boldsymbol{0}_{K\times 1}, E_s \mathbf{I}_K)$ and $\boldsymbol{n} \sim \mathcal{CN}(\boldsymbol{0}_{M\times 1}, N_0 \mathbf{I}_M)$ we have

$$p(\boldsymbol{s}) = \frac{1}{(\pi E_s)^K} \exp\left(-\frac{\|\boldsymbol{s}\|^2}{E_s} \right), \tag{20}$$

$$p(\boldsymbol{y}|\boldsymbol{H},\boldsymbol{s}) = \frac{1}{(\pi N_0)^M} \exp\left(-\frac{\|\boldsymbol{y}-\boldsymbol{H}\boldsymbol{s}\|^2}{N_0} \right), \tag{21}$$

which can be substituted in (19). Given the singular value decomposition (SVD) of the channel matrix, $\boldsymbol{H} = \boldsymbol{U}\boldsymbol{\Sigma}\boldsymbol{V}^{\mathrm{H}}$,[32] if we expand the norms and perform some matrix manipulations over (19) (with (20) and (21)) we reach

$$\begin{aligned} p(\boldsymbol{y}) = \frac{\exp\left(-\frac{\|\boldsymbol{y}\|^2}{N_0}\right)}{(\pi E_s)^K (\pi N_0)^M} \quad & \mathbb{E}_{\boldsymbol{H}} \left\{ \int_{\tilde{\boldsymbol{s}}\in\mathbb{C}^K} \exp\left(-\frac{\|\tilde{\boldsymbol{s}}\|^2}{E_s} \right) \right. \\ & \left. \times \exp\left(-\frac{\tilde{\boldsymbol{s}}^{\mathrm{H}} \boldsymbol{\Lambda} \tilde{\boldsymbol{s}}}{N_0} \right) \exp\left(\frac{2}{N_0} \Re\{ \boldsymbol{y}^{\mathrm{H}} \boldsymbol{U} \boldsymbol{\Sigma} \tilde{\boldsymbol{s}} \} \right) d\tilde{\boldsymbol{s}} \right\}, \end{aligned} \tag{22}$$

where $\boldsymbol{\Lambda} = \boldsymbol{\Sigma}^{\mathrm{H}}\boldsymbol{\Sigma}$ is the diagonal matrix with the eigenvalues of $\boldsymbol{H}^{\mathrm{H}}\boldsymbol{H}$, and where we have considered the change of integration variable to $\tilde{\boldsymbol{s}} = \boldsymbol{V}\boldsymbol{s}$. Further expanding the norms and multiplications leads to

$$\begin{aligned} p(\boldsymbol{y}) = & \frac{\exp\left(-\frac{\|\boldsymbol{y}\|^2}{N_0}\right)}{(\pi E_s)^K (\pi N_0)^M} \, \mathbb{E}_{\boldsymbol{H}} \left\{ \prod_{k=1}^{K} \int_{\tilde{s}_k\in\mathbb{C}} \exp\Big(\right. \\ & \left. - \frac{(E_s\lambda_k + N_0)|\tilde{s}_k|^2}{E_s N_0} + \frac{2}{N_0} \Re\{ \boldsymbol{y}^{\mathrm{H}} \boldsymbol{u}_k \sigma_k \tilde{s}_k \} \Big) d\tilde{s}_k \right\}, \end{aligned} \tag{23}$$

[32] Note that, assuming (5), the SVD of $\boldsymbol{H}$ is given by (6) after including the scaling of the singular values $\sqrt{\beta}$.

where λ_k is the kth eigenvalue of $\boldsymbol{H}^{\mathrm{H}}\boldsymbol{H}$, $\boldsymbol{u}_k$ is the kth column of $\boldsymbol{U}$, and $\sigma_k = \sqrt{\lambda_k}$ is the kth singular value of $\boldsymbol{H}$. The integrals from (23) can be solved in closed form by considering the real and imaginary part of each $\tilde{s}_k$ (see [22, Entry 3.323.2]). Thus, after integrating and performing trivial operations we get

$$p(\boldsymbol{y}) = \frac{\exp\left(-\frac{\|\boldsymbol{y}\|^2}{N_0}\right)}{\pi^K (\pi N_0)^{M-K}} \mathbb{E}_{\boldsymbol{H}} \left\{ \prod_{k=1}^{K} \frac{1}{\lambda_k E_s + N_0} \times \exp\left(\frac{\lambda_k E_s \|\boldsymbol{u}_k \boldsymbol{y}^{\mathrm{H}}\|^2}{N_0(\lambda_k E_s + N_0)} \right) \right\}. \tag{24}$$

Given the orthogonality constraint on the channel (5) with (6), we can substitute the eigenvalues $\lambda_k = \beta$ for $k \leq K$, and eigenvectors $\boldsymbol{u}_k$, directly corresponding to the kth row of $\widetilde{\boldsymbol{U}}$ from (5), which is itself a sub-matrix (6) of $\boldsymbol{U}$ hereby assumed to be uniformly distributed on the unitary space $\mathcal{U}(M)$. By substituting in (24) and regrouping we reach

$$p(\boldsymbol{y}) = \frac{\exp\left(-\frac{\|\boldsymbol{y}\|^2}{N_0}\right)}{\big(\pi(\beta E_s + N_0)\big)^K (\pi N_0)^{M-K}} \times \mathbb{E}_{\boldsymbol{U}} \left\{ \exp\left(\frac{\beta E_s \|\widetilde{\boldsymbol{U}} \boldsymbol{y}^{\mathrm{H}}\|^2}{N_0(\beta E_s + N_0)} \right) \right\}, \tag{25}$$

which, after expanding the expectation and operating, leads to

$$p(\boldsymbol{y}) = \frac{\exp\left(-\frac{\|\boldsymbol{y}\|^2}{N_0}\right)}{\big(\pi(\beta E_s + N_0)\big)^K (\pi N_0)^{M-K}} \int_{\boldsymbol{U} \in \mathcal{U}(M)} p(\boldsymbol{U}) \times \exp\Big(\mathrm{trace}\Big(\gamma \boldsymbol{y}\boldsymbol{y}^{\mathrm{H}} \boldsymbol{U} \widetilde{\boldsymbol{I}} \boldsymbol{U}^{\mathrm{H}}\Big)\Big)\, d\boldsymbol{U}, \tag{26}$$

where $p(\boldsymbol{U})$ is the PDF of an isotropically distributed unitary matrix, and where we have defined

$$\gamma = \frac{\beta E_s}{N_0(\beta E_s + N_0)} \tag{27}$$

$$\widetilde{\boldsymbol{I}} = \mathrm{diag}\left(\begin{bmatrix} \mathbf{1}_{K\times 1} \\ \mathbf{0}_{(M-K)\times 1} \end{bmatrix} \right). \tag{28}$$

The integral (26) has closed-form solution [23], [24], giving

$$p(\boldsymbol{y}) = \frac{\exp\left(-\frac{\|\boldsymbol{y}\|^2}{N_0}\right)}{\big(\pi(\beta E_s + N_0)\big)^K (\pi N_0)^{M-K}} \frac{\prod_{m=1}^{M-1} m! \det(\boldsymbol{G})}{\Delta(\gamma \boldsymbol{y}\boldsymbol{y}^{\mathrm{H}})\Delta(\widetilde{\boldsymbol{I}})}, \tag{29}$$

where $\Delta(\boldsymbol{A}) = \prod_{1 \le i < j \le T}(\lambda_j(\boldsymbol{A}) - \lambda_i(\boldsymbol{A}))$ corresponds to the Vandermonde determinant of the decreasing eigenvalues $\lambda_i(\boldsymbol{A})$ of some $T \times T$ positive semi-definite matrix $\boldsymbol{A}$, and where the (i,j)th entry of $\boldsymbol{G}$ is given by

$$[\boldsymbol{G}]_{i,j} = \exp\left(\lambda_i(\gamma \boldsymbol{y}\boldsymbol{y}^{\mathrm{H}})\lambda_j(\widetilde{\boldsymbol{I}})\right). \tag{30}$$

Given the rank deficiency of $\widetilde{\boldsymbol{I}}$, which has K non-zero eigenvalues $\lambda_j(\widetilde{\boldsymbol{I}}) = 1$ for $j = 1, \dots K$, as well as of $\gamma \boldsymbol{y}\boldsymbol{y}^{\mathrm{H}}$, which has only one non-zero eigenvalue $\lambda_1(\gamma \boldsymbol{y}\boldsymbol{y}^{\mathrm{H}}) = \gamma \|\boldsymbol{y}\|^2$, the right quotient in (29) evaluates to an indeterminate form $0/0$. Let us define $\boldsymbol{G}$ in function form as $\boldsymbol{G} = \{g_i(a_j)\}$ for $1 \le i, j \le M$, where $a_j = \lambda_j(\widetilde{\boldsymbol{I}})$, which leads to

$$g_i(x) = \exp\left(\lambda_i(\gamma \boldsymbol{y}\boldsymbol{y}^{\mathrm{H}})x\right). \tag{31}$$

We can then apply [25, Lemma 2] to find the limit

$$\lim_{\substack{a_1,\dots,a_K \to 1 \\ a_{K+1},\dots,a_M \to 0}} \frac{\det(\{g_i(a_j)\})}{\Delta(\widetilde{\boldsymbol{I}})} = \frac{\det(\boldsymbol{F})}{(-1)^{K(M-K)} \prod_{k=1}^{K-1} k! \prod_{n=1}^{M-K-1} n!}, \tag{32}$$

where the ith column of $\boldsymbol{F}$ is given by

$$[\boldsymbol{F}]_{i,:} = \left[g_i(1) \;\; \cdots \;\; g_i^{(K-1)}(1) \;\; g_i(0) \;\; \cdots \;\; g_i^{(M-K-1)}(0)\right]. \tag{33}$$

Note that $g_i^{(n)}(a)$ corresponds to nth derivative of $g_i(x)$ at $x = a$, which is given by

$$g_i^{(n)}(x) = \lambda_i^{n-1}(\gamma \boldsymbol{y}\boldsymbol{y}^{\mathrm{H}}) \exp\left(\lambda_i(\gamma \boldsymbol{y}\boldsymbol{y}^{\mathrm{H}})x\right). \tag{34}$$

After substituting (34) into (33), we can also define $\boldsymbol{F}$ in function form as $\boldsymbol{F} = \{f_j(b_i)\}$ for $1 \le i, j \le M$, where $b_i = \lambda_i(\gamma \boldsymbol{y}\boldsymbol{y}^{\mathrm{H}}))$, leading to

$$f_j(x) = \begin{cases} x^{j-1}\exp(x), & j \le K \\ x^{j-1}, & K < j \le M, \end{cases} \tag{35}$$

with $\tilde{j} = j - K$. We can then apply [25, Lemma 2] again to find the limit

$$\lim_{\substack{b_1 \to \gamma \|\boldsymbol{y}\|^2 \\ b_2, \ldots, b_M \to 0}} \frac{\det(\{f_j(b_i)\})}{\Delta(\gamma \boldsymbol{y}\boldsymbol{y}^{\mathrm{H}})} = \frac{\det(\boldsymbol{Z})}{(-\gamma \|\boldsymbol{y}\|^2)^{M-1} \prod_{q=1}^{M-2} q!}, \tag{36}$$

where the jth column of $\boldsymbol{Z}$ is given by

$$[\boldsymbol{Z}]_{:,j} = \left[f_j(\gamma \|\boldsymbol{y}\|^2) \;\; f_j(0) \;\; f_j' \;\; \cdots \;\; f_j^{(M-2)}(0) \right]^{\mathrm{T}}, \tag{37}$$

with the nth derivative of $f_j(x)$ given by

$$f_j^{(n)}(x) = \begin{cases} \sum_{k=0}^{n} \binom{n}{k} \prod_{l=1}^{n-k} x^{j-n+k-1} \exp(x), & j \leq K \\ \prod_{l=1}^{n} (\tilde{j} - l) x^{\tilde{j}-n-1} \exp(x), & K < j \leq M, \end{cases} \tag{38}$$

Substituting (38) in (37) and operating leads to (15). Furthermore, substituting (29) with the obtained limits leads directly to (14), which concludes the proof.

References

[1] T. L. Marzetta, "Noncooperative cellular wireless with unlimited numbers of base station antennas," *IEEE Transactions on Wireless Communications*, vol. 9, no. 11, pp. 3590–3600, 2010.

[2] E. Björnson, L. Sanguinetti, H. Wymeersch, J. Hoydis, and T. L. Marzetta, "Massive MIMO is a reality—what is next?: Five promising research directions for antenna arrays," *Digital Signal Processing*, vol. 94, pp. 3–20, 2019, Special Issue on Source Localization in Massive MIMO.

[3] T. Van Chien and E. Björnson, "Massive MIMO communications," in *5G Mobile Communications*, W. Xiang, K. Zheng, and X. S. Shen, Eds., Cham: Springer International Publishing, 2017, pp. 77–116.

[4] N. Jindal, "MIMO broadcast channels with finite-rate feedback," *IEEE Transactions on Information Theory*, vol. 52, no. 11, pp. 5045–5060, 2006.

[5] F. Rusek, D. Persson, B. K. Lau, *et al.*, "Scaling up MIMO: Opportunities and challenges with very large arrays," *IEEE Signal Processing Magazine*, vol. 30, no. 1, pp. 40–60, 2013.

[6] S. Hu, F. Rusek, and O. Edfors, "Beyond massive MIMO: The potential of data transmission with large intelligent surfaces," *IEEE Transactions on Signal Processing*, vol. 66, no. 10, pp. 2746–2758, 2018.

[7] C. Huang, A. Zappone, G. C. Alexandropoulos, M. Debbah, and C. Yuen, "Reconfigurable intelligent surfaces for energy efficiency in wireless communication," *IEEE Transactions on Wireless Communications*, vol. 18, no. 8, pp. 4157–4170, 2019.

[8] E. Basar, M. Di Renzo, J. De Rosny, M. Debbah, M.-S. Alouini, and R. Zhang, "Wireless communications through reconfigurable intelligent surfaces," *IEEE Access*, vol. 7, pp. 116 753–116 773, 2019.

[9] J. Vidal Alegría and F. Rusek, "Channel orthogonalization with reconfigurable surfaces," in *2022 IEEE Globecom Workshops (GC Wkshps)*, 2022, pp. 37–42.

[10] M. Z. Chowdhury, M. Shahjalal, S. Ahmed, and Y. M. Jang, "6G wireless communication systems: Applications, requirements, technologies, challenges, and research directions," *IEEE Open Journal of the Communications Society*, vol. 1, pp. 957–975, 2020.

[11] O. Ozdogan, E. Björnson, and E. G. Larsson, "Using intelligent reflecting surfaces for rank improvement in MIMO communications," in *ICASSP 2020 - 2020 IEEE International Conference on Acoustics, Speech and Signal Processing (ICASSP)*, 2020, pp. 9160–9164.

[12] H. Guo, Y.-C. Liang, J. Chen, and E. G. Larsson, "Weighted sum-rate maximization for reconfigurable intelligent surface aided wireless networks," *IEEE Transactions on Wireless Communications*, vol. 19, no. 5, pp. 3064–3076, 2020.

[13] Y. Zhang, C. Zhong, Z. Zhang, and W. Lu, "Sum rate optimization for two way communications with intelligent reflecting surface," *IEEE Communications Letters*, vol. 24, no. 5, pp. 1090–1094, 2020.

[14] R. Long, Y.-C. Liang, H. Guo, G. Yang, and R. Zhang, "Symbiotic radio: A new communication paradigm for passive internet of things," *IEEE Internet of Things Journal*, vol. 7, no. 2, pp. 1350–1363, 2020.

[15] E. Basar, "Reconfigurable intelligent surface-based index modulation: A new beyond MIMO paradigm for 6G," *IEEE Transactions on Communications*, vol. 68, no. 5, pp. 3187–3196, 2020.

[16] W. Tang, J. Y. Dai, M. Chen, *et al.*, "Programmable metasurface-based rf chain-free 8PSK wireless transmitter," *Electronics Letters*, vol. 55, no. 7, pp. 417–420, 2019. eprint: `https://ietresearch.onlinelibrary.wiley.com/doi/pdf/10.1049/el.2019.0400`.

[17] W. Yan, X. Yuan, and X. Kuai, "Passive beamforming and information transfer via large intelligent surface," *IEEE Wireless Communications Letters*, vol. 9, no. 4, pp. 533–537, 2020.

[18] J. Ye, S. Guo, S. Dang, B. Shihada, and M.-S. Alouini, "On the capacity of reconfigurable intelligent surface assisted MIMO symbiotic communications," *IEEE Transactions on Wireless Communications*, vol. 21, no. 3, pp. 1943–1959, 2022.

[19] A. Paulraj, R. Nabar, and D. Gore, *Introduction to Space-Time Wireless Communications*, 1st. USA: Cambridge University Press, 2008.

[20] T. M. Cover and J. A. Thomas, *Elements of Information Theory (Wiley Series in Telecommunications and Signal Processing)*. USA: Wiley-Interscience, 2006.

[21] T. Marzetta and B. Hochwald, "Capacity of a mobile multiple-antenna communication link in rayleigh flat fading," *IEEE Transactions on Information Theory*, vol. 45, no. 1, pp. 139–157, 1999.

[22] I. S. Gradshteyn and I. M. Ryzhik, *Table of integrals, series, and products*, Seventh. Elsevier/Academic Press, Amsterdam, 2007, pp. xlviii+1171, Translated from the Russian, Translation edited and with a preface by Alan Jeffrey and Daniel Zwillinger, With one CD-ROM (Windows, Macintosh and UNIX).

[23] Harish-Chandra, "Differential operators on a semisimple lie algebra," *American Journal of Mathematics*, vol. 79, no. 1, pp. 87–120, 1957.

[24] C. Itzykson and J. Zuber, "The planar approximation. ii," *Journal of Mathematical Physics*, vol. 21, no. 3, pp. 411–421, 1980. eprint: `https://doi.org/10.1063/1.524438`.

[25] R. Couillet and M. Guillaud, "Performance of statistical inference methods for the energy estimation of multiple sources," in *2011 IEEE Statistical Signal Processing Workshop (SSP)*, 2011, pp. 673–676.